

A NEW GEOTHERMAL BRIDGE DE-ICING SYSTEM WITH ATTACHED
HYDRONIC HEATING LOOPS: FIELD TESTS, NUMERICAL MODELING,
AND ECONOMIC ASSESSMENT

by

Omid Habibzadeh-Bigdarvish

Presented to the Faculty of the Graduate School of
The University of Texas at Arlington
in Partial Fulfillment of the Requirements for the Degree of

Doctor of Philosophy
In
Civil Engineering

THE UNIVERSITY OF TEXAS AT ARLINGTON

August 2021

A NEW GEOTHERMAL BRIDGE DE-ICING SYSTEM WITH ATTACHED
HYDRONIC HEATING LOOPS: FIELD TESTS, NUMERICAL MODELING,
AND ECONOMIC ASSESSMENT

The members of the Committee approve the doctoral dissertation of Omid
Habibzadeh-Bigdarvish:

Prof. Xinbao Yu, Chair _____

Prof. Anand J. Puppala _____

Prof. Kathleen M. Smits _____

Prof. Ankur Jain _____

Copyright © by Omid Habibzadeh-Bigdarvish 2021

All Rights Reserved



To my parents, for endless love and support.

TABLE CONTENTS

TABLE CONTENTS	v
LIST OF FIGURES	x
LIST OF TABALES	xviii
ACKNOWLEDGEMENTS	xx
VITA AND PUBLICATIONS	xxiii
ABSTRACT	xxv
CHAPTER 1: INTRODUCTION	1
1.1 Motivation	1
1.2 Problem Description	3
1.3 Research Objectives	6
1.4 Dissertation Outline	6
CHAPTER 2: BACKGROUND	9
2.1 Introduction	9
2.2 Geothermal Snow-Melting and De-icing System	11
2.3 Thermal Performance of the Vertical Ground heat exchanger (GHE).....	18
2.3.1 Experimental Studies	18
2.3.1 Numerical Studies.....	21
2.4 Economic Assessment of Bridge deck de-icing using geothermal heat pump system.	25
CHAPTER 3: EXPERIMENTAL SETUP	26

3.1 Introduction	26
3.2 Overview	27
3.3 Instrumentation and Data Acquisition System (DAQ)	29
3.2 Construction of the Geothermal Mock-Up Bridge.....	32
CHAPTER 4: A NOVEL FULL-SCALE EXTERNAL GEOTHERMAL HEATING SYSTEM	
FOR BRIDGE DECK DE-ICING	46
4.1 Abstract	46
4.2 Introduction	47
4.3 Description of De-icing and Monitoring System	51
4.3.1 Test Site	51
4.3.2 Design of the Mock-up Geothermal Bridge	53
4.3.3 Construction of the Bridge Deck Prototype	61
4.3.4 Instrumentation and Monitoring System	65
4.4. Results and Discussion of The Operation Tests.....	67
4.4.1 Winter Test Process	67
4.4.2 De-icing Tests.....	70
4.4.3 System Performance	77
4.4.4 Heat Flux Analysis and Heating Efficiency	83
4.5 Summary and Conclusions.....	87

CHAPTER 5: A U-TUBE GROUND HEAT EXCHANGER FOR BRIDGE DE-ICING: SOLAR COLLECTOR AND DE-ICING TEST, GROUND HEAT RECOVERY, AND OPERATION STRATEGY	89
5.1 Abstract	89
5.2 Introduction and Background.....	90
5.3 External geothermal bridge deck de-icing system	98
5.3.1 Experimental Set-up and Monitoring System	98
5.3.2 Testing site.....	101
5.4 Energy performance assessment methodology	106
5.5 Field Investigation Result.....	108
5.5.1 Bridge Solar-Collector Test.....	108
5.5.2 Bridge De-icing Test	114
5.5.3 Heat Storage and Extraction Analysis	122
5.5.4 Ground Thermal Balance and Operation Strategy	125
5.6 Conclusions	127
CHAPTER 6: ON THE MODELLING OF A U-TUBE GROUND HEAT EXCHANGER: A PROPOSED COMPUTATIONALLY EFFICIENT NUMERICAL MODEL AND EXPERIMENTAL VERIFICATION.....	128
6.1 Abstract	128
6.2 Introduction	128

6.3 Numerical Model Development	133
6.3.1 Theoretical Basis of The Heat Transfer Processes	133
6.3.2 Experimental Set-up and Monitoring System	138
6.3.3 The Conventional FEM Model.....	141
6.3.4 A Proposed simplified Model.....	143
6.3.5 Mesh schema	146
6.4 Results and Discussion.....	147
6.4.1 Model Verification	147
6.4.2 Accuracy and Computational Time	159
6.4.3 Thermal behavior inside the borehole.	162
6.5 Conclusions	165
 CHAPTER 7: LIFE-CYCLE COST-BENEFIT ANALYSIS OF BRIDGE DECK DE-ICING USING GEOTHERMAL HEAT PUMP SYSTEM: A CASE STUDY OF NORTH TEXAS.....	
7.1 Abstract	166
7.2 Introduction	166
7.3 Background	170
7.3.1 Conventional snow/ice removal system (CSRS).....	170
7.3.2 Geothermal heat pump de-icing system (GHDS).....	171
7.4 Methodology	178

7.4.1 Framework.....	178
7.4.2 LCCBA.....	182
7.5 Results and Discussion:.....	193
7.5.1 Base case analysis.....	193
7.5.2 Sensitivity analysis.....	196
7.6 Conclusions.....	200
CHAPTER 8: SUMMARY AND CONCLUSIONS.....	202
8.1 Summary.....	202
8.2 Conclusions.....	202
8.2.1 De-icing Operations and Bridge Deck Thermal Response.....	203
8.2.2 GHE Performance and Subsurface Thermal Response.....	203
8.2.3 Overall system de-icing performance.....	204
8.2.4 Numerical Simulations of the U-tube heat exchanger.....	205
8.2.5 Economic Assessment.....	206
8.3 Lessons Learned.....	207
8.4 Future Direction.....	208
REFERENCES.....	210

LIST OF FIGURES

Figure 1.1 Conceptual diagram of the geothermal heat pump de-icing system (GHDS) (Habibzadeh-Bigdarvish et al. 2019)	3
Figure 2.1. 133-car pileup in Fort Worth, TX after freezing rain coats the bridge on I-35W and Northside Drive on Thursday, February 11, 2021 (Marfin et al. 2021).....	9
Figure 2.2. Schematic plot of a GSHP for space heating and cooling (Yu and Olson 2018).....	10
Figure 2.3. SERSO Project in Switzerland: (a) Overview of the system; (b) system under operation (Eugster 2007).....	12
Figure 2.4. Typical hydronic snow-melting system: (a) Plan view; (b) Cross-Sectional View. ..	13
Figure 2.5. Heat transfer mechanisms in a hydronically-heated bridge deck (Chiasson and Spitler 2001; Spitler and Ramamoorthy 2000).....	13
Figure 2.6. First geothermal snow-melting study in Turkey (Balbay et al. 2010).....	14
Figure 2.7. Sidewalk snow-melting project in Aomori, Japan: (a) Hydronic heating loop; (b) System under operation (Morita and Tago 2005)	15
Figure 2.8. The proposed snow melting system in Japan: (a) system overview; (b) Bridge deck condition during a snow-storm (Yoshitake et al. 2011).....	16
Figure 2.9. Comparison of the heated and unheated zone during a snowstorm (Bowers Jr 2016)17	
Figure 2.10. A lab experiment of the external heating system; (a) attached hydronic loops to the bottom of the concrete slab; (b) Applied spray foam to the bottom surface for thermal insulation (Hurley 2019).....	18
Figure 2.11. Experimental setup for the SBTES system in San Diego, California : (a) Plan view; (b) Elevation view (Başer and McCartney 2020)	20

Figure 2.12. Schematic and finite element representation of a single U-shape heat pipe (Al-Khoury et al. 2005)	24
Figure 3.1. Photo of the construction site located in Fort Worth, TX	26
Figure 3.2. 3D model of the experimental setup.....	27
Figure 3.3. (a) Layout of the heated bridge deck; (b) A-A cross-section view of the bridge deck, left: external heating zone, and right: internal heating zone (unit: in.).....	28
Figure 3.4. System operation modes: (a) full load operation mode; (b) bypass operation mode .	29
Figure 3.5. Data loggers and multiplexers used in the data acquisition system: (a) 25-channel solid-state thermocouple multiplexer; (b) Pile Dynamics TAP; (c) CR 1000X data logger; (d) 32-channel relay multiplexer.....	31
Figure 3.6. Construction process of stage 1: Bridge deck set-up.....	33
Figure 3.7. The construction process of stage 2: Internal hydronic loop and concrete casting ...	34
Figure 3.8. The construction process of stage 2: External hydronic loop and applying insulation foam.	35
Figure 3.9. Hydronic loops inlet and outlet pipes.....	36
Figure 3.10. Stage 3 of the fieldwork: Bridge deck instrumentation.....	37
Figure 3.11. Plan view of sensor locations in the externally heated zone (Unit: in.): (a) Z=0; (b) Z=5 cm; (c) Z= 10 cm; (d) 17.5 cm.	38
Figure 3.12. Plan view of sensor locations in the internally heated zone (Unit: in.): (a) Z=0; (b) Z=5 cm; (c) Z= 10 cm; (d) 17.5 cm.	39
Figure 3.13. Overview of the control room	40
Figure 3.14. Inlet/outlet temperature sensors: (a) GHE; (b) Bridge deck hydronic loops.....	41
Figure 3.15. The wiring diagram of the heat pump and thermostat.....	42

Figure 3.16. Subsurface soil and underground loop instrumentation	42
Figure 3.17. Stage 6 of construction activities: Borehole drilling and underground loop installation.....	44
Figure 3.18. Header pipes' thermistor string	45
Figure 4.1. Test site weather information (Source: U.S. Climate Data).....	52
Figure 4.2. Test site ground temperature profile.....	53
Figure 4.3. Schematic diagram of the mock-up geothermal bridge design (only the externally heated zone is tested in this study).....	54
Figure 4.4. The design of the mock-up bridge deck: (a) Plan view of the bridge deck, (b) Cross- sectional view of the bridge deck.....	55
Figure 4.5. GLHE design diagram.....	59
Figure 4.6. The final design of the GLHE	61
Figure 4.7. Installation of the hydronic loops: (a) Hydronic loops installed on the bottom surface of the externally heated zones, then covered by a cement paste, (b) A layer of polyurethane foam applied to the deck bottom.....	62
Figure 4.8. Construction of the GLHE: (a) Drilling the boreholes, (b) Insertion of the ground loop into the geothermal borehole, (c) Insertion of TMB's PEX pipe, (d) Connection of the ground loop pipes to the header pipes in the trench.....	64
Figure 4.9. Overview of the control room	64
Figure 4.10. Instrumentation: (a) The temperature sensor node from Pile Dynamics thermal wire cable at 2.5 cm below the deck surface, (b) Bridge deck inlet/outlet temperature sensors, (c) Geothermal borehole inlet/outlet temperature sensors	66
Figure 4.11. Collected weather data from different sources for the period of Jan. to Mar. 2019.	68

Figure 4.12. Summary of the externally heated surface temperature during freezing air temperatures for each test	70
Figure 4.13. Temperature variations inside the insulation foam and ambient during test #5.....	71
Figure 4.14. Inlet and outlet temperatures of the bridge deck hydronic pipes.....	71
Figure 4.15. Time-lapse of the bridge deck condition before, during, and after the de-icing test	73
Figure 4.16. Comparison of the heated and non-heated zone temperature variation during test #5	73
Figure 4.17. Surface temperature measurement of the bridge deck using thermal imager during test #5	74
Figure 4.18. Geothermal borehole inlet and outlet temperatures during winter test #5	75
Figure 4.19. Comparison of the heated and non-heated zone temperature variation during test #7	77
Figure 4.20. Power input to the heat pump and circulating pumps during the test; (a) Test#5, (b) Test #7.....	79
Figure 4.21. Comparison of the system input power, thermal energy output, and COP: (a) Test #5; (b) Test #7	80
Figure 4.22. Details of heat pump operation during test #5.....	81
Figure 4.23. Relationship between the thermal energy output of the heat pump and the total power input to the system	82
Figure 4.24. Relationship between the system COP and thermal energy output of the heat pump	82
Figure 4.25. Temperature variations of the bottom surface and the plane at 2.5 cm below the surface during winter test #5.....	85

Figure 4.26. Comparison of the heat flux on the bridge deck surface and supplied heat flux during winter test #5	85
Figure 5.1. Schematic of the external geothermal heat pump de-icing system	99
Figure 5.2. (a) Control room; (b) Bridge deck hydronic pipes	99
Figure 5.3. (a) Final stage of installation of the GHE and TMBs before excavation of trench and GHE connection to the header pipe; (b) Thermistor string attached to the heat exchanger pipe (c) Thermistor string attached to the PEX pipe that is filled with rebar for installation in TMB.....	100
Figure 5.4. On-site recorded temperatures at the Geothermal Bridge in Arlington, TX: (a) Air temperature; (b) Subsurface soil temperature.	102
Figure 5.5. Subsurface soil characteristics profile	103
Figure 5.6. Simplified boring log of the testing site's nearby bridge.	104
Figure 5.7. Variation of volumetric heat capacity and thermal conductivity with water content	105
Figure 5.8. Thermal response test apparatus at the site	105
Figure 5.9. The on-site GHE thermal response test result	106
Figure 5.10. Inlet/Outlet fluid temperature for bridge solar-collector test	109
Figure 5.11. (a) Heat rate and COP variation; (b) Heat injection and collection rate during the bridge solar-collector test.....	110
Figure 5.12. Ground temperature profile during bridge solar-collector test at different radial distances from GHE: (a) 0.45 m; (b) 0.9 m; (c) 1.5 m; (d) Far-field.....	112
Figure 5.13. Radial temperature profiles (a) and thermal gradient (b) at 14 m below the ground surface during the bridge solar-collector test.....	113

Figure 5.14. Temperature distribution of GHE’s surrounding soil at 14 m below the ground surface: (a) Before system onset, (b) 15 days after system onset, (c) 50 days after system onset. (Habibzadeh-Bigdarvish et al. 2020).....	114
Figure 5.15. Comparison of Inlet/Outlet fluid temperature with bridge deck and ambient temperature: (a) Test A; (b) Test B.....	116
Figure 5.16. Heat rate and COP variation: (a) Test A; (b) Test B	117
Figure 5.17. GHE extraction rate and supplied heat flux to the bridge deck: (a) Test A; (b) Test B.....	117
Figure 5.18. Ground temperature profile during Test A at different radial distance from GHE: : (a) 0.45 m; (b) 0.9 m; (c) 1.5 m; (d) Far-field.....	119
Figure 5.19. Ground temperature profile during Test B at different radial distances from GHE: : (a) 0.45 m; (b) 0.9 m; (c) 1.5 m; (d) Far-field.....	120
Figure 5.20. Radial temperature profiles (a) and thermal gradient (b) at 14 m below the ground surface during the de-icing Test A.....	121
Figure 5.21. Radial temperature profiles (a) and thermal gradient (b) at 14 m below the ground surface during the de-icing Test B	121
Figure 5.22. Ground temperature variation at the depth of 14 m and different radial distances (RD) from bridge solar collector test in summer to 1 st bridge de-icing test in the winter	123
Figure 6.1. Temperature distribution across the pipe wall (Gawecka et al. 2020)	134
Figure 6.2. Illustration of reducing 3D flow problem to a 2D or 3D curve (Comsol 2018).....	135
Figure 6.3. Schematic of the experimental setup.....	140
Figure 6.4. Average monthly air temperature and solar radiation data for the testing site.....	143

Figure 6.5. Schematic diagrams of GHE: (a) physical model; (b) Conventional model with 1-D pipe flow and pseudo pipe; (c) Proposed model.....	144
Figure 6.6. Finite element meshes for the optimum case: (a) Proposed model; (b) Conventional model.....	147
Figure 6.7. Monthly average ground temperature profile: numerical simulation vs experimental data.....	149
Figure 6.8. Comparison between the experimental data and the simulated fluid temperatures by the conventional and proposed efficient model.	150
Figure 6.9. Vertical temperature profile comparison between the experimental data from TMB 1 and the simulated by the conventional and proposed efficient model.....	151
Figure 6.10. Comparison between the experimental data from TMB 1 and the simulated soil by the conventional and proposed efficient model.	153
Figure 6.11. Vertical temperature profile comparison between the experimental data from TMB 3 and the simulated by the conventional and proposed efficient model.....	154
Figure 6.12. Comparison between the experimental data from TMB 3 and the simulated soil by the conventional and proposed efficient model.	155
Figure 6.13. Vertical temperature profile comparison between the experimental data from TMB 4 and the simulated by the conventional and proposed efficient model.....	156
Figure 6.14. Comparison between the experimental data from TMB 4 and the simulated soil by the conventional and proposed efficient model.	157
Figure 6.15. Radial temperature profile comparison at 14 m below the ground surface between the experimental data and the simulated by the conventional and proposed efficient model.....	158

Figure 6.16. Element size distribution on a plane located on the central axis of the borehole along the GHE: (a) Proposed model; (b) Conventional model.....	161
Figure 6.17. Temperature profile at Time=74 days and enlarged view for 15 m below the ground surface: (a) Proposed model; (b) Conventional model	163
Figure 6.18. Temperature profile inside the borehole.....	164
Figure 6.19. Radial temperature profile comparison at 14 m below the ground surface between the conventional and proposed model inside and borehole and surrounding soil	164
Figure 7.1. Conceptual diagram of the geothermal heat pump de-icing system (GHDS)	172
Figure 7.2. Cost items of GHDS	173
Figure 7.3. The framework of the economic analysis.....	179
Figure 7.4. Outline of the scenario's bridge	180
Figure 7.5. Cash flow diagram of corrosion maintenance activities.....	185
Figure 7.6. (a) An average daily minimum temperature of January 2015 (PRISM Climate Group 2015); (b) Texas annual precipitation in 2015 (PRISM Climate Group 2017); (c) Texas regions prone to road icing.	187
Figure 7.7. Cash flow of GHDS over one life cycle of the bridge deck.....	196
Figure 7. 8. The estimated range of GHDS costs PV	198
Figure 7.9. The estimated range of GHDS benefit PV	198
Figure 7.10. The estimated range of cost and benefit PV and NPV of GHDS	199
Figure 7.11. Variations of NPV and BCR of GHDS with respect to average daily traffic (ADT)	200

LIST OF TABALES

Table 3. 1. Type and quantity of the thermal sensors used in each area.....	30
Table 3. 2 Instrumentation list	31
Table 3. 3. Details of GHE and TMBs thermistor string	45
Table 4.1. Required heat flux at steady-state conditions (Source: ASHRAE, 2015)	56
Table 4.2. Summary for required heat flux at the mock-up bridge deck surface	58
Table 4.3. Required heating loads.....	60
Table 4.4. GLHE design and operational parameters	60
Table 4.5. Instrumentation list	65
Table 4.6. The details of operation tests and weather conditions	69
Table 4.7. Summary of System Performance during Tests #5 and #7	79
Table 4.8. Summary of the heat flux analysis and heat transfer efficiency	86
Table 5.1. Details of installed thermistor string in the soil.....	101
Table 5.2. Selected tests highlights.....	115
Table 5.3. Summary of the soil thermal and energy response during the study period from bridge solar-collector test in summer to 1 st bridge de-icing test in the winter.....	125
Table 5.4. Annual GHE energy performance	126
Table 6.1. The geometrical details of the borehole and heat exchanger pipe.....	139
Table 6.2. Details of installed thermistor string.....	140
Table 6.3. The material properties of the GHE in this study	141
Table 6.4. Automatic free tetrahedral element mesh settings.....	146
Table 6.5 Study period details	148
Table 6.6. The error of the numerical simulations results	160

Table 6.7. Comparison of the number of elements and computational time between proposed and conventional model.....	162
Table 7.1. Information on chloride-based and abrasives products used as a de-icing material (Fay et al. 2015)	171
Table 7.2. Construction cost information of previous projects (Boyd 2003; Minsk 1999).....	173
Table 7.3. Estimated unit construction costs of the GHDS for bridges and pavements.	174
Table 7.4. Summary of the environmental effects of chloride-based de-icers (Fischel 2001) ...	177
Table 7.5. List of costs and benefits for each alternative.....	183
Table 7.6. Corrosion maintenance schedule	185
Table 7.7. Texas statewide car crashes due to slippery road surface conditions	187
Table 7.8. Number of bridges in TxDOT Districts that are located in zones prone to icy road surface conditions (Texas Department of Transportation (TxDOT) 2016)	189
Table 7.9. Texas statewide crashes and injuries occurring in work zones and expected cars crashes on bridges.	189
Table 7.10. Traffic data of the scenario’s bridge	191
Table 7.11. Hourly travel time value per vehicle.....	192
Table 7.12. Travel delay scenario due to corrosion maintenance events.....	192
Table 7.13. Results of the base case analysis.....	195
Table 7.14. Input variables distributions of the Monte Carlo Simulation (MCS)	197
Table 7.15. Benefit-cost ratios for different reliabilities.....	199

ACKNOWLEDGEMENTS

First and foremost, I would like to express my sincere gratitude to my advisor Dr. Xinbao Yu. This journey of my research career at the University of Texas at Arlington (UTA) would not have been possible without his continuous support, patience, and encouragement. I cannot imagine coming to this point in my research without the benefit of his immense knowledge and intellectual curiosity. He has helped me grow personally, academically, research-wise, and professionally.

I am very thankful to my dissertation committee members Dr. Anand Puppala, Dr. Kathleen Smits and, Dr. Ankur Jain, for their encouragement and positive feedback. My professors and advisors were always there to support me with their insightful comments, recommendations, and constructive feedback. Their guidance and mentorship have benefited me in every step. I am forever grateful.

Furthermore, I would like to thank the financial support provided by the Texas Department of Transportation (TxDOT). I also wish to thank everyone at Civil Engineering Department at UTA, for being supportive, encouraging, and kind since day one. I could not wish for a better environment than here for achieving a doctorate degree.

I would also like to thank my colleagues, Dr. Aritra Banerjee, Dr. Mohammad Rakib Hasan, Dr. Shi He, Dr. Xuelin Wang, Dr. Teng Li, Gang Lei, Rahul Yadav, Mark Hurley, Sunil Adhikari, Taryn DiLorenzo, Hussein Hashemi Senejani, Nice Kaneza, Subhas Kandel, Samrat Raut, Hiramani Chimaurya, Maedot Abebe, which I enjoyed a lot working with them, for their assistance and encouragement during the dissertation research. We have broadened our knowledge with insightful research discussions and have helped each other in every way we could during our studies. I am also grateful to my friends who have been there to help me in any way possible until the last moment.

Last but not least, I would like to express my sincere gratitude and indebtedness to my parents, my wife, my sister, and my brothers for their love, support, and encouragement throughout the years. Without their presence, none of my success would have been possible.

Chapter 4 of this dissertation is based on the materials published by the Journal of Applied Thermal Engineering titled “A novel full-scale external geothermal heating system for bridge deck de-icing” with authors, Omid Habibzadeh-Bigdarvish, Xinbao Yu, Teng Li, Gang Lei, Aritra Banerjee, and Anand J. Puppala. (2021). In addition, this chapter partially used the materials published by the 4th International Conference on Transportation Geotechnics titled “De-icing Test of the Externally Heated Geothermal Bridge in Texas.” with authors Omid Habibzadeh-Bigdarvish, Teng Li, Gang Lei, Aritra Banerjee, Xinbao Yu, and Anand J. Puppala (2021).

Chapter 5 of this dissertation is based on material from a manuscript under preparation for publication, tentatively titled “A U-tube ground heat exchanger for bridge de-icing: solar collector and de-icing test, ground heat recovery, and operation strategy” with authors, Omid Habibzadeh-Bigdarvish, Gang Lei, Xinbao Yu, and Anand J. Puppala (2021). In addition, this chapter partially used the materials published by the 2nd International Conference on Energy Geotechnics titled “Externally heated geothermal bridge deck: Performance analysis of the U-tube ground heat exchanger” with authors Omid Habibzadeh-Bigdarvish, Xinbao Yu, and Anand J. Puppala (2020).

Chapter 6 of this dissertation is based on material from a manuscript under preparation for publication, tentatively titled “On the modeling of a U-tube ground heat exchanger: A proposed computationally efficient numerical model and experimental verification” with authors, Omid Habibzadeh-Bigdarvish, Xinbao Yu, and Anand J. Puppala (2021). In addition, this chapter partially used the materials published by the IFCEE 2021 titled “Numerical Study and Experimental Validation of the Thermal Performance of a U-Tube Borehole Heat Exchanger for a Geothermal De-Icing

System.” with authors Omid Habibzadeh-Bigdarvish, Teng Li, Gang Lei, Anand J. Puppala, and Xinbao Yu (2021).

Chapter 7 of this dissertation is based on the materials published by the Journal of Sustainable Cities and Society titled “Life-Cycle cost-benefit analysis of Bridge deck de-icing using geothermal heat pump system: A case study of North Texas.” with authors, Omid Habibzadeh-Bigdarvish, Xinbao Yu, Gang Lei, Teng Li, and Anand J. Puppala (2021).

July 30th, 2021

VITA AND PUBLICATIONS

2009-2014	Bachelor of Science in Civil Engineering, Islamic Azad University, Iran
2014-2017	Master of Science in Civil Engineering for Risk Mitigation The Polytechnic University of Milan, Italy
2017-2021	Doctor of Philosophy in Civil (Geotechnical) Engineering The University of Texas at Arlington, USA

Publications:

Habibzadeh-Bigdarvish, O., Yu, X., Lei, G., Li, T., and Puppala, A. J. A. J. (2019). “Life-Cycle cost-benefit analysis of Bridge deck de-icing using geothermal heat pump system: A case study of North Texas.” *Sustainable Cities and Society*, Elsevier, 47, 101492.

Habibzadeh-Bigdarvish, O., Yu, X., and Puppala, A. J. (2020). “Externally heated geothermal bridge deck: Performance analysis of the U-tube ground heat exchanger.” *E3S Web of Conferences*, EDP Sciences, 7006.

Habibzadeh-Bigdarvish, O., Li, T., Lei, G., Banerjee, A., Yu, X., and Puppala, A. J. (2021). “De-icing Test of the Externally Heated Geothermal Bridge in Texas.” *4th International Conference on Transportation Geotechnics, ICTG 2021*.

Habibzadeh-Bigdarvish, O., Li, T., Lei, G., Puppala, A. J., and Yu, X. (2021). “Numerical Study and Experimental Validation of the Thermal Performance of a U-Tube Borehole Heat Exchanger for a Geothermal De-Icing System.” *IFCEE 2021*, American Society of Civil Engineers, Reston, VA, 109–118.

Habibzadeh-Bigdarvish, O., Yu, X., Li, T., Lei, G., Banerjee, A., and Puppala, A. J. (2021). “A novel full-scale external geothermal heating system for bridge deck de-icing.” *Applied*

Thermal Engineering, Elsevier, 185, 116365.

Habibzadeh-Bigdarvish, O., Lei, G., Yu, X., and Puppala, A. J. (2021). “A U-tube ground heat exchanger for bridge de-icing: solar collector and de-icing test, ground heat recovery, and operation strategy.” To be submitted to: *ASCE Journal of Geotechnical and Geoenvironmental Engineering*.

Habibzadeh-Bigdarvish, O., Yu, X., and Puppala, A. J. (2021). “On the modeling of a U-tube ground heat exchanger: A proposed computationally efficient numerical model and experimental verification.” To be submitted to: *Geothermics*.

ABSTRACT

A NEW GEOTHERMAL BRIDGE DE-ICING SYSTEM WITH ATTACHED HYDRONIC HEATING LOOPS: FIELD STUDY, NUMERICAL MODELING, AND ECONOMIC ASSESSMENT

Omid Habibzadeh-Bigdarvish

The University of Texas at Arlington, 2021

Supervising Professor: Dr. Xinbao Yu

Each year, ice and snow adversely impact U.S. transportation infrastructure during the cold season, causing an extensive impact on the U.S. economy. Bridges are key elements in the transportation network and the most vulnerable sections of the road to ice and snow. Conventional snow and ice removal system (CSRS) is proven not to be a satisfactory solution as it causes induced damages and issues, such as accelerating bridge deck corrosion, safety issues, travel delays, and environmental damages. Thus, the geothermal heat pump de-icing system (GHDS) is introduced as a sustainable solution for bridge deck de-icing, which utilizes renewable geothermal energy and prevents the problems associated with CSRS. Current GHDS designs mostly rely upon embedded hydronic loops in concrete decks. To extend the GHDS for existing bridges, a new external hydronic deck has been developed, which employs attached hydronic heating pipes to the bottom surface of the bridge deck.

In this study, a novel external geothermal heating system is developed and implemented on a full-scale bridge deck, located in the Dallas-Fort Worth metroplex in Texas, USA. Primarily, this study presents the design and implementation procedure of a novel external geothermal

heating system on a full-scale bridge deck for de-icing operations in field conditions for the first time. It tests and analyzes the system's heating performance and the bridge deck's thermal response under multiple winter events. The details and information pertaining to the design and construction of the hydronic loops, a ground heat exchanger (GHE), and the monitoring system, are presented and can be pivotal for the designers of similar projects. The test results showed that the system was successful in de-icing the bridge deck and maintaining the bridge deck surface temperature above freezing in the event with a minimum ambient temperature of $-6.2\text{ }^{\circ}\text{C}$. Experimental results also indicated that the external heating system was able to transfer about 55% of the supplied heat to the bridge deck surface. Moreover, this study investigates the thermal and energy performance of the 131 m borehole heat exchanger as well the subsurface ground temperature distribution during heat injection and extraction due to bridge solar collector and de-icing tests. According to the result, the heat injection by bridge solar-collector test resulted in a noticeable rise in the ground temperature surrounding the heat exchangers. The result proved that the stored thermal energy can be preserved for utilization in the winter de-icing test. Also, the field tests' results proved the feasibility of the bridge solar collector to address the thermal imbalance issue in the ground.

Moreover, in this study, a 3D transient FE model is developed in COMSOL Multiphysics to assist in further investigation of the GHE performance and overcome the limitation of the experimental tests. As one of the disadvantages of the finite element (FE) models is huge computational time, a computationally efficient model is developed which sacrifices the temperature distribution inside the borehole and simulates the borehole wall temperature with less computational time, a high level of accuracy, and convenient meshing. The proposed model is verified against the experimental data and was found to be as accurate as of the conventional model in simulating outlet fluid temperature, borehole wall temperature, and soil temperature surrounding

the borehole. The outcome of the analysis confirmed, application of the proposed model greatly reduced the required number of mesh elements and consequently computational time in comparison to the conventional model.

Finally, this study performs a scenario-based life-cycle cost-benefit analysis (LCCBA) on the geothermal heat pump de-icing system (GHDS) to investigate the economic viability of this system for the case of North Texas. The result of the base case analysis showed the benefits of the GHDS outweigh its costs. In addition, the results of the sensitivity analysis, using the Monte Carlo Simulation (MCS), indicated traffic flow enhancement is the most dominant variable affecting the overall result. However, for the daily traffic volume of 24000 vehicles, the benefits were estimated to be 2.32 times greater than the costs with 95% reliability. Generally, the analysis output demonstrated, for the bridges with a minimum daily traffic volume of 7000 vehicles, the application of the GHDS is economically viable.

CHAPTER 1: INTRODUCTION

1.1 Motivation

Severe winter weather conditions adversely affect the functionality of roads and endanger the safety of motorists. Approximately 70% of the United States' population and transportation network are affected by snowy weather and receive more than 13 cm average snowfall annually (Perkins et al. 2012). Bridges are considered as the key elements of the transportation infrastructure as they ensure the accessibility of roads. However, they are vulnerable to cold weather and highly prone to accumulating ice and snow due to exposed top and bottom surfaces to the atmosphere. Therefore, winter maintenance of bridges is one of the crucial and recurring tasks during winter in snowy and icy regions.

Commonly, de-icing salt is utilized in the conventional snow/ice removal system (CSRS) as it is inexpensive and redundant. However, de-icing salt can cause a phenomenon known as a “chloride attack” which provokes a significant durability problem for concrete pavements and structures. The output of a chloride attack is the corrosion of steel reinforcement, which results in cracking and spalling of the concrete, and eventually deteriorates the bridge deck surface. Several studies have focused on this topic (Baboian 1992; Granata and Hartt 2009; White et al. 2005; Yunovich et al. 2003). The reinforcement area is decreased as a consequence of the bridge corrosion, which leads to the overstress of the steel cross-section and ultimately causes a reinforced concrete bridge deck to collapse (Ghasemi-Fare et al. 2015). There are several cases of reinforced concrete bridge decks that collapsed due to the corrosion of steel reinforcements (Naito et al. 2010). According to recent studies, resilient steel can be used on new construction projects, but this does not address concerns relating to the existing infrastructure.

There is a growing concern nationwide about the condition of the bridges. The total cost of bridge corrosion has been estimated at 6-10 billion dollars annually by Koch et al. (2002). Yunovich et al. (2003) found that indirect costs account for 10 times of the total direct cost. According to the FHWA (2008), one-fourth of the U.S. bridges contain structural defects or are functionally obsolete. One of the main challenges for highway administration is to extend the service life of infrastructures, with minimal maintenance cost and efforts (AASHTO 2005). Besides the problems discussed above, utilization of de-icing salt also cause delays for motorists and result in massive financial damages due to excessive fuel consumption and additional travel time cost (Zeroual et al. 2017). As a result of bridge deck corrosion more frequent maintenance is required, which might involve closing lanes or even the whole bridge to fix the problem, again causing delays for travelers. There are also environmental risks associated with de-icing agents, including contamination, roadside vegetation damage and mortality, reduced soil stability, and increased permeability and salinity of water (Fischel 2001). Moreover, the conventional bridge de-icing method also leads to some safety concerns for the motorists since the application of this system does not always provide an ice-free surface; for example, it is very likely that drivers face an icy surface on the bridge deck after freezing rain. Therefore, it is imperative to apply new approaches and technologies, which can prevent the aforementioned problems.

Geothermal energy is a renewable and green source of energy, proven to be a reliable alternative to fossil fuels. The shallow geothermal energy (SGE) is extracted using the ground heat exchangers (GHE) or energy geostructures (e.g., foundations, diaphragm walls, tunnel liners, or anchors) (Barla et al. 2016; Brandl 2006; Mimouni et al. 2014; Nam and Chae 2014; Sterpi et al. 2018a). The output of the geothermal energy system is used for a variety of purposes, such as heating and cooling of a building. A novel application of geothermal energy is for snow melting

or de-icing the bridge deck surface. Thus, a geothermal heat pump de-icing system (GHDS) was developed which utilizes geothermal energy as a reliable and renewable source of energy. In this system, the heat carrier fluid, mostly water-based antifreeze solution, circulates between the ground loop heat exchangers (GLHE) and hydronic heating loops embedded in the bridge deck (Figure 1.1). The study of the life-cycle cost-benefit analysis (LCCBA) of this system has indicated that its application is economically viable for the bridges with a minimum annual daily traffic volume of 7000 vehicles, and benefit to cost ratio (BCR) of 2.6 can be achieved for the 50-year life-cycle and daily traffic volume of 24000 vehicles (Habibzadeh-Bigdarvish et al. 2019).

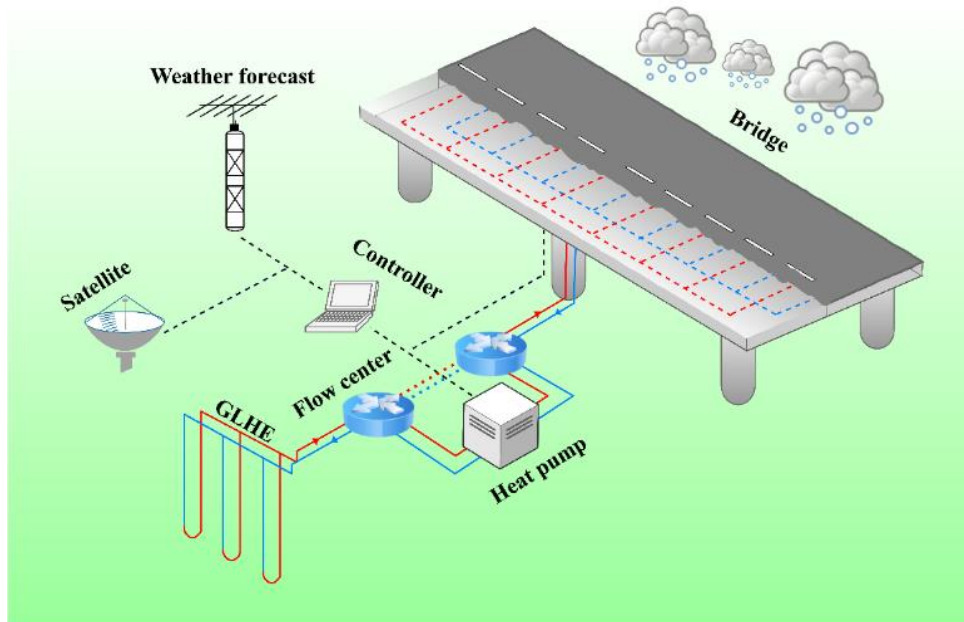


Figure 1.1 Conceptual diagram of the geothermal heat pump de-icing system (GHDS) (Habibzadeh-Bigdarvish et al. 2019)

1.2 Problem Description

Most previous geothermal de-icing/snow-melting studies have focused on geothermal heat pump de-icing systems in which hydronic heating loops are embedded within the concrete slab of the new bridges, which actually cannot be employed in the existing bridges where the demand for de-

icing is the greatest. In recent years, a UTA research team has been collaborated with the Texas Department of Transportation (TxDOT), to develop an external geothermal de-icing system that can be implemented for existing bridges. So far, preliminary studies have been carried out through experimental and numerical analysis (Hurley 2019; Li et al. 2020; Yu et al. 2017, 2019). The experimental studies are limited to the laboratory-scale concrete slab and only focused on the hydronic heating loops and heating performance of the bridge deck. Therefore, they have never studied the overall system performance of the externally heated bridge deck, as they did not employ any geothermal systems in the test setup. However, due to the lack of research concerning the performance of the full-scale external geothermal heating system for bridge deck de-icing, there is still a need for investigating the thermal and energy performance, heat transfer efficiency, and feasibility of the full-scale external geothermal heating system under actual winter weather.

The most critical component of the geothermal de-icing systems is the ground heat exchangers (GHEs), as they play a vital role in keeping the system running efficiently. A significant disadvantage of GHEs is the long-term variation in subsurface thermal conditions due to heat extraction or sink in the ground (You et al. 2018; You and Yang 2020). The ground thermal imbalance problem is a potential threat to the efficiency of the geothermal bridge deck snow melting/de-icing system due to single-mode operation, i.e., heating mode. Because, despite the thermal conditioning of a building in which the GHE operates under both heating and cooling load, geothermal snow-melting/de-icing systems only need to work in heating mode, i.e., heat extraction from the ground, which provoke ground thermal imbalance issue. However, the solution lies in the application of the bridge deck as a solar collector. Several studies are available in the literature that have investigated the application of the bridge deck as a solar collector to address the thermal imbalance issue in the ground (Bowers Jr and Olgun 2015; Wu et al. 2020). To date, no study has

been found in the literature that comprehensively investigated the bridge solar-collector impact on the thermal condition of the ground. Moreover, the energy performance, soil thermal storage capacity, and thermal imbalance ratio (IR) due to the bridge solar-collector operation of GHDS are also open questions. Besides, very few full-scale experimental studies have investigated the GHE performance and heat transfer surrounding the GHE; studying the GHE performance in a geothermal snow-melting/de-icing system is even a rarer topic.

Another challenge is that there are many Finite Element (FE) models available for the analysis of the heat transfer process inside and surrounding the GHE, and not all the models are computationally efficient as well as accurate. Al-Khoury et al. (2005) and Al-Khoury and Bonnier (2006) developed the 1D pipe element, which significantly has reduced the mesh complexity and computational time. Ozudogru et al. (2014) developed a 3D numerical model for vertical heat exchangers which utilized 1D fluid flow; also, they proposed a pseudo pipe approach to overcome the errors of the 1D pipe flow modeling. The same approach has been later used by other researchers, such as Zhang et al. (2020). In the previous studies, the meshing of the borehole and pseudo pipe model has been challenging as it presents extreme geometrical aspect ratios and requires a more advanced and efficient numerical strategy to reduce the computational time.

Lastly, an understanding of the financial performance of geothermal heat pump de-icing (GHDS) is necessary to encourage the widespread use of this technology. This issue can be clarified by conducting an economic assessment. It is a useful method to predict the expected costs and benefits of a proposal or project and to provide valuable information to assure the efficient allocation of resources. Thus, a decision-maker is then able to compare alternatives and select the most appropriate ones. However, although GHDS has proved to be a sufficient and feasible solution for de-icing the bridge decks, its financial feasibility has never been investigated.

1.3 Research Objectives

The primary objective of this research is to better understand different aspects of the novel full-scale external geothermal heating systems for bridge deck de-icing through field experiments, numerical modeling, and economic assessment. The general research objectives are:

- Development of a full-scale prototype of the external geothermal heating system to better investigate the system's thermal and energy performance as well as bridge deck's thermal response under winter events.
- Experimental Investigation of the ground heat recovery using the bridge deck as a solar collector and thermal and energy performance analysis of the GHE during the solar collector and de-icing test.
- Experimental Investigation of the heat transfer in the subsurface surrounding a full-scale vertical ground heat exchanger under heat extraction and injection load.
- Development of a computationally efficient finite element (FE) model that can overcome the extreme geometrical aspect ratios problem of the geothermal borehole components and provide accurate simulation results.
- Development of a framework and case study for the life-cycle cost-benefit analysis (LCCBA) of the geothermal heat pump de-icing system (GHDS).

1.4 Dissertation Outline

This dissertation mainly consists of four journal papers, of which two have been published, and two will be submitted for publication. The topic of each paper and the associated journal is given below:

- Chapter 4 – A novel full-scale external geothermal heating system for bridge deck de-icing

- Overview: This chapter assesses the feasibility of the de-icing system and demonstrates the winter test result. It tests and analyzes the system's heating performance and the bridge deck's thermal response under several winter events.
 - Journal: Applied Thermal Engineering
- Chapter 5 – A U-tube ground heat exchanger for bridge de-icing: a solar collector and de-icing test, ground heat recovery, and operation strategy
 - Overview: This study focuses on the evaluation of the energy performance and subsurface ground temperature distribution during the operation of a borehole ground heat exchanger in an externally heating geothermal bridge de-icing system.
 - Journal: ASCE Journal of Geotechnical and Geoenvironmental Engineering (to be submitted)
- Chapter 6 – On the modeling of a U-tube ground heat exchanger: A proposed computationally efficient numerical model and experimental verification
 - Overview: This chapter deals with developing a computationally efficient FE model which replaces the modeling of the borehole with an equivalent 1D pipe element, however providing accurate results as the conventional model with less computational time.
 - Journal: Geothermics. (to be submitted)
- Chapter 7 – Life-cycle cost-benefit analysis of bridge deck de-icing using geothermal heat pump system: a case study of north Texas
 - Overview: This chapter develops an economic analysis framework and performs a scenario-based life-cycle cost-benefit analysis (LCCBA) for a geothermal heat pump de-icing system (GHDS) located in North Texas.

- Journal: Sustainable Cities and Society

For further understanding of this research, three additional chapters are also included. Chapter 2 reviews the background and previous literature in this area of study, Chapter 3 describes the overview, construction, and layout of the field setup, and Chapter 8 summarizes the main findings of this study.

CHAPTER 2: BACKGROUND

2.1 Introduction

Bridges are the critical infrastructures of the transportation network, which are negatively affected by the severe winter weather (Figure 2.1). Traditionally, de-icing salt and other chemical deicers are used to prevent snow and ice accumulation on the bridge deck. Application of the chemical deicers is hazardous to the environment, labor-intensive, time-consuming, and corrosive to the bridge deck (Baboian 1992; Fischel 2001; Yunovich et al. 2003). Moreover, corrosion of the bridge deck eventually leads to the repair/rehabilitation actions and work zones on the bridges, which imposes delays on the travel time of the motorists and increases the risk of an accident as well (Habibzadeh-Bigdarvish et al. 2019). Thus, new technologies have been developed that use geothermal energy for snow/ice melting on the bridge deck surface, prevent the corrosion of the bridge deck, and minimize environmental footprints (Lund 1999; Minsk 1999).

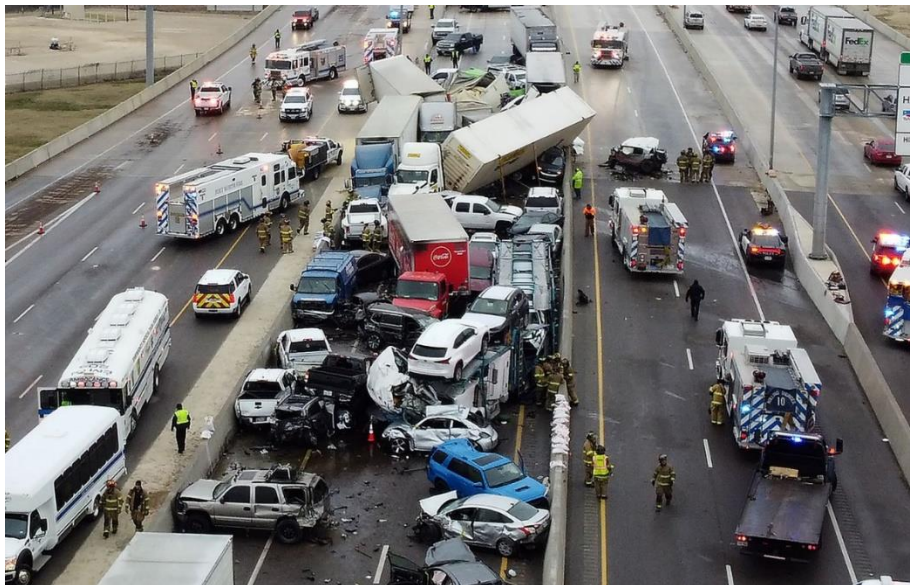


Figure 2.1. 133-car pileup in Fort Worth, TX after freezing rain coats the bridge on I-35W and Northside Drive on Thursday, February 11, 2021 (Marfin et al. 2021)

Commonly, geothermal energy is employed using a ground source heat pump system (GSHP) which is a highly efficient, renewable energy technology (Omer 2008; Spitler and Bernier 2011; Yu and Olson 2018). This technology relies on the ground heat exchangers (GHE) buried into the ground to extract heat during the cold season and depletion during the warm season (Figure 2.2). It works on the basis that the ground temperature is relatively constant, around 10-15 °C, below a certain depth, it is warmer than the air in winter and cooler than the air in summer (Brandl 2006).

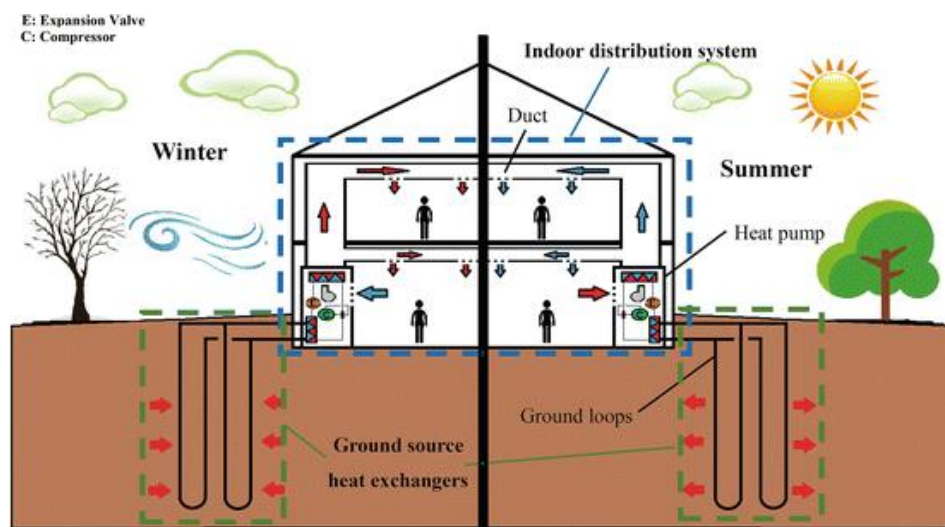


Figure 2.2. Schematic plot of a GSHP for space heating and cooling (Yu and Olson 2018)

The GSHP is mainly used for thermal conditioning of the building; however, a novel application has been developed through the implementation of a geothermal heat pump de-icing system (GHDS) for snow melting and de-icing bridge decks and pavements. GHDS is a ground source heat pump system (GSHP) that uses the system's heat output for snow melting and de-icing purposes. In these systems, the heat carrier fluid circulates between ground loop heat exchangers (GHE) and the hydronic loops in contact with the bridge deck/pavement and transfers heat to the

bridge deck/pavement surface to melt snow and ice. The heat pump in the system helps the heat carrier fluid reach the ideal temperature appropriate for snow and ice melting.

2.2 Geothermal Snow-Melting and De-icing System

The geothermal bridge/pavement heating system has been developed, implemented, and studied for several decades. As early as the 1970s, the feasibility of using geothermal energy as a heat source in a system that uses the heat pipes for de-icing and snow-melting of the pavement surface was studied by Bienert et al. (1974) in Baltimore. The study was performed at McLean, Virginia, during two winters at the Fairbank Highway Research Station. In another study by Ferrara and Brinkman (1976), it was demonstrated how the application of heat pipes contributes to avoiding the preferential freezing of highway pavement slabs and bridge decks. For de-icing roadways structures in Colorado, Griffin (1982) examined the conceptual designs, life expectancy, performance, and cost estimates for all the potential systems with non-fossil fuel heat sources. One of the pioneer applications of geothermal energy for bridge deck de-icing and snow-melting is the SERSO system in Switzerland that works since 1994 (Eugster 2007). The SERSO system has demonstrated that an underground thermal energy storage system is feasible for storing solar energy. This system utilizes 91 borehole heat exchangers 65 m deep to maintain temperatures at or above 3 °C on a bridge deck surface during the winter. Only the circulation of water within the pipes is powered by electricity, and no heat pump is used. Figure 2.3 shows the overview of the SERSO Project in Switzerland. More recently, Lund (1999) and Minsk (1999) also reported multiple applications of the geothermal heat pump de-icing system for bridge decks in the U.S. Their study focused on the design, construction, and cost data, but provided less information on the performance of the system during snow/ice events; however, they observed positive control of snow and ice on the bridge deck.

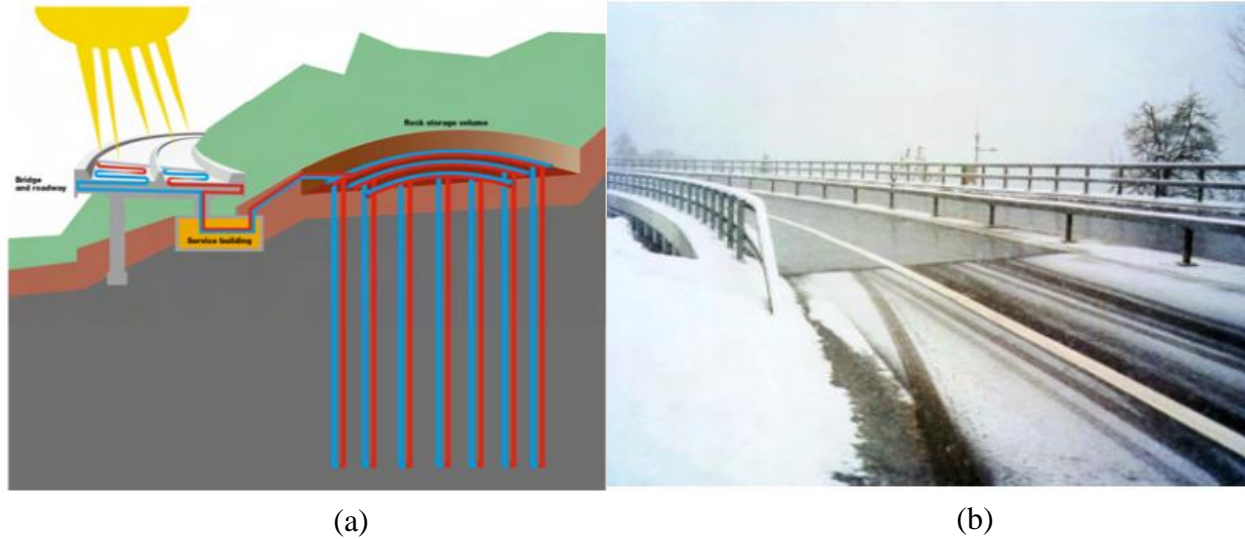


Figure 2.3. SERSO Project in Switzerland: (a) Overview of the system; (b) system under operation (Eugster 2007)

In two similar studies, Spitler and Ramamoorthy (2000) and Chiasson and Spitler (2001), investigated the design of the hydronic heating system for an interstate highway in Oklahoma. They discussed the conventional layout of hydronic heating pipes and demonstrated the heat transfer mechanism within the concrete bridge deck (Figures 2.4 and 2.5). Their design called for a vertical closed-loop ground-coupled type, which can be installed at any location where drilling and earth trenching are feasible. They mentioned that it is necessary to perform the ground thermal recharge to effectively balance the thermal loading to the ground over the annual cycle, and hence reduce the size and therefore the cost of the GLHE. They concluded that the final design consists of 16 heat pumps that will supply fluid to the bridge deck at approximately 50°C with a total flow rate of 22 l/s. Also, the de-icing system needs 250 boreholes, each 76 m deep which are running with a fluid flow rate of 57 l/s, that uses summer recharge.

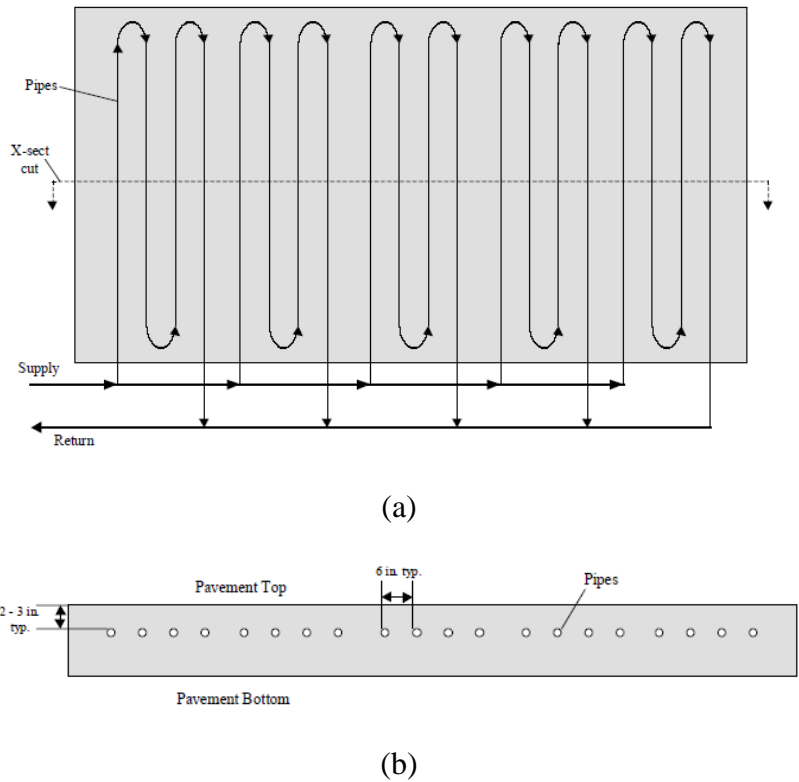


Figure 2.4. Typical hydronic snow-melting system: (a) Plan view; (b) Cross-Sectional View.

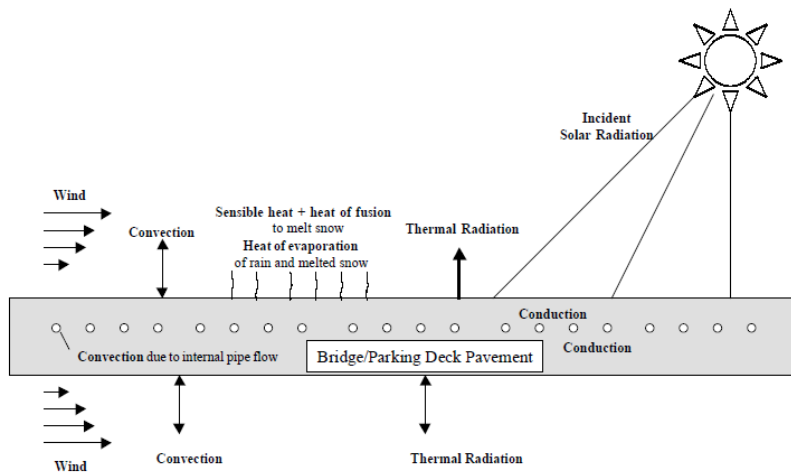


Figure 2.5. Heat transfer mechanisms in a hydronically-heated bridge deck (Chiasson and Spitler 2001; Spitler and Ramamoorthy 2000).

Liu et al. (2003) set up a bridge deck model of 18.3 m × 6.1 m where a PEX pipe heating system was installed in a 15.2 cm thick bridge deck. The underground loops system consists of 6

boreholes of 66.1 m deep and 13 cm diameter that are in a 2 by 3 configuration with 7.62 m spacing. Boreholes were employed to transport geothermal heat. Furthermore, to simulate the operation of the whole anti-icing system, they developed a model in the HVACSIM+ model and also investigated the snow melting process occurring on the surface. The same authors also developed a numerical model of snow melting on a heated pavement surface and discussed its application to a representative snow melting system. The model was successful in predicting the transient surface conditions, including the temperatures and extent of snow cover, and was experimentally validated and successfully tested (Liu et al. 2007).

Balbay and Esen (2010) were the first to study the practicality of using a ground source heat pump system for snow melting on pavements and bridge decks in Turkey (Figure 2.6). Their research demonstrates the performance of the system and provides valuable information regarding slab temperature and coefficient of performance (COP). They also investigated the energy performance of the snow melting systems using a GSHP and found that the COP values of the GSHP system were 1.99, 2.66, and 3.05 for borehole depths of 30 m, 60 m, and 90 m, respectively.



Figure 2.6. First geothermal snow-melting study in Turkey (Balbay et al. 2010)

In Japan, several studies have investigated the feasibility of the geothermal snow-melting system. Morita and Tago (2005) reported the highlights of the geothermal snow-melting project for 659 m² sidewalks in the heavy snowfall city of Aomori (Figure 2.7). The system consists of a total of 8-151.4 m downhole coaxial heat exchanger (DCHE) and 2 heat pumps. Based on the system operation in several winters, it was found that snow-melting systems have sufficient snow-melting capacity for the city.



Figure 2.7. Sidewalk snow-melting project in Aomori, Japan: (a) Hydronic heating loop; (b) System under operation (Morita and Tago 2005)

Yoshitake et al. (2011) developed a bridge deck heating system using the underground water storage tank as a heating source (Figure 2.8). The goal was to achieve a temperature $> 0.5^{\circ}\text{C}$ on the bridge deck surface during the winter. The system showed to be capable of removing snow on the bridge decks sooner than on the unheated road surface near the bridge. The authors suggested that the proposed system was an economical and effective method for snow-melting and de-icing and can be implemented in relatively mild regions, such as western Japan.

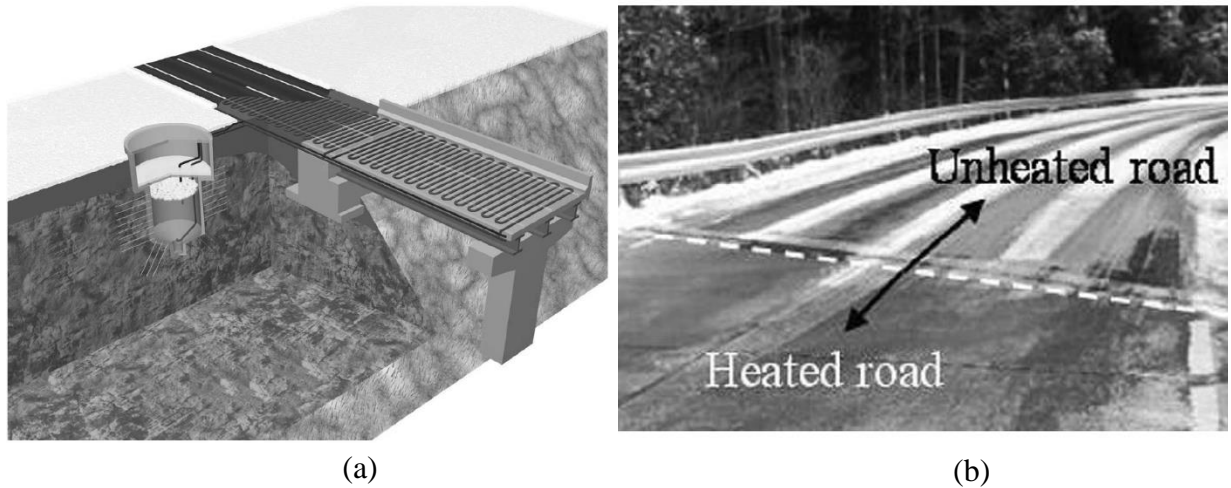


Figure 2.8. The proposed snow melting system in Japan: (a) system overview; (b) Bridge deck condition during a snow-storm (Yoshitake et al. 2011)

Ghasemi-Fare et al. (2015) examined the feasibility of the geothermal de-icing system and proved the feasibility of this technology through numerical and experimental investigation. They employed proof-of-concept testing to assess the operational basis and key design parameters.

Another study has investigated the thermal performance of a small-scale (2.6 m × 3.0 m) bridge deck de-icing system under bridge deck de-icing and thermal recharge operations (Bowers G Allen and Olgun 2014; Bowers Jr 2016). Figure 2.9 illustrates the test result during a snowstorm. The energy piles were used as a mean to harvest the geothermal energy. The authors examined both the bridge deck and the ground's temperature response during winter heating and summer recharge. According to the experiments, the system was able to draw enough energy from the energy piles to maintain the deck snow-free during moderate snowstorms.

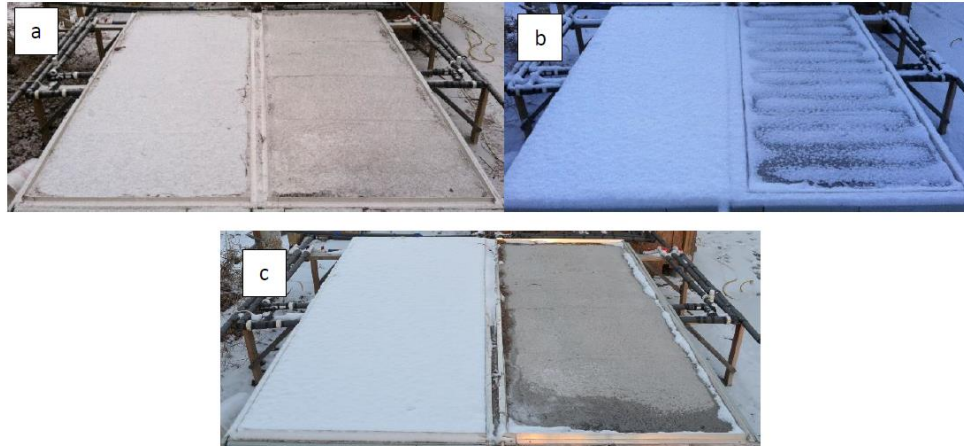


Figure 2.9. Comparison of the heated and unheated zone during a snowstorm (Bowers Jr 2016)

Over the past few years, A UTA team has been working with the Texas Department of Transportation (TxDOT) to investigate the implementation of this system on Texas bridges (Yu et al. 2017), and to develop a system that can be also used for existing bridges. Li et al. (2018) conducted preliminary research on externally heated geothermal bridge decks, using numerical analysis, and showed that the proposed externally heated geothermal bridge deck can successfully de-ice bridge decks in mild winter weather conditions (Li et al. 2018). The same research group has investigated the feasibility and performance of the externally heated geothermal bridge decks through experimental tests performed on the laboratory-scale concrete slab of 10 and 20 cm (Figure 2.10). The lab setup consists of hydronic loops, a circulating pump, and an electrically heated water tank. A series of heating tests were performed under various heating conditions to assess the efficiency of the heating performance and heat transfer of the external heating design (Hurley 2019; Yu et al. 2019). Although they showed the external heating system is a feasible solution for de-icing the bridge deck, however, the laboratory tests only focused on the hydronic heating loops and thermal response of the concrete slabs; the experiments were unable to investigate the overall performance of the externally heated bridge deck as they did not employ any geothermal systems

in the test setup. More recently, the heat transfer process and energy balance of the externally heated concrete slab have been studied using a 3D numerical model, which was calibrated using the experimental results obtained from lab experiments (Li et al. 2020).



Figure 2.10. A lab experiment of the external heating system; (a) attached hydronic loops to the bottom of the concrete slab; (b) Applied spray foam to the bottom surface for thermal insulation (Hurley 2019)

2.3 Thermal Performance of the Vertical Ground heat exchanger (GHE)

2.3.1 Experimental Studies

In recent years, there have been many studies concentrating on accurate estimation of heat transfer inside and around boreholes using numerical and experimental studies (Javadi et al. 2019; Li et al. 2018; Noorollahi et al. 2018; Zhang et al. 2018). However, in contrast to numerical modeling, only a few full-scale experimental studies are available which has investigated the heat transfer inside and around boreholes.

In one of the earlier studies, the temperature profile inside a 151.4 m downhole coaxial heat exchanger (DCHE) in a snow-melting system in Japan has been investigated (Morita and Tago 2005). The authors have studied the impact of the DCHE operation on the temperature profile

inside the geothermal borehole. Observing the temperature changes in this formation, they concluded that the DCHE temperature is sensitive to the heat balance between charged and extracted heat. The amounts of extracted heat were significantly in excess of charged heat on a fiscal year basis. They suggested that the most effective way would be to reduce unnecessary snow-melting operations, which might also lead to better performance. In another study, the subsurface thermal environmental changes caused by heat exchange with the ground have been evaluated by monitoring the ground temperature variation of heat exchanging well (Fujimitsu et al. 2010). They have also performed a numerical simulation of the underground temperature change with computer programs to predict the long-term effect. They found, according to the simulation results for a 20-year operation, there will not be a cumulative increase or decrease in subsurface temperature. Therefore, it is likely that the GSHP system does not significantly impact the subsurface thermal environment. Gao et al. (2013) focused on the development of a numerical model for groundwater heat pump (GWHP) systems to conduct a comparison of the energy efficiency and thermal interaction between pumping and injecting well groups. They concluded that the influence of thermal interaction would lead to an effect on the efficiency of the groundwater heat pump (GWHP), and the well location and their arrangement was a crucial key to the thermal breakthrough.

In a recent study, Başer et al. (2016) studied the transient changes in ground temperatures in a field-scale SBTES system installed in the vadose zone of Golden, Colorado through experimental and numerical analysis (Figure 2.11). Their experimental result showed that after 75 days of heat injection at a constant rate of 20 W/m the ground temperature in the array increased by 7 °C and only 21-42% of the total 11.5 GJ thermal energy stored in the soil. In a similar study by the same authors, transient ground temperatures have been investigated in a field-scale soil-

borehole thermal energy storage (SBTES) system in San Diego, California (Başer and McCartney 2020). The SBTES system consists of an array of thirteen 15 m-deep borehole heat exchangers at 1.5 m spacing. In a 4-month period, the heat was collected from solar thermal panels and injected into the SBTES system, which was followed by monitoring the subsurface for about a 5-month ambient cooling period. The authors also developed a numerical model for coupled heat transfer and water flow and compared the measured data compared with those predicted by the model. In general, a good match was found between the experimental measurements of ground temperature in the SBTES and those simulated.

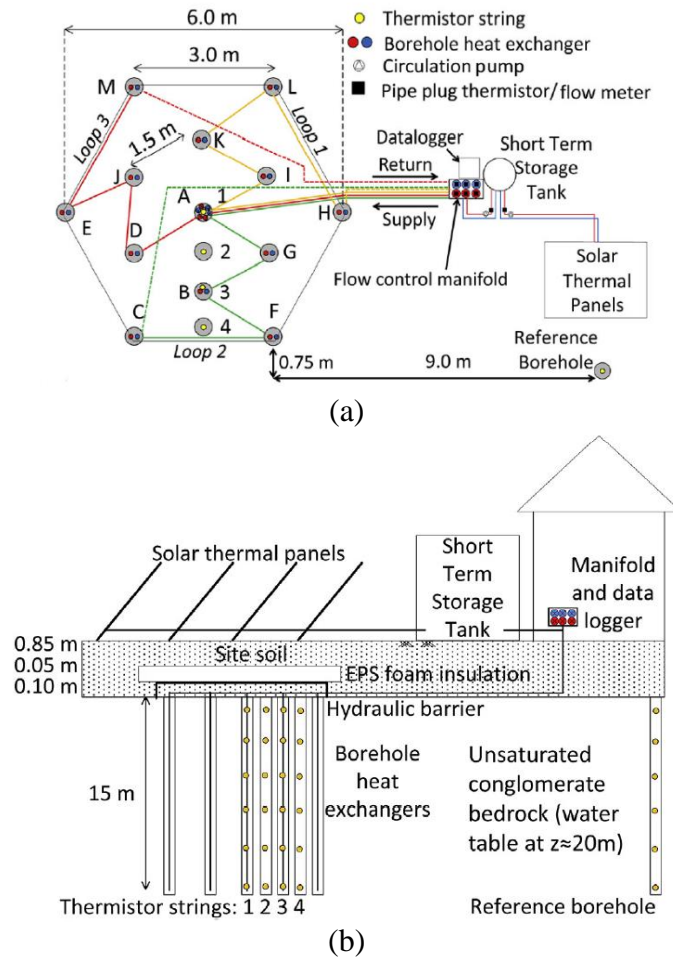


Figure 2.11. Experimental setup for the SBTES system in San Diego, California : (a) Plan view; (b) Elevation view (Başer and McCartney 2020)

Besides full-scale experimental studies, several lab-based experiments have been conducted to explore this issue. Beier et al. (2011) conducted a large laboratory sandbox experiment containing a single U-tube heat exchanger of 18 m long to provide reference data sets for researchers to test their borehole models. Similarly, Salim Shirazi and Bernier (2014) developed a small-scale experimental setup to study transient heat transfer in ground heat exchangers. Their experimental setup consists of a sand tank of 1.35 m high and 1.4 m in diameter. They compared the experimental and numerical results from the developed model for 73 hours of heat injection, which was followed by 5 days recovery period. They concluded that the agreement between experimental data numerical results indicates that accurate experimental data can be obtained with the apparatus. Moreover, for evaluating the underground thermal process of thermal injection/extraction, Giordano and his colleagues built a field-scale laboratory nearby Torino in Northern Italy using borehole thermal energy storage (Giordano et al. 2016). Zhang et al. (2020) also designed and constructed a lab-scale experimental system based on similitude laws to study the heat transfer behavior in underground soil. They proposed a transient 3D numerical model to calculate the temperature variation of full-scale GHE and performed model validation with the sandbox data set. Overall, they tried to provide more accurate reference data and foundation with less time-consuming for engineering application of underground energy storage systems, such as GSHP, ground energy pile, etc.

2.3.1 Numerical Studies

As a result of the complex transient 3D transport phenomena of ground heat exchanger (GHE), models and simulations of GHE serve as important tools in modern geothermal heat extraction technologies. Throughout the years, different numerical models of high and low complexities have been developed and utilized as a design tool for GHEs.

Signorelli et al. (2007) compared the results of analytical and 3-D numerical models to investigate the affecting phenomenon on the analysis of thermal response test data. They employed the 3-D finite-element (FE) code FRACTure developed by Kohl and Hopkirk (1995). Their study considered the effects of heterogeneous subsurface conditions and soil moisture migration. The result indicated that in contrast to the line-source model, the numerical analysis is more suitable for an accurate assessment of thermal response tests because the model is able to analyze heat injection rates as well as borehole geometry, something that the line-source model cannot do. They also found that soil moisture migration has a profound impact on the interpretation of thermal response test data when flow speeds are greatly higher than 10 cm/day. He et al. (2009) developed a dynamic three-dimensional numerical model using the finite volume method to assess the short timescale transient responses of a borehole heat exchanger (BHE) and the inter-tube flux between two U-shape pipe legs. The model included a single borehole with a diameter of 150 mm and a depth of 100 m. They found that the delayed response due to the circulation of fluid along the pipe loop is important at short time scales (10 min). Also, the result showed effective heat transfer rate may be considerable where there is an onset control system or where maximum thermal loads are critical. Lamarche et al. (2010) studied the borehole thermal resistance and developed 2D and 3D numerical models in COMSOL to evaluate and compare the different approaches and determine the resistances. They also proposed a new method to calculate the borehole resistances from in situ tests.

In order to reduce the computational time and effort, some researchers have simulated the GHE using 2D models. Austin III (1998) employed a 2D finite volume model to determine the thermal conductivity of the ground. Lazzari et al. (2010) examined the long-term performance of different borehole heat exchanger (BHE) fields configuration using 2D finite element models in

COMSOL software. For each BHE field geometry, they discussed heat load and thermal conductivity of the ground, illustrations of the minimum annual value of the fluid temperature for a period of 50 years. The authors found out that except for a single BHE, long-term performance is negatively affected for every case. Choi et al. (2013) studied the influence of groundwater flow on BHE arrays and used a 2D finite element method to simulate the heat transfer outside the borehole. For the case that a full description of the borehole geometry is required, a 3D model can be used which should deal with extreme geometrical aspect ratio problems.

Al-Khoury et al. (2005) and Al-Khoury and Bonnier (2006) proposed a new numerical technique to accommodate the extreme geometrical aspect ratios that make it necessary for an advanced and efficient numerical simulation to be employed in geothermal heating systems. Their model utilizes the combination of the finite element method with thermal resistance and capacity models, in which 1D finite element representation is used to model single and double U-pipe elements in a three-dimensional (3D) finite element model (Figure 2.12). A new expression for the thermal resistance between the GHE pipe and the grout is proposed to account for thermal interaction inside the borehole. Conduction heat transfer through the pipe wall and convective heat transfer between heat carrier fluid and pipe's inner wall is considered.

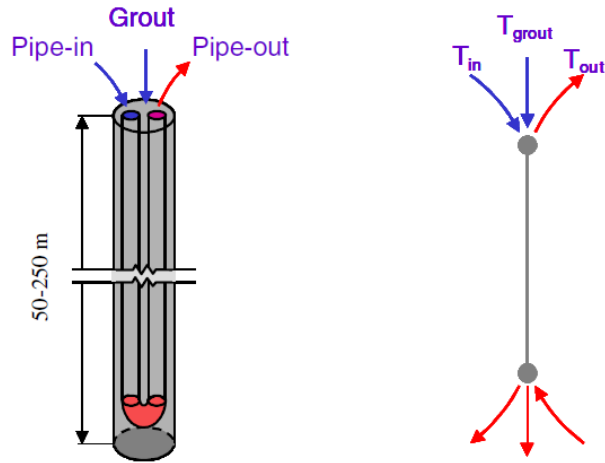


Figure 2.12. Schematic and finite element representation of a single U-shape heat pipe (Al-Khoury et al. 2005)

However, the application of the 1D pipe element causes some errors. First, in the actual physical process, the pipe-grout temperature coupling occurs at a distance of pipe outer radius from the pipe axis, while in 1D pipe element modeling, the outer pipe wall temperature is coupled to the temperature field of the grout domains at the pipe axis. Moreover, the 1D pipe element modeling does not consider the heat capacity of the pipes. To overcome the 1D pipe flow modeling errors, Ozudogru et al. (2014) developed a 3D numerical model in COMSOL and proposed the pseudo pipe approach. Pseudo pipes are two cylinders with a radius equal to the pipes outer radius and centered at the two legs axis, with a very high thermal conductivity in the radial direction and very low in the vertical direction. The heat capacity of the pipes is assigned to the pseudo pipe elements, and as a correction factor, the pipe volume ratio is used to estimate the density of the pseudo pipe elements. Han and Yu (2016) performed a series of sensitivity analyses and studied the impact of the geological, design, and operational factors on the performance of the vertical geothermal heat pump system, using a 3D finite element model in COMSOL. They utilized the 1D pipe element and simulated the steady-state and unsteady behavior of the GHE. They found

that ground thermal conductivity and circulation fluid flow rate are two critical factors significantly affecting the performance of the GHE. The result also showed that thermal energy could be extracted more efficiently, and higher COP can be achieved in an intermittent mode in comparison to the continuous operation mode. To study the heat transfer process in underground soil in the vicinity of GHE, Zhang et al. (2020) conducted a small-scale laboratory experiment and also developed a transient 3D finite element model in COMSOL in which a 1D pipe element was used to represent the GHE. They applied the pseudo pipe element approach as proposed by Ozudogru et al. (2014) to overcome the estimation errors of the 1D pipe element module. The developed model was compared with experimental data and a good match was achieved.

2.4 Economic Assessment of Bridge deck de-icing using geothermal heat pump system.

To promote the application of the geothermal heat pump de-icing system (GHDS) on a large scale, it is critical to study the financial feasibility of the system. In one of the available studies in the literature, Ghasemi-Fare et al. (2015) investigated the cost analysis of the geothermal de-icing system besides the feasibility assessment of this technology. However, their report did not explain the cost and economic feasibility of this technology and instead fully focused on the life cycle analysis (LCA) of de-icing salt. There are also multiple studies that discussed the project construction cost besides the system's performance, such as Spitler and Ramamoorthy (2000), Minsk (1999), and Boyd (2003); however, the life-cycle cost-benefit analysis (LCCBA) of the system has never studied. Moreover, a very plausible study on the economic viability of electrically conductive concrete (ECON) heated pavement systems (HPS) was studied by Anand et al. (2017). Although the research is focused on airport pavement heating using ECON, however, it successfully gives insight into the economic performance of the heating system and provided useful information regarding the economic analysis details and process.

CHAPTER 3: EXPERIMENTAL SETUP

3.1 Introduction

The selected construction site is located at the West Division Street (SH 180) and Green Oaks Boulevard Bridge (Dottie Lynn Parkway), Fort Worth, TX, as shown in Figure 3.1. The site is on an abandoned asphalt pavement which was used by TxDOT for storage of reclaimed asphalt pavement (RAP). The test site is in Tarrant County, which has a humid subtropical climate characterized by moderate rainfall, mild temperatures, and abundant sunshine. The days are hot in the summer, but temperatures exceeding 100 degrees are frequent only during periods when the rainfall is below normal. The hot summer days are moderated somewhat by the dryness of the air and by a steady south wind. The winters generally are mild except for several snowstorms in recent years.



Figure 3.1. Photo of the construction site located in Fort Worth, TX

3.2 Overview

Figure 3.2 presents the 3D model of the mockup bridge and the geothermal heating system. It illustrates the design of the heated zone on the bridge deck. The dimensions of the heated area are $4.88 \text{ m} \times 11.43 \text{ m}$; however, only a $2.44 \text{ m} \times 7.32 \text{ m}$ section was assigned for the application of the external heating system. The mock-up bridge deck consists of three zones: an externally heated zone, an internally heated zone, and a control zone. It utilizes both the traditional type of GHDS, which uses a hydronic pipe embedded in the concrete slab and the newly developed method, which utilizes an external hydronic pipe that is attached to the bottom surface of the bridge deck and covered in a layer of insulation foam. In addition to the external heating system, which is the focus of this study, the internal heating system was also designed in the mock-up bridge deck for comparison purposes. The hydronic loops at the bridge deck consisted of 1.27 cm internal diameter polyethylene (PEX) pipes with a 20.3 cm centerline spacing. Moreover, the end section of the bridge deck was considered as a control area with no heating (Figure 3.3).

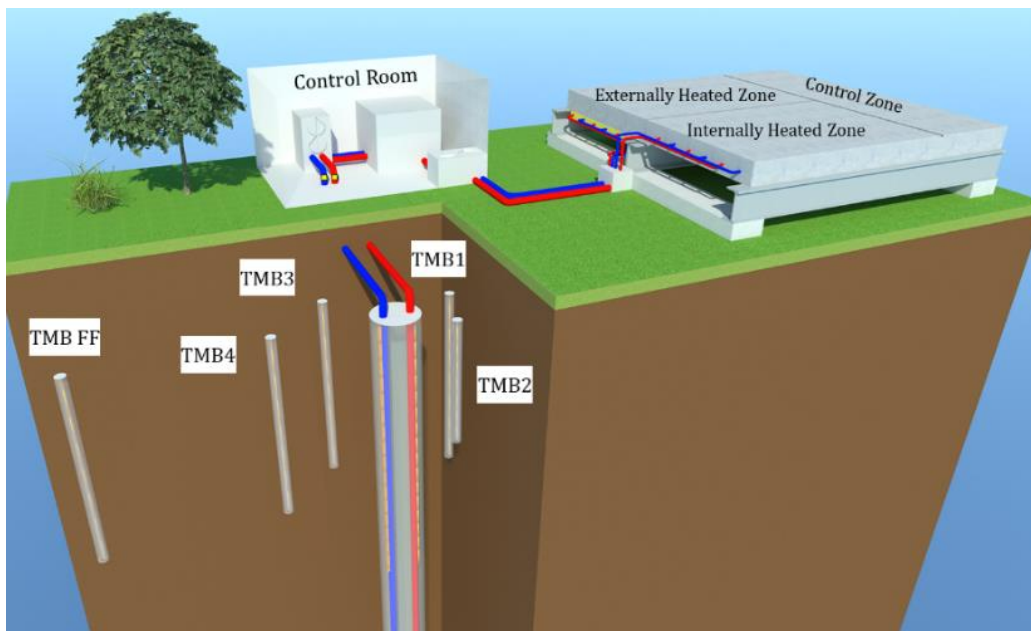


Figure 3.2. 3D model of the experimental setup

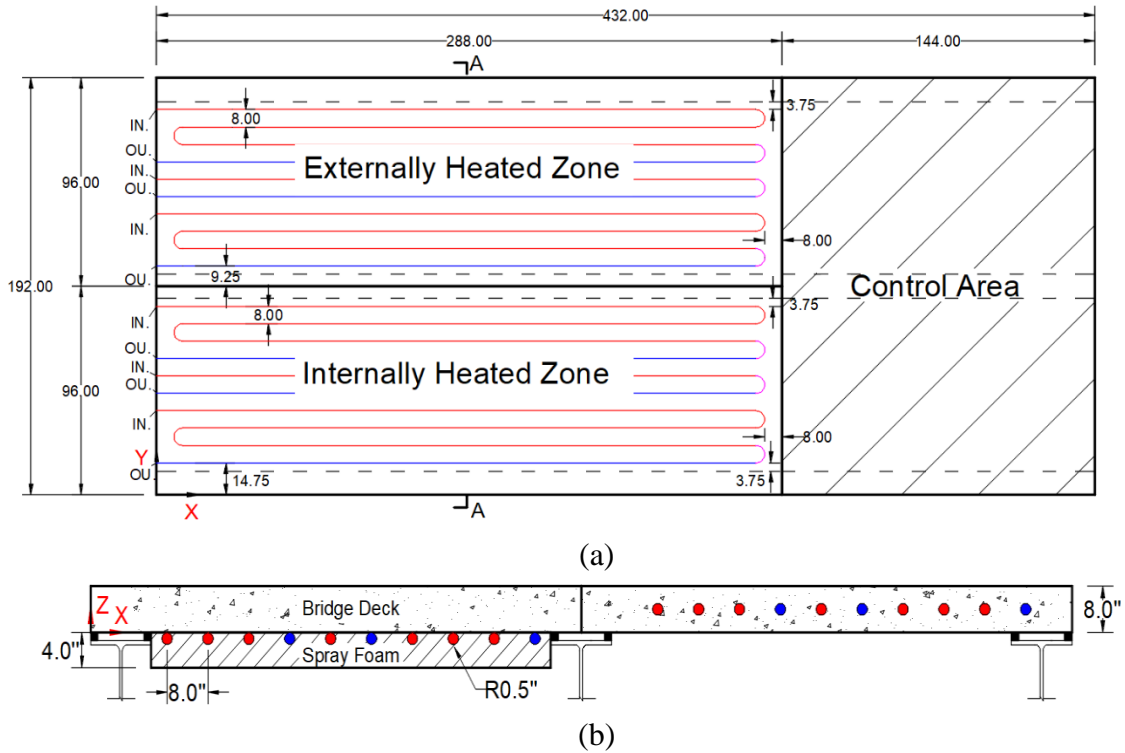


Figure 3.3. (a) Layout of the heated bridge deck; (b) A-A cross-section view of the bridge deck, left: external heating zone, and right: internal heating zone (unit: in.)

Also, the experimental field setup consists of a 3 ton heat pump, 2 flow centers (including 4 circulating pumps), an expansion tank, and a geothermal borehole of 132.5 m (from ground level) deep and 14.6 cm diameter, which hosted a single U-tube heat exchanger loops made of high-density polyethylene (HDPE) pipe with a standard dimension ratio (SDR) of 11 and 3.45 cm inside diameter. Besides 5-10 cm diameter temperature monitoring boreholes (TMBs), which were equipped with thermistor strings and radially scattered around the geothermal borehole, were drilled to investigate the temperature distribution in the soil and at different depths.

The system operates in two modes: full-load operation and bypass operation. As shown in Figure 3.4(a), the control valves at the heat pump are closed and the flow goes through the heat pump in the full-load operation mode. The geothermal heat pump is on in the full load operation

mode, which provides more heat to the bridge deck surface for snow/ice melting. In bypass mode, as shown in Figure 3.4(b), the geothermal heat pump is off, and the heat carrier fluid directly circulates through the bypass, into the hydronic loops on the bridge site and back to the ground loop. Two heated zones, i.e., the internally heated, and externally heated zones, are operated independently by a control valve. In all the tests, the goal is to melt the ice on the bridge deck surface.

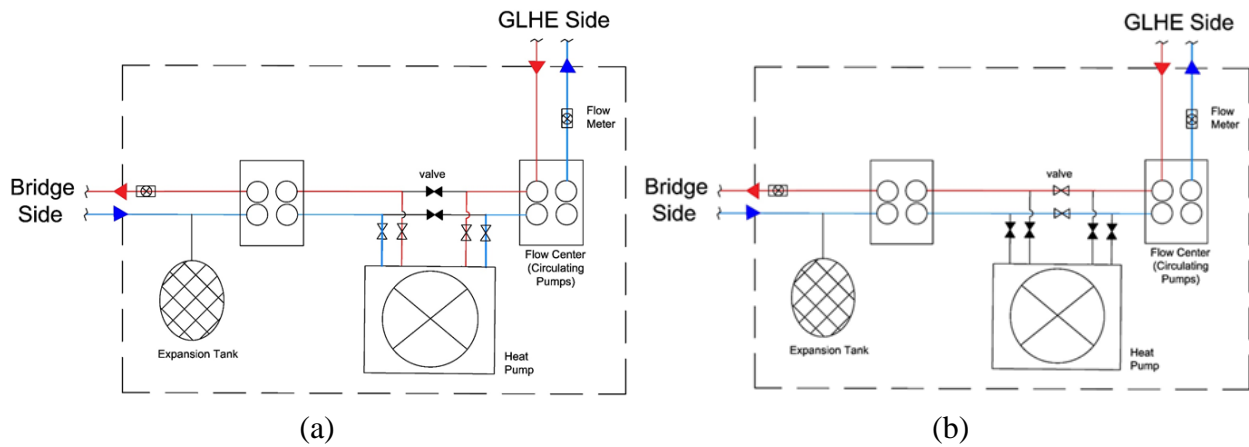


Figure 3.4. System operation modes: (a) full load operation mode; (b) bypass operation mode

3.3 Instrumentation and Data Acquisition System (DAQ)

The geothermal system and the bridge deck were instrumented with temperature sensors to monitor the system's components and the bridge deck's thermal response. Table 3.1 lists the type and number of sensors used in each section. Also, Table 3.2 lists the instruments used in this project and shows their measurement accuracy. The data acquisition system of this study consists of three multiplexers and two data loggers (Figure 3.5). The Type-T thermocouples were connected to the thermocouple multiplexer and a data logger. The thermistors and strings were connected to two multiplexers and another data logger through a bridge completion circuit. All the sensors were calibrated, and temperature outputs were recorded in the data logger.

Table 3.1. Type and quantity of the thermal sensors used in each area






Instrument	Externally Heated Zone	Internally Heated Zone	Subsurface	
Thermal wire cable (Pile Dynamics)	2	1	1	
Type-T Thermocouple (National Instrument)	22	3	2	
Thermistor probe (GEOKON)	4	2	-	
Thermistor probe w/PVC house (GEOKON)	2	3	-	
Thermistor string (GEOKON)	-	-	6	

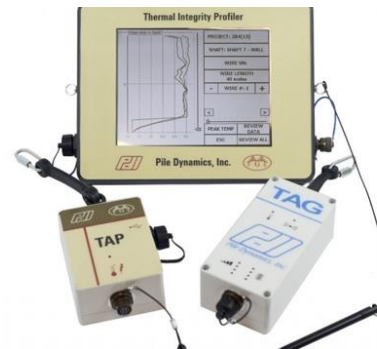
Table 3.2 Instrumentation list

Instrument	Manufacturer	Quantity	Accuracy
Thermal wire cable	Pile Dynamics (PDI)	4	$\pm 0.2^{\circ}\text{C}$
Type-T Thermocouple	National Instrument (NI)	27	$\pm 0.5^{\circ}\text{C}$
Thermistor Probe	GEOKON	6	$\pm 0.2^{\circ}\text{C}$
Thermistor Probe- PVC house	GEOKON	5	$\pm 0.2^{\circ}\text{C}$
Thermistor string	GEOKON	6	$\pm 0.2^{\circ}\text{C}$
Flow Meter	Sotera	2	$\pm 1\%$
Power Logger	Fluke	1	*Voltage: $\pm(0.2\% + 0.01\%)$ *Current: $\pm(0.2\% + 0.02\%)$

* Intrinsic Accuracy at Reference Conditions (% of Reading + % of Range)



(a)



(b)



(c)



(d)

Figure 3.5. Data loggers and multiplexers used in the data acquisition system: (a) 25-channel solid-state thermocouple multiplexer; (b) Pile Dynamics TAP; (c) CR 1000X data logger; (d) 32-channel relay multiplexer

3.2 Construction of the Geothermal Mock-Up Bridge

The construction process of the prototype of the external geothermal bridge deck de-icing system includes different stages:

- **Stage 1:** Construction of the mock-up bridge deck
- **Stage 2:** Installation of the hydronic heating loops
- **Stage 3:** Bridge deck instrumentation
- **Stage 4:** Control room and geothermal system
- **Stage 5:** Subsurface soil and underground loop instrumentation
- **Stage 6:** Borehole drilling and underground loop installation

The model bridge was constructed during February and March of 2018. TxDOT Fort Worth district has a stock of salvage I-beams and low-profile concrete traffic barriers (LPCTBs) at the Little Road Yard, Arlington. With these materials along with the purchased PCP panels, the research team built a mock-up bridge deck to implement the first full-scale prototype of the external geothermal heating system. The bridge consists of prestressed concrete panels (PCPs) and cast-in-place (CIP) concrete slabs (PCP-CIP) bridge deck of 12 - standard 2.43 m × 1.82 m × 10.16 cm PCP panels. After the materials were transported to the site, the concrete traffic barriers (CTBs) were placed in their pre-specified locations, the I-beams were affixed to them, and the PCP panels were put atop the beams. Figure 3.6 shows the construction process of the mock-up bridge deck setup.

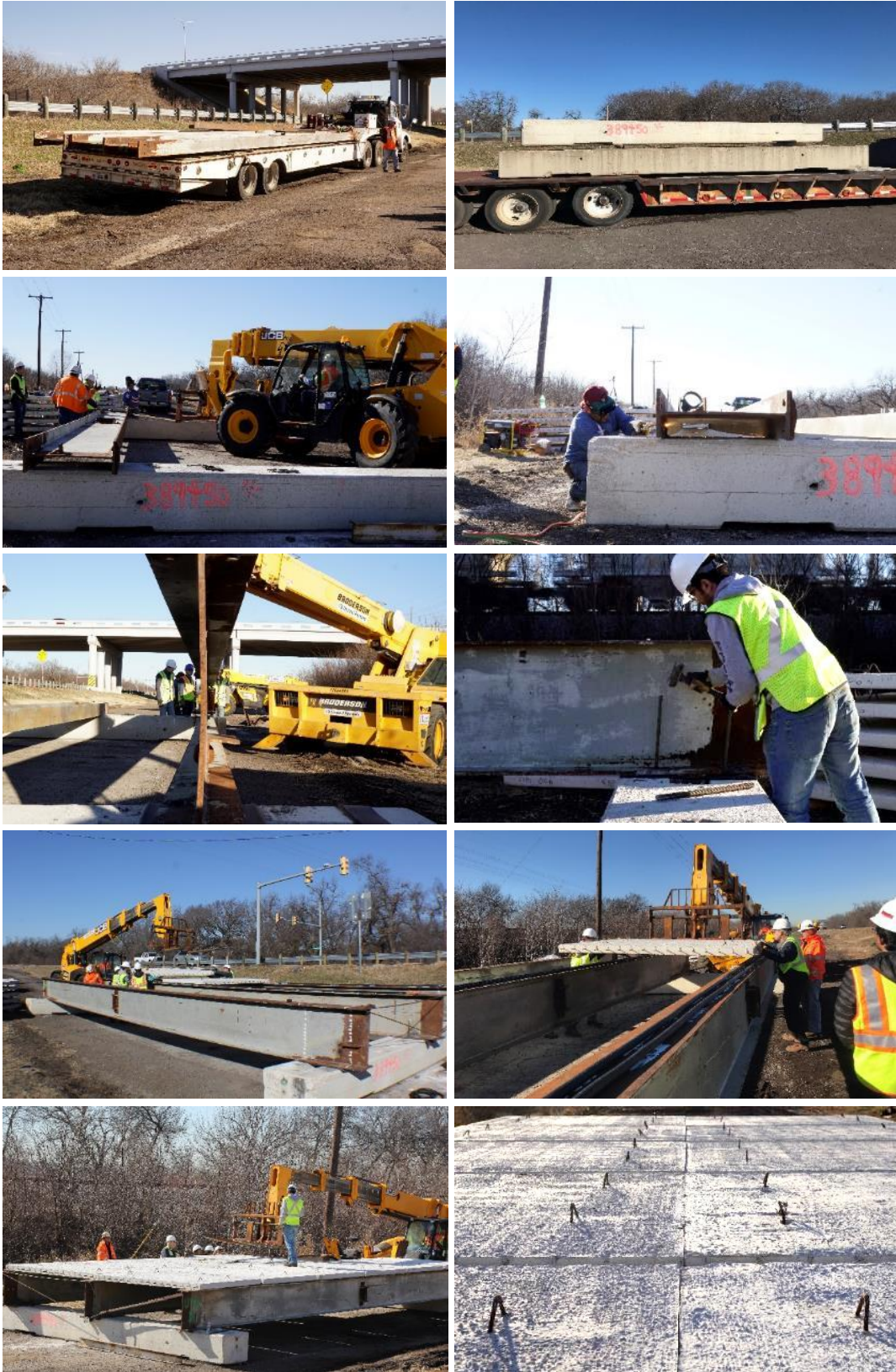


Figure 3.6. Construction process of stage 1: Bridge deck set-up

During stage 2 of the construction, the longitudinal and transverse #4 rebars were placed on top of the PCP panels, with a maximum of 22.8 cm between them, using rebar chairs to keep them at the appropriate depth. The installation of the internal heating loops followed the conventional method. They were attached to the rebar and embedded in the top 10.16 cm of the cast-in-place concrete deck, using the TxDOT Class S concrete mix, which is typically used for bridge decks in Texas. Figure 3.7 shows the installation of the internal hydronic heating loops and concrete casting during stage 2 of the construction process.

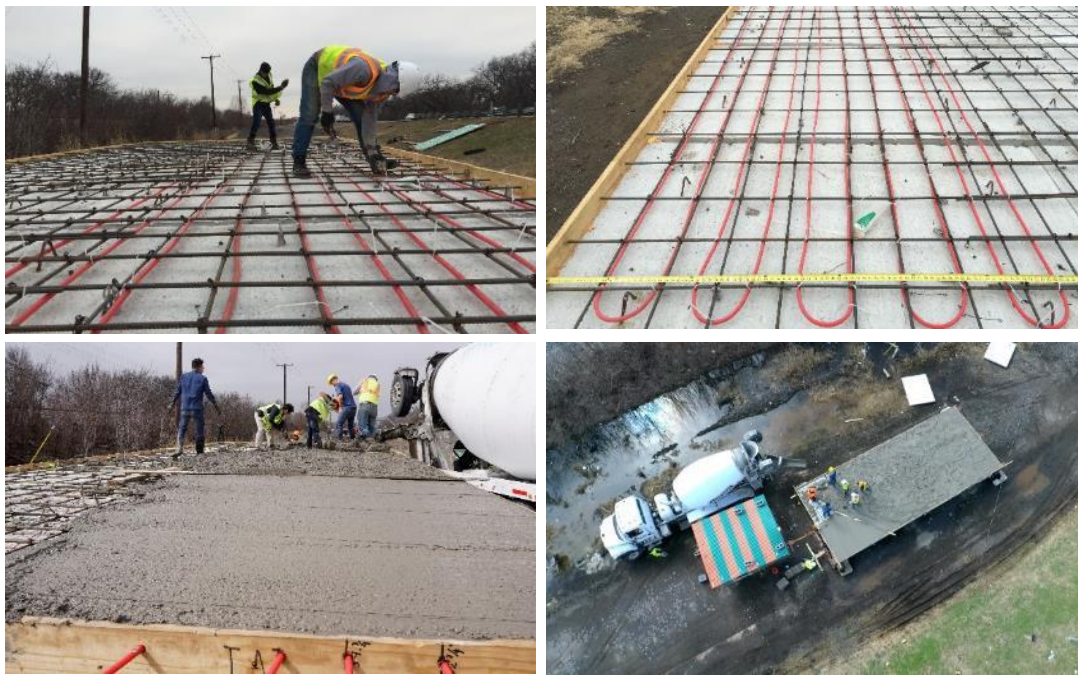


Figure 3.7. The construction process of stage 2: Internal hydronic loop and concrete casting

After the bridge deck was completed, the external heating pipes were attached to the bottom surface of the externally heated zone using two-hole straps, then the pipes were covered with cement paste to increase the thermal contact between the pipes and the concrete. Finally, thermal insulation foam was applied to the entire surface to prevent heat loss from the bottom, and valves

were installed to control the operation mode and the heated section of the bridge deck. Figure 3.8 shows the installation of the external hydronic heating loops and applying the insulation foam to the bottom surface of the externally heated zone during stage 2 of the construction.



Figure 3.8. The construction process of stage 2: External hydronic loop and applying insulation foam.

Figure 3.9 shows the inlet and outlet pipes of the externally and internally heated zone. First, PEX pipes were connected to the main HDPE pipe and then pulled into the control room to be connected to the heat pump. Several valves were also installed to control the flow direction toward the heated zone.



Figure 3.9. Hydronic loops inlet and outlet pipes

Stage 3 of the construction process was the instrumentation of the mock-up bridge deck to monitor the hydronic heating system's performance and thermal response of the bridge deck (Figure 3.10). Bridge deck instrumentation includes a total of 3 thermal strings (Pile Dynamics), 6 thermistors with bead only (GEOKON), 5 thermistors with PVC house (GEOKON), and 25 thermocouples were installed throughout the mock-up bridge deck. All the sensors are calibrated internally by the data logger. The locations of the sensors are different between external heating and internal heating. Figures 3.11 and 3.12 illustrate the sensor locations on different planes on the externally and internally heated zone, respectively.



Figure 3.10. Stage 3 of the fieldwork: Bridge deck instrumentation

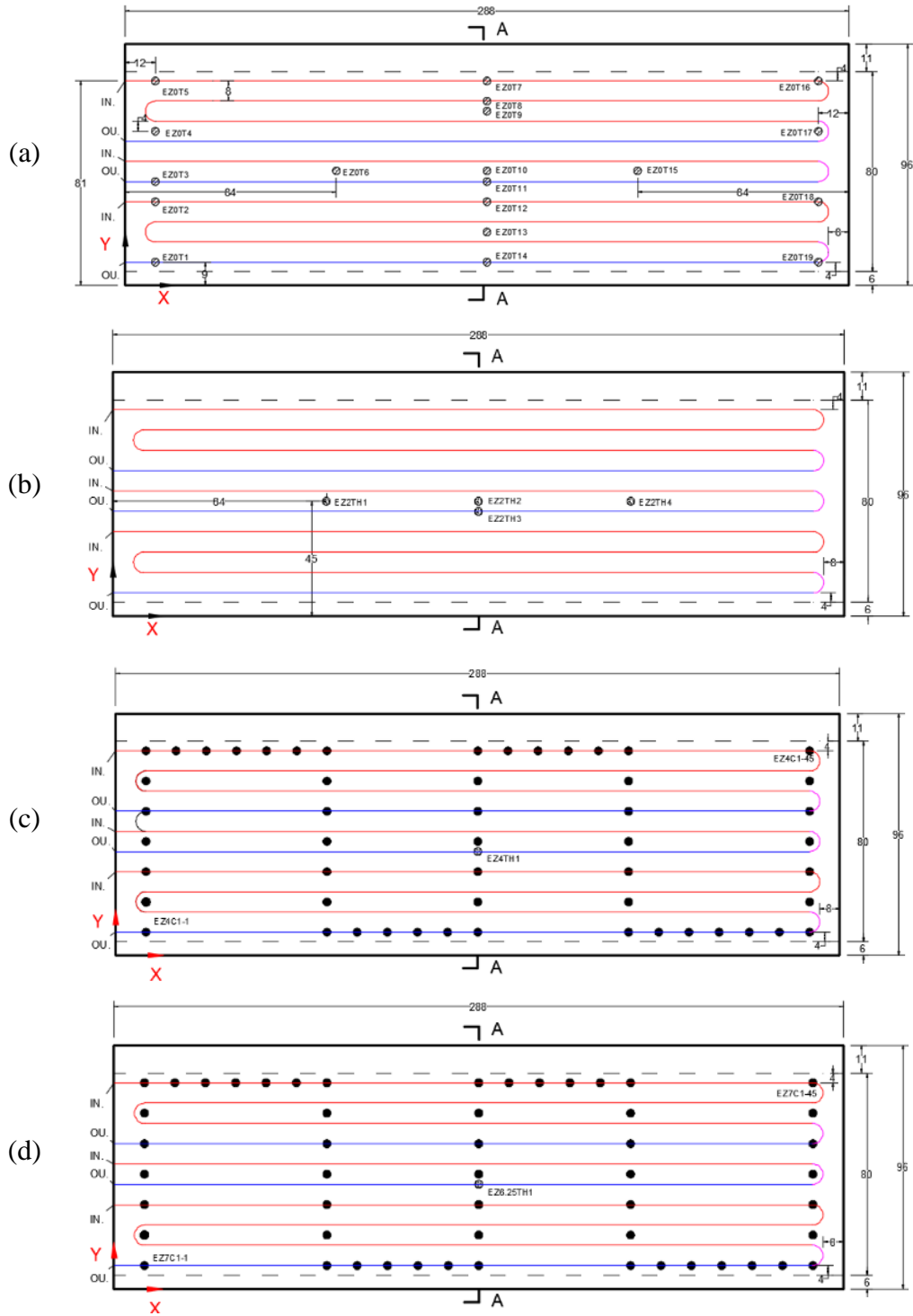


Figure 3.11. Plan view of sensor locations in the externally heated zone (Unit: in.): (a) $Z=0$; (b) $Z=5$ cm; (c) $Z=10$ cm; (d) 17.5 cm.

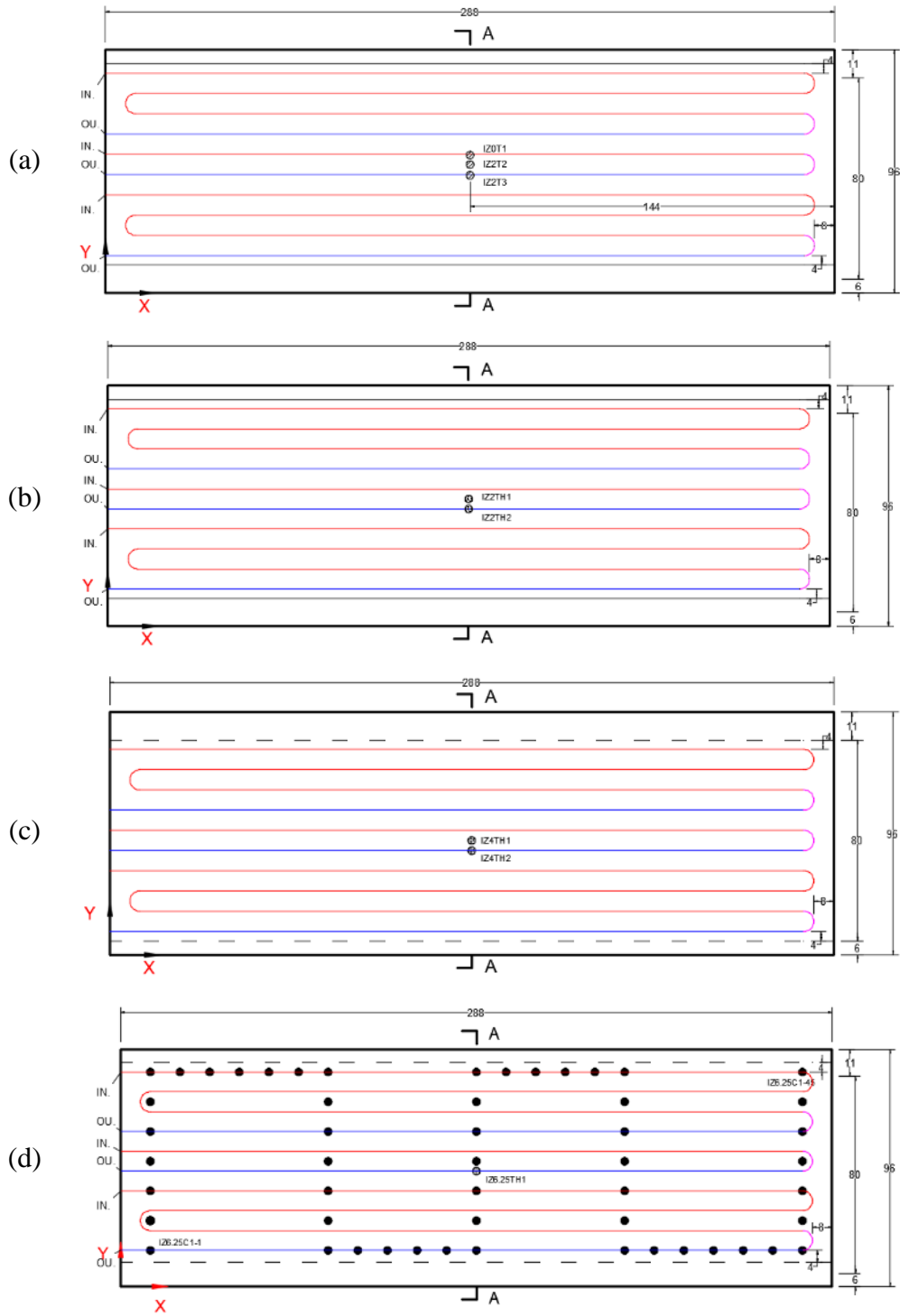


Figure 3.12. Plan view of sensor locations in the internally heated zone (Unit: in.): (a) $Z=0$; (b) $Z=5$ cm; (c) $Z=10$ cm; (d) 17.5 cm.

Stage 4 of the fieldwork was to build a control room to host the system's main components, which includes one heat pump, two flow centers, four circulating pumps, and one expansion tank. It also hosts the data acquisition system, including the data loggers and multiplexers (Figure 3.5). Figure 3.13 shows an overview of the control room and its components. Two sets of thermocouples were attached to the inlet and outlet pipes in the control room to monitor the inlet and outlet temperature of the heat carrier fluid on the ground and bridge deck side (Figure 3.14). In addition, a bypass was provided so that the system could operate in two modes: full-load and bypass. Flow meters were also installed to measure the flow rate of each side. Finally, the pipes were connected, and the system was flushed with a 20% propylene glycol solution and tested for any possible leakage.

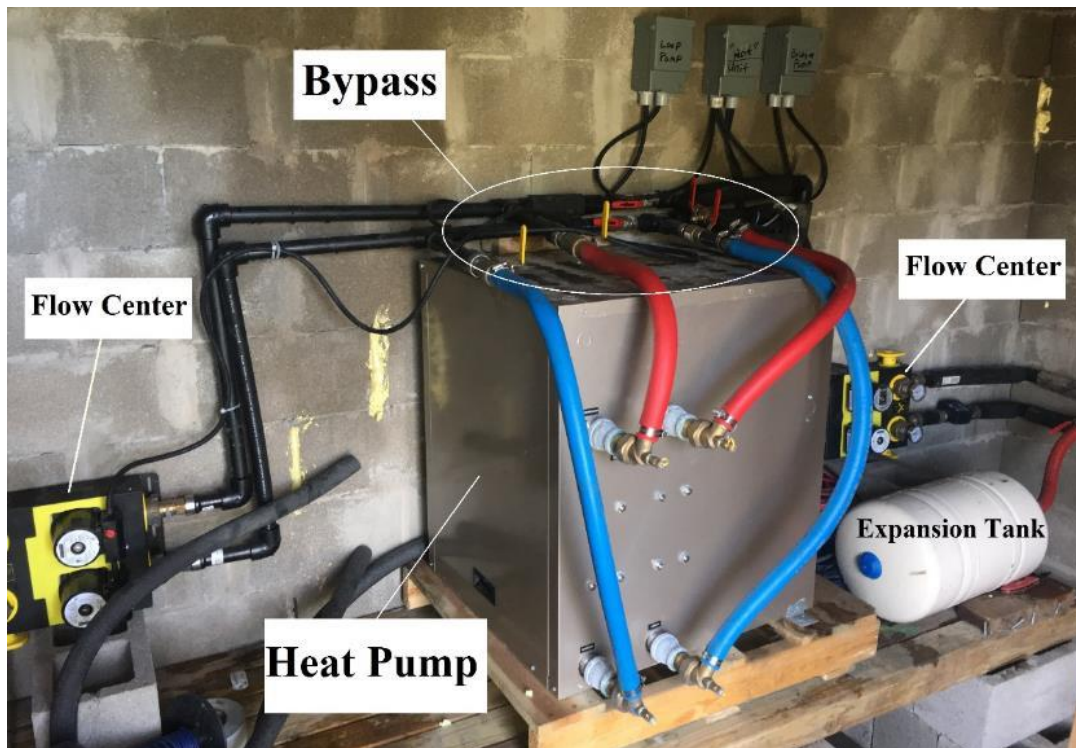


Figure 3.13. Overview of the control room

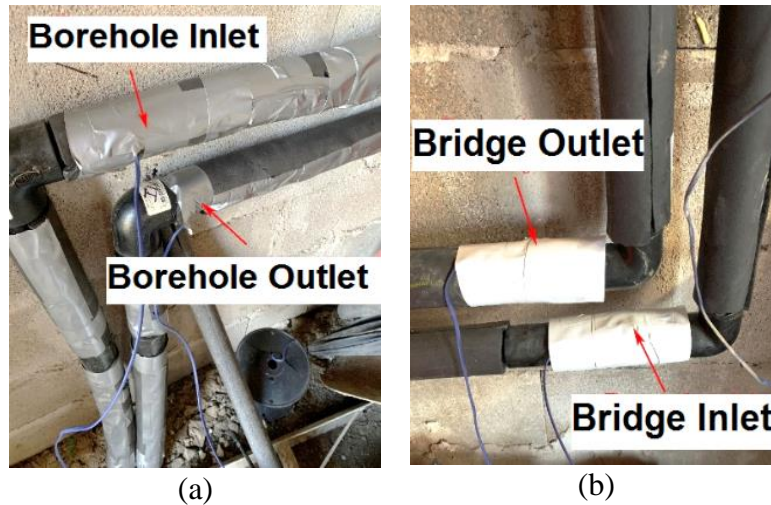


Figure 3.14. Inlet/outlet temperature sensors: (a) GHE; (b) Bridge deck hydronic loops

A very simple control system was used to control the system's operation. A simple thermostat was wired to the heat pump to control the operation of the heat pump (Figure 3.15). The thermostat was controlled by an external thermistor which was attached to the inlet pipe to the bridge deck to measure the inlet fluid temperature. This sensor controls the supplied water temperature to the bridge deck which gives this opportunity to the operator to decide the supplied heating load according to the forecasted weather. However, it should be noted that the whole system, including the four circulating pumps, was turned on/off manually and pumps were on during the entire test.

Stage 5 and 6 of the construction processes involved one geothermal borehole and five temperature-monitoring boreholes that were drilled and equipped with temperature sensors to monitor the temperature at various distances from the geothermal borehole. Boreholes were drilled in the locations specified by the design of the GHE. A 14.6 cm diameter geothermal borehole was drilled 132.5 m deep (from ground level), then the previously prepared and the instrumented ground loop was inserted in the borehole. Eventually, the borehole was grouted and allowed to settle. To facilitate the installation of the temperature sensors, which were in the form of thermistor

string, they were attached to a PEX pipe which was filled with rebars. After they were installed, the monitoring boreholes were grouted with the same material used for the geothermal borehole.

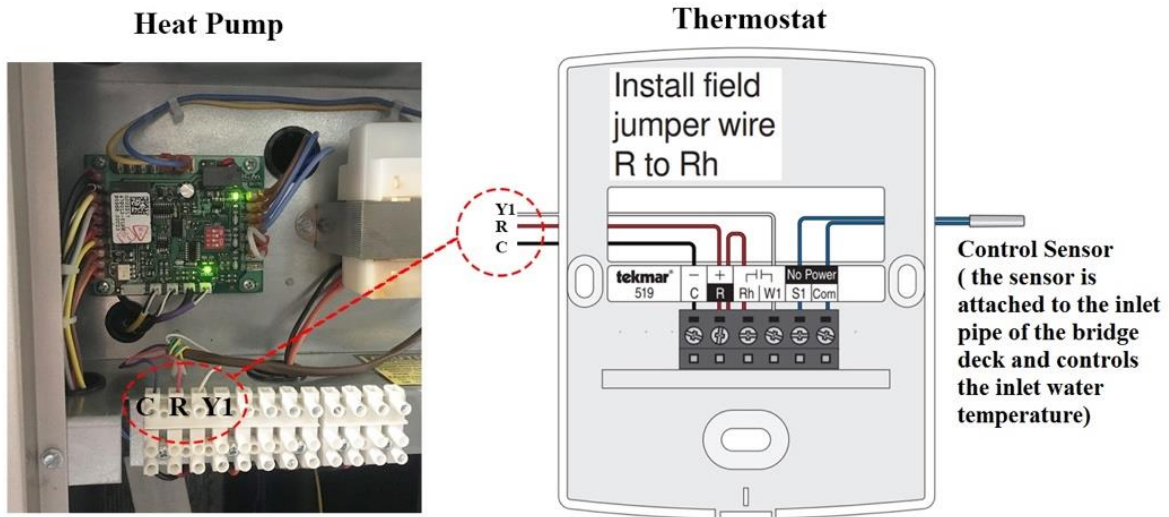


Figure 3.15. The wiring diagram of the heat pump and thermostat



Figure 3.16. Subsurface soil and underground loop instrumentation

A 1.5 m deep trench was excavated to lay the groundwork for connecting the GHE to the control room. Header pipes of 3.17 cm diameter were connected to the GHE using socket fusion coupling, and the sensor's cable was laid down on the bottom of the trench. The trench was then backfilled with the excavated soil. The horizontal header pipes were bundled together during the backfill process. The embedment depth of the HDPE pipes in the trench varied due to the bending of the pipes near the intersections of elevation changes. Due to the fragility of the sensor cables, the backfilling operation was performed with extreme caution. Figures 3.16 and 3.17 illustrate the fieldwork during stages 5 and 6 of construction.

The subsurface monitoring system consists of five 10 cm-diameter temperature monitoring boreholes (TMBs), which are equipped with thermistor strings and radially scattered around the geothermal borehole to investigate the temperature distribution in the soil and at different depths. Also, two thermistor strings were attached to the outer surface of the GHE legs to monitor the pipe and grout interface temperature variation. Table 3.3 shows the details of the radial distance to the geothermal borehole and node depth for each thermistor string. An additional thermistor string was also attached to the header pipe in the trench to investigate the soil-pipe interface temperature variation in the trench. Figure 3.18 illustrates the schematic of the thermistor string attached to the header pipe in the trench.

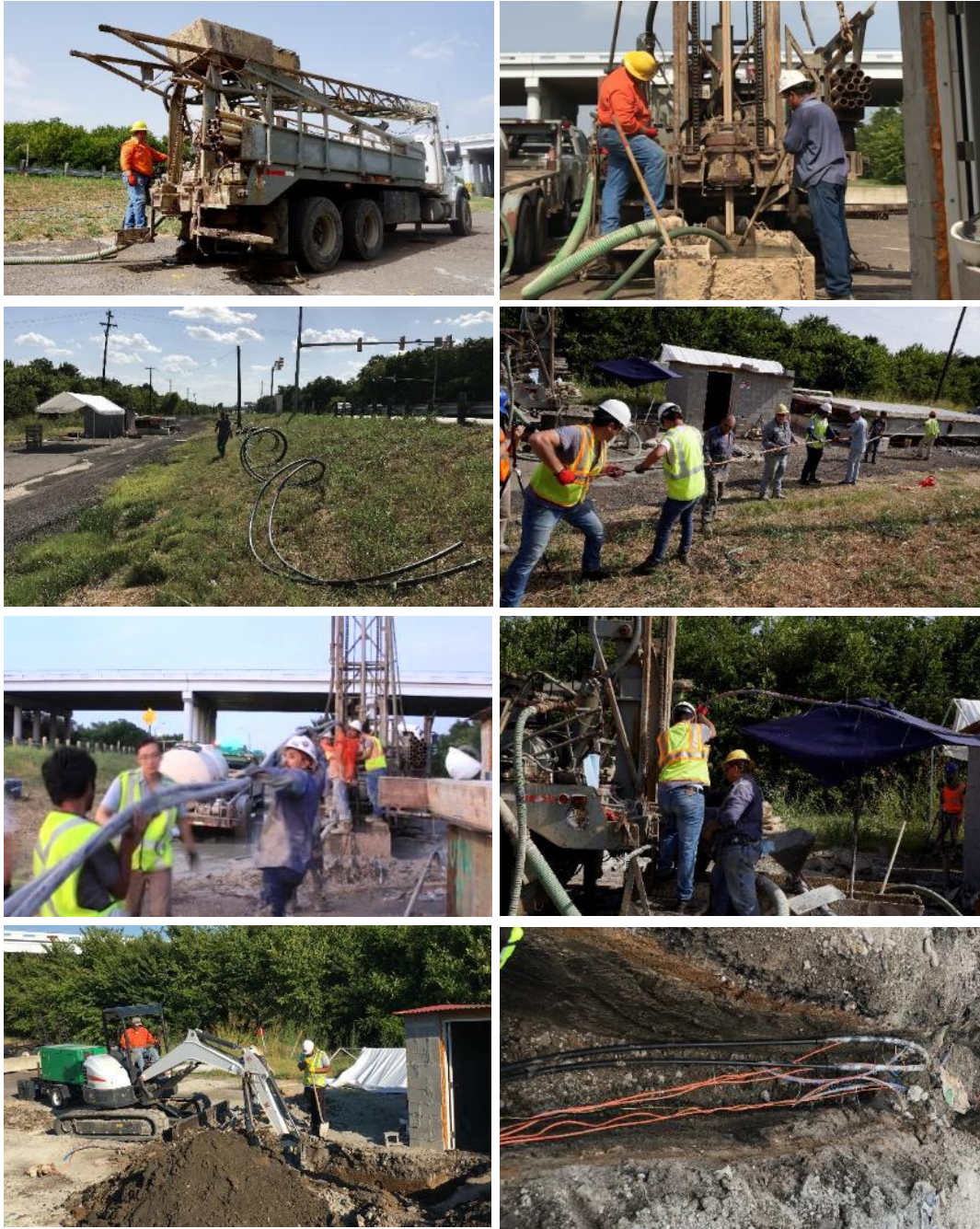


Figure 3.17. Stage 6 of construction activities: Borehole drilling and underground loop installation

Table 3.3. Details of GHE and TMBs thermistor string

Thermistor string	Inlet pipe	Outlet pipe	TMB 1	TMB 2	TMB 3	TMB 4	TMB FF
Radial Distance (m)	~0	~0	0.45	0.6	0.9	1.5	7.5
Sensor node	Depth from the surface (m)						
#1	0.8*	0.8*	0.6	0.6 m : 0.3 m : 14 m	0.9*	0.9	1.2
#2	1.1*	0.8*	1.8		1.5	1.8	4.0
#3	1.7*	1.1*	3.4		3.0	3.4	10.1
#4	2.3	2.3	6.4		6.1	6.4	19.2
#5	3.2	3.8	9.4*		9.1	9.4	n/a
#6	4.7*	5.3*	14.0		13.7	14.0	n/a
#7	6.2	6.9	18.6*		18.3*	18.6*	n/a
#8	7.8*	8.4	n/a		n/a	n/a	n/a
#9	9.3*	13.0*	n/a		n/a	n/a	n/a
#10	13.9*	17.5*	n/a		n/a	n/a	n/a
#11	18.4*	29.7	n/a		n/a	n/a	n/a
#12	30.6	n/a	n/a		n/a	n/a	n/a

* The sensor has malfunctioned.

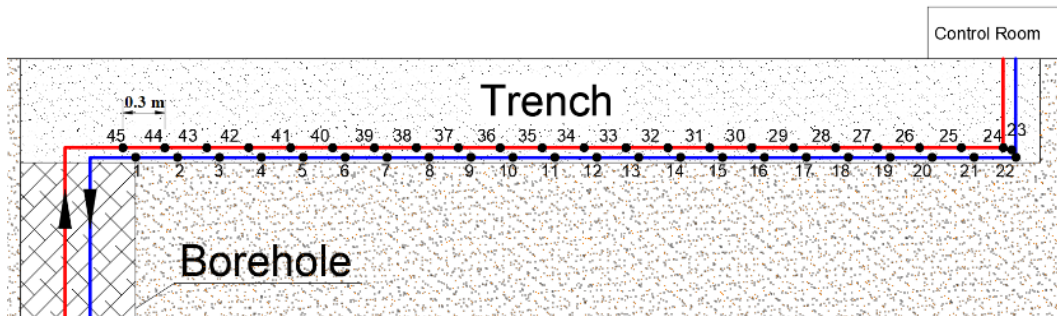


Figure 3.18. Header pipes' thermistor string

CHAPTER 4: A NOVEL FULL-SCALE EXTERNAL GEOTHERMAL HEATING SYSTEM FOR BRIDGE DECK DE-ICING

4.1 Abstract

The utilization of geothermal energy for melting snow and ice on bridge decks has been shown to be effective. However, the existing geothermal heating systems work through hydronic loops embedded inside the bridge deck and therefore are only applicable to new bridges. A new external geothermal heating design for bridge de-icing has been explored in concept and tests in the laboratory, showing great implementation potential. This study presents the design and implementation procedure of a novel external geothermal heating system on a full-scale bridge deck for de-icing operations in field conditions for the first time. It tests and analyzes the system's heating performance and the bridge deck's thermal response under several winter events. The details and information pertaining to the design and construction of the hydronic loops, a ground loop heat exchanger (GLHE) monitoring system, are presented and can be pivotal for the designers of similar projects. The test results showed that the system was successful in de-icing the bridge deck and maintaining the bridge deck surface temperature above freezing in the event with a minimum ambient temperature of $-6.2\text{ }^{\circ}\text{C}$. The de-icing system requires about 7-8 hours of pre-heating to reach its maximum performance; however, less time is required during mild events. Moreover, this research investigated the performance of the system, and the experimental results showed an average system coefficient of performance (COP) of approximately 4.6 and a heating efficiency of about 55 %.

4.2 Introduction

Severe winter weather conditions adversely affect transportation networks and endanger the safety of motorists. Bridges, key transportation network elements, are the first sections of the roads to experience freezing temperatures, due to the exposed bottom surfaces; roads are less susceptible to freezing because of the insulated bottom surface provided by the ground. De-icing salts traditionally have been used to prevent snow/ice accumulation on bridge decks, and while its application is effective, it can induce several problems, such as a phenomenon known as “chloride attack.” Corrosion of steel reinforcement is the net outcome of the chloride attack, which eventually causes serious durability problems for the concrete pavement and structures (Baboian 1992; Granata and Hartt 2009; White et al. 2005; Yunovich et al. 2003). The application of de-icing salt also provokes other problems, such as negative environmental impacts (Fischel 2001). Thus, it is essential to implement a sustainable method that prevents the corrosion of bridge decks, and enhances safety and traffic flow, while leaving minimal environmental footprints.

The heated bridge technology, utilized with geothermal energy, is a potential solution to snow-covered and icy bridge decks. Geothermal energy is a reliable source of energy and a viable alternative to fossil fuel. While the ground surface temperature fluctuates with weather conditions, the temperature below a certain depth is relatively constant (Brandl 2006). This thermal gradient provides an opportunity to harvest shallow geothermal energy. Several methods of extraction and application of shallow geothermal energy are available. Boreholes and geostructures, such as foundations, diaphragm walls, tunnel liners, and anchors, can be used to draw energy from the earth and be utilized for various heating and cooling purposes (Barla et al. 2016; Binod et al. 2012; Mimouni et al. 2014; Nam and Chae 2014; Sterpi et al. 2018a; c; Zhang et al. 2013). The application of geothermal energy that has been developed in recent years is the use of a geothermal

heat pump de-icing system (GHDS) to melt snow and de-ice pavement and bridge decks. In this system, the heat carrier fluid circulates between the ground loop heat exchangers (GLHE) and the hydronic loops installed in the bridge deck or pavement, and the heat pump helps the fluid reach the ideal temperature for melting snow and ice on the surface. However, although there are other available technologies for bridge deck and pavement heating, such as heat-pipe (Chi et al. 2019; Nydahl et al. 1987) and electrical (Malakooti et al. 2020; Zhao et al. 2010), the ground-coupled hydronic heating system has shown a higher potential.

Lund and Minsk reported multiple applications of the geothermal heat pump de-icing system for bridge decks in the U.S. (Lund 1999; Minsk 1999). Their studies focused on the design, construction, and cost data, but provided less information on the performance of the system during snow/ice events. Although their projects were among the first that employed this technology, positive control of snow and ice were observed. Spitler and Ramamoorthy investigated a bridge deck de-icing systems that used a ground source heat pump system (GSHP) (Spitler and Ramamoorthy 2000) and demonstrated the simulation methodology and design of the system. In another study, they investigated the numerical model and snow melting process occurring on the surface and described the model development (Liu et al. 2007). The model was successful in predicting the transient surface conditions, including the temperatures and extent of snow cover (Liu et al. 2007), and was experimentally validated and successfully tested (Liu et al. 2007). Balbay and Esen were the first to study the practicality of using a ground source heat pump system for snow melting on pavements and bridge decks in Turkey (Balbay et al. 2010). Their research demonstrated the performance of the system and provided valuable information regarding slab temperature and coefficient of performance (COP). Ghasemi-Fare et al. examined the feasibility of the geothermal de-icing system and proved the feasibility of this technology through numerical

and experimental investigation (Ghasemi-Fare et al. 2015). They employed proof-of-concept testing to assess the operational basis and key design parameters. Similar to the bridge deck application, the geothermal heat pump de-icing system has also been effective in heating road units (Mirzanimadi et al. 2020; Zhao et al. 2020). In an attempt to reduce the installation cost of geothermal bridge snow melting system, the feasibility of employing energy piles for bridge deck snow melting system has investigated in which it is found the system performance is dependent upon the geological and snow conditions of a particular region, as well as the design snow removal criteria, and usually is applicable only to regions with high underground temperature (Han and Yu 2018, 2017; Liu et al. 2019). A more recent study showed that the application of a geothermal heat pump de-icing system could be economically viable for bridges that have a minimum daily traffic volume of 7000 vehicles, while a benefit-cost ratio (BCR) of 2.6 can be achieved for a daily traffic volume of 24000 vehicles (Habibzadeh-Bigdarvish et al. 2019). All of the aforementioned studies utilized the typical form of geothermal heat pump de-icing system in which hydronic loops are embedded in the concrete slab, which is unfortunately limited to new bridges. A new method has been developed, however, that employs an external hydronic pipe that is attached to the bottom surface of the slab and encapsulated in a layer of insulation materials, such as insulation foam (Yu et al. 2019).

The Texas Department of Transportation (TxDOT) has been investigating the implementation of this system on Texas bridges over the past few years (Yu et al. 2017), to develop a system that can be used for both existing and to be constructed bridges. Li et al. conducted preliminary research on externally heated geothermal bridge decks, using numerical analysis, and showed that the proposed externally heated geothermal bridge deck can successfully de-ice bridge decks in mild winter weather conditions (Li et al. 2018). The same research group conducted

another study on the feasibility of externally heated geothermal bridge decks and tested the system performance of a laboratory-scale bridge deck in the environmental chamber. A series of heating tests were performed under various heating conditions to assess the efficiency of the heating performance and heat transfer of the external heating design (Yu et al. 2019). Moreover, a comprehensive analysis of the heat transfer mechanism and energy balance of the externally heated deck was conducted using a 3D numerical model, which was calibrated using the experimental results obtained in the environmental chamber (Li et al. 2020). However, the previous experimental studies on the externally heated bridge deck are limited to the laboratory-scale test on the 1.8 m × 1.2 m concrete slab with 10.16 cm thickness while the bridge deck thickness is usually double in thickness. The laboratory tests were limited to the room temperature as low as 4.4 °C, and no test under actual freezing winter weather has been performed. Moreover, the laboratory tests only focused on the hydronic heating loops and heating performance of the bridge deck; they never studied the overall system performance of the externally heated bridge deck as they didn't employ any geothermal systems in the test setup. Therefore, the implementation of the novel externally heated geothermal heating system on a full-scale bridge deck is needed to comprehensively investigate the performance of the proposed system under operational conditions and in real winter events.

The primary objective of the current study is to test and analyze the full-scale external geothermal heating system performance in de-icing the bridge deck surface under actual winter weather conditions. Also, it demonstrates the design, construction, and implementation procedure of the first full-scale external geothermal heating system for bridge deck de-icing. The remainder of this paper discusses the de-icing system performance and the thermal response of the bridge deck during cold winter events. The heating efficiency of the de-icing system is investigated, and

the design surface heat flux of the system is compared with the actual heating performance of the system. Finally, an equation is presented based on the heating efficiency of the de-icing system to be used for the future design of the required heating load of the external geothermal heating system for bridge deck de-icing.

4.3 Description of De-icing and Monitoring System

4.3.1 Test Site

The mock-up of the externally heated bridge deck was constructed in the Dallas-Fort Worth metroplex in Texas, USA. The test site has a humid subtropical climate that is characterized by moderate rainfall, mild temperatures, and abundant sunshine (Koppen 1936). Figure 4.1 shows the weather information of the region from the nearest weather station to the test site (DFW International Airport). The region has annual high and low temperatures of 25 °C and 14 °C, respectively (Gardiner et al. 2019). In general, July and August are recorded as the hottest months, with an average high of 35.5 °C. January is typically regarded as the coldest month, with an average low of 2.9 °C (Gardiner et al. 2019). The average annual rainfall accumulation is 95.3 cm, with an average of 81 days with precipitation. Most of the precipitation is due to thunderstorm activity that occurs most frequently in the spring and is classified by occasional heavy rainfall over short periods. On average, the region experiences 5 cm of snowfall annually (Gardiner et al. 2019). Although the region is known for mild winters, it has experienced several snowstorms in recent years, such as the snowstorm on March 4-5, 2015, which was the fourth-largest ever recorded in the region in a 24-hour period during March. Over two days, 8.89 cm of snow fell, and the average ambient temperature recorded was approximately -2.2°C .

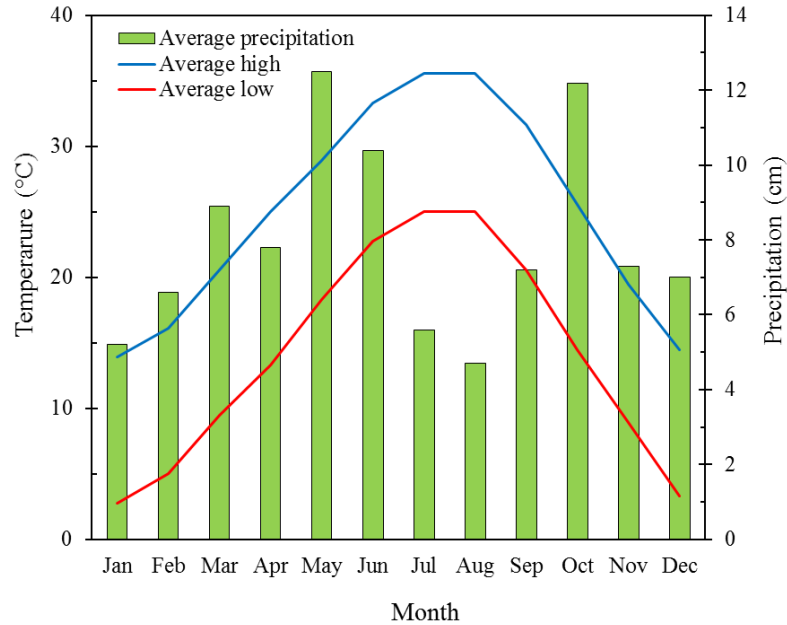


Figure 4.1. Test site weather information (Source: U.S. Climate Data)

The boring logs of a nearby bridge show that the site has relatively uniform soil layers: sandy clay with alternating sand/gravel seams covers the top 12.2 m, followed by a limestone layer. The boring logs stop at 18.3 m. Based on local knowledge of the region, it is estimated that the limestone extends to a depth that is of interest to the study. The groundwater table was encountered at 4.6 m below the ground surface at the time of drilling. Figure 4.2 illustrates the ground temperature profile recorded by one of the on-site temperature-monitoring boreholes, and the result represents the average monthly ground temperature variations up to 14 m below the surface. The formation thermal response test was carried out on-site by a contractor from July 30 to August 1, 2019, and the results showed that the soil formation has a thermal conductivity of 1.99 W/m.K and thermal diffusivity of 0.078 m²/day. The undisturbed temperature of the soil was observed to be about 21.4 °C during the test.

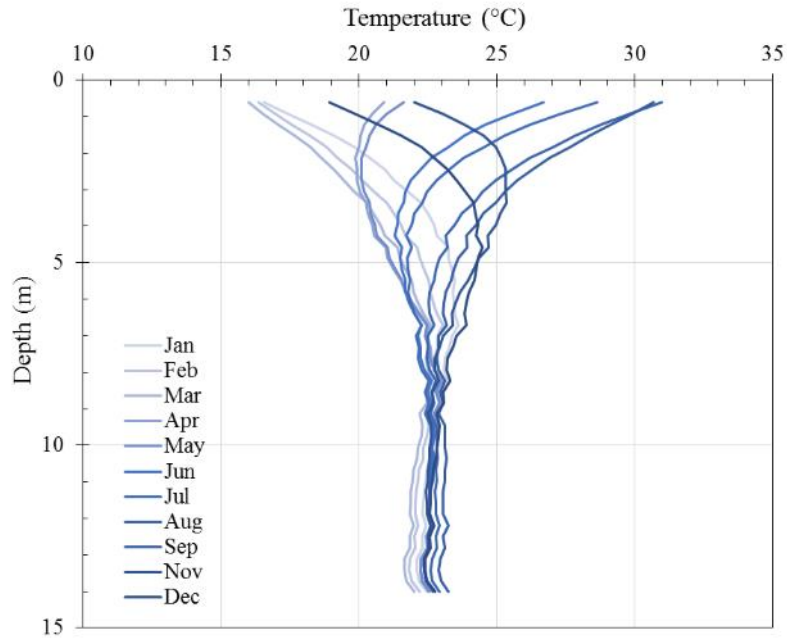


Figure 4.2. Test site ground temperature profile

4.3.2 Design of the Mock-up Geothermal Bridge

4.3.2.1 Overview

The purpose of the mock-up geothermal bridge was to provide a bridge deck surface on which to practice melting snow and ice. The geothermal heat pump de-icing system (GHDS), a ground-coupled heat pump system that utilizes the heat output of the system to de-ice and melt snow on the surface, was utilized for heating the bridge deck. The heat carrier fluid circulated in a closed loop between the ground loop heat exchangers and hydronic pipes in contact with the deck to transfer the heat from the ground to the bridge deck surface. Figure 4.3 shows the schematic diagram of the mock-up geothermal bridge and the different components of the GHDS. The mock-up bridge deck consists of three zones: an externally heated zone, an internally heating zone, and a control zone. It utilizes both the traditional type of GHDS, which uses a hydronic pipe embedded

in the concrete slab, and the newly developed method, which utilizes an external hydronic pipe that is attached to the bottom surface of the bridge deck and encapsulated in a layer of foam. In addition to the external heating system, which is the focus of this study, the internal heating system was also designed in the mock-up bridge deck for comparison purposes. However, as a sufficient number of tests have not yet been performed on the internally heated zone, no comparison has been carried out, and only external heating system performance is discussed in this study. Moreover, the end section of the bridge deck was considered as a control area with no heating.

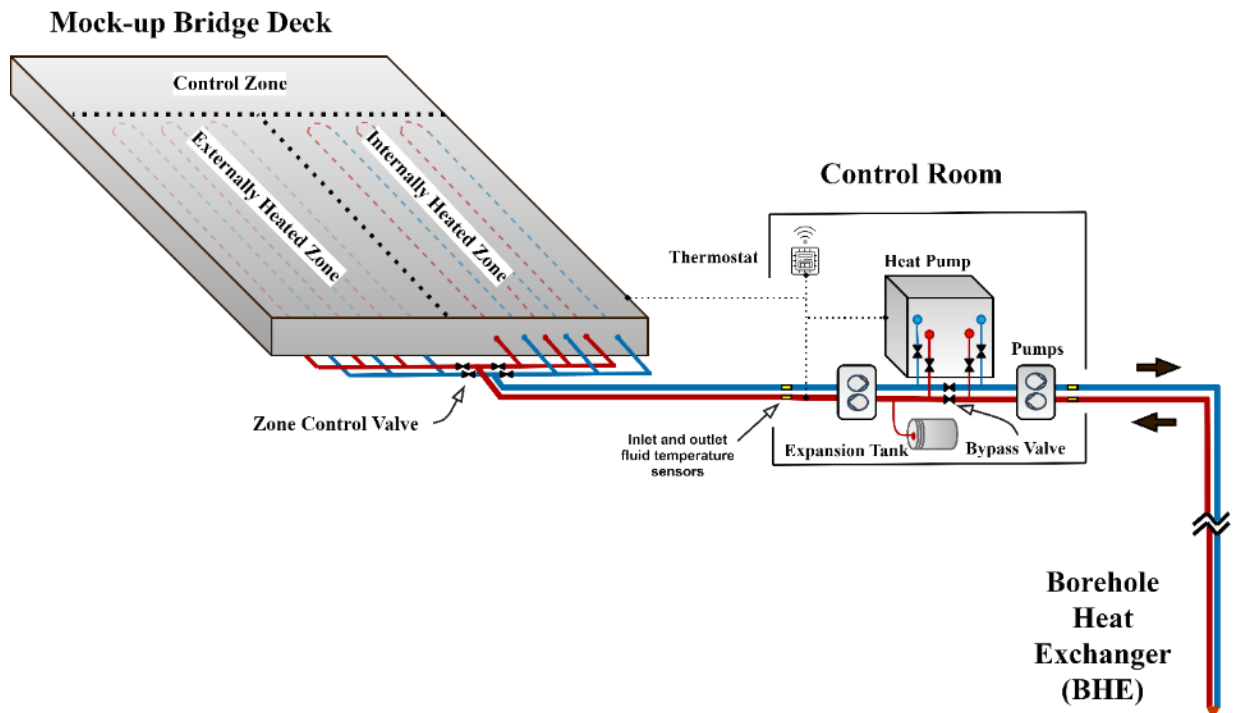


Figure 4.3. Schematic diagram of the mock-up geothermal bridge design (only the externally heated zone is tested in this study)

4.3.2.2 Mock-up Bridge and Hydronic Heating System

The mock-up bridge was designed to represent most of the bridges owned by TxDOT, which are CIP-PCP bridges consisting of precast, prestressed concrete panels (PCPs) and a cast-in-place

(CIP) concrete deck (Merrill 2002). The model bridge deck was designed to be constructed of 12 standard 2.43 m × 1.82 m × 10.16 cm PCP panels, 12 m I-beams, and two standard concrete traffic barriers (CTBs). The bridge was designed so that the PCP panels would rest on the I-beams, and the whole structure would be supported by the CTBs on both ends. The plan called for 10.16 cm of concrete to be cast on the surface, to complete the 20.32 cm thick bridge deck.

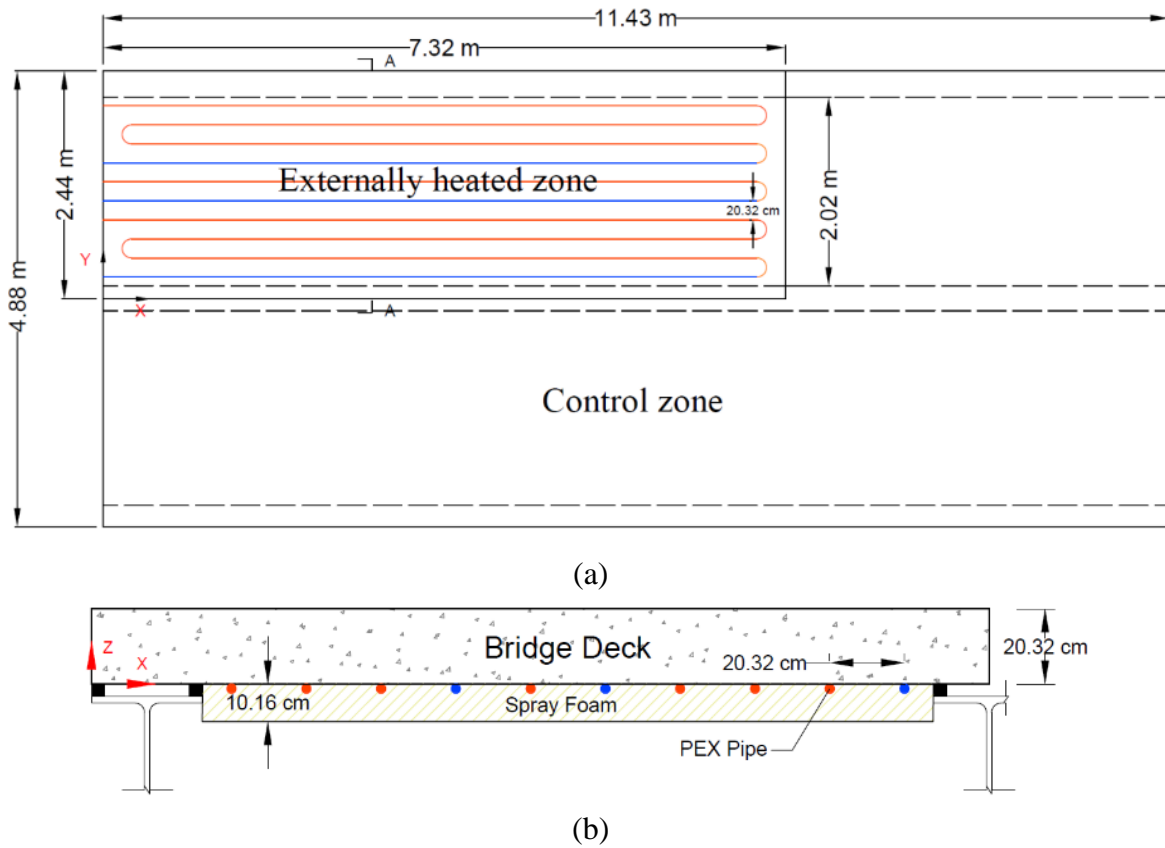


Figure 4.4. The design of the mock-up bridge deck: (a) Plan view of the bridge deck, (b) Cross-sectional view of the bridge deck

Figure 4.4 shows the plan and cross-sectional view of the mock-up bridge and illustrates the design of the externally heated zone on the bridge deck. The dimensions of the bridge slabs were 4.88 m × 11.43 m, and included 12 standard PCP panels; however, only a 2.44 m × 7.32 m section was assigned for the application of the external heating system. The hydronic loops at the

bridge deck consisted of 1.27 cm internal diameter polyethylene (PEX) pipes with a 20.32 cm centerline spacing. The remaining portion of the bridge deck was considered as the control section, which would aid in assessing the efficiency of the heating system. It should be noted that the internally heated zone was completely inactive during this study, therefore, assumed as a controlled zone.

4.3.2.3 Required Heat Flux

Geothermal snow melting systems provide sufficient heat flux to melt snow or ice on the bridge deck surface. The heat flux required is determined and maintained in order to prevent snow/ice formation under specified winter weather conditions. The objective of this section is to estimate the required heat flux for the mock-up bridge under specified weather conditions. The ASHRAE handbook design table and Chapman and Katurnich prediction equation were used to estimate the required heat flux (American Society of Heating and American Society of Heating 2015; Chapman and Katunich 1956).

The ASHRAE handbook provides the required heat flux for different cities in the USA. Amarillo is the only city in Texas included in the handbook for which the required heat flux for 64 hours of annual snowfall for different snow-free area ratios and reliability percentages is provided, as shown in Table 4.1.

Table 4.1. Required heat flux at steady-state conditions (Source: ASHRAE, 2015)

Location	Snowfall Hours per Year	Snow-Free Area Ratio (Ar)	Heat Fluxes Not Exceeded During Indicated Percentage of Snowfall Hours from 1982 Through 1993 (W/m ²)					
			75%	90%	95%	98%	99%	100%
Amarillo, TX	64	1	356.2	472.9	529.6	668.3	718.8	1002.5
		0.5	223.8	277.4	340.5	390.9	447.7	961.5
		0	75.7	145.0	195.5	280.6	362.5	920.5

Chapman and Katunich (1956) their provided a general equation (Equation 1) for computing the steady-state energy balance for required total heat flux (q_o) at the upper surface of a snow-melting slab during a snowfall(Chapman and Katunich 1956). Their equation is based on four environmental factors that determine the heating requirement for snow melting: rate of snowfall, air temperature, relative humidity, and wind velocity.

$$q_o = q_s + q_m + A_r(q_h + q_e) \quad (4.1)$$

Where q_o is heat flux required at the snow-melting surface in W/m^2 , q_s is the sensible heat flux in W/m^2 , q_m is the latent heat flux in W/m^2 , A_r is a dimensionless snow-free area ratio, q_h is the convective and radiative heat flux from the snow-free surface in W/m^2 , and q_e is the heat flux of evaporation in W/m^2 .

Table 4.2 presents a summary of the two approaches taken to estimate the heat fluxes for melting snow on the mock-up bridge. The first approach assumed that the bridge was located in Amarillo, Texas (data are taken from the ASHRAE Handbook) (American Society of Heating and American Society of Heating 2015), and applied a heat flux corresponding to a snow-free area ratio of 0.5 and 95% reliability. It is worth noting that in 1999, a similar geothermal de-icing system with smaller heat flux was implemented for two bridges in Amarillo. Although the required heat flux of the project was considered as $129 W/m^2$, the objective of the project was ice prevention (anti-icing) rather than snow melting. The hydronic heating loops in these two bridges were embedded in the concrete deck (internally heated bridge deck) (Minsk 1999). The second approach considered the snowstorm at DFW in March 2015, an extreme case, and applied Equation 1, even though, considering the weather history of the DFW metroplex, it would have been acceptable to select a more moderate case for the required heat flux. In conclusion, It was decided to design the geothermal system based on the required heat flux of $340.2 W/m^2$.

Table 4.2. Summary for required heat flux at the mock-up bridge deck surface

Scenario	Required heat flux
Amarillo, TX (1)	340.2 W/m ²
DFW, TX (2)	1080 W/m ²

4.3.2.4 The Ground Loop Heat Exchanger (GLHE)

The main objective in designing the GLHE was to determine the smallest size that could provide sufficient heat output for melting the snow and ice. The proper design was of utmost importance because an undersized bore field can cause performance failures, and an oversized bore field results in an uneconomical system (Monzó et al. 2016). A variety of geological formations and properties complicate the design of vertical ground heat exchangers and eventually affect the thermal performance (Kavanaugh 1997). Figure 4.5 shows the design procedure followed in this study for determining the proper size of the GLHE in this study. First, the design weather condition was chosen. In this step, weather data were collected, and the weather history of the region was investigated. Then the required heat flux for bridge deck snow/ice melting was calculated based on the weather data. The process of calculating the required heat flux is shown in section 2.2.3 and the result is shown in Table 4.2. Then, the peak hourly and monthly heating loads were calculated according to the area of the bridge deck and snowfall hours, respectively. The result is shown in Table 4.3. In the calculation of the monthly heating load, it was assumed that 64 hours of snowfall per year (refer to Table 4.1) is only happening during the three months of the winter season i.e. 21.3 hours in December, January, and February, respectively. Next, a heat pump was selected which was able to work in a system with the calculated heating load; EWT and flow rates were specified and heat pump and GLHE heating loads were selected from the heat pump heating performance datasheet. Afterward, the design and operational parameters were selected (Table 4.4). If the

required data were not available, a reasonable assumption was made. Finally, all data were inputted to the design tool software e.g. GLHEPro and the GLHE size was computed.

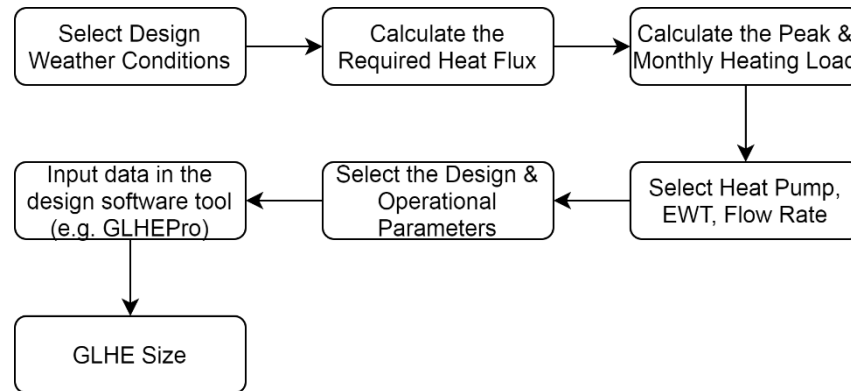


Figure 4.5. GLHE design diagram

In this study, GLHEPro software, which was developed based on the g-functions method presented by Eskilson (Eskilson 1987), was utilized to calculate the size of the GLHE (Spitler 2000). It was found that a single borehole that is 132.5 m deep and 14.6 cm wide is sufficient to supply enough heat for snow melting/de-icing the mock-up bridge deck. Figure 4.6 shows the details of the geothermal borehole design. However, since this was the first attempt in designing the GLHE size for use in the external geothermal heating system, there were many uncertainties in calculating the design heating load for snow melting and de-icing the bridge deck surface. The difference between the external and internal heating system is located in the installation details. In the external heating system, there is a greater distance between the heating source and the bridge deck surface which yields to more heat loss and the need for a larger heat supply. However, it was tried to consider some overestimations and underestimations to account for the additional heat requirement of the external heating systems. Firstly, greater required heat flux was assumed in comparison with a similar project as explained in section 2.2.3. Secondly, the operational parameters such as entering water temperature (EWT) were selected with underestimation in

comparison to the ground temperature potential. Also, the design peak hourly heating load was estimated with 50% overestimation in comparison to the required heating load, i.e. the design peak hourly heating load on the heat pump and GLHE considered as 9.34 kW and 6.94 kW, respectively. It means the design surface heat flux is equal to 524.7 W/m², assuming 35% heat loss in the bridge deck. lastly, the ground thermal recharge was neglected, and the design was conducted only based on the heating operation mode. The outcome of all these considerations led to an overestimation of GLHE size. However, a more proper design can be performed after the external geothermal heating system is tested and the heating efficiency of the system is investigated. The heating efficiency of the system determines how much overestimation should be considered in designing the GLHE of an external geothermal heating system.

Table 4.3. Required heating loads

Required heat flux	Area of snow melting	Peak hourly heating	Monthly snow	Total monthly heating
340.2 W/m ²	17.8 m ²	6.07 kW	21.3 hours	129 kWh

Table 4.4. GLHE design and operational parameters

Parameters	Value
Undisturbed soil formation temperature (T _g)	21.4°C
Soil thermal conductivity (K _{soil})	1.99 W/m.K
Grout thermal conductivity (K _{grout})	1.38 W/m.K
Diameter of borehole (D _{bore})	13.97 cm
Diameter of pipe (D _{pipe})	3.17 cm
Flow regime	Turbulent
Bore layout	1x1
Heat carrier fluid	20% Propylene Glycol solution
Heat pump full-load heating performance data	
Heat pump size	3 Ton
Minimum entering water temperatures (EWT _{min})	7.2°C
Flow Rate	3.78 l/min
Heat pump heating capacity (CAP)	9.34 kW
GLHE heat extraction (HE)	6.94 kW
COP	3.9

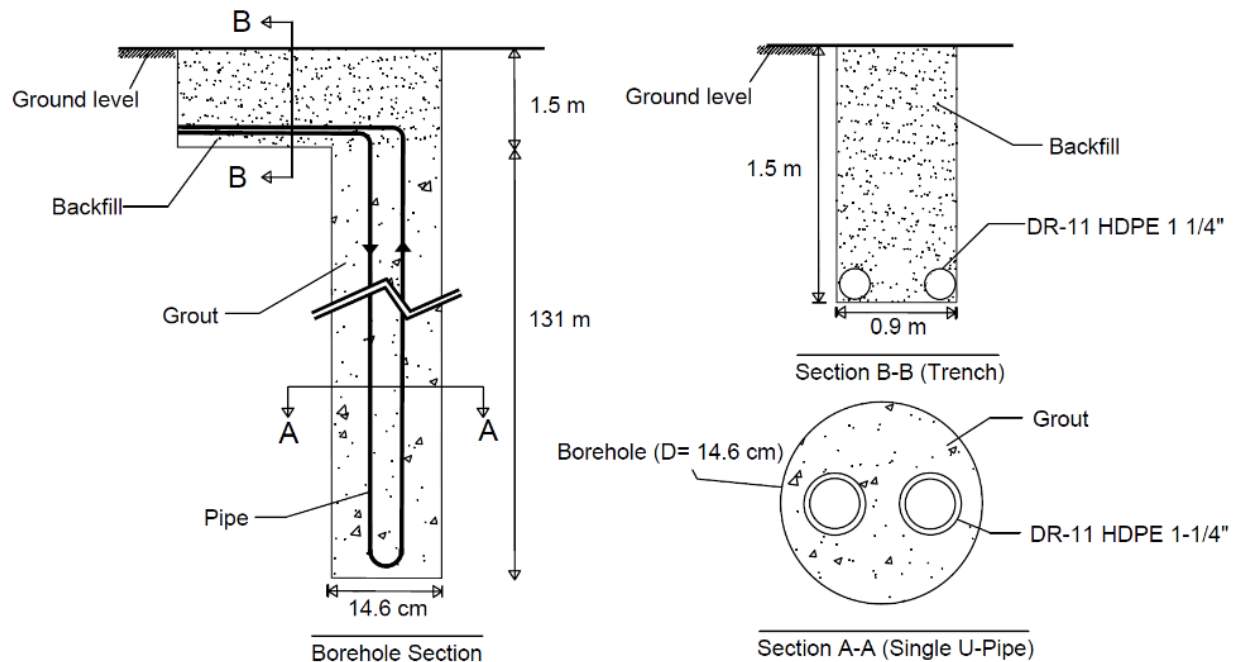


Figure 4.6. The final design of the GLHE

4.3.3 Construction of the Bridge Deck Prototype

The mock-up bridge was constructed during February and March of 2019, and the various stages of construction are depicted in Figure 4.7. After the materials were transported to the site, the concrete traffic barriers (CTBs) were placed in their pre-specified locations, the I-beams were affixed to them, and the PCP panels were put atop the beams. The longitudinal and transverse #4 rebars were then placed on top of the PCP panels, with a maximum of 22.8 cm between them, using rebar chairs to keep them at the appropriate depth. The installation of the internal heating loops followed the conventional method. They were attached to the rebar and embedded in the top 10.16 cm of the cast-in-place concrete deck, using the TxDOT Class S concrete mix, which is typically used for bridge decks in Texas. After the bridge deck was completed, the external heating pipes were attached to the bottom surface of the externally heated zone, using two-hole straps, then the pipes were covered with cement paste to increase the thermal contact between the pipes and

the concrete. Finally, thermal insulation foam was applied to the entire surface to prevent heat loss from the bottom, and valves were installed to control the operation mode and the heated section of the bridge deck.



Figure 4.7. Installation of the hydronic loops: (a) Hydronic loops installed on the bottom surface of the externally heated zones, then covered by a cement paste, (b) A layer of polyurethane foam applied to the deck bottom

The construction of the ground loop heat exchangers (GLHE) involved one geothermal borehole and five temperature-monitoring boreholes that were drilled and equipped with temperature sensors to monitor the temperature at various distances from the geothermal borehole. Boreholes were drilled in the locations specified by the design of the GLHE. A 14.6 cm diameter geothermal borehole was drilled 132.5 m deep (from ground level), then the previously prepared and the instrumented ground loop was inserted in the borehole. Eventually, the borehole was grouted and allowed to settle. To facilitate the installation of the temperature sensors, which were in the form of thermo-string, they were attached to a PEX pipe. After they were installed, the borehole was grouted with the same material used for the geothermal borehole.

A 1.5 m deep trench was excavated to lay the groundwork for connecting the GLHE to the control room. Header pipes of 3.17 cm diameter were connected to the GLHE using socket fusion coupling, and the sensor's cable was laid down on the bottom of the trench. The trench was then backfilled with the excavated soil. The horizontal header pipes were bundled together during the backfill process. The embedment depth of the HDPE pipes in the trench varied due to the bending of the pipes near the intersections of elevation changes. Due to the fragility of the sensor cables, the backfilling operation was performed with extreme caution. Figure 4.8 illustrates the construction stages of the geothermal and temperature-monitoring boreholes.

The last step in construction was to build a control room to host the system's main components, which included one heat pump, two flow centers, four circulating pumps, and one expansion tank. Figure 4.9 shows an overview of the control room and its components. In the control room, the pipes of the bridge side were connected to the ground side, and a simple single-stage heating thermostat was wired to the heat pump to control its operation. In addition, a bypass was provided so that the system could operate in two modes: full-load and bypass. In the full-load operation mode, the control valves of the heat pump are closed and the flow goes through the heat pump. In the full load operation mode, the geothermal heat pump is active; while in bypass mode, the geothermal heat pump is off, and the heat carrier fluid circulates directly through the bypass. Flow meters were also installed to measure the flow rate of each side. Finally, the pipes were connected, and the system was flushed with a 20% propylene glycol solution and tested for any possible leakage.

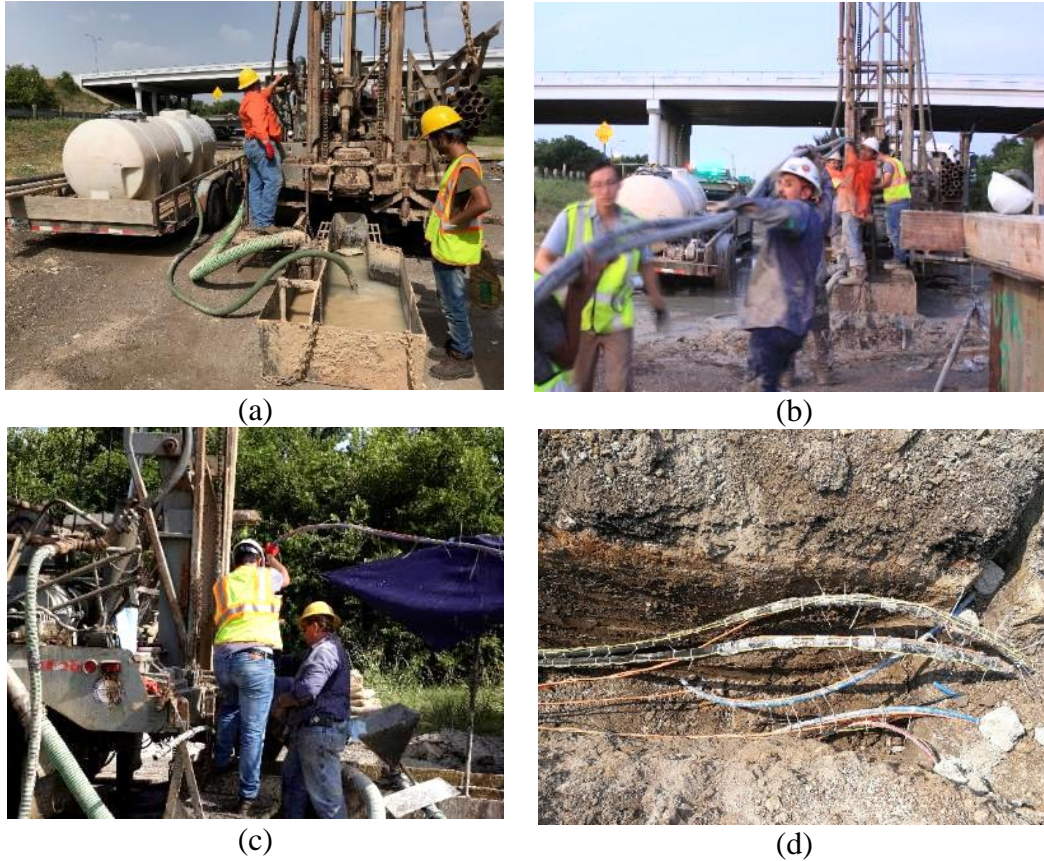


Figure 4.8. Construction of the GLHE: (a) Drilling the boreholes, (b) Insertion of the ground loop into the geothermal borehole, (c) Insertion of TMB's PEX pipe, (d) Connection of the ground loop pipes to the header pipes in the trench.

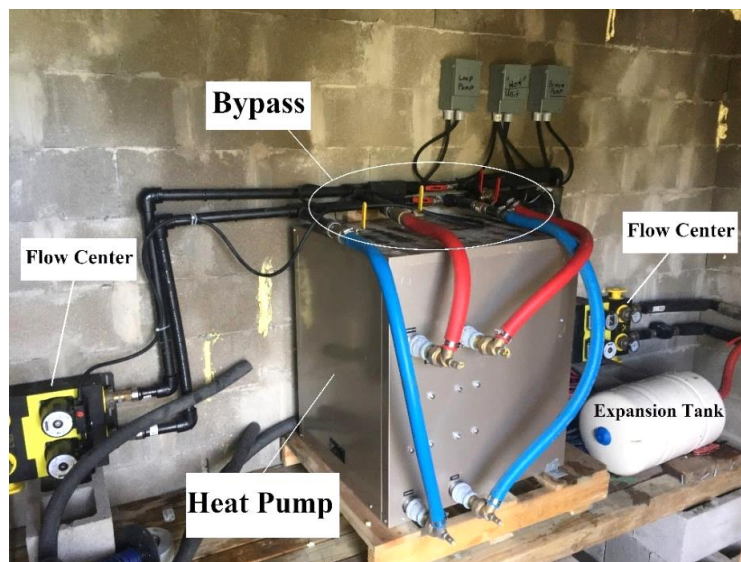


Figure 4.9. Overview of the control room

4.3.4 Instrumentation and Monitoring System

The geothermal system and the bridge deck were instrumented with temperature sensors to monitor the system's component and bridge deck's thermal response. Table 4.5 lists the instruments of this study and shows their measurement accuracy. The data acquisition system of this study consisted of three multiplexers and two data loggers. The T-type thermocouples were connected to the thermocouple multiplexer and a data logger. The thermistors and strings were connected to two multiplexers and another data logger through a bridge completion circuit. All the sensors were calibrated, and temperature outputs were recorded in the data logger. Although multiple temperature sensors at different coordinates were installed on the bridge deck, this study has only utilized the data of the two representative sensors located at 2.5 cm below the deck surface on the heated and non-heated zone, respectively (Figure 4.10 (a)). Moreover, the Type-T thermocouple was utilized to monitor the inlet/outlet fluid temperature of the bridge deck and the underground loop (Figure 4.10 (b) and (c)). The thermocouples were attached to the outer surface of the pipes and then insulated and protected.

Table 4.5. Instrumentation list

INSTRUMENT	MANUFACTURER	QUANTITY	ACCURACY
Thermal wire cable	Pile Dynamics (PDI)	4	$\pm 0.2^{\circ}\text{C}$
Type-T Thermocouple	National Instrument (NI)	27	$\pm 0.5^{\circ}\text{C}$
Thermistor Probe	GEEKON	6	$\pm 0.2^{\circ}\text{C}$
Thermistor Probe- PVC house	GEEKON	5	$\pm 0.2^{\circ}\text{C}$
Thermistor string	GEEKON	6	$\pm 0.2^{\circ}\text{C}$
Flow Meter	Sotera	2	$\pm 1\%$
Power Logger	Fluke	1	*Voltage: $\pm(0.2\% + 0.01\%)$ *Current: $\pm(0.2\% + 0.02\%)$

* Intrinsic Accuracy at Reference Conditions (% of Reading + % of Range)

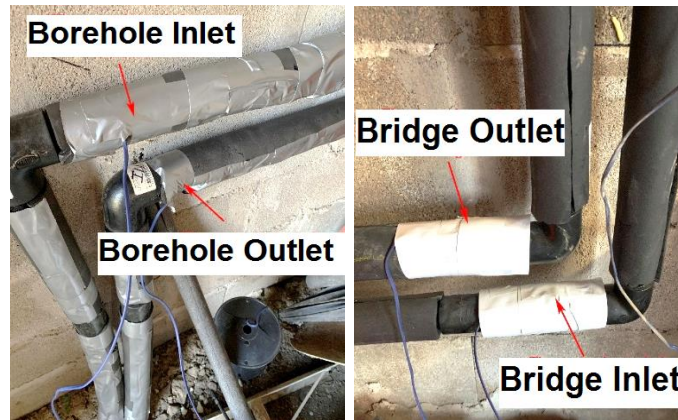
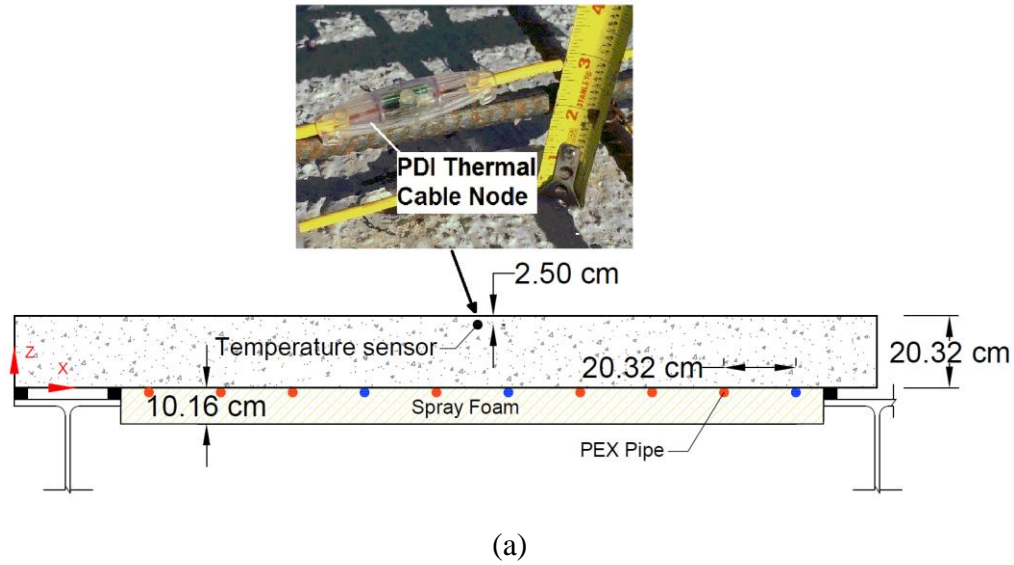


Figure 4.10. Instrumentation: (a) The temperature sensor node from Pile Dynamics thermal wire cable at 2.5 cm below the deck surface, (b) Bridge deck inlet/outlet temperature sensors, (c) Geothermal borehole inlet/outlet temperature sensors

A very simple control system was used in this study. A simple thermostat was wired to the heat pump to control the operation of the heat pump. The thermostat was controlled by an external thermistor which was attached to the inlet pipe to the bridge deck to measure the inlet fluid temperature. This sensor controls the supplied water temperature to the bridge deck which gives this opportunity to the operator to decide the supplied heating load according to the forecasted

weather. However, it should be noted that the whole system, including the four circulating pumps, was turned on/off manually and pumps were on during the entire test. It should be noted that the focus in the initial tests was more on the heating performance and de-icing feasibility of the external hydronic pipes and less attention has been paid to the optimal control system. However, the research team is going to design a more advanced control system in the future which works automatically according to the weather condition and is able to control all components of the system.

4.4. Results and Discussion of The Operation Tests

4.4.1 Winter Test Process

Winter climatic conditions were closely monitored from November of 2018 to March 2019. The geothermal system was operated when a cold front with below-freezing temperatures was forecasted. Figure 4.11 presents the collected weather data from different sources, namely thermocouple measurements on-site, weather station (Vaisala WXT530) data from the site, and online data from various sources (Weather Underground 2019). The on-site thermocouple was located approximately 30 cm above the roof of the control room. The air temperature measurements from the on-site thermocouple were in good agreement with the data obtained from the online source, which was recorded from a weather station located at the DFW International Airport, 15 miles from the site. Time delays in temperature measurement were observed as a result of different locations. This comparison shows that the ambient temperature measurement, using the thermocouple on site, is a reliable source for air temperature since it matches the on-site weather station data and is very close to the online source data.

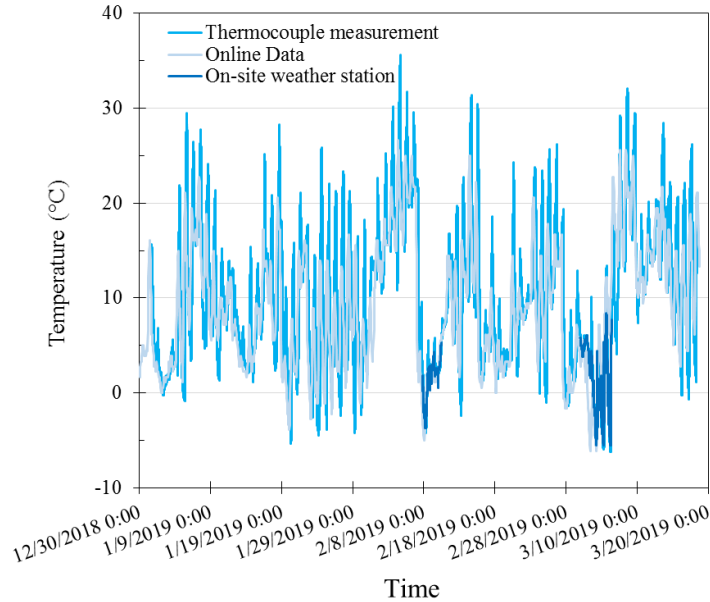


Figure 4.11. Collected weather data from different sources for the period of Jan. to Mar. 2019

The de-icing system was operated in several modes, depending on the operational condition of the geothermal heat pump and the heated deck. The geothermal heat pump was switched off when the winter event was mild and the heat demand was less - i.e. when the minimum ambient temperature was greater than -2.5°C . In all the tests, the goal was to melt the ice on the bridge deck surface. Table 4.6 summarizes the seven winter tests performed in the winter of 2018-2019. The start and end times were the operation period when the geothermal system was switched on. The number of freezing hours were determined from the air temperature measured by the thermocouple installed at the bridge site. The number of freezing hours, minimum air temperature, and average air temperature during the freezing period were obtained to characterize the winter events. The last column of Table 4.6 describes the operation mode of the geothermal system during each winter test.

Table 4.6. The details of operation tests and weather conditions

Test	Start	End	Ambient temperature			Operation mode
			# Hr. of freezing	Average (°C)	Minimum (°C)	
#1	11/13/18 13:00	11/16/18 12:00	9.00	-1.3	-2.2	Bypass
#2	12/31/18 16:00	1/5/19 13:32	5.47	-0.3	-0.8	Full load
#3	1/19/19 11:28	1/22/19 16:49	9.87	-2.4	-5.3	Full load
#4	1/24/19 11:25	1/29/19 12:55	14.90	-1.7	-4.2	Full load
#5	2/7/19 22:02	2/12/19 9:19	11.70	-2.4	-4.3	Full load
#6	2/17/19 16:50	3/3/19 11:17	12.48	-0.7	-1.4	Bypass
#7	3/4/19 2:50	3/6/19 9:53	36.10	-3.5	-6.2	Full load

average and minimum surface temperatures during the freezing period were obtained from the sensor node, which was embedded in the concrete, approximately 2.5 cm below the deck surface (Figure 4.10 (a)). This sensor was selected as representative of the bridge deck's temperature response during the coldest period of the winter test. The bridge deck temperature during the other periods of operation was higher than the temperature recorded when the air temperature was below freezing. Figure 4.12 shows that the system was capable of keeping the heated surface temperature above freezing during all of the events. Unfortunately, the surface temperature data of the externally heated zone are not available for Test #6 and not presented in Figure 4.12. Test #5 was selected as the example of the winter tests, and a detailed discussion of the system performance is presented in the following section. It should be noted that only some representative sensors were used in discussing the system performance; all of the data collected from the tests are not presented. Also, due to an issue in the data acquisition system, the thermistor strings measurements in the geothermal borehole and four TMBs malfunctioned and no data during the first winter operation has been collected from these sensors.

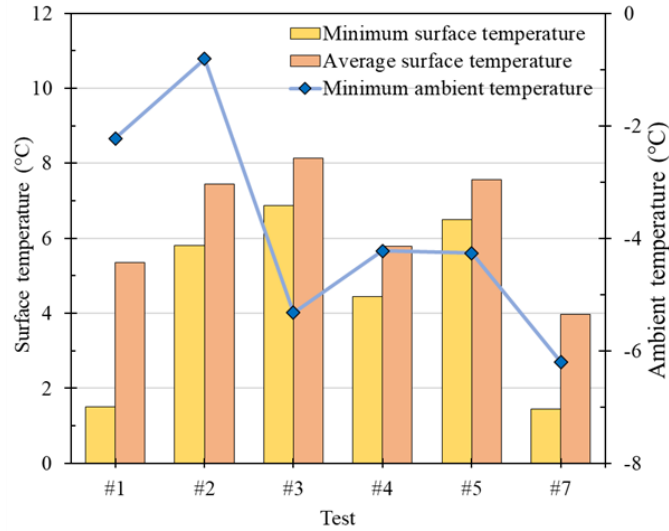


Figure 4.12. Summary of the externally heated surface temperature during freezing air temperatures for each test

4.4.2 De-icing Tests

Winter test #5 was primarily selected to discuss the performance of the system due to the observed low ambient temperature of $-4.3\text{ }^{\circ}\text{C}$. This test spanned from 10 p.m. on 2/7/2019 to 7 p.m. on 2/8/2019. The geothermal heat pump was turned on at 10 p.m. on 2/7/2019 to provide 7 hours of pre-heating before the bridge experienced the minimum freezing temperature of $-4.3\text{ }^{\circ}\text{C}$ that was reached at 5 a.m. on 2/8/2019. Only the external heating hydronic system was active. As no precipitation was forecasted or experienced during that time, the project team decided to make snow/ice on the bridge deck surface, using a snow gun. It was an excellent opportunity for the application of snowmaking devices due to the low ambient temperature of $-4.3\text{ }^{\circ}\text{C}$, a temperature suitable for making snow; however, the snowmaking was not successful due to the high humidity (greater than 60 percent). The water drops became ice pellets, and a uniform ice layer was observed on the non-heated zone surface, which was a good simulation of freezing rain. Figure 4.13 compares the temperature of the insulation foam, captured from a thermocouple installed in the

middle of the 10.16 cm layer of insulation foam (Figure 4.7 (b)), with the ambient temperature during the system operation. As expected, the temperature of the insulation foam fluctuated less with the ambient temperature. It can be concluded that the thermal resistance of the insulation foam was effective.

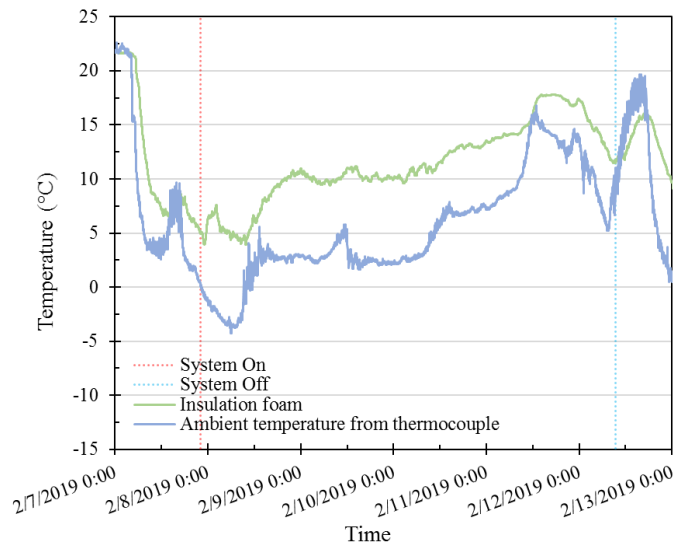


Figure 4.13. Temperature variations inside the insulation foam and ambient during test #5

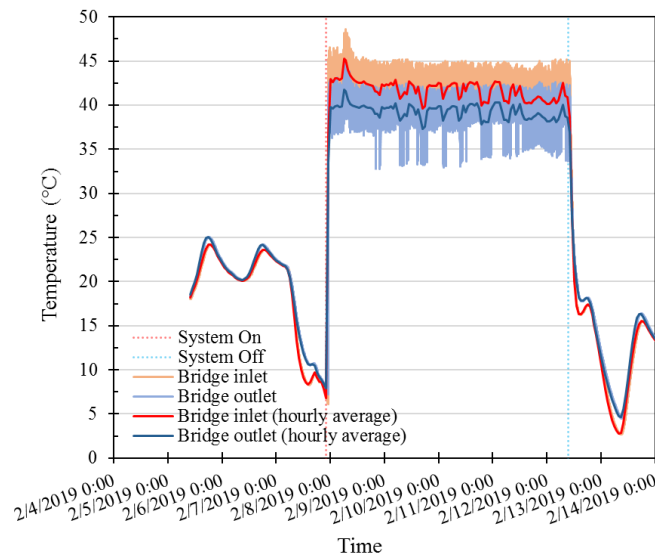


Figure 4.14. Inlet and outlet temperatures of the bridge deck hydronic pipes

Figure 4.14 shows the temperature variations of the bridge deck supplying and returning heat carrier fluid. These data are pivotal as they represent the inlet and outlet temperature variations on the condenser side of the heat pump and will be used to study the system performance. The monitoring data illustrates that the bridge deck was heated with heating fluid with an average temperature of 41.4 °C at the inlet. The average outlet temperature was recorded as 38.9 °C, with an approximately 2.5 °C temperature drop.

Figure 4.15 illustrates the condition of the bridge deck during snow/ice making and the de-icing process. It shows that no ice accumulation was observed on the heated surface during the ice-making process after the snow gun was turned on at 5:40 a.m. on 2/8/2019. However, the temperature of the non-heated zone dropped quickly, and the surface was covered with ice. It was observed that the surface of the heated zone started to dry, while the non-heated zone was fully covered with ice.

Figure 4.16 compares the temperature variations of the heated and non-heated zones, along with the ambient temperature data. The temperature data for both the heated and non-heated zone were obtained from the sensor node, 2.5 cm below the surface, in the center of each zone. Before the system was turned on, the heated and non-heated zone deck temperatures were very similar and followed the same trend as the ambient temperature. After the onset of the geothermal heat pump, the temperature on the heated zone began to increase and followed trends that were different from those of the non-heated zone. The temperature in the non-heated zone still closely matched the ambient temperature, which also validated the monitored data. When the test was over and the system had been turned off, the temperature in the heated zone dropped and slowly rose to the non-heated zone temperature, with both following the ambient temperature variations.

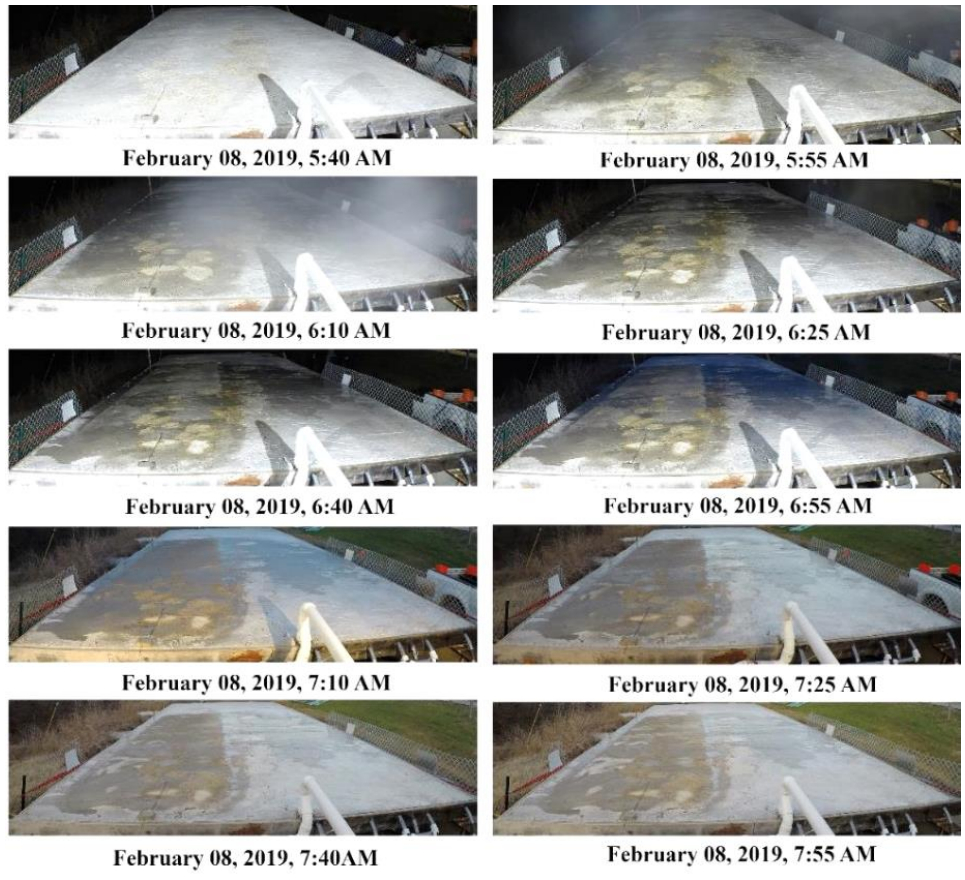


Figure 4.15. Time-lapse of the bridge deck condition before, during, and after the de-icing test

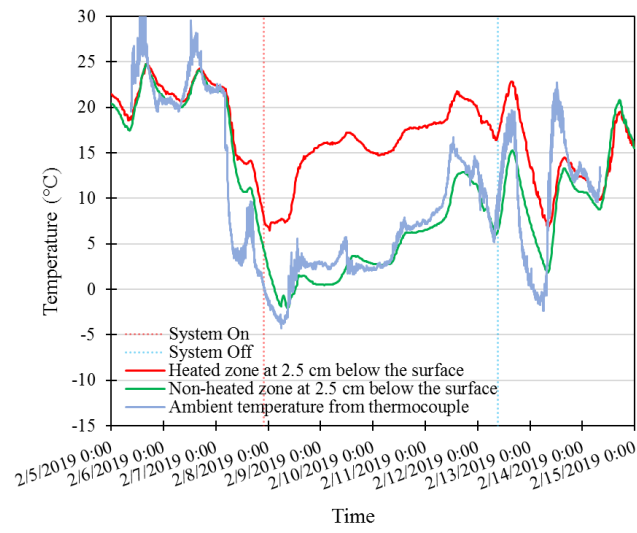


Figure 4.16. Comparison of the heated and non-heated zone temperature variation during test #5

The surface temperature was monitored by using a Fluke 50Ti thermal imager at various time intervals. Although the temperature measurement of the thermal imager is slightly different from that of other sources, it is a useful tool for visually illustrating the heated section and the temperature variations across a large area. Figure 4.17 shows the thermal images of the bridge deck during event #5. It clearly shows that when the test began, the surface temperature was below freezing, while after about 7 hours of operation, the surface temperature on the externally heated zone rose to 1.1 °C. The minimum ambient temperature was -4.3 °C.

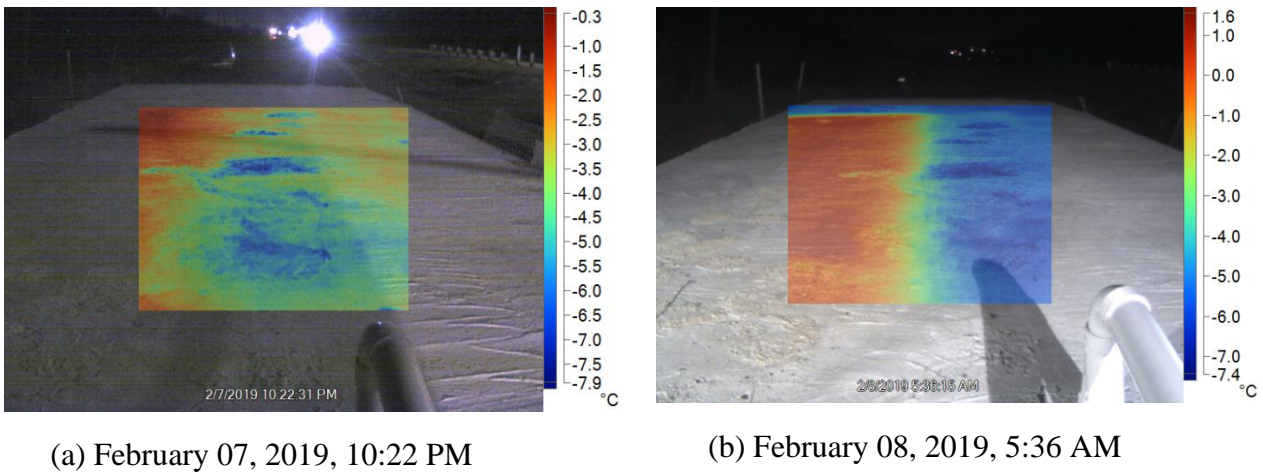


Figure 4.17. Surface temperature measurement of the bridge deck using thermal imager during test #5

The efficiency of the geothermal system primarily depends on the ground loop heat exchangers (GLHE). One of the key parameters significantly affecting the design of the geothermal system is the outlet water temperature of the geothermal borehole. Figure 4.18 shows the inlet and outlet temperatures of the geothermal borehole during the event. The monitored data illustrates an average temperature of 16.5 °C for the inlet water to the borehole, while the water returning from 131 m deep borehole was recorded as about 16.9 °C during the system's operation.

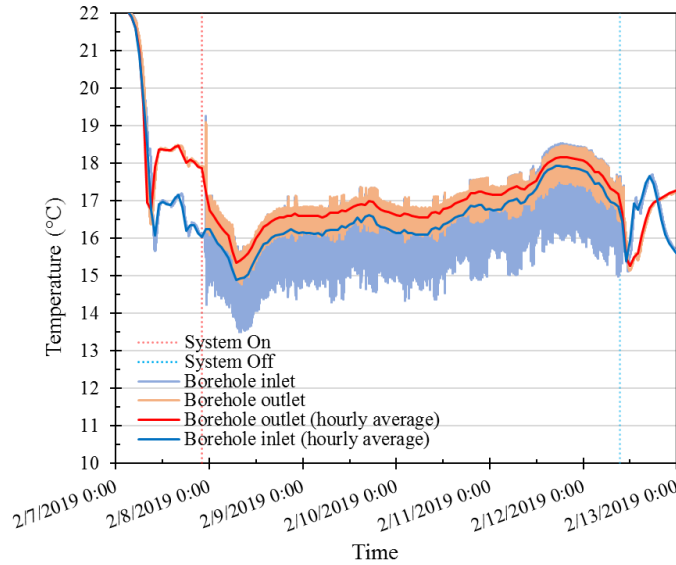


Figure 4.18. Geothermal borehole inlet and outlet temperatures during winter test #5

Moreover, the highlight of the system’s performance during Test #7, coldest event which was experienced by the system during winter 2018-2019, is briefly discussed in the following; however more details can be found in (Habibzadeh-Bigdarvish et al. 2021a). In this specific event, the system was operated from 3/4/19 2:50 a.m. through 3/6/19 9:53 a.m. in full-load mode in the externally heated zone and the bridge experienced 7 hours of freezing temperatures before the system was turned on. The monitoring data showed that the bridge deck was heated with heating fluid with an average temperature of 42.2 °C at the inlet; the outlet temperature was recorded as 39.4 °C as the average temperature, with approximately 2.8 °C temperature drop. Figure 4.19 compares the temperature variation of the heated zone and the non-heated zone, along with ambient temperature data. The temperature data for both the externally heated zone and internally heated zone (not active, therefore referred to as a non-heated zone) are obtained from the sensor at 2.5 cm below the surface in the center of each zone as shown in Figure 4.10 (a). However, it should be noticed that the difference between temperature in the heated and non-heated zone before

the test began is due to the system operation in the previous test in which the system was operating in bypass mode for the external & internal heated section and ended at 3/3/19, 11:17 a.m. As mentioned earlier, the bridge experienced 7 hours of freezing temperature before the system was switched on for this test. The idling gap of the geothermal system between the previous and this test is about 15.5 hours. The heat stored from the previous test gradually dissipated and the bridge was close to being in equilibrium with the ambient temperature before the start of the system. However, after the onset of the geothermal heat pump, the temperature on the heated zone starts to increase and follows a different trend concerning the non-heated zone. The temperature in the non-heated zone still closely matches the ambient temperature, which also indicates the validity of the monitored data. In the end, when the test was over, and the system turned off, the temperature in the heated zone drops and slowly merges to the non-heated zone temperature and both follow the ambient temperature variation. The on-site observation proved the 8 hours of idling time was required when the bridge deck of the control zone was in close equilibrium with the ambient temperature. The hours required to raise the bridge deck surface temperature to 0 °C is considered as the time re-quired for pre-heating. It is worthwhile to mention that the recorded temperatures in Figure 4.19 belong to 2.5 cm below the surface and it has a slightly higher temperature with respect to exact surface temperature on the heated zone. The minimum of 0.3 °C on the heated zone is recorded slightly after the test began in the early morning of 3/4/2019 when the air temperature reached -5.5 °C. Following about 24 hours of operation, the heated surface temperature achieved 11.1°C, while air and non-heated surface temperatures are dropped to about -5.8 °C. However, after approximately 48 hours of operation, the heated surface temperature is reached 14.4 °C, while air and the non-heated surface temperature recorded as -6.2 °C and -2.2 °C, respectively.

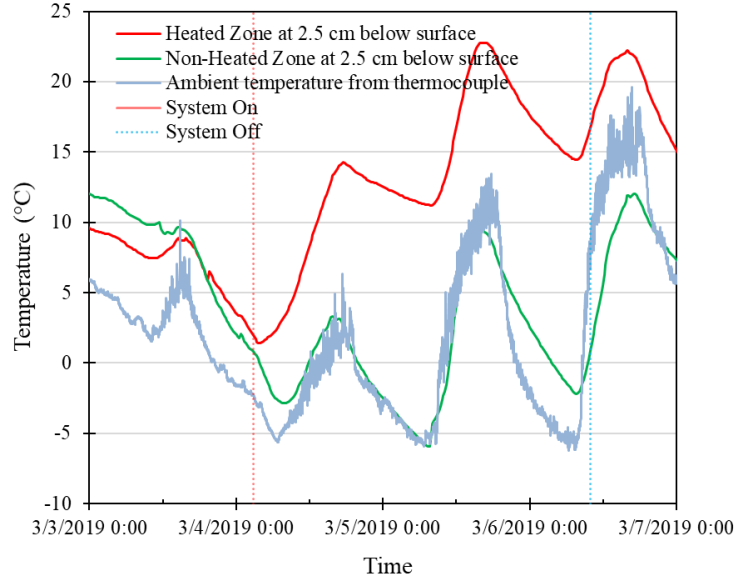


Figure 4.19. Comparison of the heated and non-heated zone temperature variation during test #7

4.4.3 System Performance

In this study, the input power of the entire system was monitored, using a Fluke 1736 power logger during tests #5 and #7, and the data were utilized to study the system performance. The GHDS was tested under the heating mode; therefore, the energy efficiency of the system can be evaluated by using the coefficient of performance (COP), which is defined as follows:

$$COP_{sys} = \frac{\dot{Q}_c}{\dot{W}_{in,total}} \quad (4.2)$$

Where \dot{Q}_c and $\dot{W}_{in,total}$ are the thermal energy output produced by the heat pump (heat transferred in the condenser) and total input power, respectively. They are calculated using equations (4.3) and (4.4), respectively.

$$\dot{Q}_c = \dot{m}C_p(T_{c,o} - T_{c,i}) \quad (4.3)$$

$$\dot{W}_{in,total} = \dot{W}_{hp} + \dot{W}_p \quad (4.4)$$

Where \dot{m} , C_p , $T_{c,o}$, and $T_{c,i}$ are the mass flow rate, the specific heat of the fluid, outlet, and inlet fluid temperatures of condenser, respectively. In this study, the flow rate of the heat carrier fluid was measured by the installed flow meter in the system and was equal to 2158 l/h on the bridge deck side. The outlet and inlet fluid temperatures of the condenser were monitored by the two thermocouples which measured the inlet/outlet fluid temperature of the bridge side (Figure 4.10 (c)). The heat capacity of the heat carrier fluid, i.e., 20% propylene glycol solution was estimated as 4038 J/kg°C. Moreover, \dot{W}_{hp} and \dot{W}_p are the power input to the heat pump unit and the pumps, respectively.

Figure 4.20 shows the monitored power input to the heat pump and the circulating pumps during Test #5 and #7. As described previously, the circulating pumps were on during the entire test and drew relatively constant power. However, the heat pump had on-off cycles which depends on the heating load requirements of the bridge deck. The increase in heating demand results in a more operational time of the heat pump and more input power. The result showed the circulating pumps electricity consumption accounts for about half of the total energy consumption. However, if the control system was able to control the on-off cycling of the circulating pumps as well as the heat pump operation, the energy consumption of the circulating pumps could be greatly reduced due to the huge reduction in the operational time. In that case, the operational time of the circulating fluid would be the same as the heat pump.

Table 4.7 shows a summary of the system performance during tests #5 and #7. Despite the different weather conditions during the tests, the overall performance of the systems was similar: the average hourly input power was approximately 1.4 kW for both tests. Moreover, although the average hourly operational time of test #7 was higher than that of test #5, the system average COP was similar.

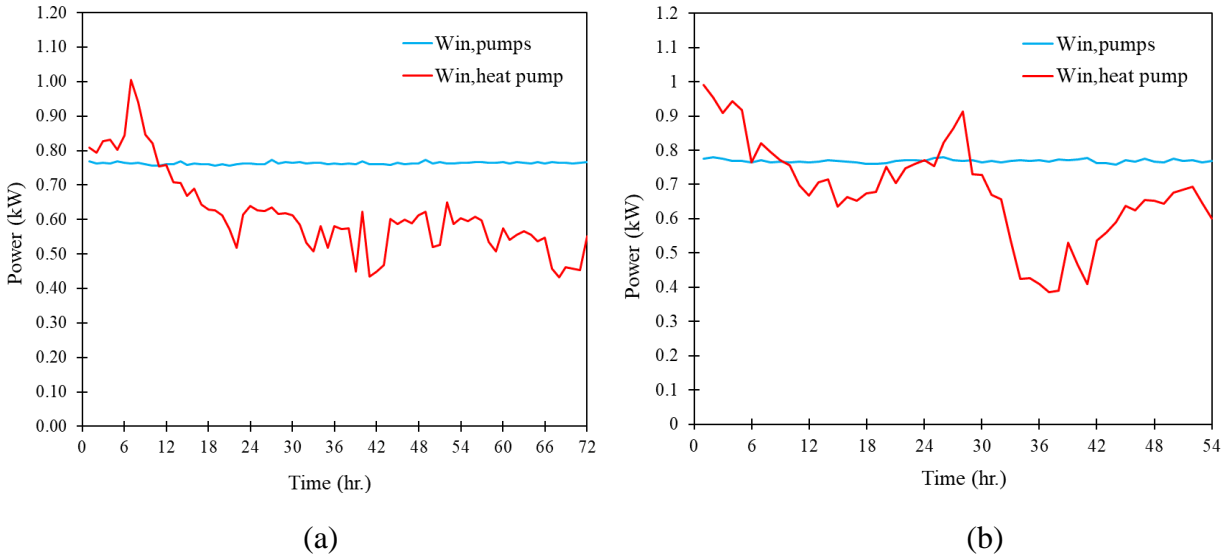


Figure 4.20. Power input to the heat pump and circulating pumps during the test; (a) Test#5, (b) Test #7

Table 4.7. Summary of System Performance during Tests #5 and #7

Test	#5	#7
Monitoring duration (hr.)	72.0	54.0
Total input energy (kWh)	99.2	78.0
Average ($T_{c,o} - T_{c,i}$) (°C)	2.5	2.8
Total thermal energy output (kWh)	455.6	360.1
Average COP _{sys}	4.6	4.6
Standard deviation (SD) of COP _{sys}	0.24	0.36
Average heat pump hourly operating time (min)	16.5	18.2
Average heat pump number of cycles per hour	5.4	5.6
Average cycle duration (min)	3.1	3.2

Figure 4.21. presents hourly fluctuations of the thermal energy output of the heat pump (kW), the total electricity consumption of the system (kW), and the COP of the system for Test #5 and #7. While there was a slight variation in the electricity consumption of the system, the thermal output from the heat pump varied more due to the ambient and bridge deck temperatures and resulted in variations in the COP_{sys}. The COP_{sys} was recorded above 4 throughout the test, and 4.6 as the test's average COP_{sys}.

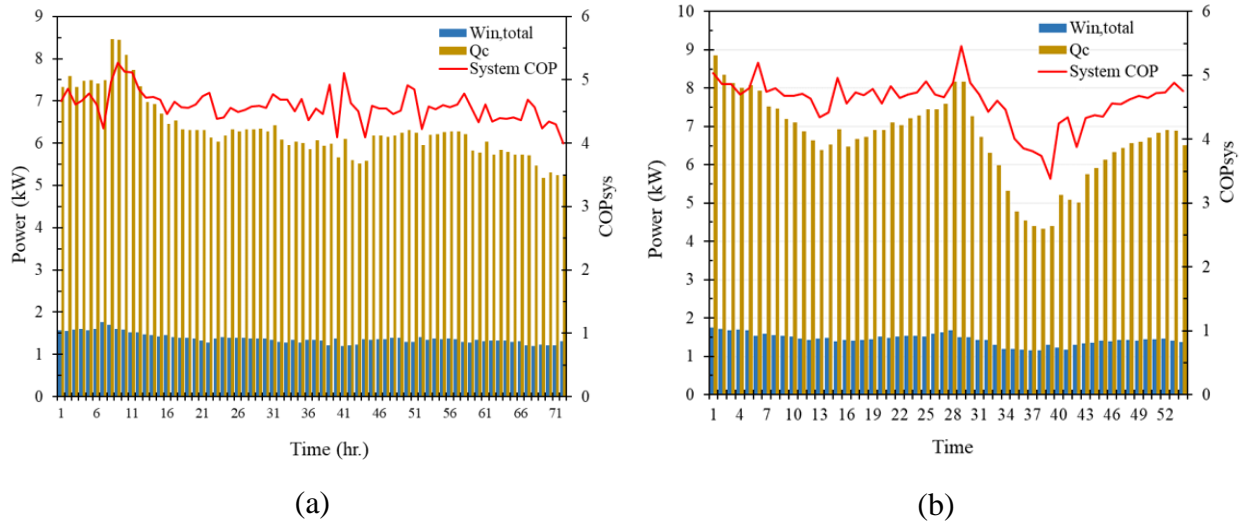


Figure 4.21. Comparison of the system input power, thermal energy output, and COP: (a) Test #5; (b) Test #7

The heat pump’s operational details were investigated since the system’s performance highly depends on them. Figure 4.22 illustrates the number of cycles and the operational time of the heat pump during each hour of the test. The heat pump usually has 6 cycles per hour; however, when the ambient temperature rises, the number of cycles and operational time decrease due to the smaller heat demand. The results demonstrated that the operational time has a direct relationship with the COP_{sys} , meaning that an increase in the time that the heat pump operates results in more heat generation and an eventual increase in COP_{sys} .

With all the available power data, it is possible to determine the effectiveness of the various parameters on the system’s performance. Figure 4.23 shows the relationship between the total input power and the thermal energy output. A more prolonged heat pump operation uses more electricity, which results in higher thermal energy output by the heat pump. Similarly, as shown in Figure 4.24, as the thermal energy output increases, the COP of the system increases. The results

showed that while the thermal energy output of the system varied from 4.4 kW to 8.8 kW, the COP of the system varied between 3.7 and 5.4.

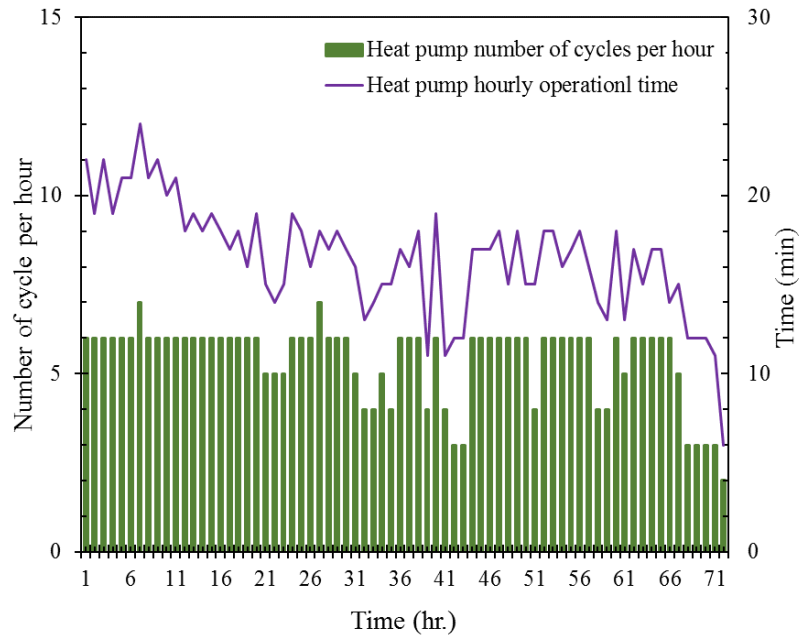


Figure 4.22. Details of heat pump operation during test #5

However, there is uncertainty in the calculation of the COP. The uncertainty in the calculation of the COP lies in the uncertainties of the measurement of the parameters used in the calculation. The accuracy of the instrument has already shown in Table 4.5. The high/low bound value of each parameter can be calculated using the possible error in the measurements. The result of the uncertainty analysis showed the COP varies from a minimum of 3.65 to a maximum of 5.55. It worth mentioning that the COP outcome of the uncertainty analysis is in good correspondence with Figure 4.24 which shows the COP of the systems varied between 3.7 and 5.4 at different hours.

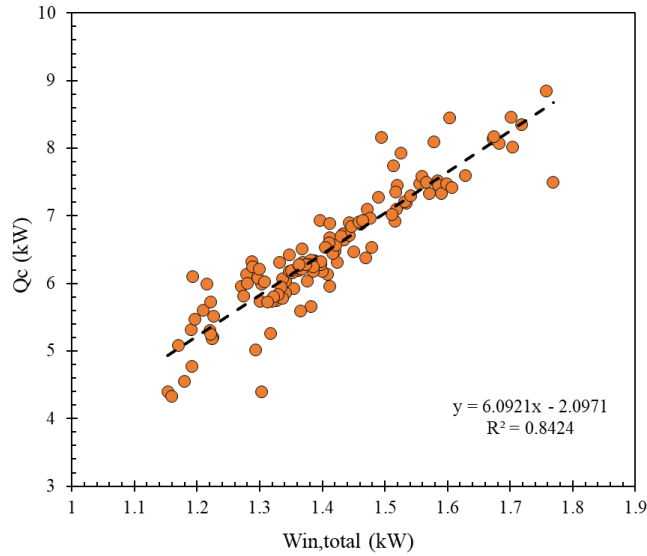


Figure 4.23. Relationship between the thermal energy output of the heat pump and the total power input to the system

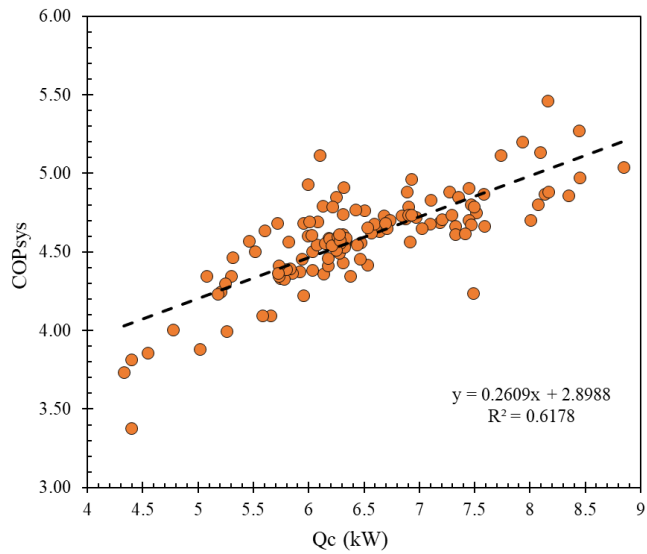


Figure 4.24. Relationship between the system COP and thermal energy output of the heat pump

A comparison of the system performance of this study with a similar GSHP system demonstrated that the system used in this study was efficient. Many research groups have studied the performance of the GSHP systems, including (Al-Habaibeh et al. 2018; Bakirci 2010; Bi et al. 2009; Kong et al. 2017; Liu et al. 2017; Ozyurt and Ekinci 2011; Roy et al. 2020). (Al-Habaibeh

et al. 2018) investigated the application of GSHP for mine water, in which the single-shaft system used the energy from flooded coal mines. For this specific case, the average daily COP of the whole system was about 1.5 (Al-Habaibeh et al. 2018). Ozyurt and Ekinici studied the performance of a ground-source heat pump system with a vertical ground heat exchanger that was to be used to heat a building in Turkey (Ozyurt and Ekinici 2011). They found the COP of the system to be in the range of 2.07–3.04. (Bakirci 2010; Bi et al. 2009) also presented different studies on the performance of the GSHP system, and reported the system COP to be in the range of 3.2–4 and 2.6–2.9, respectively. As GHDSs are less common, only a few researchers, such as [19], studied their performance. Balbay and Esen investigated the performance of the snow melting systems using a GSHP and found that the COP values of the GSHP system were 1.99, 2.66, and 3.05 for borehole depths of 30 m, 60 m, and 90 m, respectively.

4.4.4 Heat Flux Analysis and Heating Efficiency

The objective of the heat flux is to maintain an average bridge surface temperature above freezing during cold weather. However, the heat flux only demonstrates the maximum potential output of the system; it conveys no information about the actual energy consumption of the system over the course of a heating period since it is only specified for extreme weather conditions (Spitler and Ramamoorthy 2000). The supplied and surface heat flux of the bridge deck can be calculated using Equations 4.5 and 4.6, respectively.

$$q_{supplied} = \frac{Q_c}{A_{heated}} \quad (4.5)$$

$$q_{surface} = k \frac{dT}{dX} \quad (4.6)$$

Where Q_c is the thermal energy output produced by the heat pump (heat transferred in the condenser) can be calculated from Equation 4.3, A_{heated} is the area of the heated zone; k is the

thermal conductivity of the deck concrete; dT/dX is the temperature gradient. It is assumed that the heat transfer inside the concrete slab is one-dimensional and upward. The thermal conductivity of the mock-up bridge deck is 2.16 W/m.K according to the on-site measurements.

The supplied heat flux (q_{supplied}) represents the supplied heat flux of the geothermal heat pump system to the bridge, while bridge deck surface heat flux (q_{surface}) is the actual heat flux on the plane 2.5 cm below the top surface of the bridge deck. q_{surface} is the key outcome of the system and a critical parameter in designing the de-icing system. The temperature measurements of the two sensors located in the middle of the externally heated zone at two different depths were used to calculate the heat flux on the bridge deck surface (q_{surface}). As the temperature at the exact top surface of the bridge deck was not available, the sensor at 2.5 cm below the surface plane (Figure 4.10 (a)) was selected. Another node sensor, Type-T thermocouple, at the same coordinate, was installed at the bottom surface 0.6 cm into the concrete, to represent the temperature at the bottom surface of the bridge deck. The distance between the two sensors was 17.14 cm. It is assumed the heat flux on the top surface is similar to the plane at 2.5 cm below the surface. Figure 4.25 illustrates the temperature variations of the bottom surface and the plane at 2.5 cm below the surface. The temperature measurements of the two planes were similar before and after the test, with some time delays; however, during the test, there was a huge temperature difference between the two locations. Also, Figure 4.26 compares the supplied and surface heat flux of the bridge along with the ambient temperature variations. It can be observed that the heat flux increases when the ambient temperature decreases. The results show that the heat flux of the bridge deck varies with ambient temperatures and heating conditions. On average, the actual heat flux of the bridge deck surface was about 150 W/m² less than the supplied heat flux to the bridge, which can be explained by the heat loss.

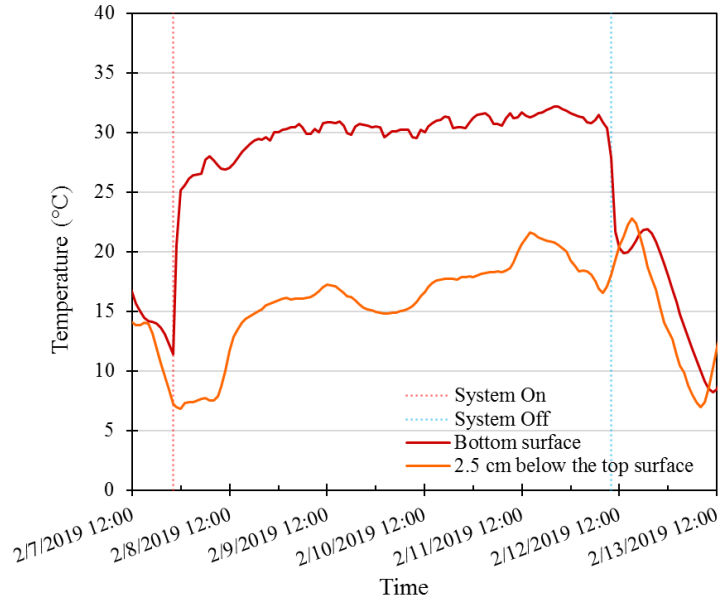


Figure 4.25. Temperature variations of the bottom surface and the plane at 2.5 cm below the surface during winter test #5

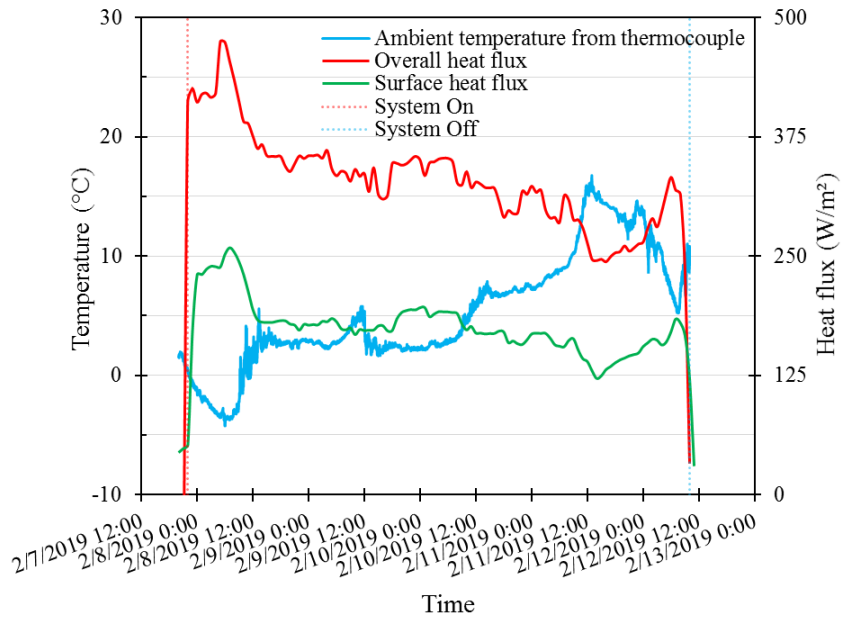


Figure 4.26. Comparison of the heat flux on the bridge deck surface and supplied heat flux during winter test #5

Table 4.8 list the summary of the heat flux analysis during the freezing ambient of Test #5.

It was found that during freezing ambient temperatures, the average supplied, and surface heat flux

was about 433.4 W/m² and 236.2 W/m², respectively. The supplied heat flux to the bridge deck, however, was different than the heat flux at the bridge deck surface due to heat loss. Insufficient insulation of the pipes and bottom surface of the externally heated zone were among the main causes of heat loss. The heat transfer efficiency of the system can be calculated by Equation 4.7. The system allows approximately 55% of the supplied heat, to the bridge deck surface. Also, comparing the external heating system efficiency of the field and laboratory test shows a nearly similar result, however, about 5 % less efficient in the field performance which is mostly due to the greater thickness of the concrete slab and colder environmental conditions.

$$\text{Heat Transfer Efficiency (\%)} = \left(\frac{q_{\text{surface}}}{q_{\text{supplied}}} \right) \times 100 \quad (4.7)$$

Table 4.8. Summary of the heat flux analysis and heat transfer efficiency

Parameter	Value
Required surface heat flux	340.2 W/m ²
Preliminary design surface heat flux	524.7 W/m ²
Initial guess of heat transfer efficiency	65%
Average supplied heat flux of Test #5	433.4 W/m ²
Average surface heat flux of Test #5	236.2 W/m ²
Actual Heat transfer efficiency	55 %

Finally, a comparison between the required surface heat flux for de-icing the bridge deck surface and actual surface heat flux shows the system was not able to provide the required heat flux on the surface in this test. As mentioned previously, in the external heating system, the large distance between the heating source (hydronic pipe) and bridge deck surface results in more heat loss in comparison with an internal heating design where hydronic loops are embedded in the concrete deck and installed in the vicinity of the bridge deck surface. The result shows the initial

guess for the heat transfer efficiency was close to the actual heat transfer efficiency of the system during Test #5. However, to provide the heat flux of 340.2 W/m^2 on the bridge deck surface, the design surface heat flux of the external geothermal heating system should have been considered as 618.5 W/m^2 , which recognizes 45% heat loss in the bridge deck. Thus, when designing the external heating system, it is critical to consider the accurate amount of heat loss in the design step. The design snow melting/de-icing of the external geothermal heating system ($q_{external\ design}$) in the future should follow Equation 4.8.

$$q_{external\ design} = \frac{\text{required surface heat flux}}{0.55} \quad (4.8)$$

4.5 Summary and Conclusions

An externally heated geothermal de-icing system was developed and implemented on a 20 cm thick concrete full-scale bridge deck, located in the Dallas-Fort Worth metroplex in Texas, USA. The de-icing system consists of eight PEX pipe loops attached to the bridge deck, one single-U 131 m deep GLHE, four water pumps, and one 3-ton GSHP. The design, construction, and implementation procedure of the de-icing system are first presented. The geothermal bridge was fully instrumented and tested during a series of winter events. The collected data were analyzed to evaluate the heating performance and efficiency of the de-icing system. The conclusions are drawn as follows:

- The 17.8 m² heated area on the bridge deck was observed free of ice and maintained minimum surface temperature above freezing during all seven winter events.
- Among all the seven winter tests, the minimum surface temperature of 1.4 °C was observed during a severely cold winter with a minimum freezing temperature of -6.2 °C. The

supplied fluid from the GLHE to the bridge deck was observed to have a temperature around 40°C in this coldest winter test.

- It took a minimum of 7-8 hours for the de-icing system to reach its peak performance at –3.9 °C ambient temperature. The time was less for mild winter weather.
- The monitored data illustrates an average temperature of 16.5 °C for the inlet water to the borehole, while the water returning from 131 m deep borehole was recorded as about 16.9 °C during the system’s operation in Test #5. Also, the use of a bypass operation with no geothermal heat pump in de-icing was found to be practical for mild winter weather conditions, in which the bridge deck was heated with about 16.6 °C fluid rather than 40 °C from the geothermal heat pump.
- On average, the power input to the water pumps and heat pump was about 1.4 kW. The system thermal energy output rate varied from 4.4 kW to 8.8 kW; and the system COP varied between 3.7 and 5.4, with an average of 4.6. An increase in the heat pump operating time resulted in the higher thermal energy output of the heat pump and an increase in the COP of the system.
- In winter test #5, the supplied and surface heat fluxes were estimated to be about 433.4 W/m² and 236.2 W/m² respectively, when the ambient temperature was below freezing. The surface heat flux on the bridge deck was sensitive to the ambient temperature and heating conditions.
- The external heating system was able to transfer about 55% of the supplied heat to the bridge deck surface, implying that 45 % of the total heat is lost during the heating process. Thus, it is suggested to consider 45% heat loss of the system when calculating the design surface heat flux of the external geothermal heating system.

CHAPTER 5: A U-TUBE GROUND HEAT EXCHANGER FOR BRIDGE DE-ICING: SOLAR COLLECTOR AND DE-ICING TEST, GROUND HEAT RECOVERY, AND OPERATION STRATEGY

5.1 Abstract

This study focuses on the evaluation of the energy performance and subsurface ground temperature distribution during the operation of geothermal foundation system for externally heating and de-icing of the bridge from freezing to de-icing conditions. The geothermal system consists of a single U-tube ground heat exchanger of 131 m-deep, and a mock-up bridge deck of 17.8 m². In addition to monitoring the temperature of the fluid entering and exiting the heat exchanger, thermistor strings were embedded in temperature monitoring boreholes around the GHE to monitor changes in ground temperature with depth. The system performance for a 99-day period was monitored which includes a bridge solar-collector test in which heat carrier fluid transferred the heat from the bridge deck to the ground, and a de-icing test during which heat was extracted from the ground and transferred to the bridge deck. The heat injection during the bridge solar-collector test with an average of 5.7 W/m, resulted in a noticeable rise in the ground temperature surrounding the heat exchangers. The result showed 31.7-39.4% of stored thermal energy was preserved for utilization in the first winter de-icing test depending on the definition of the control volume. The influence zone radius of the GHE operation was also found to be 3.45 m which is equivalent to 2 times of the bridge deck surface area. Overall, two de-icing operation modes were studied, and the result showed the application of the heat pump in the system increases the heat extraction rate by 237%. The coefficient of performance (COP) was recorded 2.9 and 1.1 for the tests with and without the heat pump, respectively. The outcome of the field experimental studies and data collection performed over a year of operations showed that the heat injection into the soil by bridge solar-

collector was 54% more effective than heat extraction from the ground during the several de-icing tests performed in 2019 to 2020.

5.2 Introduction and Background

The harvest and utilization of shallow geothermal energy have increased in recent decades (International Energy Agency 2014). Geothermal energy has shown great potential due to the lack of environmental footprint, redundancy, and cost-effectiveness. It is a green and renewable source of energy and a reliable alternative to fossil fuels. The geothermal energy is harvested through the application of ground heat exchangers or energy geostructures including foundations, diaphragm walls, tunnel liners, or anchors and has been used for a variety of purposes such as thermal conditioning of a building (Barla et al. 2016; Binod et al. 2012; Brandl 2006; Laloui and Di Donna 2013; Laloui and Loria 2019; McCartney et al. 2016; Mimouni et al. 2014; Sterpi et al. 2018b). A more recent application of geothermal energy is used for de-icing or snow-melting of the bridge deck surfaces (Spitler and Ramamoorthy 2000). Many bridges become treacherous and experience snow or freezing related accidents due to bridge deck being iced during prolonged cold periods or during winter storm conditions. As, over 70% of the united states' roads and population are located in snowy regions, which receive more than 13 cm average snowfall annually, many accidents are reported due to the slippery road surface condition. Weather-related car accidents are responsible for 24% of all crashes each year, including accidents on snowy, slushy or icy pavement, and 15% during snowfall or sleet. Approximately 1,300 people are killed and 116,800 injured annually in car crashes as result of snowy, slushy, and icy pavements (FHWA 2020).

Transportation agencies use various methods for de-icing operations. Chemical methods include using solid chemicals and liquid-spraying equipment with a variety of de-icing and anti-icing chemicals and mechanical methods include the use of snow-removal equipment such as snow

plows, snow blowers, snow brooms, and sweepers (Anand et al. 2017). Majority of them are not effective and some may have environmental issues. One of the promising technologies that has been under research evaluation by both UTA and TAMU researchers is the geothermal based shallow foundation system. A geothermal heat pump de-icing system (GHDS) was developed which is powered by geothermal energy. GHDS is a ground source heat pump system (GSHP) that uses the heat output of the system for snow melting and de-icing purposes. In this system, the heat carrier fluid, mostly water-based antifreeze solution, is circulated between the ground loop heat exchanger (GHE) and hydronic heating loops in contact with the bridge deck. Moreover, the heat pump is employed in the system to help the heat carrier fluid reach the ideal temperature appropriate for melting snow and ice on the surface. The life-cycle cost-benefit analysis (LCCBA) of this system indicated that its application is economically viable for the bridges with a minimum annual daily traffic volume of 7000 vehicles, and benefit to cost ratio (BCR) of 2.6 can be achieved for the 50-year life-cycle and daily traffic volume of 24000 vehicles (Habibzadeh-Bigdarvish et al. 2019).

The ground heat exchangers (GHEs) are the main components of the geothermal systems, and they play a vital role in keeping the system running efficiently. A high initial cost on GHE prevents the widespread application of the technology. An in-depth understanding of the heat transfer characteristics of GHEs is paramount to designing an underground soil energy system with high efficiency and low operating costs. Investigation of the heat transfer of GHEs is therefore essential (Zhang et al. 2020). In recent years, there have been many studies concentrating on accurate estimation of heat transfer inside and around borehole using numerical and experimental studies (Javadi et al. 2019; Noorollahi et al. 2018; Zhang et al. 2018). However, in contrast to numerical modeling, only a limited number of full-scale experimental studies are available which

has investigated the heat transfer inside and around boreholes. In one of the earlier studies, the temperature profile inside a 151.4 m downhole coaxial heat exchanger (DCHE) in a snow-melting system in Japan was investigated (Morita and Tago 2005). The authors studied the impact of the DCHE operation on the temperature profile inside the geothermal borehole. Observing the temperature changes in this formation, they concluded that the DCHE temperature is sensitive to the heat balance between charged and extracted heat. The amounts of extracted heat were significantly more than charged heat on a fiscal year basis. They suggested the most effective way would be to reduce unnecessary snow-melting operations, which might also lead to better performance.

Another study examined the temperature fluctuations of heat exchange wells to determine how thermal changes in the subsurface are caused by heat exchange with the ground. A computer program was used to simulate the long-term effects of underground temperature change by the authors (Fujimitsu et al. 2010). Gao et al. (2013) studied the thermal interaction between pumping and injecting well groups, and it was found that the impact of thermal interaction would result in an influence on the performance efficiency of the system. The result revealed the well location and their layout was a vital key to the thermal breakthrough. In a recent study, the transient changes in ground temperatures in a field-scale SBTES system installed in the vadose zone of Golden, Colorado, were experimentally and numerically studied. The experiment result showed that after 75 days of heat injection at a constant rate of 20 W/m, the ground temperature in the array increased by 7 °C. The result also showed that only 21-42% of the total 11.5 GJ thermal energy is stored in the soil (Başer et al. 2016). In a similar study by the same authors, transient ground temperatures was investigated in a field-scale soil-borehole thermal energy storage (SBTES) system in San Diego, California (Başer and McCartney 2020). The SBTES system consists of an array of thirteen

15 m-deep borehole heat exchanger at 1.5 m spacing. In a 4-month period, heat collected from solar thermal panels and injected into the SBTES system, which followed by monitoring the subsurface for about 5-month ambient cooling period. Authors also developed numerical model for coupled heat transfer and water flow and compared the measured data compared with those predicted by the model. In general, a good match was found between the experimental measurements of ground temperature in the SBTES and those simulated. Also, several lab-based experiments have been conducted to explore this issue. For example, Zhang et al. (2020) designed and constructed a lab-scale experimental system based on similitude laws to study the heat transfer behavior in underground soil. They proposed a transient 3D numerical model to evaluate the variation of temperature around full-scale GHE and performed model validation with the sandbox data set. Overall, they tried to produce a more reliable source of data and foundation with fast engineering applications for underground energy storage systems, such as GSHP, ground energy pile, etc.

A significant disadvantage of GHEs is the long-term variation in subsurface thermal conditions due to heat storage or removal in the ground (You et al. 2018; You and Yang 2020). The primary cause of this issue is GHE imbalance heat loading, which is more severe in hot summer and cold winter regions (Hakkaki-Fard et al. 2015). Several solutions have been suggested to address this problem. Current methods are typically dependent on refining design parameters, adjusting operation parameters, or implementing ground thermal recovery methods (Sedaghat et al. 2020). An analysis of GSHP system performance and the size of a vertical GHE system was conducted based on the variation of various design parameters (Cho and Choi 2014). The authors found that the ratio of GHE length to unit capacity was greatly affected by the thermal conductivity of the soil and the separation distance between GHEs, meaning they play an important role in the

thermal recovery of the soil and thermal exchange between GHEs. Also, the ground thermal load was numerically studied in relation to ground temperature (Baek et al. 2017). According to them, lowering the geothermal load and extending the recovery time would increase thermal recovery. Furthermore, they noted that using recovery time in the design method reduces the duration of GHE design.

Another solution proposed by many researchers is the intermittent operation of the GSHP (Choi et al. 2011; Chong et al. 2013; Shang et al. 2011; Zarrella et al. 2015). The intermittent operation allows the accumulated heat around the GHE to diffuse into the ground as the system is powered down. The efficiency of a GSHP system with varying thermal imbalance and heat recovery ratios was also investigated (Zhao et al. 2018). It was found that heat recovery not only improves system efficiency but is also cost-effective in hot summer and cold winter climates. A hybrid ground source heat pump (HGSHP) is paired with solar energy, waste heat, and ambient air to correct the thermal imbalance of a ground heat exchanger, depending on the local temperature. Optimization of configuration and control parameters is critical in these systems for ground thermal recovery. Coupling GSHPs with solar thermal collectors is a solution for imbalanced heat loads in cold-winter regions (Emmi et al. 2015).

Yang et al. (2015) studied the effect of combining the GSHP with a solar thermal collector experimentally. Their findings showed that the collected solar energy improves the GSHP's performance throughout the day. Additionally, the nighttime performance of the GHSP was improved by taking advantage of the excess solar energy that was collected during the day and stored in the ground. In another study, GSHP systems efficiency with borehole heat exchangers, solar thermal collectors, storage tanks, and ice thermal storage were examined (Rohde et al. 2018).

Using their modeling data, the models conclude that a greater amount of heat is absorbed from the ground during the winter than solar energy is injected during the summer.

The pavement solar collector (PSC) is another alternative for harvesting thermal energy that can be used for ground thermal compensation (Ahmad et al. 2019). In a PSC, pipe systems are commonly integrated into the upper layers of road constructions. A pavement surface absorbs solar radiation during sunny days, and that energy is transferred to the fluid inside the pipes, where it may be used to heat the fluid or stored for later use (Bobes-Jesus et al. 2013). Another benefit the PSC offers is that it reduces pavement temperatures. Lower temperatures are also a benefit for concrete pavements since smaller temperature fluctuations reduce thermal stresses in concrete slabs (Dehdezi 2014). Pavement solar collectors have been the subject of a number of experiments showing their ability to harvest energy. In the Netherlands, Loomans et al. (2003) investigated the energy efficiency of a pavement collector during summer with an average air temperature of 14 °C. Their results showed an energy efficiency of approximately 30%, indicating that 30% of the solar heat incoming on the pavement surface could be harvested. Mirzanimadi et al. (2018) examine the feasibility of the coupled Hydronic Heating Pavement (HHP) system to a Horizontal GHE (HGHE) for harvesting solar energy during summer and anti-icing road surfaces during winter. They found the amount of collected solar energy during summer is, on average, 99 kWh/m².year.

In a geothermal bridge deck snow melting/de-icing system, the ground thermal imbalance problem is a potential threat for the system efficiency due to single-mode operation. Because, despite the thermal conditioning of a building in which the GHE operates under both heating and cooling load, which automatically help the ground thermal balance, geothermal snow-melting/de-icing system only need to work in heating mode, i.e., heat extraction from the ground, which

provoke ground thermal imbalance. However, the solution lies in the application of the bridge deck as a solar collector. Bridge solar-collector is similar to pavement solar-collector, which uses the bridge deck for collecting solar energy. One of the pioneer applications of bridge solar-collector is the SERSO snow-melting system in Switzerland that works since 1994 (Eugster 2007). The SERSO system has demonstrated that an underground thermal energy storage system is feasible for storing solar energy. This system utilizes 91 borehole heat exchangers of 65m deep to maintain temperatures at or above 3°C on a bridge deck surface during the winter. Only the circulation of water within the pipes was powered by electricity, and no heat pump was used.

Bowers Jr and Olgun (2015) studied the thermal performance of a small-scale (2.6 m × 3.0 m) bridge deck de-icing system under bridge deck de-icing and thermal recharge operations. The energy piles were used as a means to harvest the geothermal energy. The authors examined both the bridge deck and the ground's temperature response during winter heating and summer recharge. Following the injection of thermal energy in the summer, the system was able to increase the temperature of the ground. The experimental result showed that the average of 0.16 °C of temperature rises along the pile at 1.7 m radial distance. The measured difference in temperature for the ground at 1.7 m radial distance was relative to the temperature difference of the ground at a distance of 3.5 m from the pile. Recently, Wu et al. (2020) also studied the performance of a bridge deck as a solar collector in a thermal energy storage system. The focus of the study was on the bridge deck, and the GHE performance and ground thermal condition were not studied. They found that about 26~47% of solar energy was collected by the bridge deck. However, although bridge solar collector was tested in few studies to address the thermal imbalance issue in the ground, so far, no study was found in the literature that fully investigated the bridge solar-collector impact on the thermal condition of the ground. Moreover, the energy performance, soil thermal

storage capacity, and thermal imbalance ratio (IR) due to the bridge solar-collector operation of GHDS are also open questions. Besides, very few full-scale experimental studies have investigated the GHE performance and heat transfer surrounding the GHE; Studying the GHE performance in a geothermal snow-melting/de-icing system is even a rarer topic.

In the past few years, the present research team has been working with Texas Department of Transportation (TxDOT), to develop an external geothermal de-icing system that can be implemented for existing bridges. First, the feasibility of the external geothermal de-icing system was studied through numerical simulation (Li et al. 2020, 2021). Then, several lab-scale experiments were also conducted, and the system performance was tested (Hurley 2019; Yu et al. 2019). Finally, a full-scale external geothermal de-icing system was implemented on a mock-up bridge and tested under actual winter weather conditions (Habibzadeh-Bigdarvish et al. 2021c). It allowed to fully study the externally attached hydronic heating system performance and thermal response of the bridge deck. Test results showed that the system was successful in de-icing the bridge deck and maintaining the bridge deck surface temperature above freezing. Moreover, this project provided an opportunity to study the GHE performance, soil thermal response in process of heat injection and extraction, application of the bridge deck as a solar collector as well as investigating thermal balance and thermal storage in the soil, which are the main objectives of the current study.

In this paper, first, an overview of the experimental setup, monitoring system, and testing site conditions for full scale bridge decks in the field conditions are reviewed. Then energy performance assessment methodology of geothermal system is discussed. It follows by investigating the thermal and energy performance of GHE during the heat injection and extraction tests on the bridge decks. Temperature variation of the soil mass surrounding the GHE in the events

of heat injection and extraction were collected with embedded sensors, thermal imagery and instrumentation and these results are analyzed extensively here. Both heat storage and thermal balance in the soil and temperature rise due to bridge solar-collector tests are determined and presented. Finally, it discusses the operation strategies of ground thermal system for better performance and de-icing operations of bridge deck.

5.3 External geothermal bridge deck de-icing system

5.3.1 Experimental Set-up and Monitoring System

A mock-up bridge has been constructed and an external geothermal heat pump de-icing system has been investigated to de-ice the snow/ice on the bridge deck surface. Figure 5.1 illustrates the schematic diagram of the mock-up geothermal bridge. The dimensions of the whole bridge slabs are 4.9 m × 11.4 m, including 12 standard PCP panels. The mock-up bridge deck consists of three zones: an external heating zone, an internal heating zone, and a control zone. It utilizes both the traditional type of GHDS, which uses internal hydronic pipe embedded in the concrete slab, and the newly developed method, which utilizes external hydronic pipe attached to the bottom surface of the bridge deck. Figure 5.2 (b) shows the overview of the hydronic heating systems on the bridge deck. The end section of the bridge deck is also considered as a control area with no heating. Also, the experimental field test setup consists of a geothermal borehole of 132.5 m (from ground level) deep and 14.6 cm diameter which hosted a single U-tube heat exchanger loops made of high-density polyethylene (HDPE) pipe with 3.45 cm inside diameter. The GHE was tested under combinations of operational modes and thermal loads. For the de-icing purpose, the system was operated in bypass or full-load mode, while the system was only worked in the bypass mode for bridge solar-collector operation. In the full-load operation mode, the control valves of the heat

pump are closed, and the flow goes through the heat pump. In the full load operation mode, the geothermal heat pump is active; while in bypass mode, the geothermal heat pump is off, and the heat carrier fluid circulates directly through the bypass which connects the bridge deck hydronic loops to the ground heat exchangers. Figure 5.2 (a) shows the control room and its components.

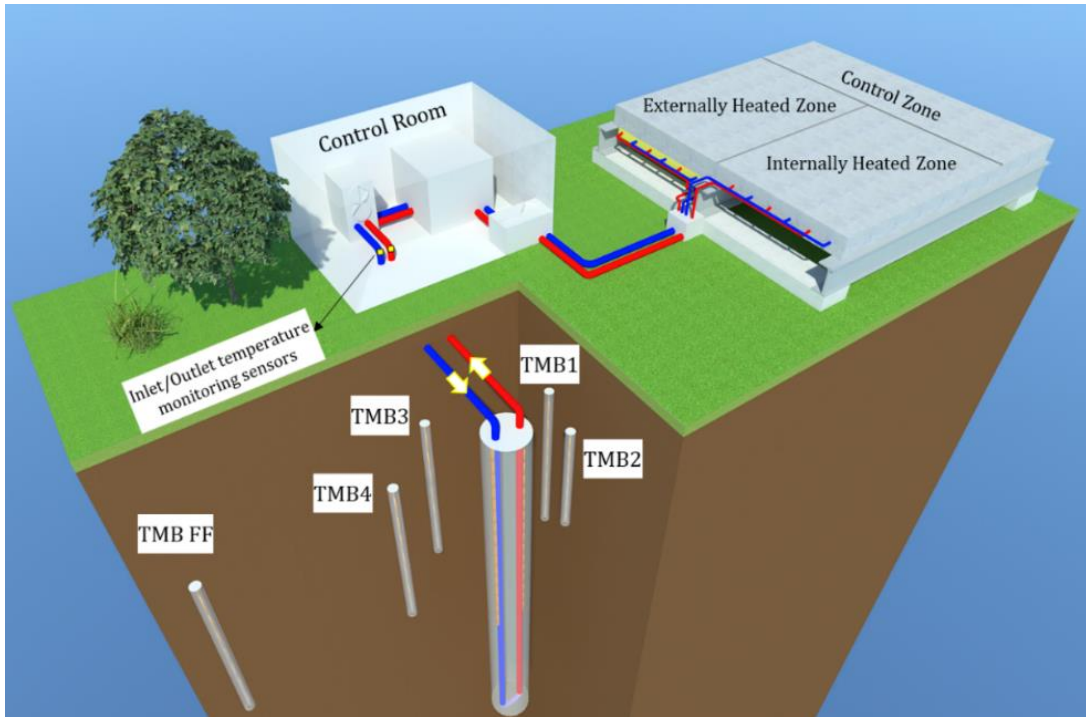
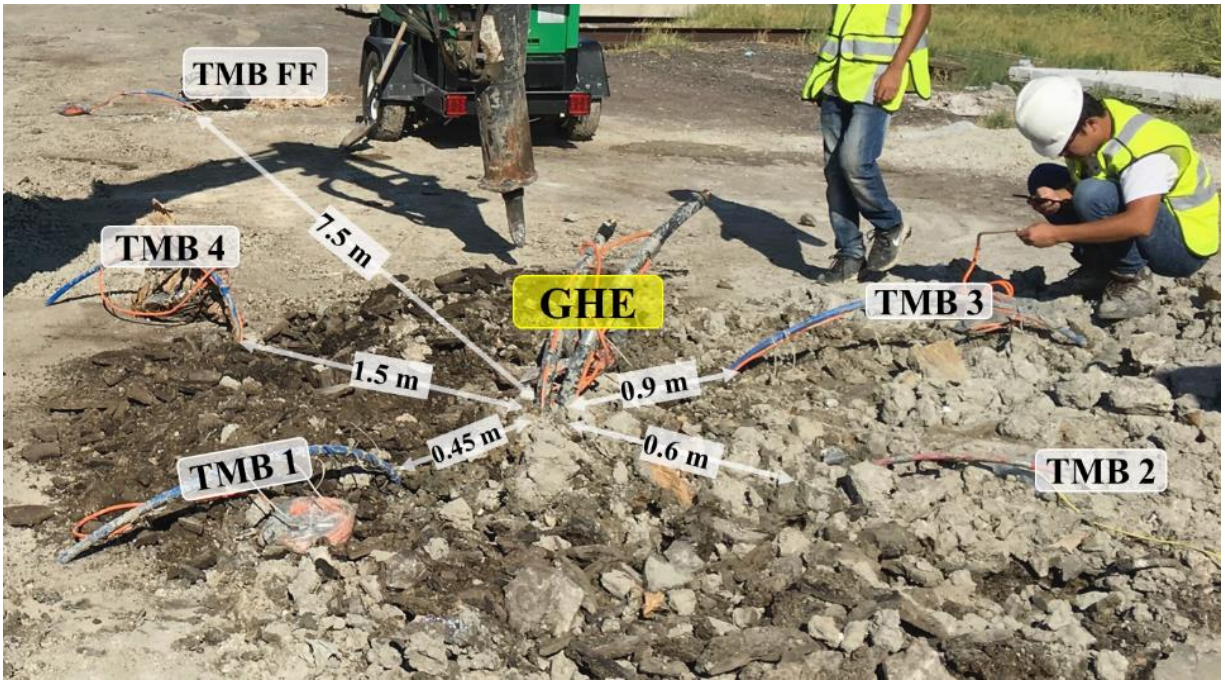


Figure 5.1. Schematic of the external geothermal heat pump de-icing system



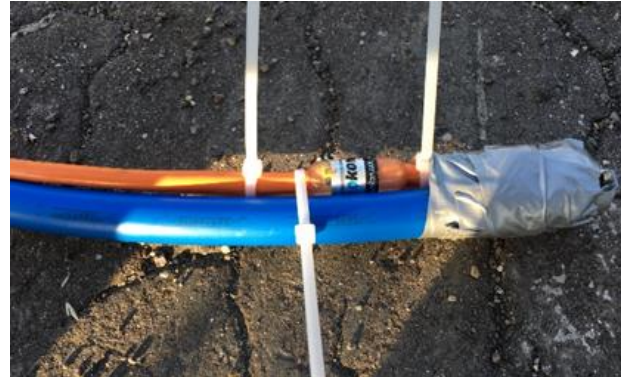
Figure 5.2. (a) Control room; (b) Bridge deck hydronic pipes



(a)



(b)



(c)

Figure 5.3. (a) Final stage of installation of the GHE and TMBs before excavation of trench and GHE connection to the header pipe; (b) Thermistor string attached to the heat exchanger pipe (c) Thermistor string attached to the PEX pipe that is filled with rebar for installation in TMB.

The subsurface monitoring system consists of five 10 cm diameter temperature monitoring boreholes (TMBs), which are equipped with thermistor strings and radially scattered around the geothermal borehole to investigate the temperature distribution in the soil and at different depths (Figure 5.3). Also, two thermistor strings were attached to the outer surface of the GHE legs to monitor the pipe and grout interface temperature variation. Table 5.1 shows the detail of the

thermistor strings' radial distance from the geothermal borehole central axis and the depths of sensor nodes on each string. An additional thermistor string was also attached to the header pipe in the trench to investigate the soil-pipe interface temperature variation in the trench.

Table 5.1. Details of installed thermistor string in the soil

Thermistor string	Inlet pipe	Outlet pipe	TMB 1	TMB 2	TMB 3	TMB 4	TMB FF
Radial Distance (m)	~0	~0	0.45	0.6	0.9	1.5	7.5
Sensor node	Depth from the surface (m)						
#1	0.8*	0.8*	0.6	0.6 m : 0.3 m : 14 m	0.9*	0.9	1.2
#2	1.1*	0.8*	1.8		1.5	1.8	4.0
#3	1.7*	1.1*	3.4		3.0	3.4	10.1
#4	2.3	2.3	6.4		6.1	6.4	19.2
#5	3.2	3.8	9.4*		9.1	9.4	n/a
#6	4.7*	5.3*	14.0		13.7	14.0	n/a
#7	6.2	6.9	18.6*		18.3*	18.6*	n/a
#8	7.8*	8.4	n/a		n/a	n/a	n/a
#9	9.3*	13.0*	n/a		n/a	n/a	n/a
#10	13.9*	17.5*	n/a		n/a	n/a	n/a
#11	18.4*	29.7	n/a		n/a	n/a	n/a
#12	30.6	n/a	n/a		n/a	n/a	n/a

* The sensor has malfunctioned.

5.3.2 Testing site

The mock-up of the externally heated bridge deck is constructed during February and March of 2018 in the Dallas-Fort Worth metroplex, Texas, USA. Figure 5.4 (a) shows the daily and monthly air temperature from August 2019 to August 2020. The minimum and maximum daily temperature of the testing site were recorded to be about 0 and 35 °C, respectively. Also, the weather history of the region showed the average annual rainfall precipitation is 95.3 cm for the average 81 days with precipitation per year. Moreover, on average, the region has experienced 5 cm of annual snowfall (Climate data of DFW international airport 2021). Although the region is familiar with mild winters, several snowstorms in recent years are experienced, such as the snowstorm on March

4-5, 2015, which was the fourth-largest ever recorded in a 24-hour period during March in the region. Over two days, 8.9 cm of snowfall and the average air temperature during snowfall was recorded around -2.2°C . Also, a very recent snowstorm on February 14-17, 2021, with 12.7 cm of snowfall. The minimum air temperature of -18.9°C was recorded, which was the second-lowest minimum temperature recorded in the history of the DFW metroplex (NOAA’s National Weather Service 2021). Moreover, Figure 5.4 (b) illustrates the average monthly ground temperature at different depths during a year at the testing site recorded by the Far-field TMB. The result shows that ground temperature beyond 10 m is relatively constant, but the soil closer to the ground surface shows huge variation.

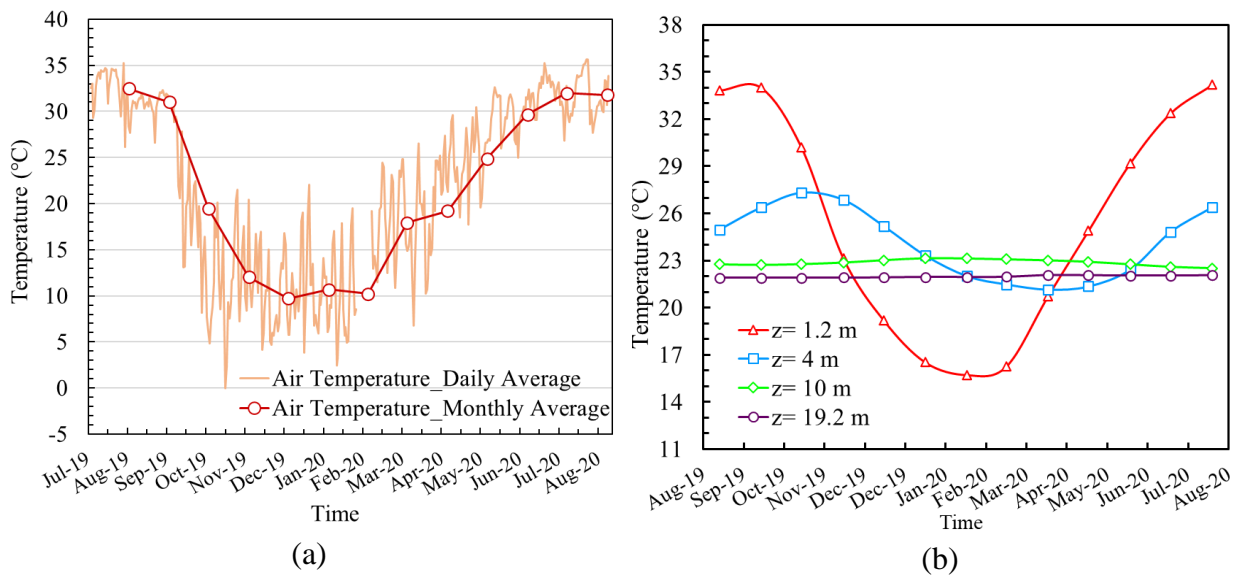


Figure 5.4. On-site recorded temperatures at the Geothermal Bridge in Arlington, TX: (a) Air temperature; (b) Subsurface soil temperature.

The subsurface investigation was carried out using the collected soil samples during the drilling of the geothermal borehole. Figure 5.5 illustrates a simplified boring log of the testing site. Soil classification has been carried out according to the Unified Soil Classification System (USCIS). The result shows that the site has relatively uniform soil layers: clayey sand (SC) covers

the top 24.3 m, followed by an 18.3 m layer of poorly graded sand (SP). A lean clay (CL) layer is extended from 42.7 m up to 134.1 m below the ground surface. Figure 5.5 also shows the density, thermal conductivity, and volumetric heat capacity variation along with the geothermal borehole profile for three different water content. The lab equipment did not allow for testing higher water content.

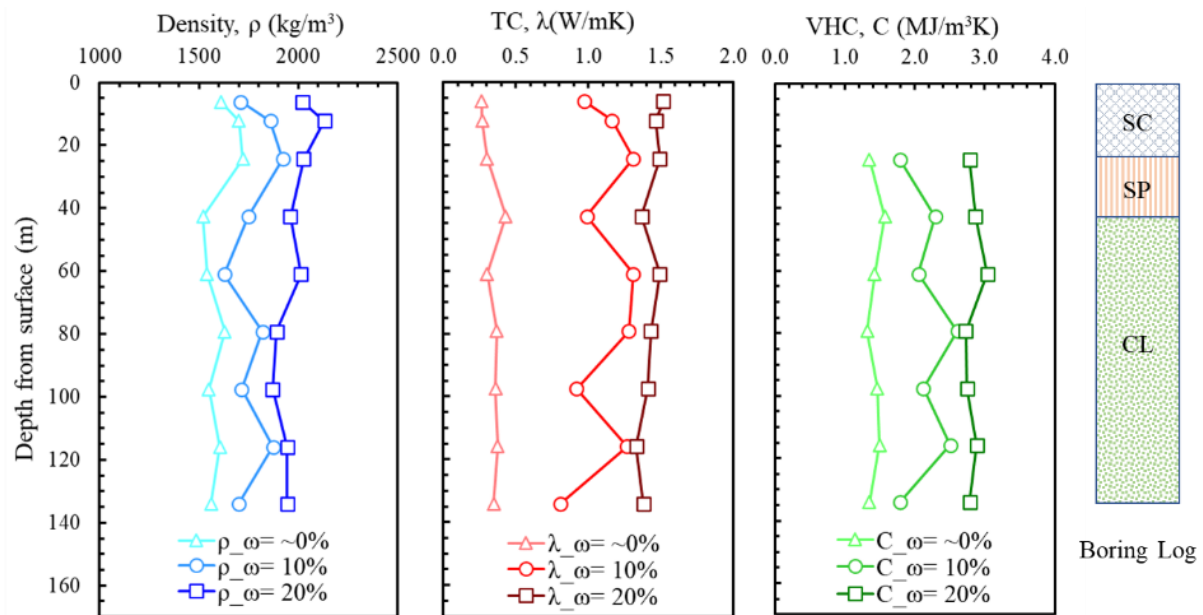


Figure 5.5. Subsurface soil characteristics profile

Moreover, the subsurface soil was studied using the boring logs of a nearby bridge provided by TxDOT. A selected simplified boring log is shown in Figure 5.6. According to the boring log, the site has relatively uniform soil layers which include a top layer of 4.5 m lean clay which follows by a 6.8 m layer of clayey sand. The boring log shows limestone layer below 11.3 m. The boring logs stop at 18.3 m. Based on the provided report, it is estimated that limestone is extended to a great depth beyond the interest of the project. Groundwater table encountered at 4.5 m below ground surface at the time of drilling.

Depth (m)	Symbol	Material Description
4.5	CL	Clay, brown, firm to very stiff, sandy, w/calcareous particles
11.3	SC	Clayey sand, brown, loos to dense, w/limestone gravel
18.3	Limestone	Limestone, shaly, gray, w/dark gray shale seams, w/calcite crystals

Figure 5.6. Simplified boring log of the testing site's nearby bridge.

There are some discrepancies between the TxDOT's boring log and the lab test results at UTA for the collected samples during drilling of the geothermal borehole. The authors believe, the provided boring log tends to be more accurate as limestone is more likely covers the great portion of the soil below 20 m. There might be error in the lab result mostly because the collected samples are disturbed and might have a mixture of soils at different depth. Also, Drillers used bentonite during the drilling for stability of the borehole wall which might have affected the collected soil samples. Additionally, samples are collected at discrete depths, 6 m for the top layers and every 20 m for the deep layers, so no information is available for the soil layers in between.

The thermal property of the grouting material was also tested for different water content in the lab. The grouting material was a mixture of 85% of bentonite and 15% of graphite. Figure 5.7 shows the relationship between thermal conductivity and volumetric heat capacity of the grout with water content. The lab test also revealed the grouting material had a dry and saturated density of 750 and 1200 kg/m³, respectively.

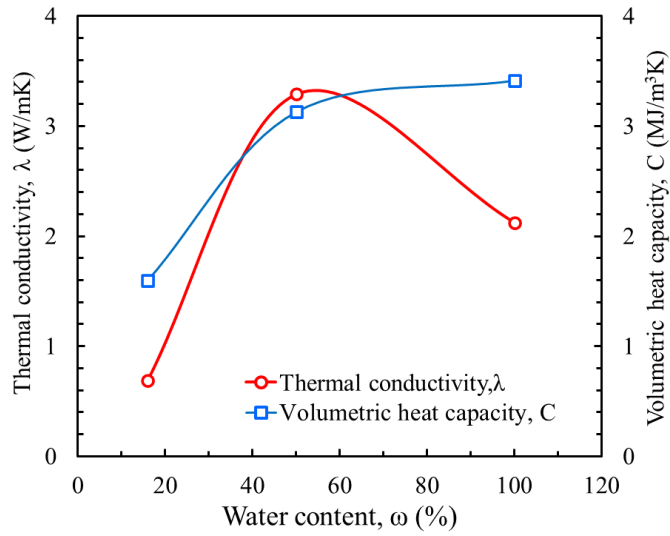


Figure 5.7. Variation of volumetric heat capacity and thermal conductivity with water content



Figure 5.8. Thermal response test apparatus at the site

Moreover, a formation thermal response test was carried out on site by a testing company (Figure 5.8). Figure 5.9 shows the result of the test which compares the GHE temperature and input heat rate versus the natural log of elapsed time. The company analyzed the temperature data versus time using the line source method. A linear curve fit was applied to the average of the

supply and return loop temperature data between 10 and 40.0 hours. The slope of the curve fit was found to be 5.54. Thermal conductivity was determined to be 1.99 W/mK. The calculated formation thermal conductivity was used along with an estimate of heat capacity to obtain the diffusivity value. This formation has been estimated to have a thermal diffusivity of 0.078 m²/day. Also, the undisturbed temperature of the soil was found to be about 21.5°C.

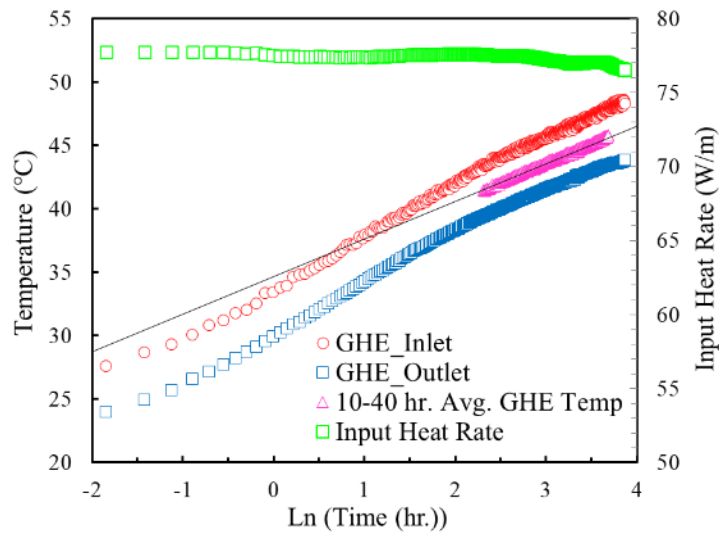


Figure 5.9. The on-site GHE thermal response test result

5.4 Energy performance assessment methodology

The energy performance of the GHE can be evaluated by using the coefficient of performance (COP). COP indicates the ratio of the total output energy of a system to its total consumption energy. The COP for the GHE in the process of heat extraction in bypass and full-load mode can be calculated using Equation 5.1 and 5.2, respectively. Also, Equation 5.3 can be used to compute the COP for the GHE during the bridge solar-collector operation.

$$COP_{Ext_bypass} = \frac{\dot{Q}_{Ext}}{\dot{W}_p} \quad (5.1)$$

$$COP_{Ext_full-load} = \frac{\dot{Q}_{Ext} + \dot{W}_{in,total}}{\dot{W}_{in,total}} \quad (5.2)$$

$$COP_{Inj_bypass} = \frac{\dot{Q}_{Inj}}{\dot{W}_p} \quad (5.3)$$

Where $\dot{Q}_{Ext/Inj}$, $\dot{W}_{in,total}$ are the heat transferred between GHE and ground, and total input power to the system, respectively. They are calculated using equations (5.4) and (5.5), respectively.

$$\dot{Q}_{Ext/Inj} = \dot{m}C_p(T_i - T_o) \quad (5.4)$$

$$\dot{W}_{in,total} = \dot{W}_{hp} + \dot{W}_p \quad (5.5)$$

Where \dot{m} , C_p , T_o , and T_i are the mass flow rate, the specific heat of the fluid, outlet, and inlet fluid temperatures of GHE, respectively. Moreover, \dot{W}_{hp} and \dot{W}_p are the power input to the heat pump unit and the circulating pumps, respectively.

The accumulated heat extraction during de-icing operation and the accumulated heat injection during bridge solar-collector operation can be calculated as:

$$Q_{AHE} = \sum_{i=1}^m \dot{Q}_{i,Ext} \times t_i \quad (5.6)$$

$$Q_{AHI} = \sum_{i=1}^n \dot{Q}_{i,Inj} \times t_i \quad (5.7)$$

Where m and n represent the number of heat extraction and injection events, and t_i is the duration of the event.

A thermal imbalance classification of GSHPS is determined by IR and is defined as (Zhao et al. 2018) :

$$IR = \frac{Q_{AHI} - Q_{AHE}}{\max(Q_{AHI}, Q_{AHE})} \times 100 \quad (5.8)$$

A positive IR means that the heat injected into the soil outweighs the extracted heat, a negative IR expresses heat extraction exceeds the heat injection to the ground. A lower IR indicates a smaller discrepancy between heating and cooling loads.

The average total thermal energy storage in the cylindrical soil mass surrounding the GHE can be quantified as follow (Claesson 1981):

$$Q_{Stored} = (T_s - T_a)C_v\pi r^2 H \quad (5.9)$$

Where T_s and T_a are the soil temperature in the storage zone and unaffected soil temperature in the surrounding subsurface; C_v represent the volumetric heat capacity of the soil; r is the radius of a cylindrical soil mass volume, and H is the height of the soil mass.

5.5 Field Investigation Result

This section discusses the thermal and energy performance the GHE and ground's thermal response due to GHE operation at two different tests, namely: heat injection during bridge solar-collector test, and heat extraction during bridge de-icing test. Soil temperatures were investigated using TMB,1,3, and 4; TMB2 was not utilized due to different string sensor type and availability of the data. Also, since studying the temperature variation inside the borehole and trench is not the focus of the current study they are not discussed in here.

5.5.1 Bridge Solar-Collector Test

5.5.1.1 Heat injection performance of GHE

To investigate the ground thermal recovery, the bridge solar-collector test was performed in the first summer following the completion of the mock-up geothermal bridge deck construction. The test spans from 8/8/2019 to 10/20/2019. The system was operated through the bypass mode in

which heat carrier fluid transferred the heat from the bridge deck to the ground. In this test, the fluid flow rate in GHE was 0.51 l/s. Figure 5.10 illustrate the inlet/outlet fluid temperature variation in comparison with ambient and bridge deck temperature during this test. Bridge deck temperature was recorded at 2.5 cm below the top surface. The average ambient temperature during the 74 days of the test was 29.4 °C. The bridge deck temperature shows a similar trend however with an average of 1.6 °C higher temperature with respect to ambient. This highlights the important role of solar radiation on the bridge deck temperature. Also, the average inlet and outlet fluid temperature from the GHE was recorded as 26.5 and 26.1 °C, respectively.

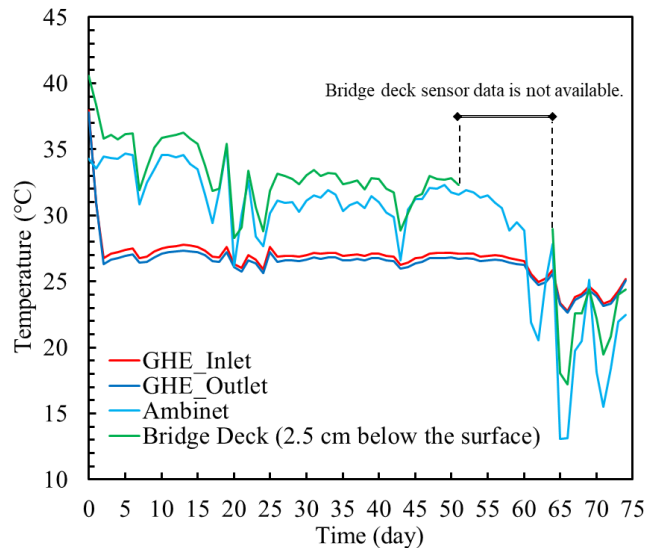


Figure 5.10. Inlet/Outlet fluid temperature for bridge solar-collector test

The heat transfer rate is calculated using Equation 5.4 and the result is shown in Figure 5.11(a). The average heat injection rate throughout the test was 0.75 kW. Overall, 1332 kWh of energy was injected into the soil. The bridge solar collector operation COP is also illustrated in Figure 5.11(a). It is calculated using Equation 5.3. For the bypass operation mode, the circulating pump power is recorded as 0.76 kW (Habibzadeh-Bigdarvish et al. 2021c). In the Bridge solar-

collector test, the system yielded an average COP of about 1; this means the amount of heat injected into the ground was equal to the amount consumed by circulating pumps. Moreover, the heat injection rate per unit length of GHE and heat collection rate by the bridge deck is shown in Figure 5.11(b). The average heat injection rate per unit length of the GHE was calculated as 5.7 W/m. The average heat collection by the bridge deck is 42.2 W/m².

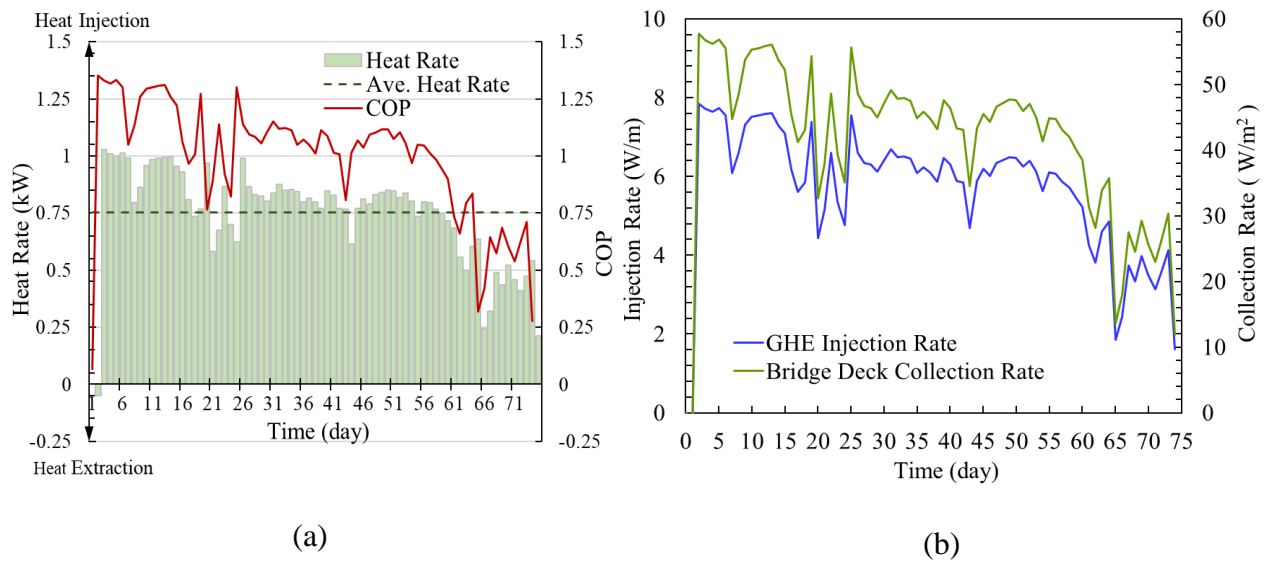


Figure 5.11. (a) Heat rate and COP variation; (b) Heat injection and collection rate during the bridge solar-collector test

5.5.1.2 Temperature profile of underground soil in the process of heat storage

The subsurface soil temperature variation was monitored for different depth and radial distances from GHE using the TMBs as shown previously. Figure 5.12 illustrates the average daily soil temperature profile for different radial distances and different times during the bridge solar-collector test. The day equal to zero represents the initial condition of the site before the test begins. In general, it is observed that the temperature of ground soil increases with time and changes more gradually at the further radial distances from GHE. Figure 5.12 (d) shows the far-field temperature

profile which receives no impacts from the GHE operation. The soil temperature below 10 m was relatively constant throughout the test and was not influenced by the atmospheric condition. It can be interpreted that the atmospheric condition influence zone at the testing site ranges from the ground surface up to around 10 m below the ground surface. The soil temperature in the influence zone was mostly increased following the hot air temperature during the test, however, in the final stages of the test soil temperature in the vicinity of the ground surface was decreased due to the air temperature drop in the last 14 days of the test. This observation is valid for all the TMBs.

Investigation of the soil temperature variation beyond the influence zone of the atmospheric condition is of high importance as the direct impact of the GHE operation on the soil temperature can be observed. The deepest sensor node (i.e. 14 m below the ground surface) of the TMB 1,3 and 4 is a good candidate to further explore the temperature variation due to GHE operation. The overall soil temperature following an increasing trend during the test, although the cold air temperature during the final stage of operation caused some temperature decrease in the soil. In all stages of the operation, the soil temperature reaction at 0.45 m radial distance shows a greater influence by the GHE operation than at 1.5 m radial distance. For the soil below the 10 m and for 0.45, 0.9, and 1.5 m radial distances, the bridge solar-collector test increased the soil temperature by 0.75, 0.48, and 0.35 °C, respectively.

Figure 5.13(a) illustrates the radial temperature profile at 14 m below the ground surface. The temperature at a radial distance equal to zero represents the average fluid temperature at the inlet and outlet point, However, the other temperature nodes are the soil temperature recorded by TMBs. For the initial time, the average inlet and outlet temperature has not been illustrated in the figure as it is not a good representative of the average fluid temperature due to lack of fluid circulation.

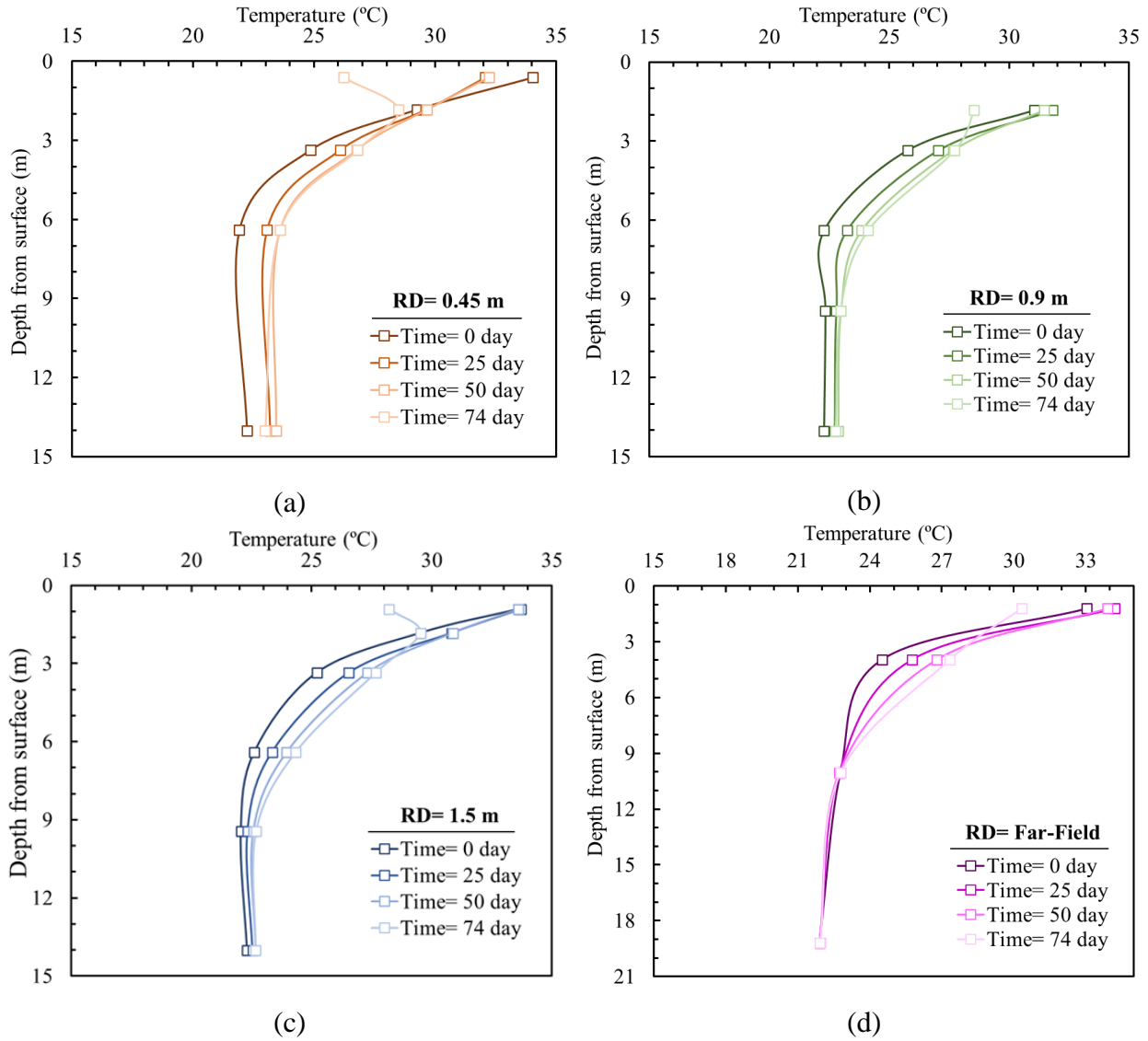


Figure 5.12. Ground temperature profile during bridge solar-collector test at different radial distances from GHE: (a) 0.45 m; (b) 0.9 m; (c) 1.5 m; (d) Far-field.

Figure 5.13 (a) shows a constant temperature at the initial condition however the operation of the system increased the temperature in soil, more temperature increase for the closer soil to the GHE and less for the further distance. Figure 5.13 (a) can also be used for the investigation of the temperature gradient (G) between the GHE fluid and the soil temperature as illustrated by the schematic. Figure 5.13 (b) shows higher thermal gradient exists for the closer soil to the GHE. The

average thermal gradient at 0.45 m radial distance is 2 and 3 times higher than that of 0.9 and 1.5 m radial distances, respectively. The maximum temperature gradients between GHE fluid and soil temperature corresponds to the peak of ambient temperature and consequently bridge deck temperature. According to the experiment results, a higher thermal gradient between the bridge deck and fluid results in a higher thermal gradient between the fluid and soil.

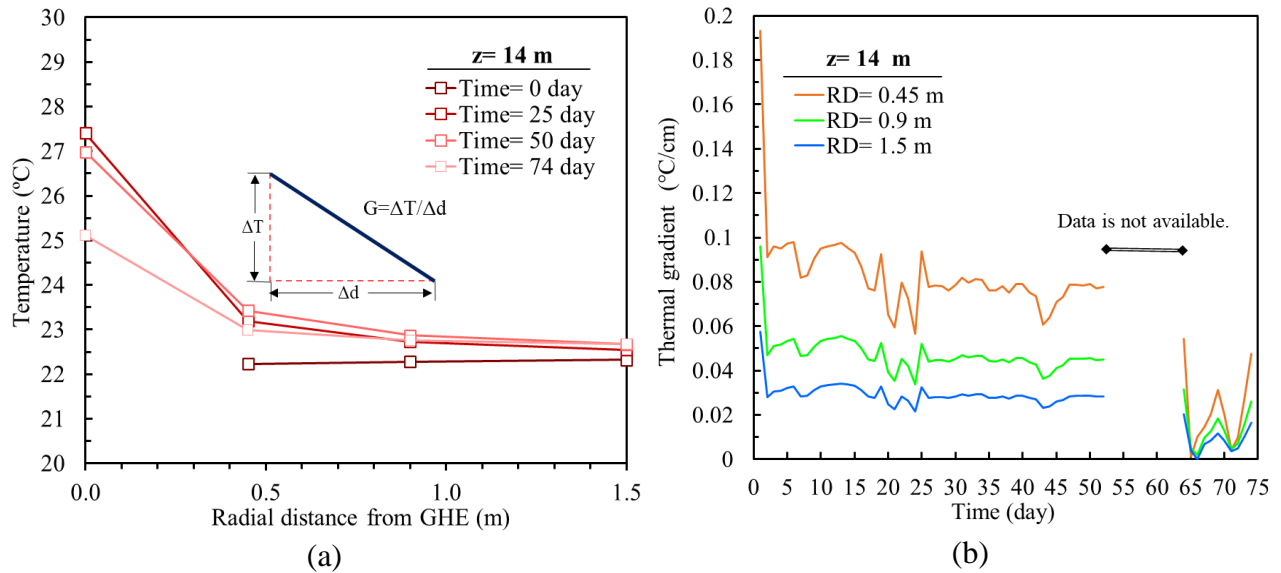


Figure 5.13. Radial temperature profiles (a) and thermal gradient (b) at 14 m below the ground surface during the bridge solar-collector test

Figure 5.14 illustrates the radial temperature distribution around GHE at 14 m below the surface and at different times of the bridge solar collector test. The radial temperature distribution plots were generated using MATLAB software employing the cubic interpolation method for scattered data collected from TMBs. Also, it is assumed that the temperature distribution is uniform in each direction around the GHE. It can be observed how the temperature in the soil has changed following the circulation of hot fluid in the GHE during the tests. The result states, the temperature

in the soil at 0.45 m, 0.9 m, and 1.5 m from geothermal borehole was increases by 0.82 °C, 0.6 °C, and 0.36 °C after 50 days of system operation.

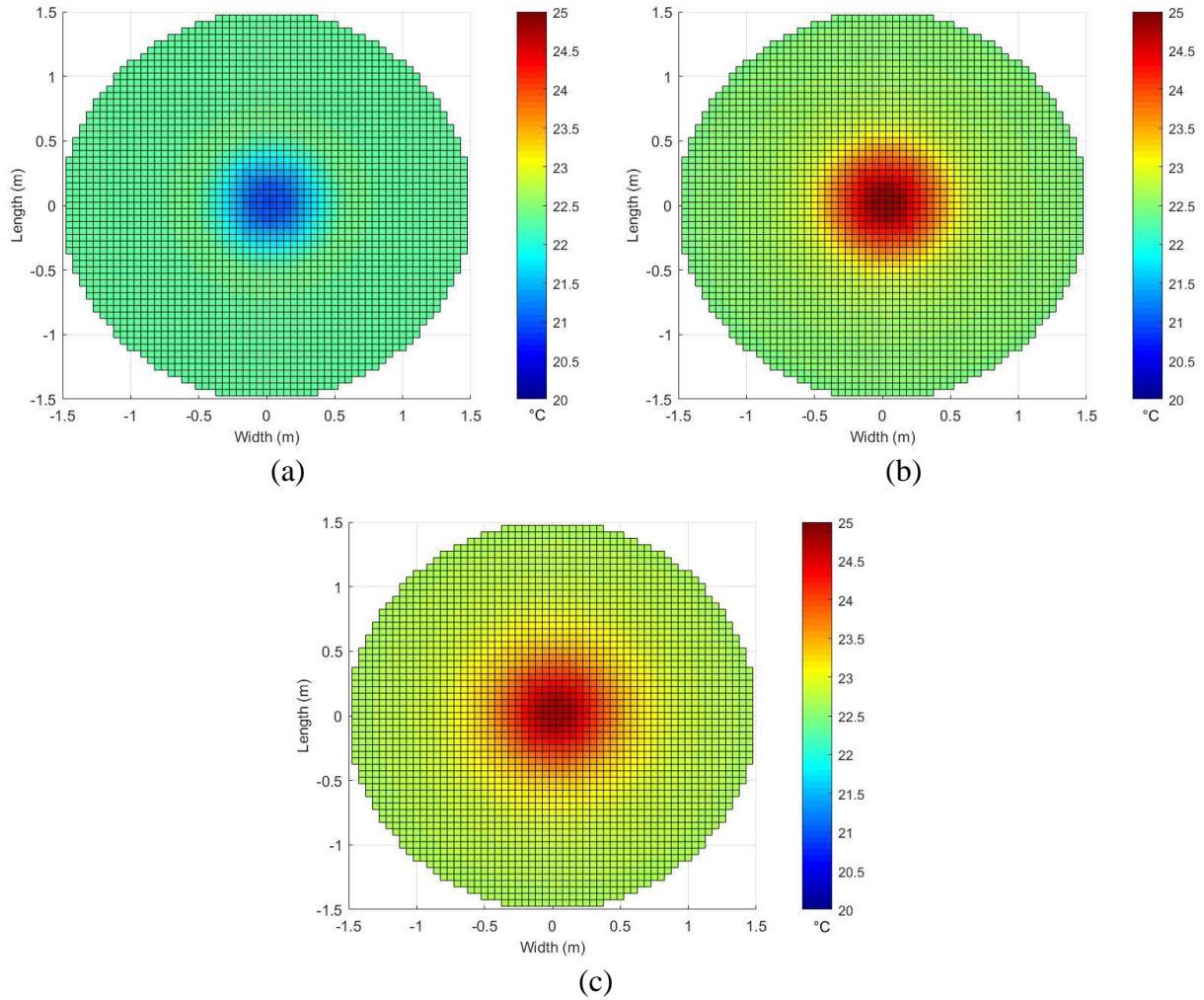


Figure 5.14. Temperature distribution of GHE’s surrounding soil at 14 m below the ground surface: (a) Before system onset, (b) 15 days after system onset, (c) 50 days after system onset. (Habibzadeh-Bigdarvish et al. 2020)

5.5.2 Bridge De-icing Test

During winter 2019-2020, a total of six de-icing tests were conducted. In this section, two representative de-icing tests has selected for discussion. The operation mode is the key difference between the two tests. For Test A, the system was operated in bypass mode however the Test B

worked in full-load mode and utilized the heat pump in the system. Table 5.2 highlights the key details of each test.

Table 5.2. Selected tests highlights

Test	Operation Mode	Duration (hr.)	GHE Flow Rate (l/s)	Freezing ambient temperature		
				# hr.	Average (°C)	Minimum (°C)
A	Bypass	80	0.56	25.00	-3.6	-5.9
B	Full-load	76	0.51	6.75	-1.2	-2.5

5.5.2.1 Heat extraction performance of GHE

The first de-icing test was performed in the first cold-weather following the bridge solar-collector test in summer. Test A spans from 11/11/2019 to 11/14/2019 and was performed in a bypass operation mode for a total of 80 hours in which the bridge deck was heated with heat carrier fluid directly circulated between the GHE and hydronic heating loops. The average ambient temperature during the 80 hours of the test was -3.6 °C and the minimum ambient temperature was recorded as -5.9 °C. During this test, the average inlet and outlet fluid temperature from the GHE was recorded as 16.6 and 17 °C, respectively. Bridge deck surface temperature was above freezing during the test with an average temperature of 8.6 °C.

The second test represents the de-icing tests which utilized a heat pump and operated in full-load mode. The test occurred on 2/5/2020 through 2/8/2020. The average inlet and outlet fluid temperatures during 76 hours of operation were 9.6 and 10.9 °C, respectively. Despite the milder winter weather condition, the result shows the heat pump has enhanced the heat extraction process as the inlet and outlet fluid temperatures were decreased in comparison to bypass mode operation. Also, although the fluid flow rate is smaller in Test B in comparison to Test A there is a larger gap between inlet and outlet temperature in comparison to that of bypass mode operation which is

another indicator that proves more heat was extracted in Test B due to application of the heat pump. The surface temperature for this test was monitored using a thermocouple installed on the top surface of the heated zone. Overall, the heating system maintained above freezing temperature on the surface. Figure 5.15 presents the heat carrier fluid temperature variation at the inlet and outlet point of the GHE and compares it with the bridge deck and ambient temperature.

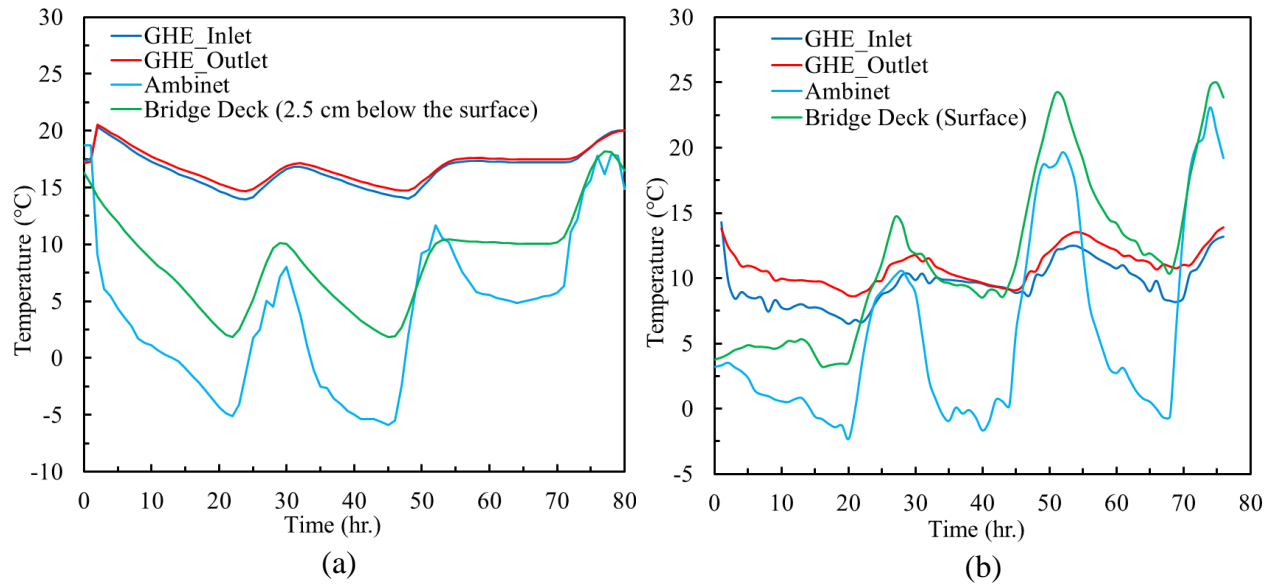


Figure 5.15. Comparison of Inlet/Outlet fluid temperature with bridge deck and ambient temperature: (a) Test A; (b) Test B.

The average hourly heat rate of the GHE for Test A and B is presented in Figure 5.16. The heat extraction rate was greatly affected by the ambient temperature, it was peaked during the minimum ambient temperature due to a larger gap between inlet and outlet temperature. In Test A, an average of 0.8 kW of energy was extracted per hour. The average heat extraction rate was increased to 2.7 kW for Test B, showing a 237% increase in heat extraction in comparison to test A. The system power during Test A is similar to the bridge solar-collector test and equal to 0.76 kW. However, as the electricity consumption was not monitored for Test B, the average power of 1.4 kW was considered for system operation in a full-load mode according to previous tests'

monitored result as discussed in the author's other paper (Habibzadeh-Bigdarvish et al. 2021c).

The average COP during Test A and B are 1.1 and 2.9, respectively.

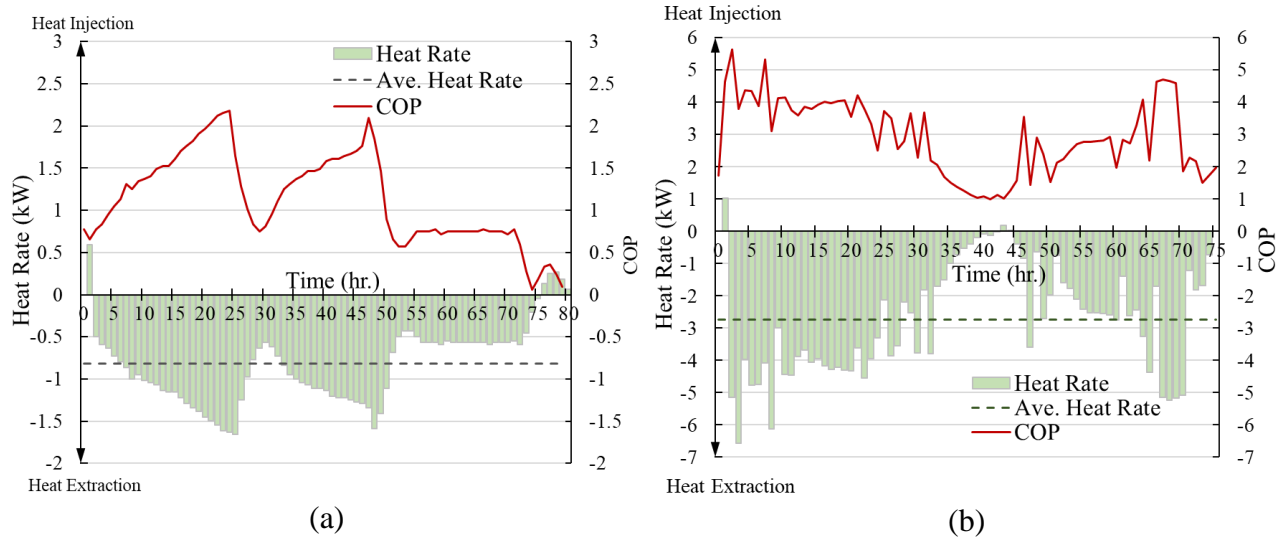


Figure 5.16. Heat rate and COP variation: (a) Test A; (b) Test B

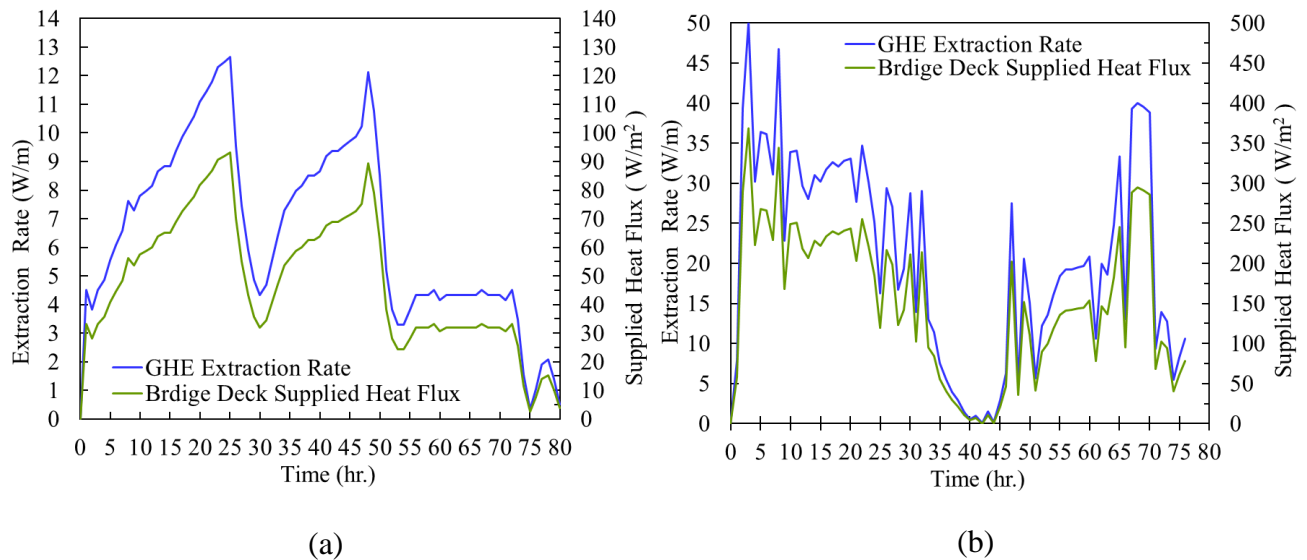


Figure 5.17. GHE extraction rate and supplied heat flux to the bridge deck: (a) Test A; (b) Test B.

Figure 5.17 illustrates the GHE extraction rate and supplied heat flux to the bridge deck for Test A and B. For Test A, the average GHE extraction rate was 6.5 W/m and supplied heat flux to

the heated area in the bridge deck recorded as 48.1 W/m^2 . However, for Test B the average GHE extraction and supplied heat flux was increased to 20.7 W/m and 152.6 W/m^2 , respectively.

5.5.2.2 Temperature profile of underground soil in the process of heat extraction

The ground temperature was reduced due to the operation of the system for de-icing Tests. Figures 5.18 and 5.19 illustrate the ground temperature in the vicinity of the GHE during Test A and B. During Test A, the temperature decreased in the top 4 m soil due to the atmospheric temperature drop as can be seen in Figure 5.18 (d). Below the 4 m, the temperature change is the pure outcome of the geothermal de-icing system operation. From the TMBs' result, the greatest impact was experienced by the soil at 0.45 m from GHE, the temperature drops can be seen for the entire length. For Test A, the average temperature drop along the vertical profile for the soil below the 4 m depth is $0.7 \text{ }^\circ\text{C}$ at 0.45 m radial distances; Temperature change is less significant for 0.9 m radial distance with $0.08 \text{ }^\circ\text{C}$ temperature decrease. It shows GHE operation impact at 0.45 m radial distance was about 9 times greater than that of 0.9 m radial distance. The soil temperature at 1.5 m radial distance showed no change due to GHE operation for the depth below the 4 m.

For Test B, the initial ground temperature for the near-surface soil shows a colder temperature than that of Test A. It is due to the 83 days gap between the two tests and the influence of atmospheric conditions on the near-surface soil during this time. Similarly, ground temperature was decreased during Test B as the heat was extracted by the GHE. The soil temperature at 0.45 m and 0.9 m radial distances were decreased by 1.3 and $0.17 \text{ }^\circ\text{C}$ along the vertical profile below the 4 m depth, respectively. The soil at 1.5 m radial distance has again received no impact by GHE operation. Following an analysis of all data, it was found that the GHE operation lasting less than 13 days would have little impact on soil temperature at 1.5 m radial distance, i.e., the soil temperature change would be less than $0.1 \text{ }^\circ\text{C}$. The GHE operation requires a minimum 10 hours

and 3 days period for soil temperatures at 0.45 and 0.9 m radial distances to be affected by a temperature change greater than 0.1 °C. Nevertheless, it is important to note that the intensity of the heating and cooling load, subsurface conditions, and thermal property of the soil can influence how quickly the soil temperature changes.

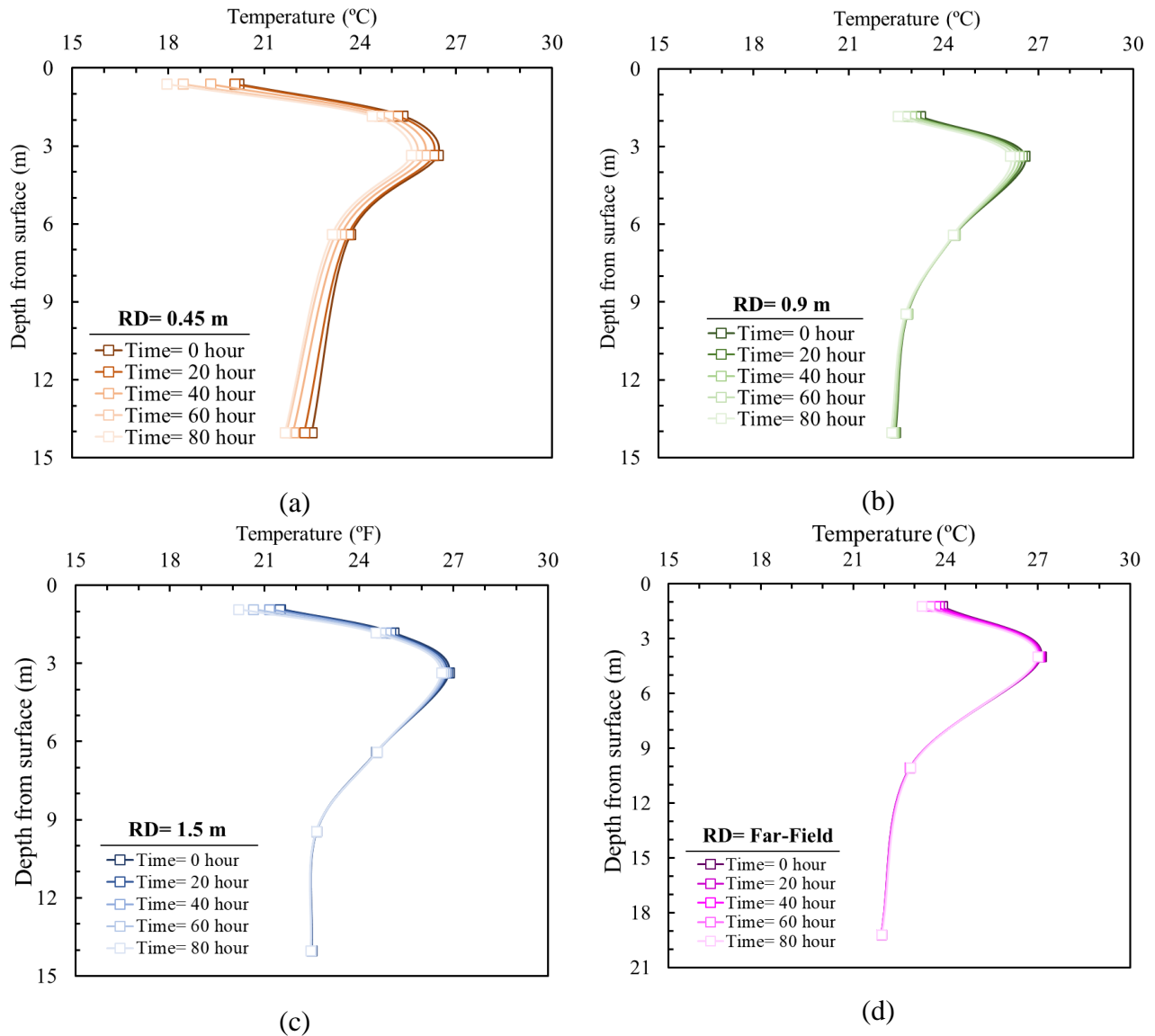


Figure 5.18. Ground temperature profile during Test A at different radial distance from GHE: : (a) 0.45 m; (b) 0.9 m; (c) 1.5 m; (d) Far-field.

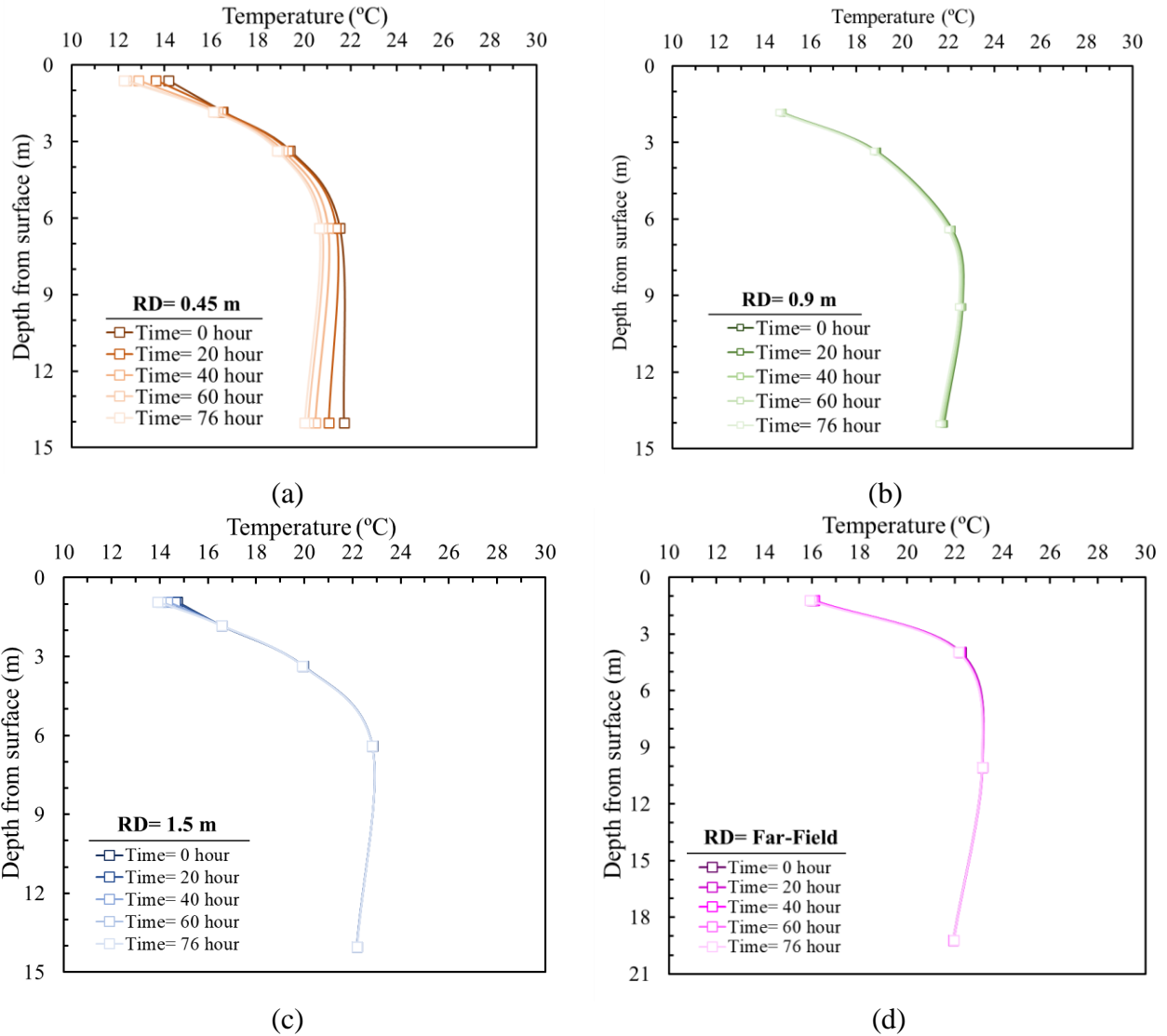


Figure 5.19. Ground temperature profile during Test B at different radial distances from GHE: : (a) 0.45 m; (b) 0.9 m; (c) 1.5 m; (d) Far-field.

The radial temperature profile at 14 m below the ground surface and thermal gradient were also investigated for Test A and B as illustrated in Figures 5.20 and 5.21. Both tests showed a constant radial temperature profile at the initial condition, however, Test B was about 0.6 °C colder. This is mainly due to the heat extraction in two previous tests since Test A was the first and Test B was the third de-icing test of the winter season. Although the initial temperature conditions in Test B were different from Test A, the heat pump's potential for higher heat extraction resulted in a greater

temperature gradient in Test B. The result shows on average the thermal gradient in Test B is 2 times higher than that of Test A.

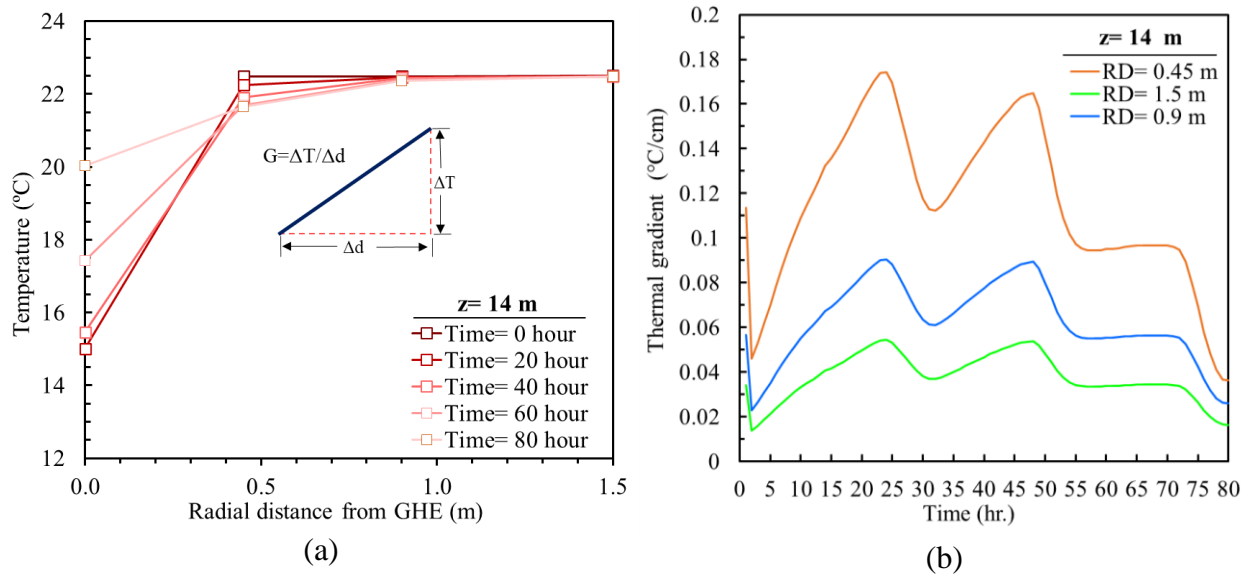


Figure 5.20. Radial temperature profiles (a) and thermal gradient (b) at 14 m below the ground surface during the de-icing Test A

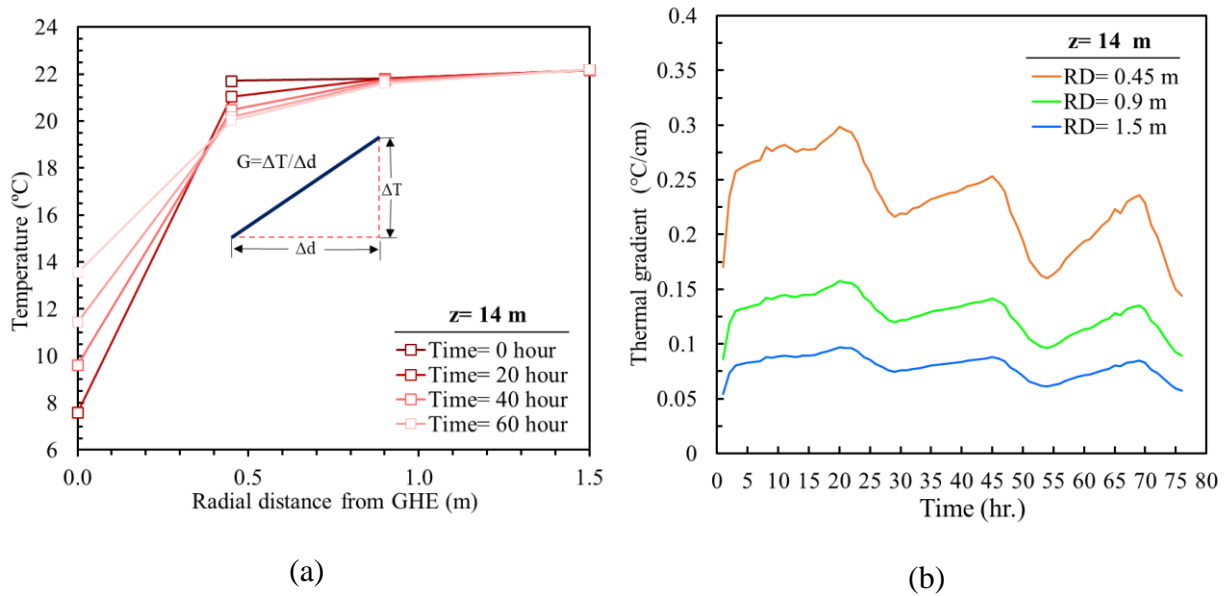


Figure 5.21. Radial temperature profiles (a) and thermal gradient (b) at 14 m below the ground surface during the de-icing Test B

5.5.3 Heat Storage and Extraction Analysis

Figure 5.22 illustrates the temperature variation in the soil at 14 m below the ground surface and for different radial distances from the start of the bridge solar-collector test until the end of the first de-icing test in the winter. The ground temperature shows a steady temperature around 22.3 °C before the start of the bridge solar-collector test. As the test began the soil temperature starts to rise; the increase in the soil is more gradual at the greater radial distances. The Bridge solar collector test can be divided into two sections, the first 60 days of operation, when the air temperature was varied between 26-35 °C, the soil temperature was increasing continuously due to high thermal difference between the bridge deck temperature and consequently fluid temperature, and the undisturbed ground temperature of 21.5 °C. Second, in the last 14 days in which the air temperature varied around 55-80 °F, the fluid temperature decreased due to the decrease in the bridge temperature following the air temperature drop. During this time, the GHE heat injection rate decreased in comparison with the first 60 days, or even its operation mode reversed and turn into heat extraction at some time instances.

Table 5.3 summarizes the key information for the thermal and energy response of the subsurface soil from bridge solar-collector test in summer to first bridge de-icing test in the winter. T_0 and T_{end} represent the temperature at the initial and final stage of the test. Overall, the ground temperature increase ($\Delta T_{Solar-collector Test}$) due to bridge solar-collector test was recorded as 0.75, 0.48, and 0.35 °C at 14 m below the ground surface and 0.45, 0.9, and 1.5 m radial distances. Also, the temperature change rate (TCR) was calculated as 0.01, 0.007, and 0.005 °C/day, for the same radial distances, respectively. From the end of the bridge solar collector test to the beginning of the first de-icing test the system was inactive for 22 days; during this time, the temperature decrease ($\Delta T_{Inactive}$) in the soil was observed as -0.52, -0.28, -0.17 °C at 0.45, 0.9, and 1.5 m radial

distances, respectively, which results in a TCR of -0.023 , -0.013 , -0.008 °C/day for the same radial distances, respectively. The overall temperature increase in the soil for the period from the initial stage of the bridge solar collector test to that of the 1st winter de-icing test ($\Delta T_{overall}$) was observed as 0.23 , 0.21 , and 0.18 °C at 0.45 , 0.9 , and 1.5 m radial distance, respectively. The result also shows that the soil mass surrounding the GHE could maintain the temperature rise for about 40 days. In other words, it took 40 days for the GHE surrounding soil mass to get in an equilibrium state with the far-field soil.

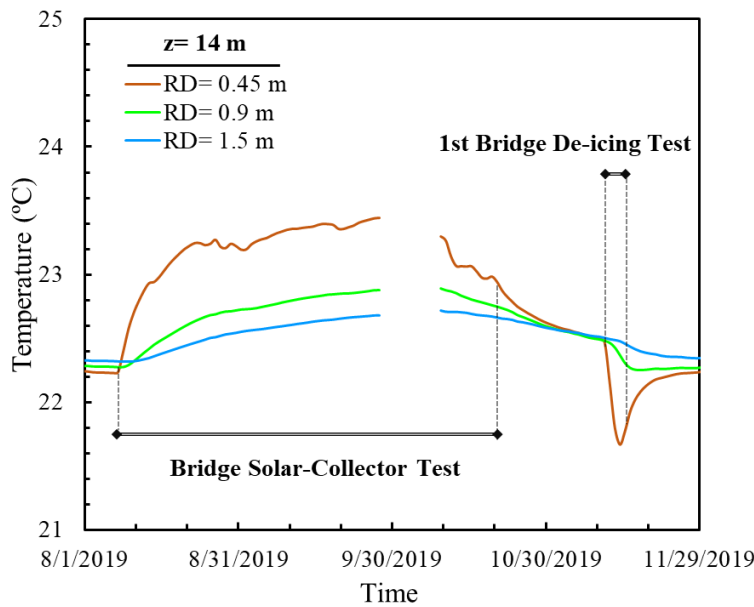


Figure 5.22. Ground temperature variation at the depth of 14 m and different radial distances (RD) from bridge solar collector test in summer to 1st bridge de-icing test in the winter

The stored thermal energy ($Q_{Solar-collector Test}$) in the cylindrical soil mass surrounding the GHE was calculated for different radius using Equation 5.9. The soil temperature at 14 m below the ground surface was used and the same temperature change was assumed along the 131 m GHE. Also, the average volumetric heat capacity for the 20% water content along the GHE depth was considered. The initial temperature of the soil was considered as the unaffected soil temperature

in the surrounding subsurface. Sensors at different radial distances were used to determine the storage volume temperature for different radii. In the 1.5 m radius, the average of all sensors was considered, while in the 0.9 m radius, the average of the sensors at 0.9 and 0.45m was considered. However, for the stored thermal energy in the cylinder of a 0.45 m radius, only the temperature measurement from the sensor at the same radial distance was considered. The test result describes how much energy is stored at varying storage volume radius after the bridge solar-collector test ($Q_{Solar-collector\ Test}$), how much energy is preserved for the first de-icing test ($Q_{Effective}$), and how much energy is lost which accounts for the dissipated heat to the far-field during the inactive period ($Q_{Heat\ loss}$). The results demonstrate that depending on the storage volume definition about 31.7-39.4% of the stored thermal energy was preserved for the utilization in the first winter de-icing test meaning about 60.6-68.3% of heat loss. It was also found that the heat loss rate was two times greater than the thermal energy storage rate for the storage volume of 1.5 m radius. The thermal energy storage rate was 5.14 kWh per day however, the heat loss during the inactive time was 10.5 kWh per day. In addition, considering the total of 1332 kWh injected energy during the bridge solar-collector test, and assuming the same temperature difference between the unaffected subsurface and the storage volume of 1.5m radius for the entire influenced zone, the radius of the thermal influence zone of the GHE after 74 days of operation is about 3.45 m. However, a more accurate estimation could be made if the soil temperature measurement beyond 1.5 m was also available.

Table 5.3. Summary of the soil thermal and energy response during the study period from bridge solar-collector test in summer to 1st bridge de-icing test in the winter

Radial Distance (RD)	0.45 m	0.9 m	1.5 m
$T_{0,Solar-collector Test}$ (°C)	22.23	22.28	22.32
$T_{End,Solar-collector Test}$ (°C)	22.98	22.76	22.67
$\Delta T_{Solar-collector Test}$ (°C)	0.75	0.48	0.35
$TCR_{Solar-collector Test} = \Delta T/Time$ (°C/Day)	0.010	0.007	0.005
$T_{0,1st De-icing Test}$ (°C)	22.47	22.48	22.50
$\Delta T_{Inactive} = T_{0,1st de-icing Test} - T_{End,Solar-collector Test}$ (°C)	-0.52	-0.28	-0.17
$TCR_{Inactive} = \Delta T/Time$ (°C/Day)	-0.023	-0.013	-0.008
$\Delta T_{Overall} = T_{0,1st de-icing Test} - T_{0,Solar-collector Test}$ (°C)	0.23	0.21	0.18
$Q_{Solar-collector test}$ (kWh)	48.9	160.1	380.8
$Q_{Heat loss}$ (kWh)	33.4	102.7	230.1
$Q_{Effective}$ (kWh)	15.5	57.4	150.7
$Soil thermal storage efficiency (\%) = (Q_{Effective}/Q_{Solar-collector test}) \times 100$	31.7	35.8	39.4

5.5.4 Ground Thermal Balance and Operation Strategy

This section studies how the bridge solar-collector test contributes to the ground thermal balance and increase in the soil temperature for the first de-icing test in the winter. Table 5.4 shows the summary of annual GHE energy performance as well as the thermal imbalance ratio (IR) in the ground. Overall, 1332 kWh of energy was injected, and 603 kWh of energy was extracted throughout the year. IR was calculated using Equation 5.8 and found to be 54%. It means the heat injection into the soil by bridge solar-collector was 54% more than heat extraction from the ground during the six de-icing tests in the winter. The outcome of the analysis confirms, that in addition to the fully recovered thermal condition of the ground, the ground temperature was also increased to improve future energy harvesting.

Table 5.4. Annual GHE energy performance

System operation	t (hr.)	$\dot{Q}_{Ext/Inj}$ (kW)	$Q_{Ext/Inj}$ (kWh)
De-icing operation in bypass mode	191	0.8	153
De-icing operation in full-load mode	167	2.7	450
Bridge solar-collector operation	1776	0.75	1332
Q_{AHE} (kWh)	603		
Q_{AHI} (kWh)	1332		
IR (%)	54		

In general, the problem of the thermal imbalance in the soil directly depends upon the number of days of the geothermal de-icing system operation. It is less critical if the number of operation days is limited. The soil temperature can be fully recovered or even increase by the bridge-solar collector test. In order to ensure ground thermal balance, the authors suggest using Equation 5.10 to estimate the time needed for bridge solar collector operation. In general, it requires the same amount of time as the bypass heating mode and four times as long as the full-load heating mode.

$$\text{Required } t_{\text{Bridge solar-collector}} = t_{\text{bypass heating mode}} + (4 \times t_{\text{full-load heating mode}}) \quad (5.10)$$

The suggested equation is valid as long as the GHE fluid flow rate is more or less the same for de-icing and bridge solar-collector operations. The bridge solar-collector operation's flow rate can be increased to reduce operating time as heat injection is enhanced as a result. The bridge solar-collector test should be conducted during hot summer weather. An automated system can use the air temperature as a criterion for the onset of the system. The test result shows a poor heat injection performance when the air temperature was below 26°C. The heat injection increases as the temperature gradient between the ambient and undisturbed ground increases. It should be avoided to perform the bridge solar-collector test when the difference between the ambient and undisturbed ground temperature is less than 5°C since the energy consumption of the circulating pump will be greater than the heat injected into the soil and the result in COP<1. As shown in this study, the

temperature rises in the GHE surrounding soil mass can also be maintained which can help the winter de-icing operation, however, the gap between the bridge solar-collecting operation and de-icing operation should be less than 40 days.

5.6 Conclusions

This study focused on the thermal and energy performance of the 131 m GHE in an external geothermal bridge deck de-icing system which was implemented on a mock-up bridge deck in the DFW metroplex, Texas, USA. The monitoring system at the site permitted the investigation of temperature distribution in the soil around the GHE as well heat storage capacity during the bridge solar-collector test and heat extraction during the de-icing tests. Two de-icing operation modes were compared, and the result highlighted the great role of the heat pump in the system and its potential to boost the heat extraction from the ground and achieving higher COP. A heat storage analysis was performed using the measured field data. The analysis result revealed that the ground temperature beyond the atmospheric condition influence zone was increased as a result of the bridge solar collector test and preserved for utilization in the first de-icing test in the winter. According to the results of the study, only a small portion of the stored heat remained within the GHE surrounding soil mass, and the majority of the injected heat was lost via lateral heat transfer. The role of bridge solar-collector operation on the ground thermal balance was also evaluated and discusses. It was observed the bridge solar-collector operation fully recovered the ground thermal condition by providing more than two times injected heat than the extracted from the ground. Moreover, the operation strategy to optimize the performance of the system was also discussed and a simple equation to calculate the optimum required number of days for bridge solar-collector operation is also presented.

CHAPTER 6: ON THE MODELLING OF A U-TUBE GROUND HEAT EXCHANGER: A PROPOSED COMPUTATIONALLY EFFICIENT NUMERICAL MODEL AND EXPERIMENTAL VERIFICATION

6.1 Abstract

As one of the disadvantages of the finite element (FE) models is huge computational time, it is essential to develop an FE model with high accuracy and minimal computational time. In this study, a computationally efficient 3D transient FE model is developed in COMSOL Multiphysics which used a 1D pipe flow to represent the physical fluid flow. In this model, an equivalent 1D pipe flow is developed using an analytical method, instead of fully modeling the borehole. The proposed model intends to sacrifice the temperature distribution inside the borehole and simulate the borehole wall temperature with less computational time, the same level of accuracy, and more convenient meshing. The proposed model is compared with a conventional model and validated against the experimental data. A good match between experimental and numerical results was found and the result showed the proposed model was successful in simulating fluid temperature, borehole wall temperature, and surrounding soil temperature. Comparison between conventional and proposed models indicated that the proposed model provides high accuracy as the conventional model and decreases the required number of elements by 90% and 67% for the optimum and extra fine mesh cases. Moreover, the computational time is reduced by 95% and 81 % for the two mesh cases, respectively.

6.2 Introduction

Geothermal energy has been increasing interest due to its potential to reduce fossil fuel consumption and consequently greenhouse gases emission. It is a green and reliable source of energy that can be utilized for a variety of purposes such as thermal conditioning of the building,

de-icing, and snow-melting of pavements or bridge decks, etc. Commonly, a ground source heat pump system (GSHP) which is a highly efficient, renewable energy technology, is used to employ geothermal energy (Omer 2008; Spitler and Bernier 2011). This technology relies on the ground heat exchangers (GHE) buried into the ground to extract heat during the cold season and depletion during the warm season. It works on a basis that, the ground temperature is relatively constant, around 10-15 °C, below a certain depth, it is warmer than the air in winter and cooler than the air in summer (Brandl 2006). GHEs are the most important part of ground source heat pumps (GSHP), which profoundly impact their performance. Frequently, boreholes are used for installing the ground heat exchangers in the soil. Vertical ground heat exchangers (VGHE) can be designed in different arrangements such as single U-shaped pipes, double U-shaped pipes, or coaxial pipes. They are inserted vertically into the borehole and then fixed by backfilling the borehole with grout. High thermal conductive grout is suggested for better heat transfer between GHE and surrounding soil.

As a result of the complex transient 3D transport phenomena of ground heat exchanger (GHE), models and simulations of GHE serve as important tools in modern geothermal heat extraction technologies. Throughout the years, different numerical models of high and low complexities have been developed and utilized as a design tool for GHEs. In an early study, Signorelli et al. (2007) compared the output of the 3-D numerical model with analytical model results to study the influencing factors on the analysis of thermal response test data. They utilized the 3-D finite-element (FE) code FRACTure developed by Kohl and Hopkirk (1995). The effects of heterogeneous subsurface conditions and soil moisture migration were considered in their study. They concluded that in contrast to the line-source model, the numerical analysis is more suitable for an accurate assessment of thermal response tests because, despite the line-source model, it can

analyze heat injection rates as well as borehole geometry. A dynamic three-dimensional numerical model using the finite volume method was developed by He et al. (2009), to assess the short timescale transient responses of a borehole heat exchanger (BHE). The model consists of a single borehole with a diameter of 15 cm and a depth of 100 m. The result showed that the delayed response due to the circulation of fluid along the pipe loop is important at short time scales i.e., 10 min. In another study, Lamarche et al. (2010) studied the borehole thermal resistance and developed 2D and 3D numerical models in COMSOL to evaluate and compare the different approaches to determine the resistances. They proposed a new method to calculate the borehole resistances from in situ tests.

In order to reduce the computational time and effort, some researchers have simulated the GHE using 2D models. Austin III (1998) employed a 2D finite volume model to determine the thermal conductivity of the ground. Lazzari et al. (2010) examined the long-term performance of different borehole heat exchanger (BHE) fields configuration using 2D finite element models in COMSOL software. For each BHE field geometry, they discussed heat load and thermal conductivity of the ground, illustrations of the minimum annual value of the fluid temperature for a period of 50 years. Based on the analysis output, they concluded that except for a single BHE, long-term performance is adversely impacted for every case. Choi et al. (2013) also studied the influence of groundwater flow on BHE arrays and used a 2D finite element method to simulate the heat transfer outside the borehole.

For the case that a full description of the borehole geometry is required, a 3D model can be used which usually results in extreme geometrical aspect ratio problems. However, as it is essential to employ an advanced and efficient numerical simulation, Al-Khoury et al. (2005) and Al-Khoury and Bonnier (2006) proposed a new numerical technique to overcome the extreme

geometrical aspect ratio problem. They used a combination of finite element method and thermal capacity models to model single and double U-pipe elements in a three-dimensional (3D), finite element model, using 1D finite element representations. A new formulation was proposed to account for thermal interaction between the GHE pipe and grout inside the borehole. There is conduction heat transfer through the pipe wall and convective heat transfer between the heat carrier fluid and the pipe's inner wall. However, the application of the 1D pipe element causes some estimation errors. First, in the actual physical process, pipe-grout temperature coupling occurs at the distance of the pipe outer radius from the pipe axis, while in 1D pipe element modeling, the outer pipe wall temperature is coupled to the temperature field of the grout domains at the pipe axis, moreover, the 1D pipe element modeling does not consider the heat capacity of the pipes (Ozudogru et al. 2014). Ozudogru et al. (2014) developed a numerical model in COMSOL that solved the problems associated with the 1D pipe flow model which applied the pseudo pipe approach to prevent the errors. A pseudo pipe is a cylinder with a radius equal to the pipe's outer radius, centered on the axis of each leg, with very high thermal conductivity in the radial direction and very low in the vertical direction. The heat capacity of the pipes is assigned to the pseudo pipe elements and as a correction factor, the pipe volume ratio is used to estimate the density of the pseudo pipe elements. They compared the developed model results with those from an analytical model and a good match was found. Han and Yu (2016) used a 3D finite element model in COMSOL and performed a series of sensitivity analyses and investigated the impact of the geological, design, and operational factors on the performance of the vertical geothermal heat pump system. The authors employed the 1D pipe element and simulated the steady-state and unsteady behavior of the GHE. They concluded that ground thermal conductivity and circulation fluid flow rate are two critical factors greatly affecting the performance of the GHE. The result

also showed that thermal energy can be extracted less costly, more efficiently, and higher coefficient of performance (COP) can be achieved in an intermittent operation mode in comparison to the continuous operation mode. Similarly, A 3-D numerical model was developed by Li et al. (2018) to assess the GSHP's performance under the impact of depth varying unsaturated soil thermal properties, the depth of the groundwater table, and the movement of saturated groundwater. Furthermore, some studies examined the soil's thermal properties and their impact on system performance using 3D numerical models that were validated with test data (Han et al. 2018; Li et al. 2019).

The finite element modeling is a strong tool in simulating the GHE operation and heat transfer process between circulation fluid to the ground, however, one of the drawbacks of the finite element models are high computational time and effort. Therefore, there are also studies focused on the development of an efficient finite element model. Boockmeyer and Bauer (2016) developed an adapted model for BHEs to simulate the geothermal application with high efficiency and accuracy. In their approach, the BHE geometry is adapted meaning that, first, circular geometries are replaced by equivalent rectangular geometries as they accommodate the mesh optimization process, and then optimal mesh density is determined. As the volume in both geometries remains constant the volumetric heat capacities were the same, however, equivalent thermal conductivities were determined following the modification of the geometry. Finally, they compared the adapted and original model output with experimental data and found a good fit between simulation results and experimental data. A study conducted by Zhang et al. (2020), focused on the heat transfer behavior in subsurface soil in the vicinity of GHE through a small-scale laboratory experiment and a 3D FE model in COMSOL software in which a 1D pipe element was utilized to represent the GHE. They applied the pseudo pipe element approach as proposed by

Ozudogru et al. (2014) to overcome the estimation errors of the 1D pipe element module. The developed model was compared with experimental data and a good match was achieved.

In this paper, a computationally efficient 3D transient FE model is developed in COMSOL Multiphysics (Comsol 2018) which utilizes a 1D pipe flow module. In this model, the modeling of the grout and pseudo pipes are replaced by modifications in the geometry and thermal properties of heat exchanger pipes. The proposed model is then compared with a conventional model which employs grout and pseudo pipe in the model and validated against the experimental data. Finally, the accuracy and computational time of the proposed and conventional model are compared and discussed.

6.3 Numerical Model Development

6.3.1 Theoretical Basis of The Heat Transfer Processes

The physics of thermal processes of the proposed numerical model which simulate the operation of the ground heat exchangers (GHE) can be divided into three steps: (1) convection heat transfer between fluid and pipe; (2) conduction heat transfer between pipe and borehole grout; (3)

conduction heat transfer between borehole grout and adjacent ground. Figure 6.1 illustrates the heat transfer process from fluid to the material outside the wall.

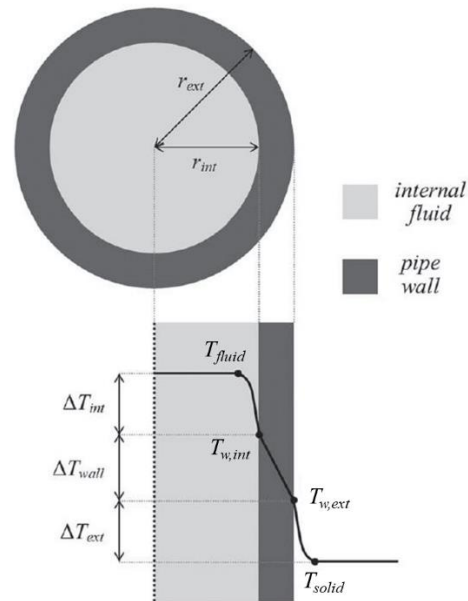


Figure 6.1. Temperature distribution across the pipe wall (Gawecka et al. 2020)

6.3.1.1 Heat transfer between heat carrier fluid and GHE pipe

The heat transfer between the fluid and GHE is physically modeled using 1D non-isothermal pipe flow (Figure 6.2). Reducing 2D or 3D problems to 1D provides a great benefit in computational efficiency. The linear pipe element approximates the heat exchanger pipe which uses built-in equations to solve the fluid flow in pipe and heat transfer problem simultaneously.

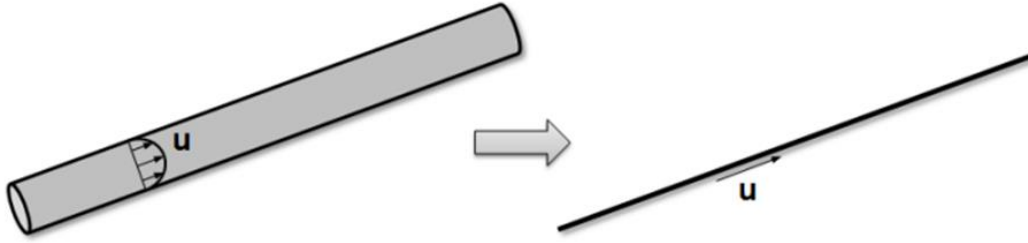


Figure 6.2. Illustration of reducing 3D flow problem to a 2D or 3D curve (Comsol 2018)

In order to determine the pipe flow problem, the momentum (Equation 6.2) and continuity (Equation 6.1) equations are solved.

$$\frac{\partial A\rho}{\partial t} + \nabla \cdot (A\rho u) = 0 \quad (6.1)$$

$$\rho \frac{\partial u}{\partial t} = -\nabla p - \frac{1}{2} f_D \frac{\rho}{d_h} |u|u + F \quad (6.2)$$

Where A is the cross-section area, ρ represents the density of the fluid, u stands for the fluid velocity, p is the fluid pressure, t is the time, T is the temperature, f_D is the Darcy friction factor, d_h represents the hydraulic pipe diameter, F is the volume force according to fluid density variation. In Equation 6.2, the second term on the right-hand side corresponds to pressure drop due to viscous shear. The Darcy friction factor represents the continuous pressure drop along the pipe segment due to viscous shear which is demonstrated as a function of the Reynolds number (Re) and the ratio of the surface roughness to the hydraulic diameter (e/d_h) (Equation 6.3).

$$f_D = f\left(Re, \frac{e}{d_h}\right) \quad (6.3)$$

The Darcy friction factor can be estimated using the (Churchill 1977) equation as follows:

$$f_D = 8 \left[\left(\frac{8}{Re} \right)^{12} + (C_A + C_B)^{-1.5} \right]^{1/12} \quad (6.4)$$

Where C_A and C_B are factors that are given as follows:

$$C_A = \left[-2.457 \ln \left(\left(\frac{7}{Re} \right)^{0.9} + 0.27 \left(\frac{e}{d_h} \right) \right) \right]^{16} \quad (6.5)$$

$$C_B = \left(\frac{37530}{Re} \right)^{16} \quad (6.6)$$

Equation 6.4 can be used for any range of Reynold numbers, which means it is valid for any flow regime. The Absolute surface roughness of the pipe is represented by e which is given as 0.0015 mm for the plastic pipe. Also, Re is the Reynolds number, a dimensionless parameter which defined as the ratio of inertia and viscous forces, such that:

$$Re = \frac{\rho_f u d_h}{\mu} \quad (6.7)$$

As mentioned earlier, the term F in Equation 6.2 represents the volume force. It accounts for density variation and assuming the heat carrier fluid is an incompressible Newtonian fluid, F set to zero.

The heat transfer in pipes problem is governed by the energy conservation equation, which involves conduction, convection, and dissipation processes. It is given as:

$$\rho A C_p \frac{\partial T}{\partial t} + \rho A C_p u \cdot \nabla T = \nabla \cdot A k \nabla T + f_D \frac{\rho A}{2 d_h} |u|^3 + Q_{wall} \quad (6.8)$$

Where C_p , k are the specific heat capacity and thermal conductivity of the heat carrier fluid, respectively. The terms on the left-hand side of the Equation 6.8 demonstrate the change of thermal energy in a fluid control volume. On the right-hand side, the first term corresponds to heat conduction and the second term on the right-hand side describes the heat generation due to viscous shear. Newton's heat dissipation theory can be used to calculate the radial heat exchange between fluid and pipe wall, Q_{wall} , which is calculated by:

$$Q_{wall} = (hZ)(T_{w,ext} - T) \quad (6.9)$$

Where T is the fluid temperature, $T_{w,ext}$ is the pipe exterior wall temperature wall, hZ is the total thermal resistance of the pipe wall and is described by Equation 6.10. An equivalent thermal

resistance term is used to account for the influence of the pipe wall on heat transfer. This term includes the contribution of the pipe's thermal resistance as well as the thermal resistances of the internal and external films with convection layers which are assumed to be in serial with each other.

$$(hZ) = \frac{2\pi}{\frac{1}{r_i h_{int}} + \frac{1}{r_o h_{ext}} + \frac{\ln\left(\frac{r_o}{r_i}\right)}{k}} \quad (6.10)$$

Where h is the convection coefficient. Z is the total thermal resistance considering those by the internal film, pipe wall, and external film, r_i , and r_o are the internal and external radius of the pipe respectively. Since the external layer is solid with no convection, h_{ext} is set as zero. For the thermal resistance of the internal fluid boundary layer, h_{int} is given by:

$$h_{int} = Nu \frac{k_f}{d_h} \quad (6.11)$$

Where Nu is the internal Nusselt number explaining the dimensionless temperature gradient at the pipe wall. The magnitude of Nu in the laminar condition is 3.66, whereas in turbulent conditions, it is calculated as follows:

$$Nu_{int} = \frac{(f_D/8)(Re-1000)Pr}{1+1.27\sqrt{f_D/8}(Pr^{2/3}-1)} \quad (6.12)$$

Where Pr is the ratio of the momentum and thermal diffusivities, such that:

$$Pr = \frac{c_p \mu}{k} \quad (6.13)$$

6.3.1.2 Heat transfer in the borehole

The borehole grouting material is considered solid. In the solid domain heat transfers through conduction. The heat exchange process in the borehole is given by Equation 6.14. It is linked with the heat carrier fluid via the heat exchange term Q_{wall} .

$$\rho_g C_{pg} \frac{\partial T_2}{\partial t} - \nabla \cdot (k_g \nabla T_2) = Q_{wall} \quad (6.14)$$

Where ρ_g is the density of the grout, C_{pg} is the specific heat capacity of the grout, and k_g is the thermal conductivity of the grout.

6.3.1.3 Heat transfer in the surrounding soil

The adjacent soil is also considered as a pure solid and the heat exchange process with the adjacent ground of the borehole involves only thermal conduction. It is given as:

$$\rho_s C_{ps} \frac{\partial T_2}{\partial t} - \nabla \cdot (k_s \nabla T_2) = Q \quad (6.15)$$

Where ρ_s is the density of the soil, C_{ps} is the specific heat capacity of the soil, and k_s is the thermal conductivity of the soil. Q represents the heat source or sink in the ground. However, as there is no extra heat source or sink in this study, this term is set as zero. $T_{w,ext}$ in Eq. 9 can be obtained by solving Equations 14 and 15. After appropriate boundary and continuity conditions are applied, the system of equations may be solved. It is then possible to determine the temperature distribution across the radial direction as well as along the GHE pipe.

6.3.2 Experimental Set-up and Monitoring System

A 56-m² mock-up geothermal bridge was constructed in Arlington, TX, to study the feasibility and performance of an external geothermal heat pump de-icing system (GHDS) (Habibzadeh-Bigdarvish et al. 2021c). Figure 6.3 illustrates the schematic of the experimental setup. The de-icing system consists of the hydronic heating pipes attached to the bottom surface of the bridge deck and is considered as external heating in contrast to conventional embedded hydronic heating systems. Also, to minimize the heat loss from the bottom, the hydronic pipes are covered by a layer of insulation foam. The mock-up bridge deck consists of three zones: an external heating zone, an

internal heating zone, and a control zone. It utilizes both the traditional type of GHDS, which uses internal hydronic pipe embedded in the concrete slab, and the newly developed method, which utilizes external hydronic pipe attached to the bottom surface of the bridge deck. The end section of the bridge deck is also considered as a control area with no heating. Also, the experimental field test setup consists of a geothermal borehole of 132.5 m (from ground level) deep and 14.6 cm diameter which hosted a single U-tube heat exchanger loops made of high-density polyethylene (HDPE) pipe with a standard dimension ratio (SDR) of 11 and 3.45 cm inside diameter. Table 6.1 shows the geometrical detail of the GHE.

The subsurface monitoring system consists of five 10 cm diameter temperature monitoring boreholes (TMBs), which are equipped with thermistor strings and radially scattered around the geothermal borehole to investigate the temperature distribution in the soil and at different depths. Also, two thermistor strings were attached to the outer surface of the GHE legs to monitor the pipe and grout interface temperature variation. Table 6.2 shows the detail of the thermistor strings' radial distance from the geothermal borehole central axis and the depths of sensor nodes on each string.

Table 6.1. The geometrical details of the borehole and heat exchanger pipe

Parameter	Value
GHE type	Single U-pipe
Pipe Material	HDPE
U-pipe Length	132.5 m
Borehole Diameter	14.6 cm
Pipe inner diameter	3.45 cm
Pipe wall thickness	0.38 cm
Pipe shank spacing	1.1 cm

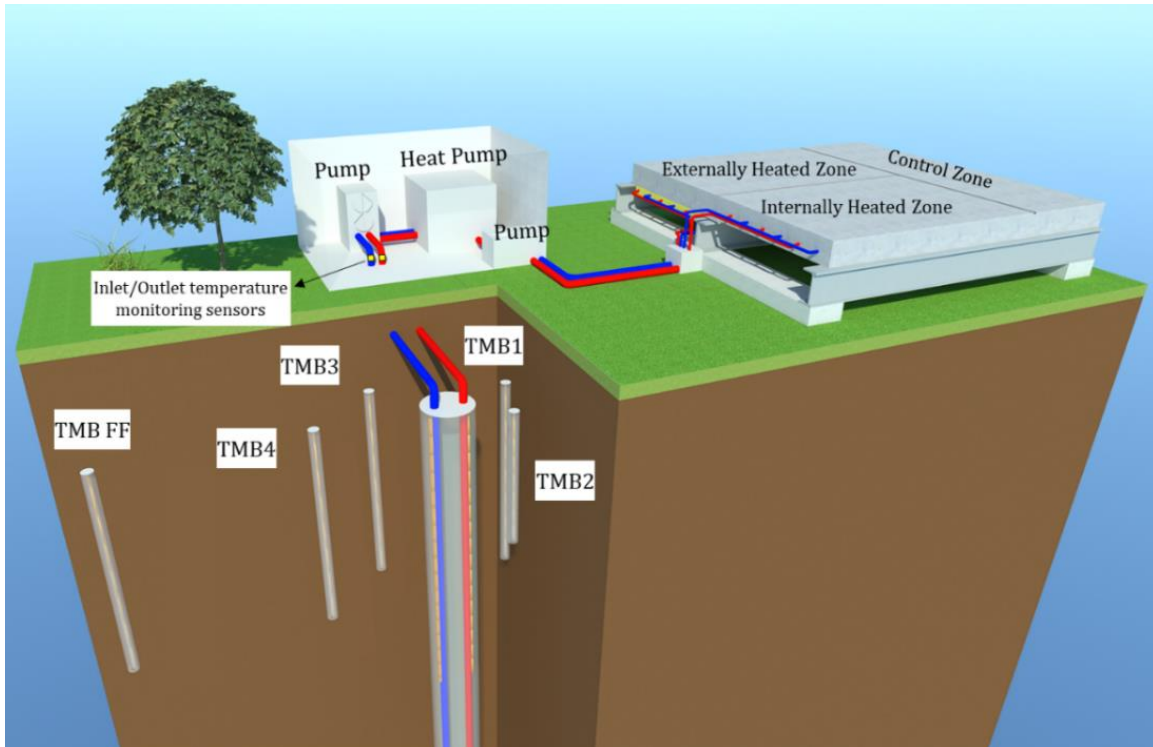


Figure 6.3. Schematic of the experimental setup

Table 6.2. Details of installed thermistor string.

Thermistor string	Inlet pipe	Outlet pipe	TMB 1	TMB 2	TMB 3	TMB 4	TMB FF
Radial Distance (m)	~0	~0	0.45	0.6	0.9	1.5	7.5
Sensor node	Depth from the surface (m)						
#1	0.8*	0.8*	0.6	0.6 m : 0.3 m : 14 m	0.9*	0.9	1.2
#2	1.1*	0.8*	1.8		1.5	1.8	4.0
#3	1.7*	1.1*	3.4		3.0	3.4	10.1
#4	2.3	2.3	6.4		6.1	6.4	19.2
#5	3.2	3.8	9.4*		9.1	9.4	n/a
#6	4.7*	5.3*	14.0		13.7	14.0	n/a
#7	6.2	6.9	18.6*		18.3*	18.6*	n/a
#8	7.8*	8.4	n/a		n/a	n/a	n/a
#9	9.3*	13.0*	n/a		n/a	n/a	n/a
#10	13.9*	17.5*	n/a		n/a	n/a	n/a
#11	18.4*	29.7	n/a		n/a	n/a	n/a
#12	30.6	n/a	n/a		n/a	n/a	n/a

* The sensor has malfunctioned.

6.3.3 The Conventional FEM Model

A conventional FE model was first developed as a source for evaluating the proposed FE model's performance. Both 3D FE models were developed in COMSOL Multiphysics (Comsol 2018) based on the GHE, as described previously. The conventional model consists of several components, namely: pipes, the borehole grout, and the soil/rock surrounding the borehole. The material properties are listed in Table 6.3. The 3D model was developed such that no thermal interactions occur across the lateral boundaries. The computational domain for the adjacent ground was set to be a cuboid of 15 m × 15 m × 137 m assuming two soil layers in which the top layer extended to 7 m below the ground surface and corresponds to the unsaturated soil above the groundwater table, moreover, the second layer represents the saturated soil. The GHE was modeled using a non-isothermal pipe flow with a 1D line element. However, to compensate for the limitation of the 1D pipe element modeling, the “pseudo pipes” were defined as proposed by Ozudogru et al. (2014).

Table 6.3. The material properties of the GHE in this study

Material	Mass density (kg/m ³)	Thermal conductivity (W/m.K)	Specific heat capacity (J/kg.K)
Circulation fluid	1021	0.48	4038
Linear pipe	0.38	n/a	n/a
Pseudo pipe	Material: 970 Effective: 328.8	{1000, 1000, 0}	1800
Borehole Grout	1200	2.1	2800
Unsaturated Soil	1700	0.75	1050
Saturated Soil	2300	2.5	1300

In this study, the model development follows the same steps as previously discussed by Habibzadeh-Bigdarvish et al. (2021b). The numerical simulation includes two models: (1) Initial ground temperature model, (2) GHE operation model. The output temperature domain of the first

model was implemented as the initial conditions for the second model. The common boundary conditions in both models are the adiabatic boundary condition on sides of the model and the Dirichlet boundary condition on the bottom boundary equal to the undisturbed ground temperature of 21.5 °C. The initial ground temperature model is fully discussed in (Habibzadeh-Bigdarvish et al. 2021b)

In the first model, the initial temperature of the whole domain was also set to be undisturbed ground temperature. The average monthly temperature of the site was applied as a Robin boundary condition at the ground surface with a constant wind velocity of 5 km/h, to describe heat exchange between ground and atmosphere. Moreover, the impact of the solar radiation on the soil temperature was simulated by the Neumann boundary condition representing the average monthly heat flux density of the soil surface. Figure 6.4 shows the average monthly air temperature and soil density at the testing site. The air temperature was monitored on-site, however, the solar radiation data were collected from an online source (Marion and Wilcox 1995) and it was assumed that the soil heat flux density to net solar radiation ratio (G/R_n) is equal to 0.12. The first simulation was repeated over the 10-year cycle with the same boundary conditions to minimize the effect of the initial boundary condition on the final result. Finally, the monthly output temperature domain of the 10th year was used as the initial ground temperature profile of the second model.

The second model simulates the GHE operation under heating and cooling load. For the month in which the operation started, the initial temperature of the whole domain was inputted from the first simulation's result. The average hourly ambient temperature, as well as the wind velocity of the site during the event, was applied as a Robin boundary condition at the ground surface boundary. The GHE operation was modeled by specifying the inlet temperature and volumetric flow rate boundary conditions in the inlet location of the GHE. Moreover, an imperfect

contact was considered by applying thermal contact between pseudo pipes and grout at the outer surface of the pseudo pipe and between the grout and surrounding soil at the borehole wall. This is due to the resistance caused by the film layer if the pipe is surrounded by water or because of contact resistance as a result of an imperfect contact between the pipe and a solid material (Gawecka et al. 2020). Basically, it is assumed the voids in the contact surfaces are filled with water.

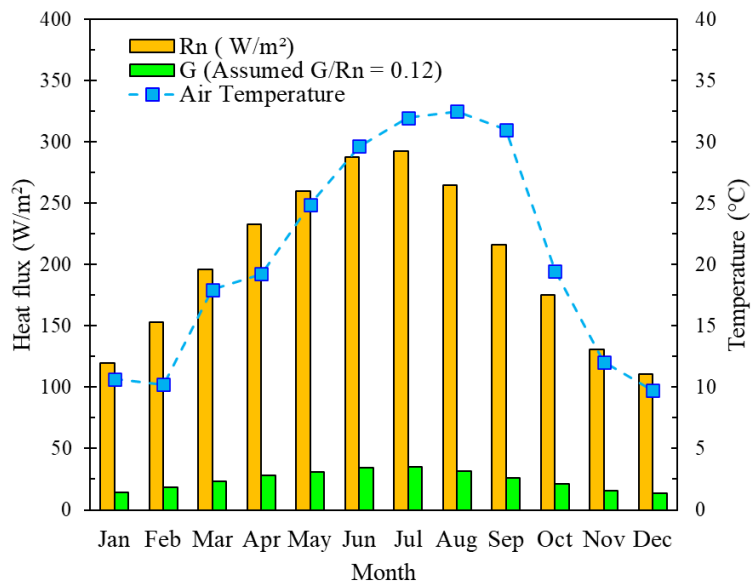


Figure 6.4. Average monthly air temperature and solar radiation data for the testing site

6.3.4 A Proposed simplified Model

In an attempt to reduce the computational time and meshing issues of the conventional model, a simplified model was proposed. In the new model, only ground heat exchangers are modeled, and the simulation of the grout and pseudo pipe is disregarded. An equivalent 1D pipe flow was developed to account for the thermal property of the pipe wall and grout. The proposed model intends to sacrifice the temperature distribution inside the borehole and simulates the borehole wall

temperature with less computational time, the same level of accuracy, and more convenient meshing. The proposed model is suitable when focusing on the fluid temperature as well as the temperature distribution in the soil. Figure 6.5 compares the schematics of the conventional, proposed, and physical models.

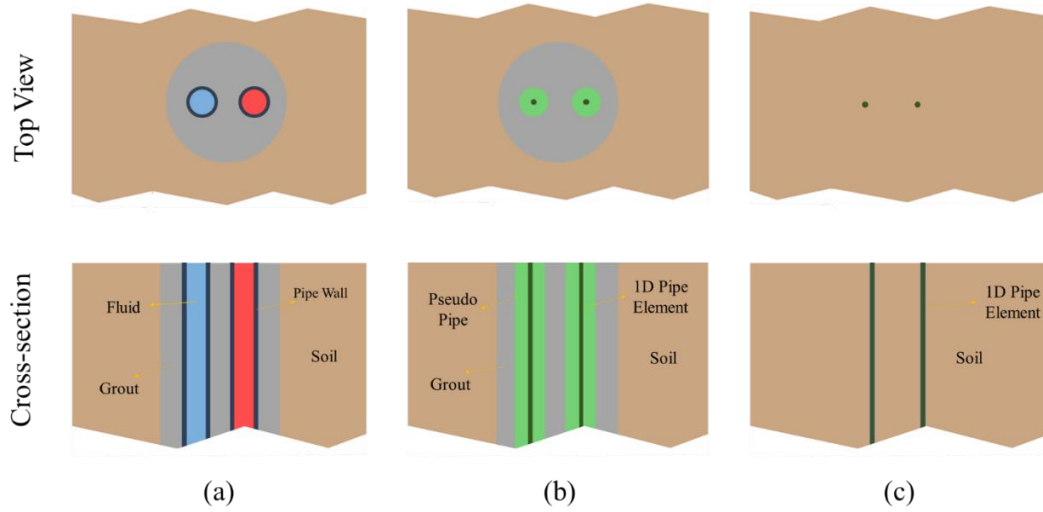


Figure 6.5. Schematic diagrams of GHE: (a) physical model; (b) Conventional model with 1-D pipe flow and pseudo pipe; (c) Proposed model.

The heat capacity of the new pipe element is the sum of the heat capacities of the grout and HDPE pipe and is given by Equation 6.16. However, since the 1D pipe element cannot account for the heat capacity of the pipe, the volumetric heat capacity of the pipe is kept constant, and the new outer pipe radius (r_{po-new}) is calculated using Equation 6.17. The new outer pipe radius can provide an equivalent volumetric heat capacity for the GHE pipe elements representing both grout and pipe.

$$2\pi(r_{po-new}^2 - r_{pi}^2)(\rho c)_p = 2\pi(r_{po}^2 - r_{pi}^2)(\rho c)_p + \pi(r_b^2 - 2r_{po}^2)(\rho c)_{gt} \quad (6.16)$$

$$r_{po-new} = \sqrt{\frac{2\pi(r_{po}^2 - r_{pi}^2)(\rho c)_p + \pi(r_b^2 - 2r_{po}^2)(\rho c)_{gt}}{2\pi(\rho c)_p}} + r_{pi}^2 \quad (6.17)$$

Where r_{pi} and r_{po} are the inner and outer radius of the pipe, respectively, r_b is the radius of the borehole, and $(\rho c)_p$ and $(\rho c)_{gt}$ are the volumetric heat capacity of the pipe and grout, respectively.

The multipole method Bennet et al. (1987) is used to calculate the thermal conductivity value of the equivalent pipe (k_{p-new}). It is evaluated so that the thermal resistance per unit length of the cylindrical layer placed between r_{pi} and r_{po-new} is the same as that of the r_{pi} and r_{gt} . The k_{p-new} is given by:

$$k_{p-new} = \frac{1}{R_{p-new}} \ln \left(\frac{r_{po-new}}{r_{pi}} \right) \quad (6.18)$$

Where R_{p-new} is the thermal resistance of the equivalent pipe which is estimated as (Bernier 2001):

$$R_{p-new} = 2 \left(R_{gt} + \frac{R_p}{2} \right) \quad (6.19)$$

Where R_{gt} and R_p are the thermal resistance of the grout and pipe, respectively. They can be calculated as:

$$R_p = \frac{1}{2\pi k_p} \ln \left(\frac{r_{po}}{r_{pi}} \right) \quad (6.20)$$

$$R_{gt} = \frac{1}{2\pi k_{gt}} \ln \left(\frac{r_b}{r_{po}\sqrt{n}} \right) \quad (6.21)$$

The new parameters were calculated and utilized in the proposed model to build the equivalent heat exchanger pipe. In this study, the r_{po-new} and k_{p-new} were found to be 13 cm and 0.7

w/m.K, respectively. Finally, similar steps as the conventional model were taken and the same boundary conditions were applied, and the proposed model was developed.

6.3.5 Mesh schema

The finite element mesh of both models was generated automatically by COMSOL for the whole domains using free tetrahedral mesh elements (Figure 6.6). The automatic mesh generation settings were adjusted to result in the optimum number of elements however avoid any bad quality mesh (i.e. distortion, thin region, element intersections, etc.) that can be detected automatically by the software. For a fair comparison between the conventional and proposed models, the same settings were applied for both models. Also, an extra-fine mesh was also generated to provide a smoother vertical temperature profile when investigating the accuracy of the numerical models and comparing them with experimental data. Table 6.4 illustrates the settings for automatic free tetrahedral finite element mesh generation. Maximum and minimum element sizes indicate the upper and lower bound of the element size, maximum element growth rate expresses the size difference of two adjacent mesh elements, curvature factor shows how big a mesh element can be along a curved boundary, and the resolution of narrow regions controls the number of layers of mesh elements in narrow regions (Comsol 2018).

Table 6.4. Automatic free tetrahedral element mesh settings

Mesh	Mesh 1: Optimum	Mesh 2: Extra fine
Maximum element size (m)	3	1.2
Minimum element size (cm)	7.5	5
Maximum element growth rate	3	2
Curvature factor	0.2	0.2
Resolution of narrow region	1	1

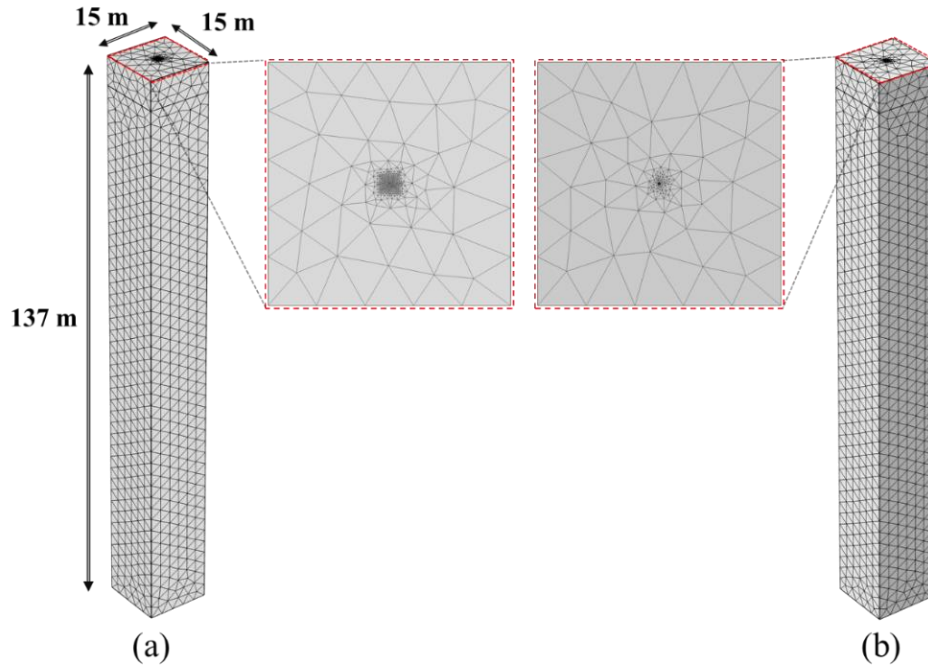


Figure 6.6. Finite element meshes for the optimum case: (a) Proposed model; (b) Conventional model.

6.4 Results and Discussion

6.4.1 Model Verification

For the verification of numerical models, a 99-day period was studied which includes both heat injection and extraction. First, the bridge solar-collector test was performed in August 2019 lasting for 74 days. During this test, heat carrier fluid transferred the heat from the bridge deck to the ground. Then the system was off for 21 days which was followed by a de-icing test for 4 days in which heat was extracted from the ground and transferred to the bridge deck. More details of each test can be found in Chapter 6 of this dissertation. Table 6.5 lists the details of the study period.

Table 6.5 Study period details

Operation	Date	Period (day)	Flow Rate (l/s)
Bridge solar-collector test	8/8/2019 - 10/20/2019	74	0.51
System off	10/20/2019 - 11/10/2019	21	0
De-icing test	11/11/2019 - 11/14/2019	4	0.56

6.4.2 Initial Ground Temperature Model

The numerical models were validated by comparing the COMSOL output against the experimental data extracted from the testing site. For both the conventional and proposed models, the output of the initial ground temperature and GHE operation models were compared with the measured data. First, the output of the initial ground temperature models were compared with the measured data of a temperature monitoring borehole at far-field (TMB FF) for the period from August 2019 to July 2020. Figure 6.7 illustrates the average monthly vertical temperature profile comparison between the experimental data and numerical simulation results. As the initial ground temperature model for both the proposed and conventional model is similar, only one result is shown here. There is a good agreement between measured data and numerical model outputs for each month. A good correspondence between the numerical analysis and the measurements justified the utilization of this result as an initial condition for the GHE operation model.

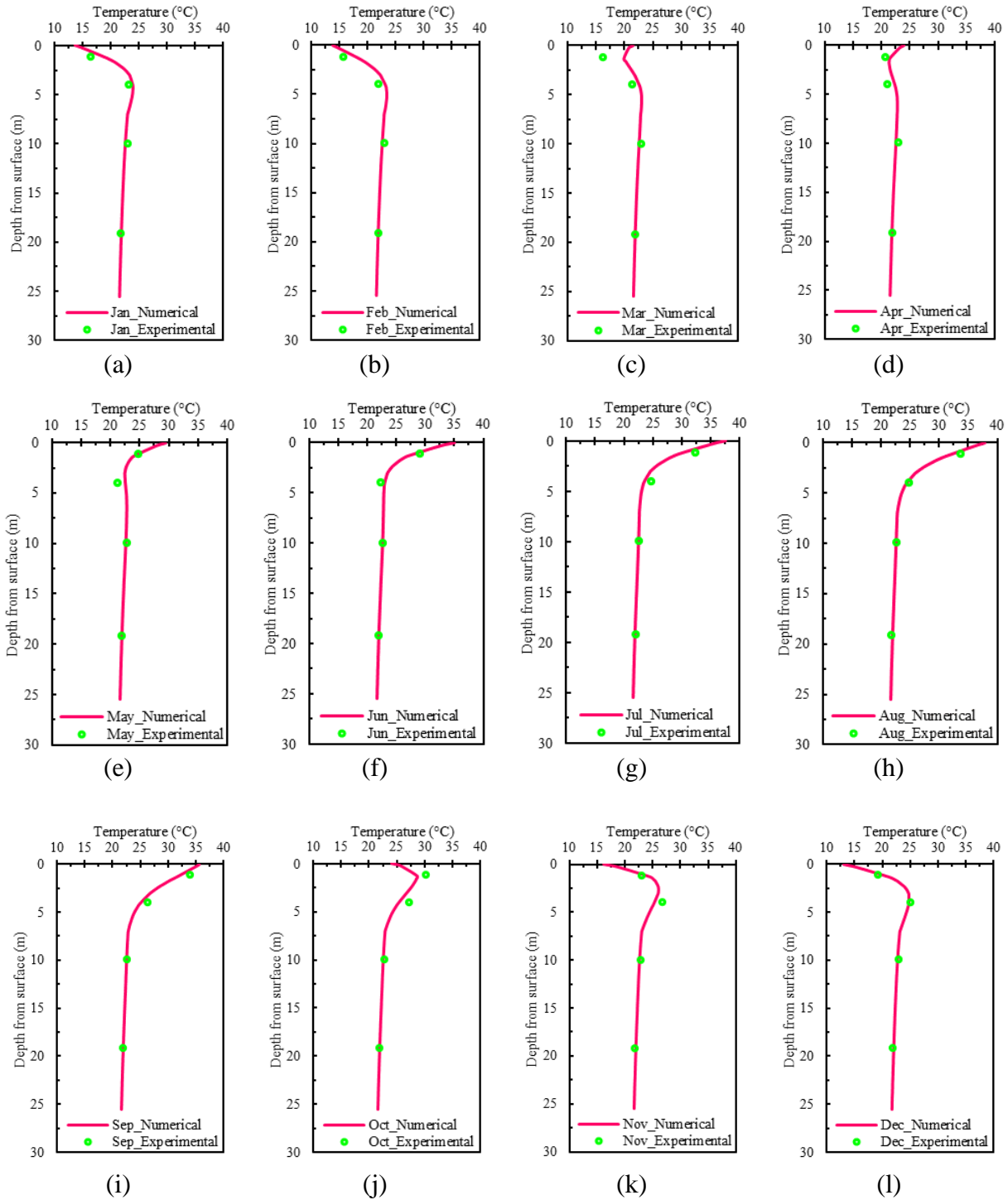


Figure 6.7. Monthly average ground temperature profile: numerical simulation vs experimental data.

6.4.3 GHE Operation Model

The average daily recorded inlet temperature during the study period was applied as the inlet boundary condition of the GHE operation model. Also, the ground temperature model output for August was selected, when the bridge solar-collector test was started, as the initial boundary conditions for the ground temperature domain. The GHE operation models were validated using the measured data during the study period from different sources, namely: GHE Outlet water temperature, TMB1, TMB3, and TMB4. As TMB2 has a similar radial distance as TMB1, it was not used for verification. The installed thermistor in TMB1, TMB3, and TMB4 is also a different type from that used in TMB2. Also, the measured data from the inlet and outlet pipe thermistor string were not used for verification as the proposed model does not simulate the pipe wall.

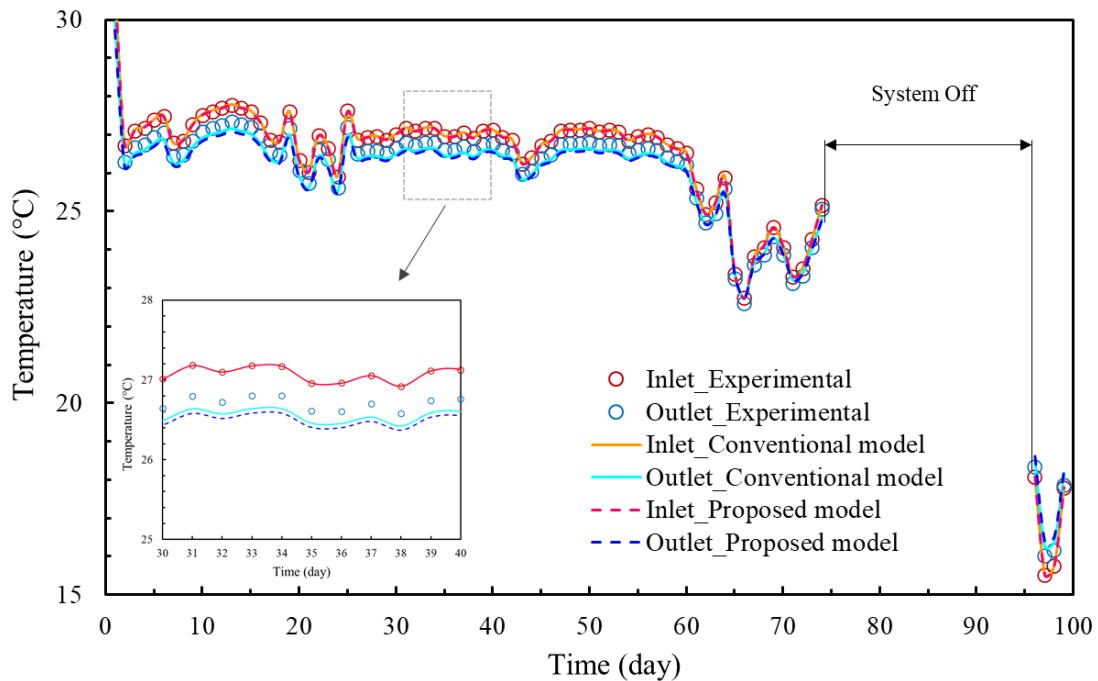


Figure 6.8. Comparison between the experimental data and the simulated fluid temperatures by the conventional and proposed efficient model.

Figure 6.8 shows the comparison between the recorded data and the simulated fluid temperatures by the conventional and proposed models. It can be observed there is a good match between the numerical models and experimental data for the outlet fluid temperature. Moreover, the proposed model can successfully duplicate the conventional model result.

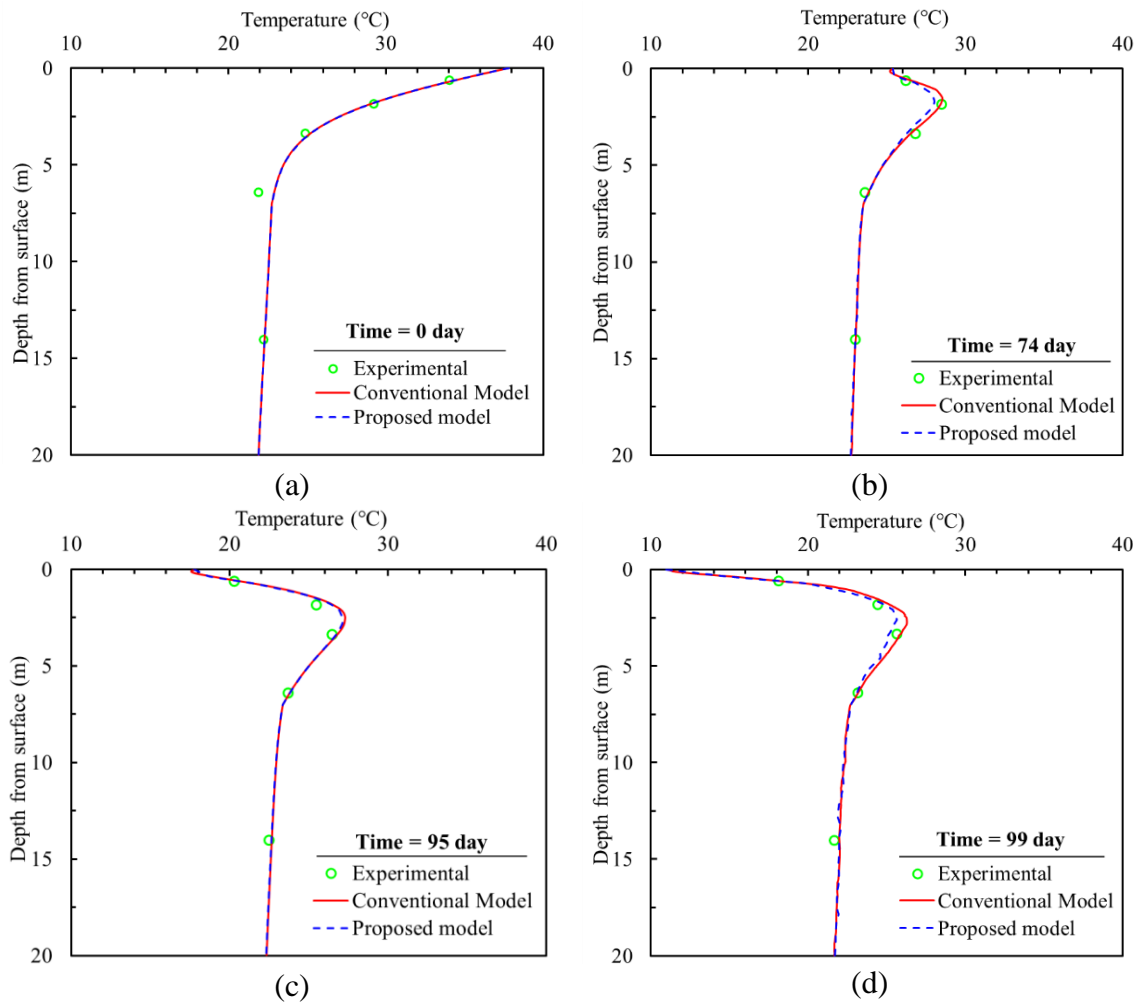


Figure 6.9. Vertical temperature profile comparison between the experimental data from TMB 1 and the simulated by the conventional and proposed efficient model.

The average daily extracted data from TMB1 were compared with soil temperature for the same radial distance from the numerical models' result. Figure 6.9 shows the vertical temperature profile during four selected critical times of the study period, namely: Time=0 day, initial condition

before the bridge solar collector test began, Time=74 day, end of bridge solar collector test, Time=95 day, initial condition before the de-icing test began and end of 21 days inactive system, Time=99 day, end of the de-icing test. Both models worked similarly, and the simulated result is very close to experimental data. The conventional model tends to work slightly better at the depth of around 1.8 m.

Figure 6.10 illustrates the time series comparison between the experimental data from TMB 1 and the simulated soil temperature for the same depth as the TMB 1's sensor nodes by the conventional and proposed model. The results are satisfactory, and it can be observed there is a minor difference between numerical models and experimental data, however, there is a noticeable mismatch for the depth 6.4 m below the ground surface which is mostly due to the mismatch for the same depth in the initial ground temperature condition.

In the same manner, as shown for TMB1 the numerical models were utilized the measured data from TMB3 for verification of the models' output. Both models worked similarly, and the simulated results are very close to experimental data. Figures 6.11 and 6.12 show vertical temperature profile and time series comparison between the experimental data from TMB 3 and the simulated by the conventional and proposed efficient model. Overall, there is a good agreement between numerical results and experimental data, and a perfect match between the proposed and conventional models.

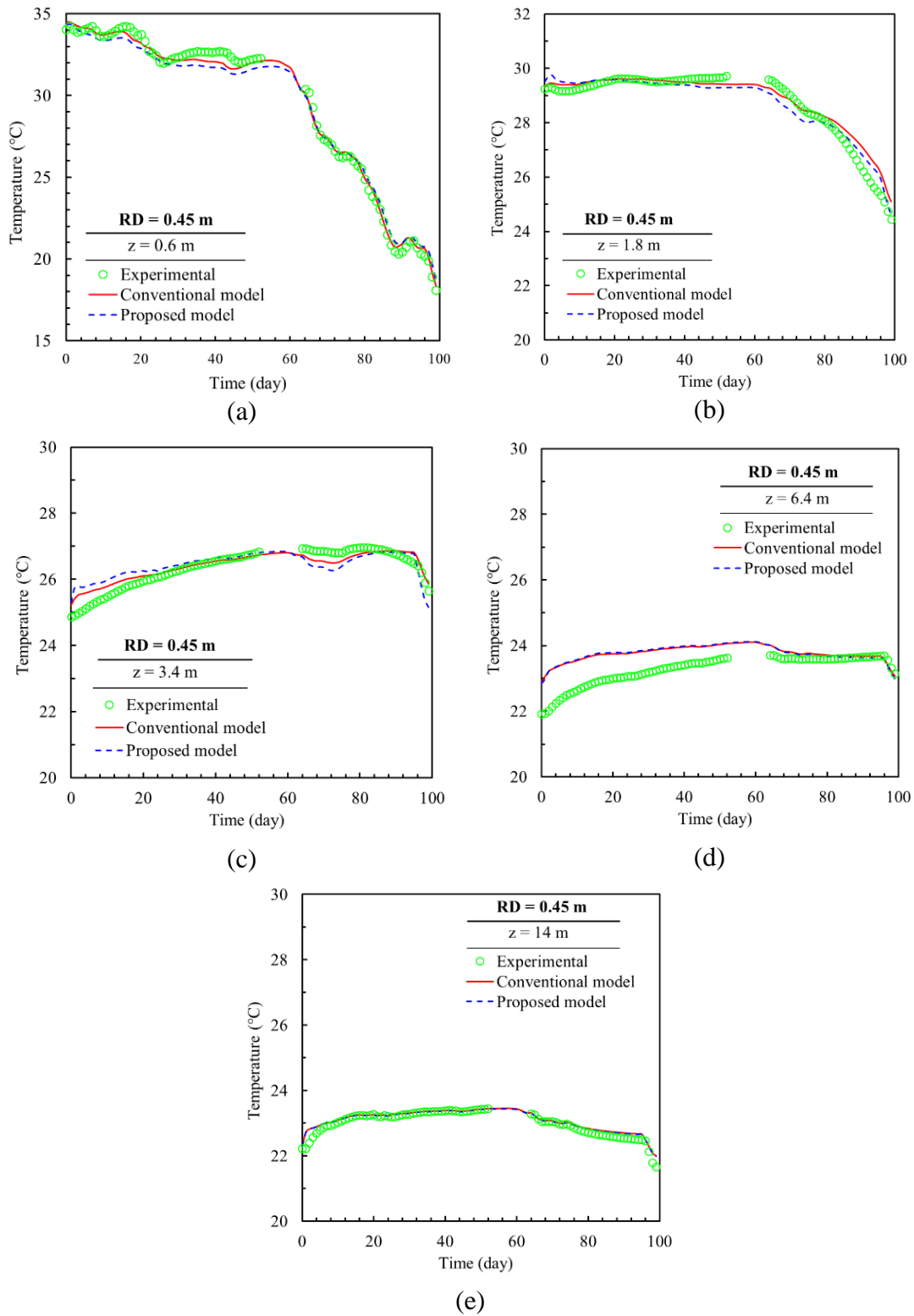


Figure 6.10. Comparison between the experimental data from TMB 1 and the simulated soil by the conventional and proposed efficient model.

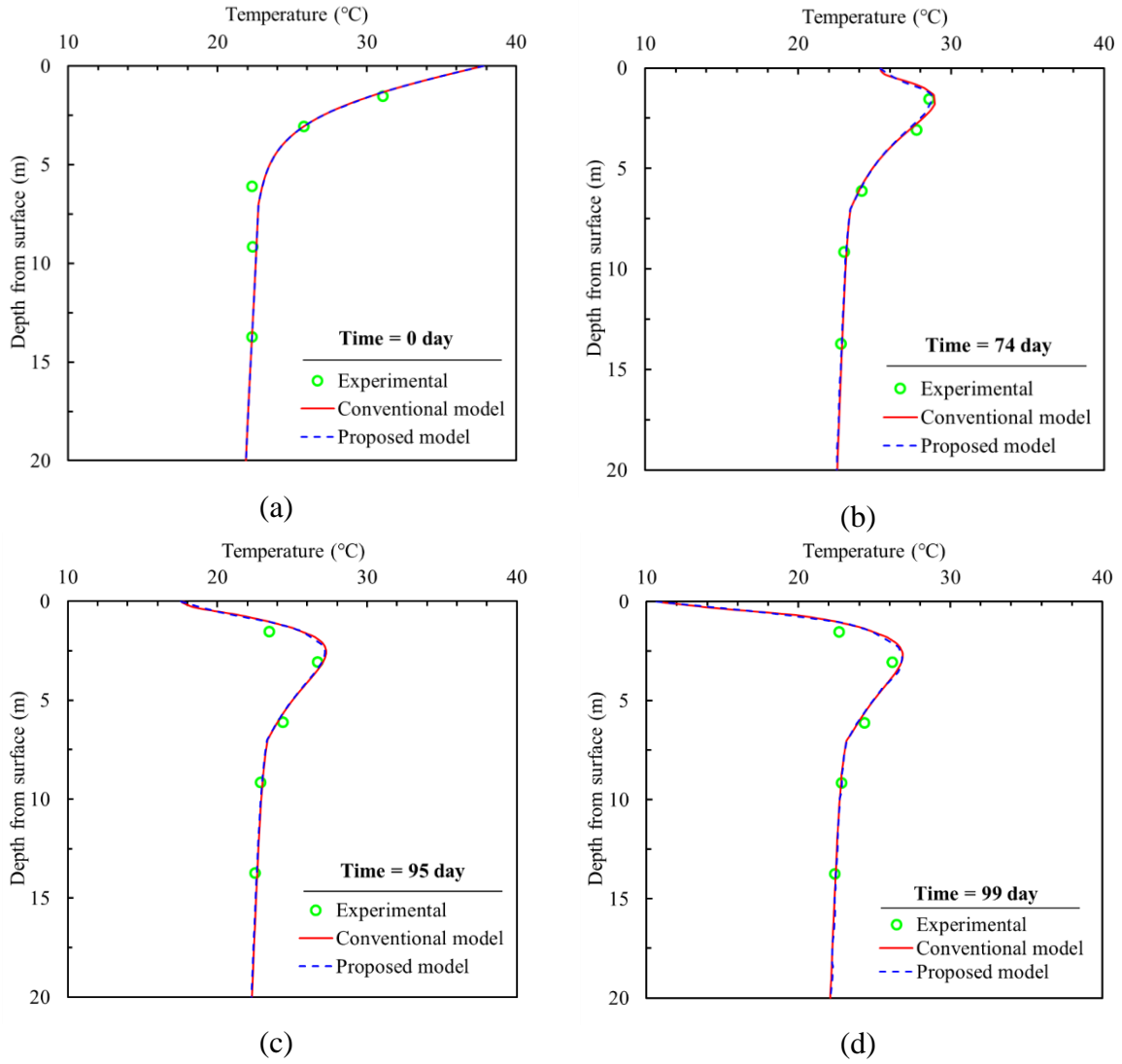


Figure 6.11. Vertical temperature profile comparison between the experimental data from TMB 3 and the simulated by the conventional and proposed efficient model.

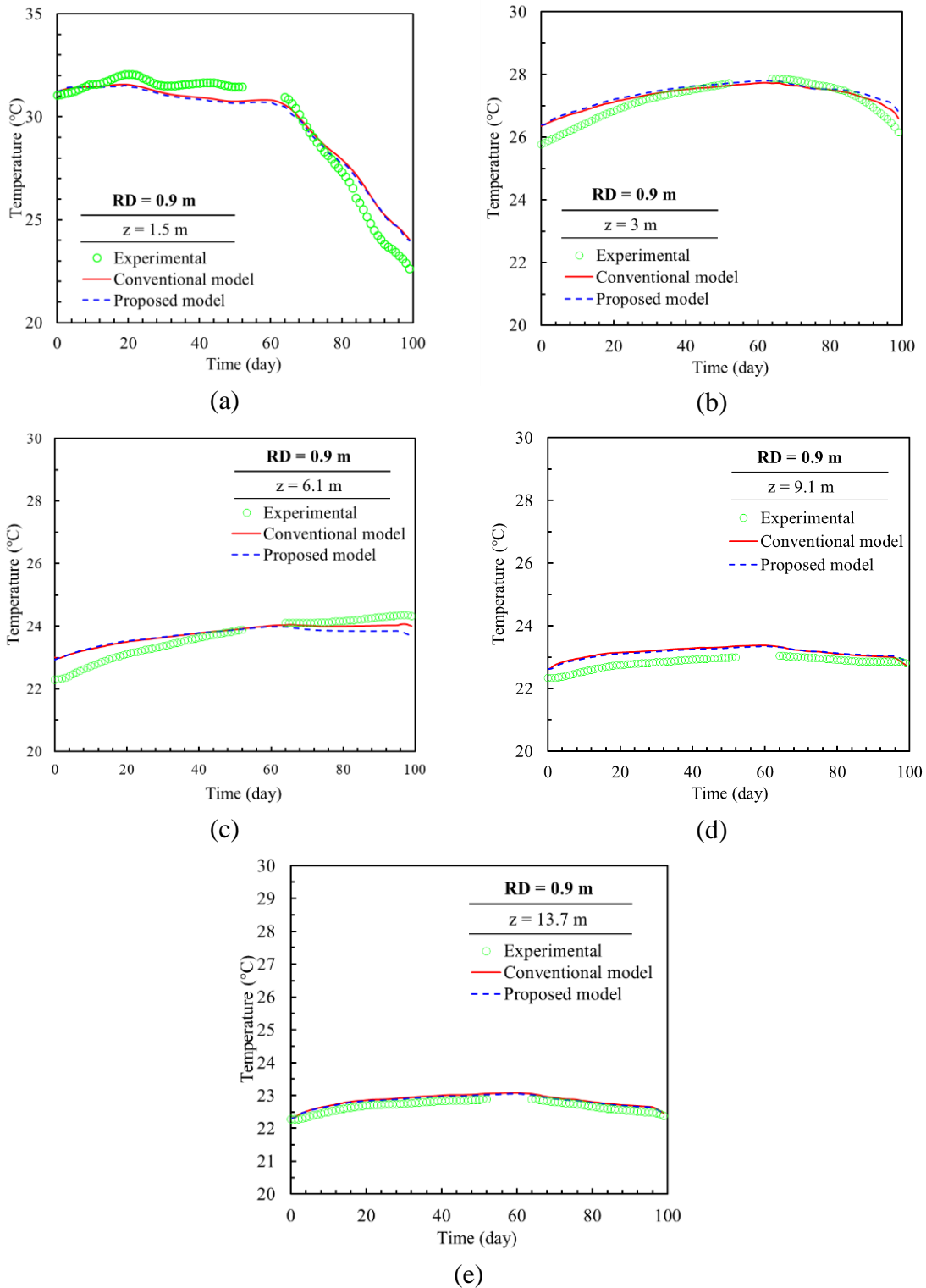


Figure 6.12. Comparison between the experimental data from TMB 3 and the simulated soil by the conventional and proposed efficient model.

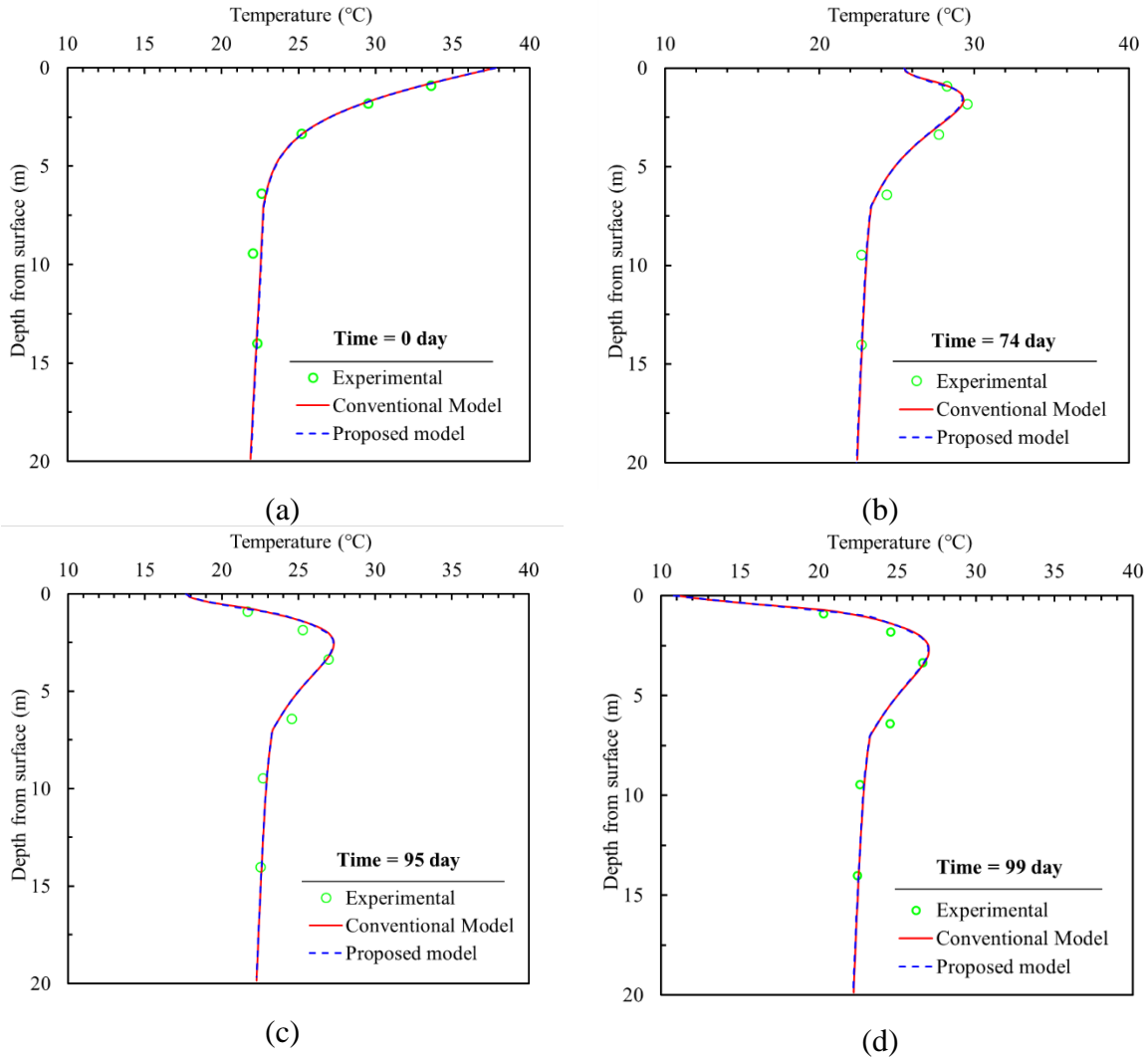
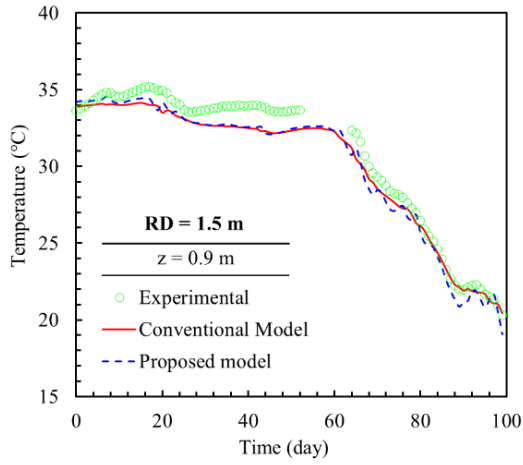
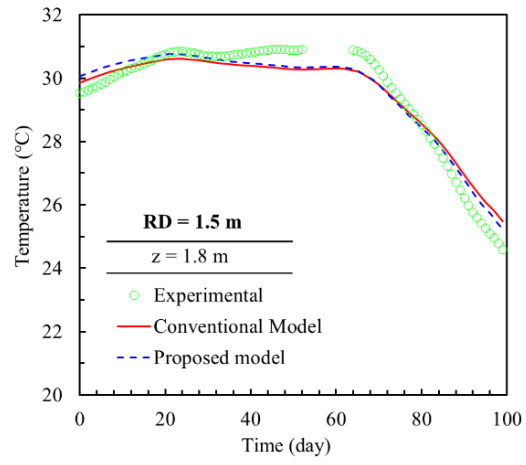


Figure 6.13. Vertical temperature profile comparison between the experimental data from TMB 4 and the simulated by the conventional and proposed efficient model.

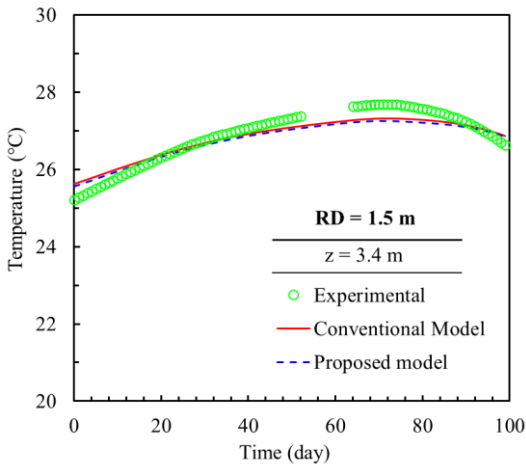
Similarly, Figures 6.13 and 6.14, also show vertical temperature profile and time series comparison between the experimental data from TMB 4 and the simulated by the conventional and proposed efficient model. The same conclusion as the result comparison for TMB1 and TMB3 is also valid here. The proposed and conventional models have a perfect match and there is good correspondence with experimental data.



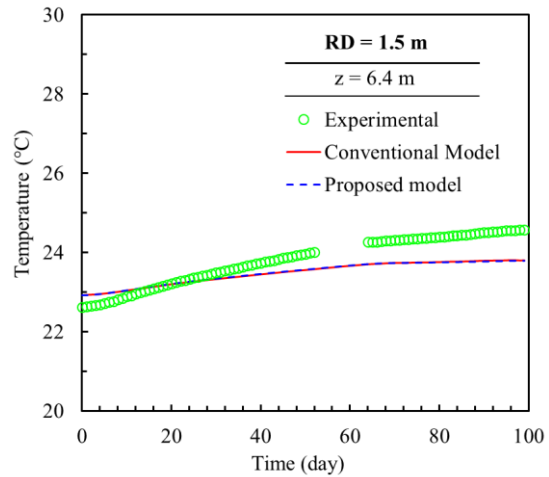
(a)



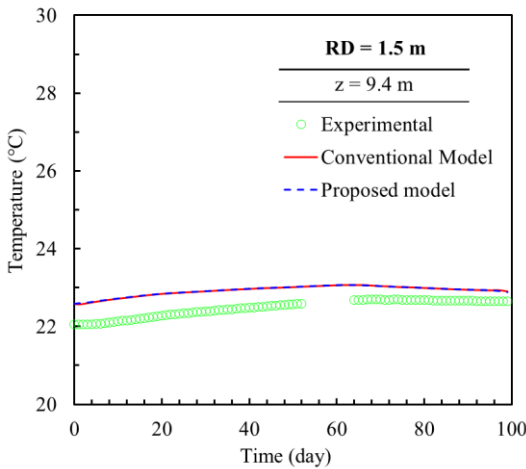
(b)



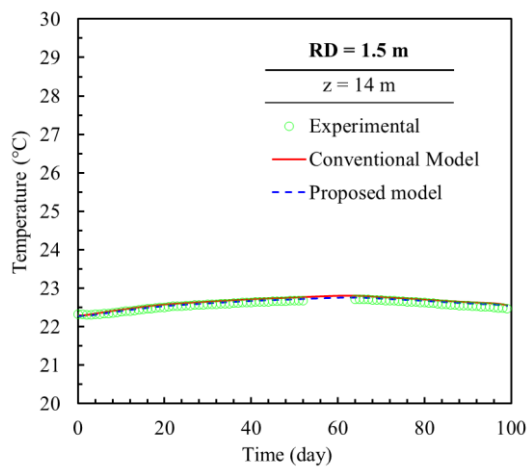
(c)



(d)

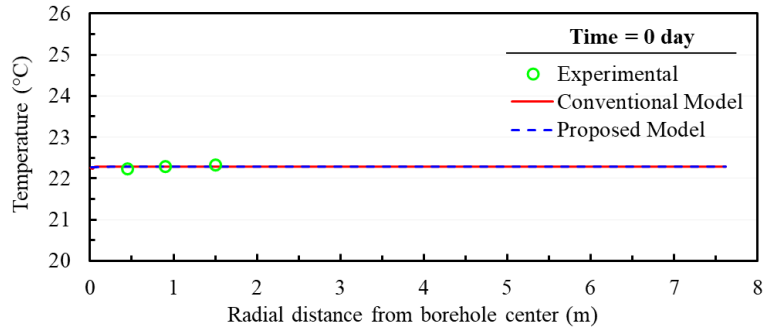


(e)

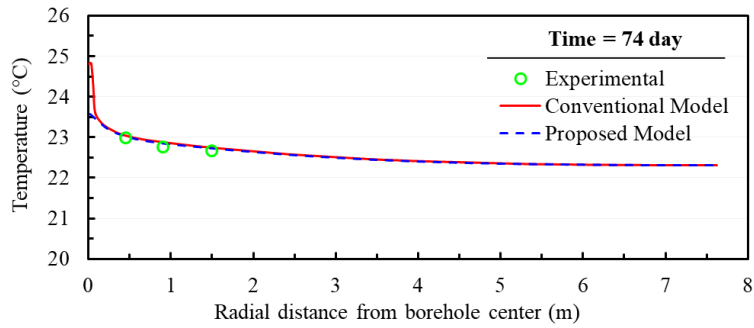


(d)

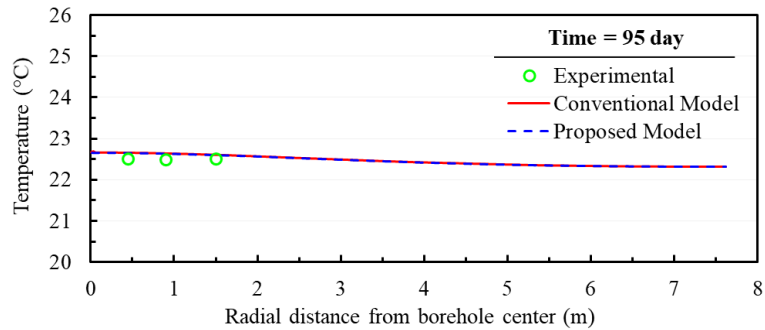
Figure 6.14. Comparison between the experimental data from TMB 4 and the simulated soil by the conventional and proposed efficient model.



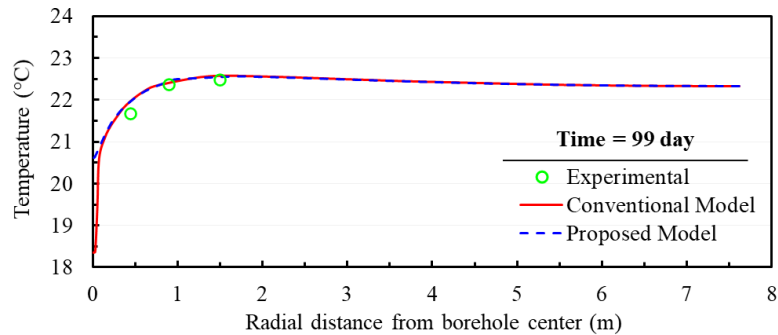
(a)



(b)



(c)



(d)

Figure 6.15. Radial temperature profile comparison at 14 m below the ground surface between the experimental data and the simulated by the conventional and proposed efficient model.

Figure 6.15 compares the radial temperature profile from conventional and numerical models with the measured data from a sensor node at 14 m below the ground surface from TMB1,3 and 4 at 14 m. The result of the proposed and conventional models are almost identical, however, there are some differences for the radial distance corresponds to the borehole wall diameter. Also, a minor difference between experimental data and numerical models proves the models are successful in simulating the ground temperature which was affected by GHE operation. Also, the result shows that the radius of the cylindrical influence zone which was affected by the GHE operation in 74 days is about 5 m.

6.4.2 Accuracy and Computational Time

To further demonstrate the accuracy and efficiency of the numerical models the error between predicted temperature by the numerical models and measured data on-site was investigated. Three common indices including root mean squared error (RMSE), mean absolute error (MAE), and mean absolute percentage error (MAPE) were used to evaluate the fitness between the model's output and experimental measurements, they are determined as:

$$RMSE = \sqrt{\frac{\sum_{i=1}^{i=n} (T_{i,Exp} - T_{i,model})^2}{n}} \quad (6.22)$$

$$MAE = \frac{1}{N} \sum_{i=1}^{i=n} |T_{i,Exp} - T_{i,model}| \quad (6.23)$$

$$MAPE = \frac{1}{N} \sum_{i=1}^{i=n} \left| \frac{T_{i,Exp} - T_{i,model}}{T_{i,Exp}} \right| \quad (6.24)$$

Where $T_{i,Exp}$ and $T_{i,model}$ are experimental and simulated temperature, respectively, and n is the number of experiment samples.

Table 6.6 lists the error of numerical models for GHE outlet fluid temperature, TMB1, TMB3, TMB4. For TMBs, first, the errors are calculated for each sensor node throughout the 99 days of the study period, then an arithmetic average was taken among all sensor nodes in each TMB. The result shows the accuracy of both models are very similar and there is only a minor difference between the proposed and conventional models. The result also demonstrates, the models' accuracy slightly declines as the radial distance from GHE increases, this is mostly due to an increase in finite element mesh size. As mentioned previously, the mesh size is increasing as moving from the central axis of the domain to the boundary.

Table 6.6. The error of the numerical simulations results

Data	Model	RMSE (°C)	MAE (°C)	MAPE (%)
Outlet	Conventional	0.19	0.15	0.60
	Proposed	0.25	0.21	0.81
TMB1 (RD=0.45 m)	Conventional	0.32	0.25	1.00
	Proposed	0.39	0.32	1.21
TMB3 (RD=0.9 m)	Conventional	0.36	0.31	1.23
	Proposed	0.38	0.33	1.19
TMB4 (RD=1.5 m)	Conventional	0.43	0.37	1.39
	Proposed	0.42	0.38	1.42

Figure 6.16 illustrates the element size of the plane located at the center and along the GHE. While the conventional model contains many small elements inside the borehole and in the vicinity of the pipes, however, the proposed model did not require generating the small elements to satisfy the model's geometry which is due to the elimination of the borehole and pseudo pipes from geometry. For the proposed model, the concentration of the elements is located at the top and bottom of the 1D pipe flow where it encounters other edges.

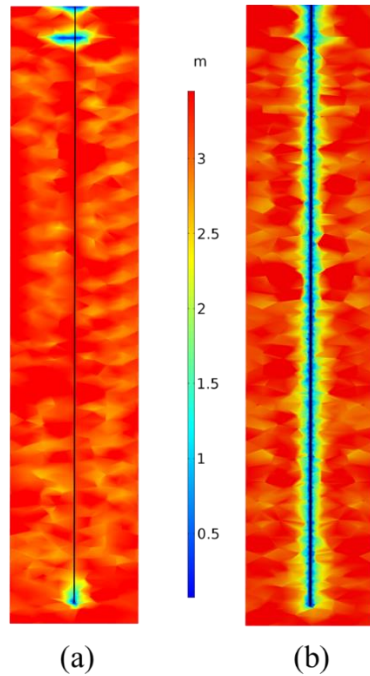


Figure 6.16. Element size distribution on a plane located on the central axis of the borehole along the GHE: (a) Proposed model; (b) Conventional model

Table 6.7 shows the number of elements and computational time for each model. All simulations were performed on a computer with an Intel(R) Xeon(R) processor running at 6 GHz using 128 GB of RAM, running Microsoft Windows 7. Two finite elements mesh were generated, and simulations were conducted for both cases. In the optimum mesh case, the conventional model was consisted of about 10 times as the proposed model, however, it is reduced to about 3 times for the extra fine mesh case. The conventional model requires 3 hours and 37 minutes to complete the initial ground temperature and GHE operation simulation when using the optimum mesh, while the proposed model only needs 11 minutes to finish the simulation. For the extra fine mesh case, the complete simulation takes 12 hours and 33 minutes with the conventional model and 2 hours and 22 minutes with the proposed model. Overall, the computational time is reduced by 95% and 81 % for the optimum and extra fine mesh cases.

Table 6.7. Comparison of the number of elements and computational time between proposed and conventional model

Mesh	Mesh 1: Optimum	Mesh 2: Extra fine
Number of Elements		
Conventional	256,184	908,208
Proposed	25,524	293,273
Computational Time: Initial ground temperature model		
Conventional	31 min	2 h 17 min
Proposed	3 min	46 min
Computational Time: GHE operation model		
Conventional	3 h 6 min	10 h 16 min
Proposed	8 min	1 h 36 min

6.4.3 Thermal behavior inside the borehole.

Figure 6.17 illustrates the temperature profile on the different planes along GHE for the last day of the bridge solar collector test. It also shows the enlarged view of the plane at 15 m below the ground surface for better comparison between the proposed and conventional models.

To better understand how the proposed model work, the vertical temperature profile along the heat exchanger pipe should be compared to the vertical temperature profile inside the borehole for the conventional model. Figure 6.18 compares the solid temperature along with the 1D pipe flow element for the inlet pipe of the proposed model with that of the conventional model as well as the pseudo pipe and borehole wall temperature. As it was the purpose of the proposed model, the heat transfer along the 1D pipe element of the proposed model can accurately simulate the heat transfer at the borehole wall of the conventional. Moreover, Figure 6.19 compares the radial temperature profile at 14 m below the ground surface along the axis which passes through both inlet and outlet pipe. It can be seen although the proposed model did not simulate the temperature

distribution inside the borehole, however, there is a good agreement for the temperature beyond the borehole wall.

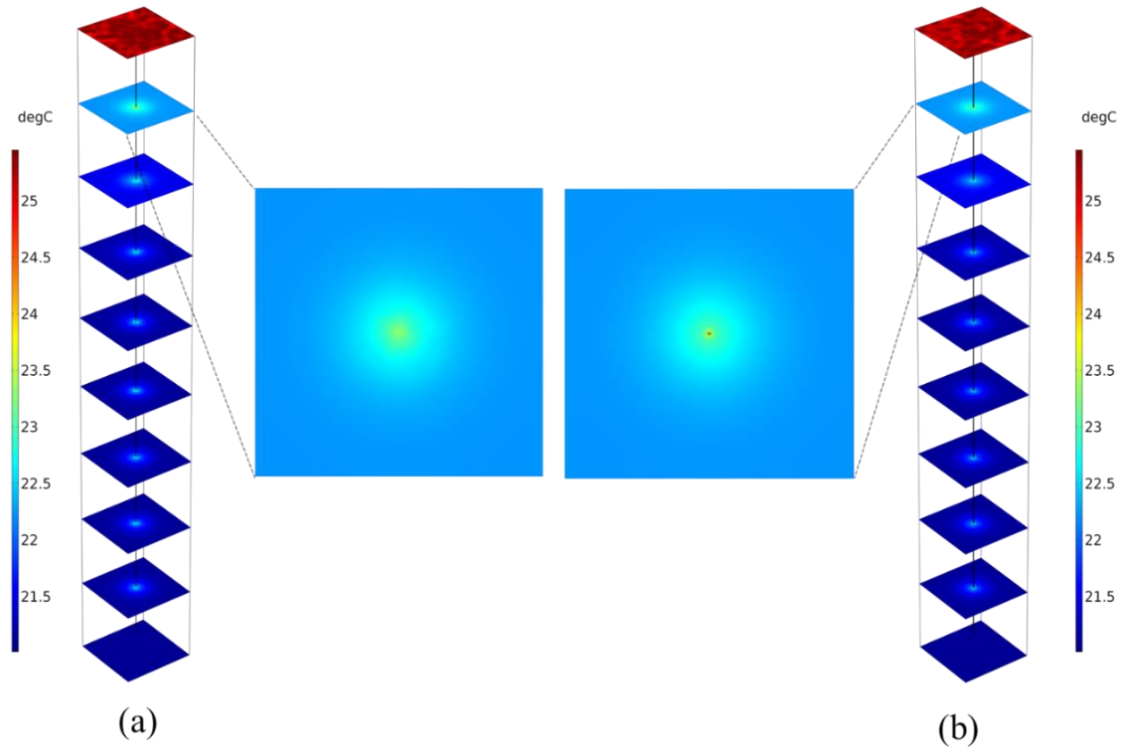


Figure 6.17. Temperature profile at Time=74 days and enlarged view for 15 m below the ground surface: (a) Proposed model; (b) Conventional model

Remembering the errors of the 1D pipe flow discussed by Ozudogru et al. (2014), the minor error in the proposed model output is because the proposed model simulates the borehole wall temperature at the central axis of the pipe location, which in reality occurs at the distance equal to borehole radius. On the plus side, the proposed model can account for the heat capacity of the heat exchanger pipe without adding to the geometrical complexity of the model which results in fewer estimation errors. The authors of the current paper observed that the error due to exact temperature coupling location is greatly less than the case of not accounting for the heat capacity in the model

for the heat exchanger pipe. Moreover, for the 2D problem the heat exchanger pipe location can be transferred to the borehole wall location to eliminate the error due to the exact temperature coupling location.

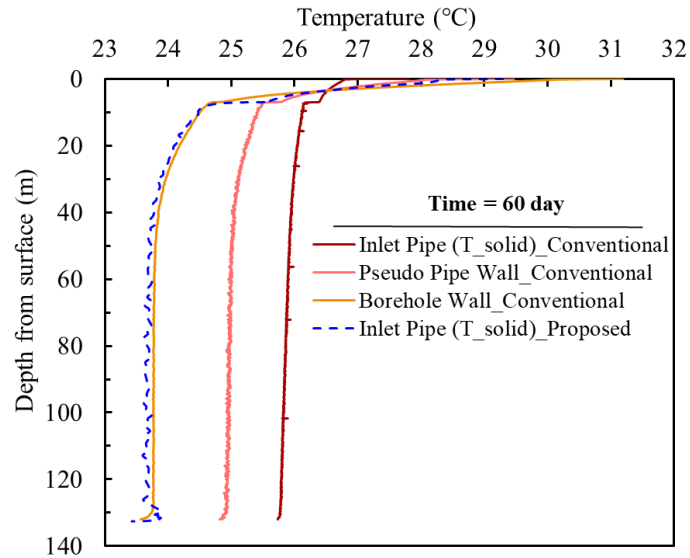


Figure 6.18. Temperature profile inside the borehole

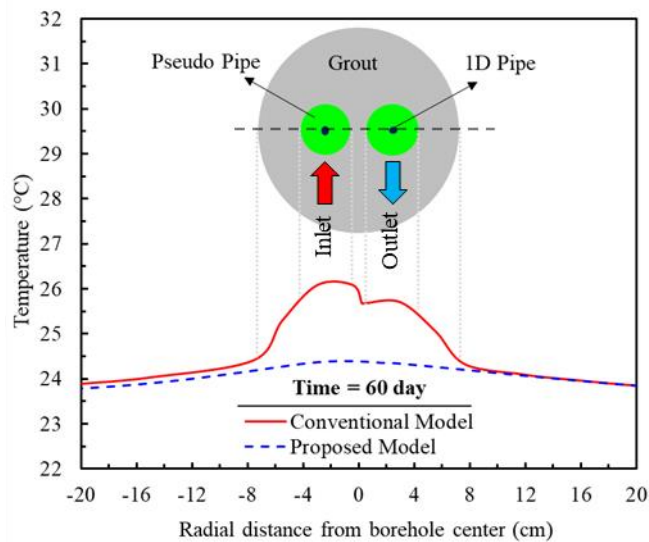


Figure 6.19. Radial temperature profile comparison at 14 m below the ground surface between the conventional and proposed model inside and borehole and surrounding soil

6.5 Conclusions

In this study, a simplified computationally efficient numerical model was developed using an equivalent 1D non-isothermal pipe flow element for the GHE, which can represent the entire borehole. The proposed model is compared with the conventional model and together are validated against the experimental data. The result showed the proposed model output almost matches perfectly with the conventional model and provides the same level of accuracy. It was observed that the application of the proposed model can significantly reduce the required number of mesh elements and consequently the computational time. The required number of elements was decreased by 90% and 67% for the optimum and extra fine mesh cases and computational time was reduced by 95% and 81 % for the same mesh cases, respectively. As the proposed model provided the same level of accuracy as the conventional model while greatly reduced the computational time, the proposed model can be used as a desirable alternative for the conventional model.

CHAPTER 7: LIFE-CYCLE COST-BENEFIT ANALYSIS OF BRIDGE DECK DE-ICING USING GEOTHERMAL HEAT PUMP SYSTEM: A CASE STUDY OF NORTH TEXAS

7.1 Abstract

Transportation infrastructures suffer major damage from ice and snow each year, negatively affecting the U.S. economy. Bridges, a key element of the transportation network, are the most vulnerable to impairment from ice and snow. The conventional snow and ice removal system (CSRS) is not a satisfactory solution, as it causes additional problems relating to the acceleration of bridge deck corrosion, motorist safety, travel delays, and environmental damages. In an attempt to provide a sustainable, economically viable alternative, this research performed a scenario-based life-cycle cost-benefit analysis (LCCBA) of the geothermal heat pump de-icing system (GHDS). The results of the analysis show that the benefits of the GHDS outweigh its cost. In addition, the output of a sensitivity analysis, using the Monte Carlo Simulation (MCS), indicates that traffic flow enhancement is the most dominant variable affecting the overall result. For a daily traffic volume of 24000 vehicles, the benefits are estimated to be 2.32 times greater than the costs, with 95% reliability. The analysis output demonstrates that the application of the GHDS is economically viable for bridges with a minimum daily traffic volume of 7000 vehicles.

7.2 Introduction

Cold climate conditions have a huge impact on the functionality of roads, as they directly influence the safety and traffic flow of transportation networks. Bridges are key elements of the infrastructure, but because they are exposed to the atmosphere from both the top and bottom

surfaces, they are highly prone to accumulating ice and snow. De-icing them is one of the critical and recurring tasks in snowy and icy regions.

The most convenient method for removing ice and snow is using salt as a de-icing agent. Unfortunately, however, applying salt can cause a phenomenon known as a “chloride attack,” which creates a significant durability problem for concrete pavements and structures. The net result of a chloride attack is the corrosion of steel reinforcement, which leads to cracking and spalling of the concrete, and ultimately deteriorates the bridge deck surface. This topic has been studied by several research groups (Baboian 1992; Daghighi and Nahvi 2014; Granata and Hartt 2009; Monsalud et al. 2015; White et al. 2005; Yunovich et al. 2003). The corrosion of steel reinforcements eventually causes a reinforced concrete bridge deck to collapse when the decreased reinforcement area overstresses the steel cross-section (Ghasemi-Fare et al. 2015). Naito et al. (2010) listed several examples of reinforced concrete bridge decks that collapsed because of the corrosion of steel reinforcements. Recent studies have suggested using resistant reinforcing steel, but this is only applicable to new projects and does not address issues relating to the existing infrastructure.

There is a growing national concern over the deterioration of bridges. Koch et al. (2002) estimated that the annual direct cost of bridge corrosion is from \$6 to \$10 billion. When indirect costs are included, the total cost is tenfold (Yunovich et al. 2003). One-fourth of the bridges in the US are either structurally deficient or functionally obsolete (FHWA 2008). Extending their service life, with minimal maintenance, is one of the main challenges facing those responsible for maintaining highway infrastructures (AASHTO 2005).

In addition to the problems caused by chloride attacks, applications of de-icing salt also cause delays for motorists and result in huge financial losses resulting from excessive fuel

consumption and additional travel time cost (Zeroual et al. 2017). The increased corrosion rate of a bridge deck also requires more frequent maintenance, which may include closing lanes or even the whole bridge to fix the issues, again imposing delays on travelers. Environmental contamination, damage and mortality of roadside vegetation, reduction in soil stability, and permeability and salinity of water are other disadvantages of employing a de-icing agent (Fischel 2001). Some of these effects, such as high salinity, cause a huge negative impact on the environment (Nahvi et al. 2018). The conventional method for de-icing a bridge deck also provokes some safety concerns for the motorists since the application of this system does not always provide a clear surface, and motorists encounter an icy surface on the bridge deck, particularly during the night when the temperature can drop below freezing quickly. Therefore, a more sustainable solution is needed.

Geothermal energy is recognized as an effective solution in a world that is moving toward using green and renewable energy sources to reduce the consumption of fossil fuels and the emission of greenhouse gases (International Energy Agency 2014). Unlike the ground surface, the soil temperature below a certain depth is relatively constant (Brandl 2006; Jalili and Habibzadeh Bigdarvish 2017). Multiple methods, ranging from boreholes to thermo-active geostructures of any kind (deep and shallow foundations, diaphragm walls, tunnel liners, or anchors), are utilized to harvest shallow geothermal energy (Barla et al. 2016; Binod et al. 2012; Mimouni et al. 2014; Nam and Chae 2014; Sterpi et al. 2017, 2018a; c; Zhang et al. 2013). A more recent use of geothermal energy is the application of a geothermal heat-pump de-icing system (GHDS) for de-icing bridge decks. In this system, heat carrier fluid extracts the geothermal energy and carries it from ground loop heat exchangers (GLHE) to the hydronic loops installed in the bridge deck. Heat is transferred from the hydronic loops to the bridge deck surface and provides the energy to melt

the ice and snow on the surface. Heat pumps are utilized to compensate for the extra required heat. The technology of the GHDS has been studied and analyzed by many research groups through experiments, numerical methods, and feasibility studies (Balbay et al. 2010; Eugster and Eugster 2007; Ghasemi-Fare et al. 2015; Lei et al. 2018; Li et al. 2018; Lund 1999; Spitler and Ramamoorthy 2000). Moreover, GHDS is a sustainable approach for de-icing the bridge deck, considering the contributing parameters in the sustainability analysis (Das et al. 2018).

Ghasemi-Fare et al. (2015) conducted research on the feasibility of this technology, and their report demonstrated the key parameters that govern the physical process and showed that utilizing the GHDS is reasonable and practical. The same report performed a cost analysis, but rather than explaining the cost and economic feasibility of the technology, it focused on the life cycle analysis (LCA) of de-icing salt. Li et al. (2018) performed a numerical feasibility study on the most recent type of this technology, externally heated bridge decks, and compared the results with an internal heating system for de-icing. It did not, however, present any information regarding the cost of the system. Nahvi et al. (2018a) studied the economic viability of electrically conductive concrete (ECON) heated pavement systems (HPS). Although their research focused on airport pavement heating using ECON, it provided insight into the economic performance of heating systems, as well as useful information regarding the economic analysis details and process.

The Texas Department of Transportation (TxDOT) recently investigated the implementation of this system on Texas bridges (Yu et al. 2017). The principal objectives of this research, however, are to assess the economic viability of utilizing the GHDS in North Texas, and to demonstrate how it can contribute to preventing corrosion, enhancing motorist safety, minimizing travel delays, conserving the environment, and saving money. This paper first reviews the literature on conventional snow and ice removal and geothermal heat-pump de-icing systems

to determine their corresponding costs and benefits. An analysis framework is developed, and a life cycle cost-benefit analysis is conducted. The results of the base case and sensitivity analysis are presented, and the results are discussed and highlighted.

7.3 Background

7.3.1 Conventional snow/ice removal system (CSRS)

The CSRS cost of de-icing a bridge deck is the same as that of de-icing pavements and includes the machinery, snow/ice control material, and labor. Several studies have estimated the cost of removing ice and snow from roads. (Nixon 2001) stated that the Oregon DOT reduced the cost of winter maintenance from \$94 to \$24 per lane mile in freezing rain conditions. (Cuelho 2010) estimated the cost of the winter operations implemented by the Colorado DOT to be \$5,200 per lane mile using conventional methods, but reported that applying anti-icing techniques reduced the cost to \$2,500 per mile lane. However, bridge decks require de-icing more frequently than pavement because they freeze earlier. Unfortunately, the literature lacks information comparing the cost of conventionally de-icing a bridge deck with the de-icing pavement.

Every year, tons of solid and liquid chemicals are used on US highways to prevent ice and snow accumulation. The two most common types are abrasives (e.g., sand) and chloride-based de-icers. Abrasives provide a temporary friction layer and improve skid resistance on icy road surfaces. They are usually applied when the temperature is lower than that at which de-icing and snow control materials are effective. Table 7.1 summarizes the information on abrasives commonly used as de-icing materials. The Colorado DOT studies reveal that abrasives are the least expensive de-icing materials (Fischel 2001). More recent research shows, however, that the overall cost of using abrasives should not be limited to the cost of the materials, but should also include

the cost of cleanup and take into account the more frequent usage required in comparison to other de-icing and ice control materials (Fay et al. 2008). Sodium chloride (NaCl) (rock salt) is the oldest and most popular de-icer in the chloride-based de-icer family; it is cheap, abundant, and has served many roads in the United States since the 1930s (Fischel 2001). Table 7.1 also summarizes the information on chloride-based products used as a de-icing material.

Table 7.1. Information on chloride-based and abrasives products used as a de-icing material (Fay et al. 2015)

Category	Product Type	Liquid/solid	Application rate	Cost
Abrasives	Sand	Solid	100-1000 lbs/l-m	\$6-16/ton
	Cinder	Solid	100-500 lbs/l-m	\$20/ton
	Crushed rock or gravel	Solid	100-500 lbs/l-m	\$11-15/ton
	Pre-wet abrasives	Pre-wet solid	100-1000 lbs/l-m	\$12-14/ton
Chlorides	NaCl	Solid	100-800 lbs/l-m	\$30-100/ton
		Liquid	10-40 gal/l-m (anti-icing) 8-20 gal/l-m (pre-wetting)	0\$0.04-0.09/gal
	MgCl ₂ and CaCl ₂	Solid	100-500 lbs/l-m	MgCl ₂ : \$100/ton
		Liquid	10-40 gal/l-m (anti-icing) 8-20 gal/l-m (pre-wetting)	MgCl ₂ : \$0.50-0.90/gal CaCl ₂ : \$120-300/ton

7.3.2 Geothermal heat pump de-icing system (GHDS)

GHDS is a ground-coupled heat pump system that utilizes the heat output of the system to de-ice and melt snow. The heat carrier fluid circulates in a closed loop between the ground loop heat exchangers (GLHE) and embedded loops in the bridge deck concrete. The hydronic loops in the bridge deck transfer the heat to the deck surface and melt the ice and snow. Moreover, the efficiency of the GHDS is studied using the coefficient of performance (COP). It is a variable depending on different parameters (e.g. GLHE size, weather condition etc.) which, for the average case COP of 2.6 can be assumed (Balbay et al. 2010). Figure 7.1 illustrates the components of GHDS.

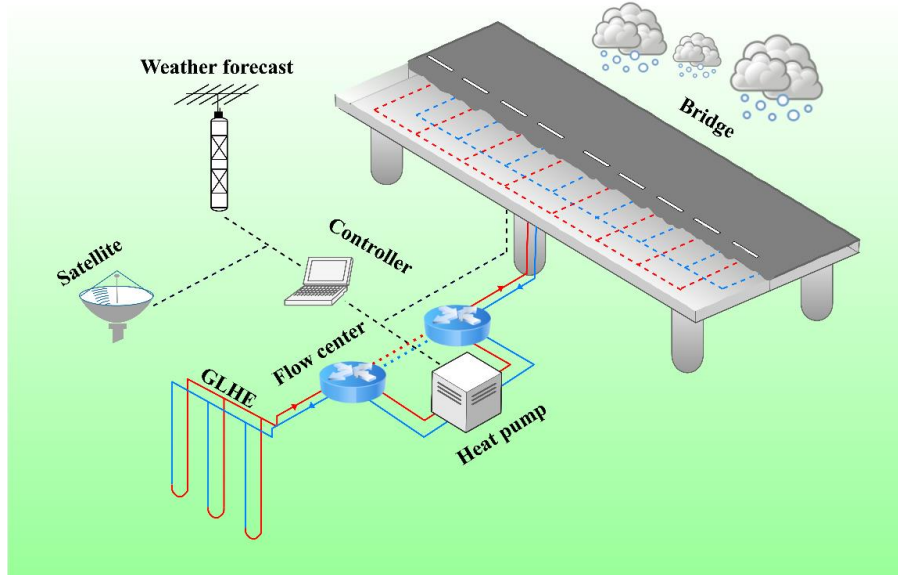


Figure 7.1. Conceptual diagram of the geothermal heat pump de-icing system (GHDS)

7.3.2.1 GHDS cost

The total cost of GHDS includes the initial start-up investment, operation, and maintenance. The initial cost refers to the cost of purchasing materials, equipment, and machinery as well as installation and labor expenses. The cost of operation corresponds to the energy (e.g., electricity, fuel etc.), required to maintain the system. Maintenance cost refers to regular inspections and repairs expenses, if needed. Figure 7.2 shows the itemized costs of GHDS.

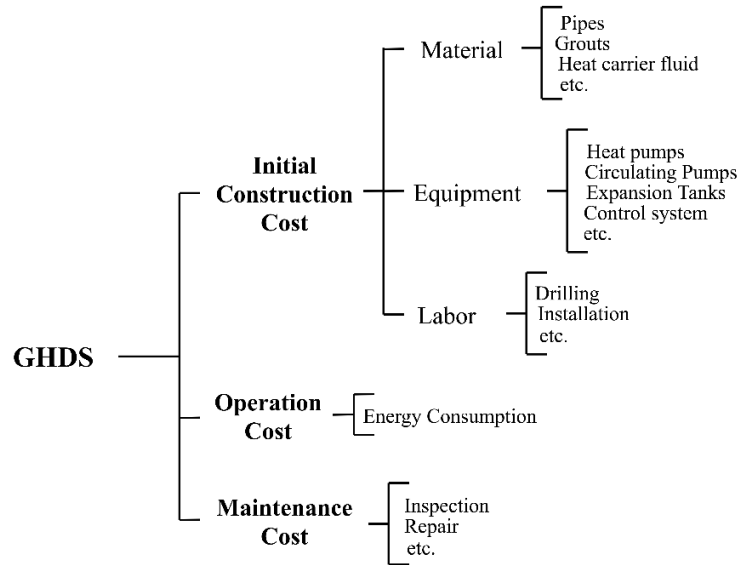


Figure 7.2. Cost items of GHDS

Cost information for all previous GHDS projects is not available in the literature; therefore, only Four real-scale GHDS projects, namely: Silver Greek, OR, I-84 Overcrossing (West Panel), OR, Amarillo, TX and Wall Street, Klamath Falls, OR, with available required data are reviewed in this paper. Table 7.2 summarizes the cost information of the aforementioned projects.

Table 7.2. Construction cost information of previous projects (Boyd 2003; Minsk 1999)

Project	Silver Greek, OR	I-84 Overcrossing (West Panel), OR	Amarillo, TX	Wall Street, Klamath Falls, OR
Year	1999	1999	1999	2003
Application	Bridge deck	Bridge deck	Bridge deck	Bridge deck
Heated Area (m ²)	576	598	1598	346
Initial Cost (\$)	411,000	307,200	1,200,000	206,000
Annual O& M Cost (\$)	9,200	9,900	8,880	N/A
Heat Output (W/m ²)	394	694	129	189
Unit Construction Cost (\$/m ²)	713	513	750	595
Unit Annual O&M Cost (\$/m ²)	16	16	3	N/A

In addition to the cost information of the few actual projects, some researchers have estimated the unit cost of the bridge deck snow melting and de-icing systems. The cost of systems for snow melting and ice control of pavement has also been included since it is the same technology, with a different application. The systems share similar components, and a significant portion of the total cost of both is the cost of drilling boreholes. Table 7.3 shows the estimated value of the unit cost for construction of geothermal bridge deck and pavement snow melting and de-icing systems by different research groups.

Table 7.3. Estimated unit construction costs of the GHDS for bridges and pavements.

Research Group	Swanson (1980)	Donnelly (1981)	Lund (2000)	Brown et al. (2014)	Anand et al. (2017)
Application	Bridge deck	Pavement	Bridge deck	Pavement	Pavement
Unit Cost (\$/m ²)	82	112	376	537	376

7.3.2.2 GHDS Benefit

The main advantages of geothermal bridge deck de-icing systems are corrosion prevention, safety enhancement, minimizing travel delays, and conservation of the environment. All the cost saving items, while using GHDS in comparison with CSRS, are considered as benefits of the GHDS.

7.3.2.2.1 Corrosion prevention

Corrosion is an issue of great importance nationally. Total annual corrosion costs include both direct and indirect costs. The direct cost includes the cost of design, manufacturing, and construction; however, other costs such as management, repair, maintenance, rehabilitation, loss of productive time, etc. are considered both direct and indirect costs. As the statistics show an increasing trend of corrosion cost (Nwaubani et al. 2014), new measures and methods should be implemented in all fields dealing with corrosion to alter the situation. One of these fields in which quick actions are necessary is highway infrastructures.

De-icing and anti-icing chemicals are used on roads to clear the surface of snow and ice, but their application has resulted in the corrosion of highway infrastructures, pipelines, utilities, and vehicles (Xi and Olsgard 2000). Bridges are most susceptible to damage from de-icing agents. Bridge decks provide a relatively thin concrete cover for embedded reinforcing steel. Salt brine affects the cracks in the deck surface, which over time results in the reinforcing steel corroding. The steel rebar expands as it corrodes, and ultimately causes the delamination of the bridge deck concrete surface (Vitaliano 1992a). Corrosion of the bridge deck ceases with the use of GHDS, and no more applications of road salt or any other type of de-icing chemical are needed.

7.3.2.2.2 Safety enhancement

Safety is a vital component of a sustainable transportation system. Transportation departments (DOTs) are continuously challenged to cost effectively provide a high level of service (LOS) on the roadways and maximize the safety of the users (Fay et al. 2015). One of the recurring challenges is a slippery road surface caused by ice or snow, an issue that concerns not only the northern states, but also the southern states, including Texas.

According to the Texas Department of Transportation (TxDOT), from 2007 to 2016, an average of 4,900 of car crashes occurred each year in Texas due to slippery road conditions (ice, snow, and/or slush). The data shows that 78% of all car crashes in this category are due to ice (Texas Department of Transportation (TxDOT) 2017). With an application of GHDS, many of those cars crashes could have been prevented.

7.3.2.2.3 Traffic flow enhancement

Many researchers believe that the main purpose of transportation projects, such as highway and public transportation improvements, is to save the users' time. Travel time is considered one of

the greatest contributors to transportation costs (Mokhtarian and Salomon 2001). Delays result in excessive fuel consumption and loss of time, which convert to increased direct and indirect costs. With the rising trend of delays and congestion on the roadways and highways, it is crucial to employ effective measures that ensure an acceptable level of service (Bivina et al. 2016).

Applying a geothermal heat-pump de-icing system enhances traffic flow and reduces the cost of travel delays; however, many cost-benefit analyses fail to address the impact that its application has on the user (indirect cost). Because the user's cost is not tangible, as other cost items are, and it is not incurred by the owner-operator, it is frequently not included as a part of the decision-making process (Yunovich et al. 2003). In this paper, travel delays are evaluated in three areas:

1. Work zones - Travel delays due to work zones refer to the maintenance activities necessitated by bridge corrosion, which slow down traffic.
2. Slippery road surface conditions – Icy and snowy road surfaces cause motorists to decelerate when passing over the bridge.
3. Car crashes – Vehicular accidents result in traffic congestion on bridges.

7.3.2.2.4 Environmental benefits

De-icing chemicals such as NaCl are inexpensive, but the environmental toll that they take makes the overall cost much higher (Cuelho 2010). Vitaliano (1992b) studied the costs of salting, and estimated that the total cost of NaCl was \$800 per ton, including the costs of the damage to roads and bridges, repair and maintenance, roadside vegetation, etc. In other research, at the Transportation Research Board (TRB), the corrosion and environmental effects of NaCl are estimated to cost about 10 times more than the initial materials(Blackburn et al. 1994). In a separate research, Blackburn (2004) mentioned that the corrosion and environmental impacts of NaCl amount to an overall annual cost of \$5 billion.

Based on research by the FHWA, the Strategic Highway Research Program (SHRP), the National Cooperative Highway Research Program (NCHRP), the Canadian Strategic Highway Research Program, and state agencies, it has been determined that de-icing chemicals adversely influence soil, air quality, vegetation, and water (both surface and groundwater) (Cuelho 2010). Table 7.4 summarizes the environmental effects of NaCl, along with other chloride-based de-icing chemicals.

Table 7.4. Summary of the environmental effects of chloride-based de-icers (Fischel 2001)

De-icing material	Environmental Impacts			
	Air	Vegetation	Soil	Surface/Ground Water
Abrasives	Increase air pollution due to the fine particulate material	Cause major damage and mortality of roadside vegetation	Affect the roadside soil composition	Decrease water quality, inhibit photosynthesis in aquatic vegetation
NaCl	The net decline in air pollution with minimizing the abrasives application	Causes major damage and mortality of roadside vegetation	Reduces soil stability and permeability; increases salinity and potential for erosion	Causes acidification of water, little increase in metals concentrations
CaCl ₂	The net decline in air pollution with minimizing the abrasives application	Causes damage and mortality of roadside vegetation	Improves soil structure, water drainage, and soil aeration	Causes acidification of water, little increase in metals concentrations
MgCl ₂	The net decline in air pollution with minimizing the abrasives application	Causes damage and mortality of roadside vegetation	Improves soil structure, Increases salinity	Causes acidification of water, little increase in metals concentrations

The benefits of GHDS are well known, but they have not been thoroughly evaluated in research. This paper intends to evaluate the monetary value of the GHDS benefits and compare it with the corresponding costs of such systems. The environmental benefit is not included in the evaluation due to the difficulty of assigning a monetary value to environmental impacts. However, it should always be remembered that the adverse environmental effect of de-icing chemicals is completely eliminated by using this technology.

7.4 Methodology

Policy and decision makers always need insight into the overall cost and benefits of a project. Life cycle cost-benefit analysis (LCCBA) is a strong, viable method of assessing the expected costs and benefits of different alternatives, and ultimately assists in making final decisions. In this section, the framework of the analysis is developed, and then the required steps are taken to perform the analysis.

7.4.1 Framework

A conceptual structure of the analysis is illustrated in Figure 7.3. It shows all of the steps required to assess the GHDS. The goal is to achieve a realistic assessment of cost and benefit for each alternative, not necessarily prove that one is more cost-effective than another.

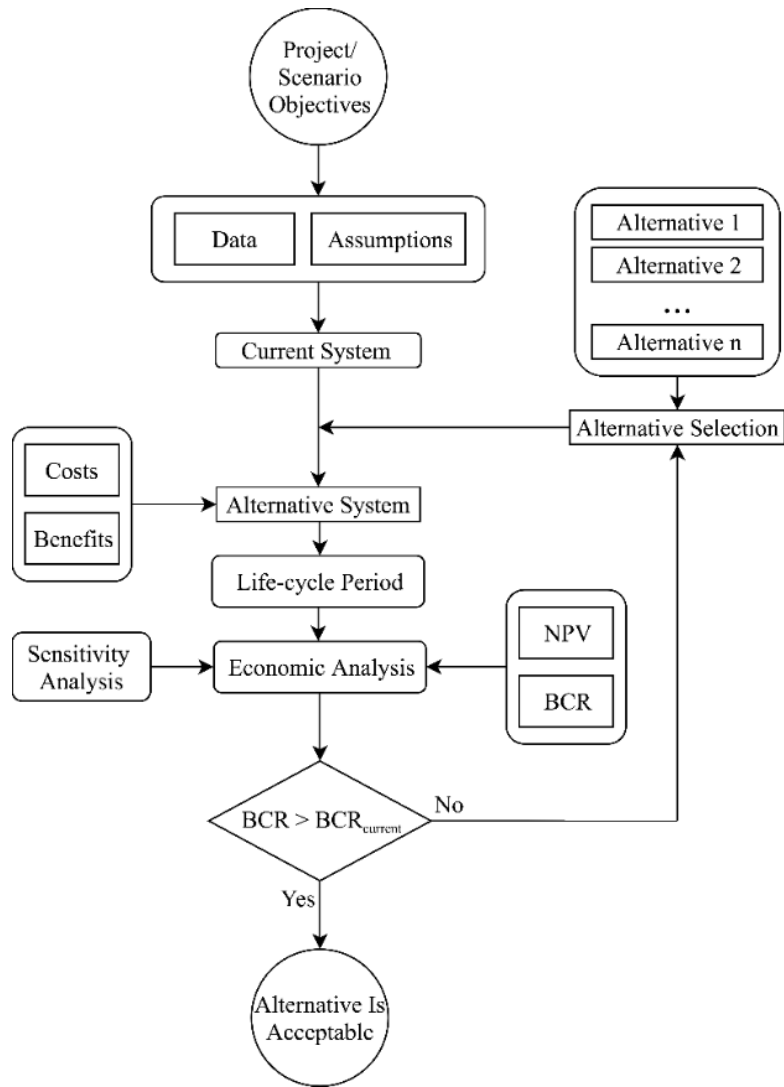


Figure 7.3. The framework of the economic analysis

The analysis is based on a scenario involving a hypothetical bridge, as shown in Figure 7.4. An “average” reinforced concrete bridge, based on the National Bridge Inventory (NBI), is assumed located on a state highway in North Texas. The bridge has two lanes and black rebar was utilized in the construction. The “average” bridge scenario is selected because it is well representative of the majority types of bridges and is fully compliant with bridge studies norms. Furthermore, it is one very commonly used by researchers, such as (Yunovich et al. 2003).

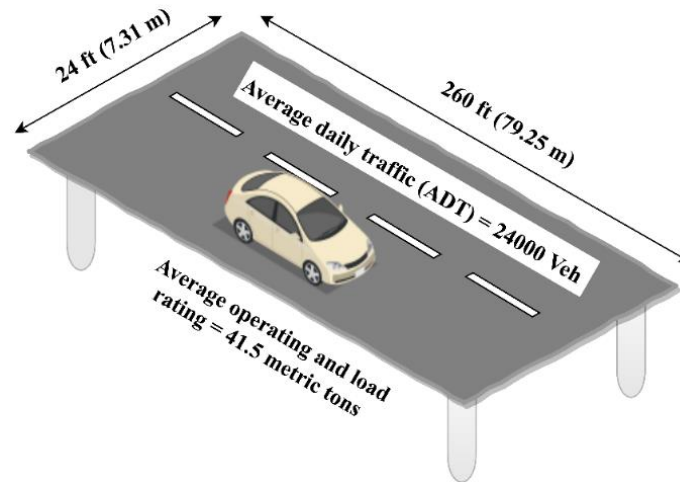


Figure 7.4. Outline of the scenario's bridge

The main objective of the project is to maintain the normal traffic flow on the bridge while clearing the bridge deck from snow and ice. In addition, it tries to prevent negative effects on the bridge deck, environment, user's safety, and traffic. This paper presents two options for addressing the project objectives, CSRS and GHDS. Data pertaining to each alternative is collected for the analysis, including details of the operation, maintenance, and other characteristics. Where no required data is available, reasonable assumptions are made. The analysis is followed by a close investigation of the costs and benefits of each alternative. Costs and benefits for alternatives are identified, and monetary value is assigned to each, based on the data collected in previous steps or by reasonable assumptions. To be reliable, an analysis has to be based on an evaluation process of sufficient length. One life cycle of a bridge deck (50 years) is considered for the analysis. Moreover, the discount rate is assumed as 5% to make sure it is not acting in favor of the construction costs of the GHDS (Thoft-Christensen, 2009). The year 2018 is considered as year 0, and all monetary values are based on the U.S. dollar.

When conducting a cost-benefit analysis on a project or proposal, it is convenient to compare and assess all future costs and benefits to their present value (PV). For this reason, the net present value (NPV) is used, which is the difference between the present value of cash inflows and outflows over the evaluation period. Net present value can be calculated by using Equation 7.1.

$$NPV = C_0 + \sum_{t=1}^T \frac{C_t}{(1+r)^t} \quad (7.1)$$

Where C_0 is the initial investment, T is time (year) of the end of the project, C_t represents the cash flow in time (year), and t and r denote discount rate.

The benefit-cost ratio (BCR), or profitability index, is an indicator that is widely used to evaluate the economic performance of an investment in a project or proposal. It serves as a management tool to identify the most efficient projects. BCR is the ratio of the present value of benefits over the costs during the studied period of time (Equation 7.2). A BCR greater than 1.0 indicates that the cost of the project is equal to its benefits or savings. A BCR of less than 1.0 indicates a poor investment. In other words, the higher the BCR, the better the investment. In this research, the present value of costs and benefits for each alternative is calculated, followed by calculating the BCR. The option that provides the highest BCR is more economically sound and should be selected.

$$BCR = \frac{PV_{benefits}}{PV_{costs}} \quad (7.2)$$

Where $PV_{benefits}$ is the present value of benefits, and PV_{costs} is the present value of costs.

Multiple assumptions, approximations and anticipations are inevitable in most cost-benefit analyses. These factors, which are due to uncertainties, can cause significant errors in the results and ultimately reduce the quality of the analysis. How much these errors affect the result of LCCBA must be clarified, firstly, for the decision makers to choose a reasonable and reliable

alternative, and secondly, to identify the degree of uncertainty associated with each alternative. A sensitivity analysis can help to mitigate these issues by investigating how different values corresponding to input variables can affect the result of the CBA and the BCR. Due to a given set of ranges for the assumptions, approximations, and anticipations, a sensitivity analysis provides the range for the outcome of the analysis and can assist in identifying the impacts of uncertainties of a different variable. Some of these variables might highly influence the outcome, while others might have an insignificant effect. In this paper, the sensitivity analysis is conducted by employing a Monte Carlo simulation, a powerful statistical analysis tool that is commonly used in both engineering and non-engineering fields and can assess the sensitivity of the output of the analysis with respect to each input variable. Moreover, it can compute the BCR with respect to the variation of input variables and eventually provide a range of possible BCRs.

7.4.2 LCCBA

A key task in the economic analysis of two systems is a comprehensive study of their individual characteristics, which leads to the identification of cost and benefit items for each alternative. The studied alternatives for snow and ice removal are a conventional snow and ice removal system (CSRS) and a geothermal heat-pump de-icing system (GHDS). In the analysis, a monetary value is assigned to each item, and then the relative costs and benefits of CSRS and GHDS are estimated. Table 7.5 illustrates the potential cost and benefit items for each alternative. Although both systems are implemented for the same purpose, which is clearing deck surfaces from ice and snow, what specifically distinguishes the two alternatives are their benefits. The GHDS minimizes the corrosion of the bridge deck, travel delays, and the risk of car crashes, while the CSRS does not. Moreover, the GHDS is an eco-friendly system, while the CSRS has proven to be destructive to the environment (Environmental impacts are not evaluated due to the difficulty of assigning a

monetary value to them). The initial investment and operating and maintenance costs of GHDS is the direct costs. The benefits of GHDS are equivalent to the total direct and indirect costs of CSRS. In other word, the overall cost savings of GHDS is the same as the overall cost of CSRS.

Table 7.5. List of costs and benefits for each alternative

Cost/benefit category	Conventional Snow/ice removal system	Geothermal heat-pump de-icing system
Initial Cost	Snow removal equipment purchase	Construction and equipment
Operation Cost	Labor, fuel, and de-icing agents	Energy source (geothermal energy, electricity, etc.)
Maintenance Cost	System maintenance	System maintenance
Benefit	-	Corrosion prevention
	-	Safety enhancement
	-	Traffic flow enhancement
	-	Environmentally friendly

7.4.2.1 Cost estimation of CSRS

An estimation of the cost of CSRS for a bridge involves many uncertainties. The initial cost of the CSRS for the bridge deck is not addressed because, as previously demonstrated, the CSRS belongs to all of the roadway, not only to the bridge. Moreover, the area of the bridge is insignificant in comparison with that of the roadways needing de-icing and snow removal, thereby making the initial cost of the bridge negligible.

The cost of snow removal on a bridge deck is basically the cost of operating and maintaining the CSRS. Operation and maintenance (O&M) costs of the CSRS are the expenses associated with all of the works and attempts to use materials and machinery for clearing snow and ice from the road surface, plus the cost of keeping the system operative. In the scenario, it is assumed that the bridge located in North Texas experienced at least ten snow/ice events a year (NOAA’s National Weather Service 2018). NaCl is assumed to be the de-icing agent used in winter maintenance for the scenario’s bridge, at a cost of \$70/ton.

7.4.2.2 Cost estimation of GHDS

In order to calculate the initial construction cost of GHDS, first, the construction unit cost (e.g. \$/m²) should be determined and then multiply by the area of the scenario's bridge. Initially, the present value (PV) of unit construction costs of actual previous projects (Table 7.2) and estimated unit construction values (Table 7.3) based on a 5% discount rate is calculated. Then simply, the average of all present values are computed and considered as the unit construction cost of the scenario's bridge. The same procedure is applied to determine the annual operation and maintenance unit cost of the scenario's bridge. Initial construction, operation and maintenance cost of the scenario's bridge is presented in Table 7.13.

7.4.2.3 Benefit estimation of GHDS

7.4.2.3.1 Benefit estimation of corrosion prevention

A primary effect of de-icing chemical application is corrosion of the bridge deck, which later requires maintenance and repair. The prevention of this phenomenon is the first major benefit of GHDS. One of the first studies on bridge corrosion costs estimated a minimum cost of \$675 per ton due to the application of de-icing salt (Vitaliano 1992b). However, the goal is to estimate the total cost of repairing and rehabilitating a deteriorated bridge deck over one life cycle. During a bridge deck's typical life cycle, it experiences at least two repairs/rehabilitation events. Four major events exist for this scenario over its life cycle. Regular maintenance and inspections are performed annually. Yunovich et al. (2003) estimated routine maintenance costs at \$1,000 per year, with no associated user cost. Major repair/patching action is carried out on a bridge deck when 2.5 percent of the deck shows delamination and spalling. When 10 percent of the deck area is spalled and

delaminated, it requires rehabilitation with latex-modified concrete (LMC). Eventually, the deck needs to be replaced when more repair and rehabilitation cannot solve the problem (Table 7.6).

Table 7.6. Corrosion maintenance schedule

Event	% of Deck Damaged	Year of Action
Routine Maintenance	N/A	Every year
Repair/Patch	2.5	25
Rehabilitation Overlay	10	32
Deck Replacement	N/A	50

When a GHDS is utilized, there is no need for repairs or rehabilitation. However, the cost of routine maintenance is not treated as a benefit of the GHDS because all bridges require this maintenance, with or without an ice and snow control system. The same logic is valid for the costs associated with bridge deck replacement.

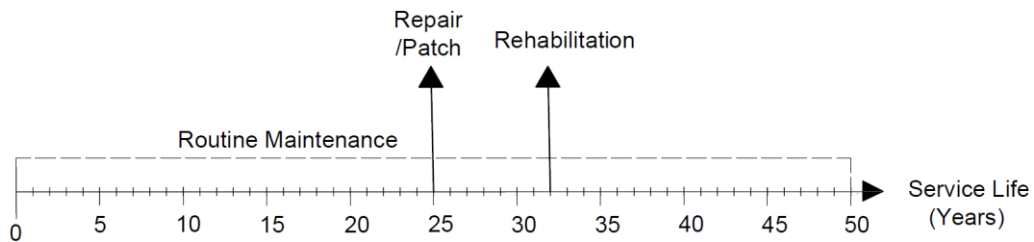


Figure 7.5. Cash flow diagram of corrosion maintenance activities

Figure 7.5 shows a cash flow diagram of corrosion maintenance activities for the scenario's bridge, over one life cycle. The main challenge is to determine the monetary value of each cash flow item. Yunovich et al. (2003) used a unit cost of \$ 90 per m² for patching and \$170 per m² unit cost for rehabilitation of a bridge deck with LMC overlay. Huang et al. (2004) suggested a range for the agency unit cost for different treatment purposes, with patching and concrete overlay recommended at \$160 and \$322 per m², respectively. However, after reviewing the literature and investigating the proposed prices, the cost due to repair/patching and rehabilitation of the

scenario's bridge deck is considered at \$215 and 484 \$/m², respectively. The total cost associated with repair/patching and rehabilitation event is the product of unit costs and area of the bridge deck, respectively. Ultimately, corrosion prevention benefit is the sum of the present value (PV) of the maintenance events cost (Equation 7.3).

$$\text{Corrosion prevention benefit} = \text{PV}_{25\text{th year}} \{ \text{patching cost} \} + \text{PV}_{32\text{nd year}} \{ \text{rehabilitation cost} \} \quad (7.3)$$

7.4.2.3.2 Benefit estimation of safety enhancement

The costs associated with traffic incidents on the scenario's bridge located in North Texas are estimated, using two factors: icy/snowy road surface conditions and work zones of corrosion maintenance activities. However, as previously stated, the safety-associated cost of conventional snow and ice removal system is considered an enhanced benefit of a geothermal heat-pump de-icing system.

Table 7.7 lists the number of car crashes in the state of Texas between 2007 to 2016 that is due to the road surfaces being affected by the cold weather. On average, 4,900 car crashes due to slippery road surface conditions in Texas are reported annually (Texas Department of Transportation (TxDOT) 2017). Unfortunately, the data considers all crashes, not only those that occurred on bridges but based on the research of (Agent and Deen 1976), a minimum of 8% percent of all crashes happen on bridges.

Table 7.7. Texas statewide car crashes due to slippery road surface conditions

Year	Ice	Slush	Snow	Total	Estimated crashes on Bridges
2007	5189	495	685	6369	509
2008	2305	231	280	2816	225
2009	4080	256	411	4747	379
2010	2442	859	1040	4341	347
2011	5914	475	919	7308	584
2012	1192	260	447	1899	152
2013	4582	488	461	5531	442
2014	6515	307	1087	7909	632
2015	5599	788	1157	7544	603
2016	376	44	108	528	42
Average	3819	420	659	4899	392

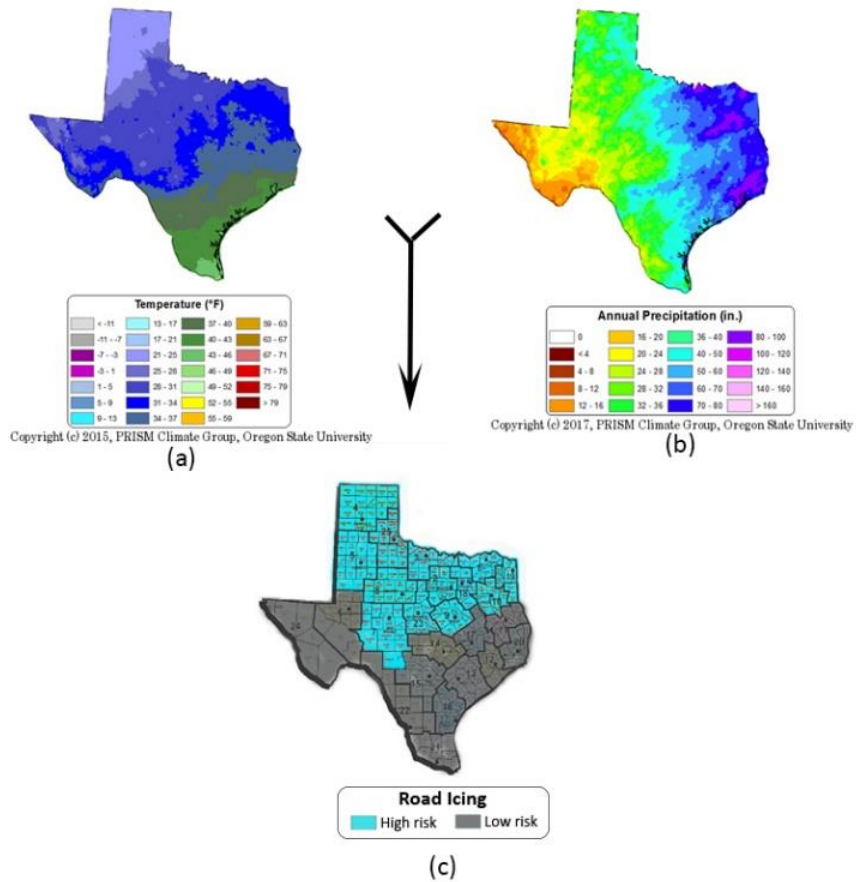


Figure 7.6. (a) An average daily minimum temperature of January 2015 (PRISM Climate Group 2015); (b) Texas annual precipitation in 2015 (PRISM Climate Group 2017); (c) Texas regions prone to road icing.

The challenge is to find the average annual number of crashes on each bridge in Texas that was caused by slippery road surface conditions. To achieve that, the total number of crashes on the bridges due to slippery roads is divided by the number of total bridges in the region prone to icing. The regions prone to icy road surfaces in Texas must be identified because Texas' weather varies widely from south to north, and not all areas suffer from icy roads. The total number of crashes on the bridges is previously calculated; therefore, the total number of bridges in the area prone to slippery road surface conditions needed to be determined.

Ice is formed on roads when precipitation coincides with freezing temperatures. In many cases, and very often in Texas, following rain during the day, the temperature drops below freezing at night, so that the water on the road surface turns to ice. In order to find the potential regions of icy roads, January 2015, one of the coldest months of the recent years in North Texas, is considered as the scenario month. Therefore, the regions in Texas prone to icy roads are determined by overlapping the annual precipitation map of 2015 (Figure 7.6 (b)) with the average daily minimum temperature map for January 2015 (Figure 7.6 (a)). The areas with more than 71 cm of precipitation that coincided with a temperature of less than 0 °C (32 °F) are selected as those that are most likely to experience icy roads during the cold season. They are presented in Figure 7.6 (c).

The counties located in the regions prone to icy roads and their number of bridges are identified in Table 7.8. Finally, the average annual number of crashes on each bridge due to slippery road surface conditions can be computed.

Table 7.8. Number of bridges in TxDOT Districts that are located in zones prone to icy road surface conditions (Texas Department of Transportation (TxDOT) 2016)

TxDOT District	Total Number of Bridges
Atlanta	1101
Abilene	1362
Amarillo	694
Brownwood	893
Dallas	3659
Fort Worth	2329
Lubbock	467
Paris	1361
San Angelo	1223
Tyler	1221
Waco	1696
Wichita Falls	1057
Total	17063

Table 7.9. Texas statewide crashes and injuries occurring in work zones and expected cars crashes on bridges.

Year	Total Crashes	Estimated Crashes on bridge
2007	19,737	1579
2008	18,633	1491
2009	15050	1204
2010	13011	1041
2011	14688	1175
2012	16732	1339
2013	17355	1388
2014	19460	1557
2015	22322	1786
2016	25814	2065
Average	18,280	1462

Every year, hundreds of car crashes happen in work zones in Texas. Table 7.9 illustrates the number of crashes and injuries occurring in work zones on bridges statewide (Texas Department of Transportation (TxDOT) 2017). Although car crashes and injuries in work zones

decreased from 2006 to 2010 statewide, they began increasing in 2010 and reached 25,814 accidents in 2016. As previously elaborated above, the data provided by TxDOT does not distinguish the number of incidents on bridges, but research shows that 8% percent of all crashes happen on bridges. Based on this assumption, an average of 1,462 incidents annually can be expected to happen on bridges in Texas due to work zones.

The annual cost of crashes on each bridge can be calculated by the product of the average crash cost, which is derived from the sample data provided in a report by FHWA (Council et al. 2005), and the average annual number of crashes that occur due to work zones and icy roads on each bridge in the regions prone to icy roads. However, following the computation of the annual crash cost, the corresponding value in each year of the life cycle is estimated by Equation 7.1. Finally, the average of the present values results in the annual safety enhancement benefit (Equation 7.4).

$$\text{Annual safety enhancement benefit} = (1/\text{life cycle}) \times \sum_{\text{year}=1}^{\text{life cycle}} \text{PV} \{ \text{crashes cost} \} \quad (7.4)$$

7.4.2.3.3 Benefit estimation of traffic flow enhancement

To calculate the travel delays cost, the unit cost (\$/hr) of travel time is multiplied by the number of estimated delays to personal, business and truck travel caused by the work zone. Mallela and Sadavisam (2011) also considered delays due to time-related depreciation and freight inventory in their analysis, but it is disregarded here because of the lack of data and a desire to simplify the problem. It is assumed that the scenario's bridge has the traffic condition presented in Table 7.10. The ADT is assumed according to the National Bridge Inventory (NBI) data regarding the average reinforced concrete bridge. The ratios of personal travel and business travel are selected, based on the 2009 National Household Transportation Survey (NHTS) (Mallela and Sadavisam 2011).

A simple procedure is followed to calculate the cost of travel delays that are due to work zones. To convert the delay time from personal hours to vehicular hours or vice-versa, an appropriate value for the average vehicle occupancy (AVO) of passenger cars is selected. The values of AVO for personal intercity, business, and truck travel are 2.3, 1.24, and 1.025, respectively. Based on the Nationwide Personal Transportation Survey (NPTS) 1990, the AVO of personal intercity travel is higher than that of local personal travel. While the AVO for local travel is 1.66, the AVO for intercity travel is 2.3. Moreover, In the absence of an AVO for trucks in the NHTS, the Highway Economic Requirement System (HERS)-ST Technical Report recommends an AVO of 1.025 (FHWA 2005). Second, the monetary value of travel time for a person is computed by multiplying person-hour monetary value as a percent of their wage rate (0.7 for personal travel and 1.0 for business travel) by the median annual income for all U.S. households reported by the U.S. Census Bureau (\$57,617 in 2016), then dividing the result by 2080 hours (the number of hours worked in a year). The median wage of a heavy tractor-trailer truck driver is \$40,260, and it only needs to be divided by the annual working hours (2080 hours).

Table 7.10. Traffic data of the scenario's bridge

Traffic data	Value	
Average daily traffic	24000	veh/day
Average daily traffic of truck travel (5 % of total)	1200	veh/day
Average daily traffic (no trucks)	22800	veh/day
Average daily traffic of personal travel (93.7%)	21363.6	veh/day
Average daily traffic of business travel (6.3 %)	1436.4	veh/day

The hourly travel time value per vehicle (Table 7.11) is computed by multiplying the hourly value of travel time and the AVO. In principle, the hourly value of travel time per person is

converted to hourly travel time value per vehicle to estimate the cost of delays. Based on the number of vehicles rather than the number of persons traveling on the bridge.

Table 7.11. Hourly travel time value per vehicle

Item	Value (\$/vehicle-hr.)
Hourly travel time value per vehicle on personal travel	\$44.60
Hourly travel time value per vehicle on business travel	\$34.35
Hourly travel time value per truck	\$19.84

The travel delay cost can be easily computed if the delay time is known. Due to the lack of actual hourly traffic volume during work zone activity, the travel delay time for the events of repair/patching and rehabilitation are assumed. Based on the common duration of the activities from online sources, the delay time during each bridge corrosion maintenance activity is assumed and is shown in Table 7.12.

Table 7.12. Travel delay scenario due to corrosion maintenance events

Event	Duration (day)	Delay (Veh-hr/day)
Repair/patching	3	0.033
Rehabilitation	15	0.083

Finally, traffic flow enhancement benefit is calculated by the product of the average daily traffic, hourly travel time value and corrosion maintenance event delays. The lack of data and unsteady traffic and weather conditions over time make it extremely difficult to calculate exact travel delay times that are due to slippery road surface conditions and car crashes on bridges. Therefore, the delay costs are assumed to be 10% of the cost of repairing and patching the bridge deck. In other words, every year, on average, icy road surface conditions cause about 4 seconds of delay for vehicles passing on a bridge during the snow and ice events. In addition, in the case of car crashes, it means 36 seconds of delay, which is imposed on the vehicles passing on the bridge

when the car crash happens. These assumptions are reasonable with respect to the number of freezing events that occur annually in North Texas (NOAA’s National Weather Service 2018). However, annual traffic flow enhancement benefit due to lack of slippery surface and crashes delays, and traffic flow enhancement benefit due to lack of corrosion maintenance activates are calculated using equation 7.5 and 7.6 respectively.

$$\text{Annual traffic flow enhancement benefit} = \frac{1}{\text{life cycle}} \times \sum_{\text{year}=1}^{\text{life cycle}} \text{PV} \{ \text{slippery surface and crashes delays cost} \} \quad (7.5)$$

$$\text{Traffic flow enhancement benefit over entire life cycle} = \text{PV}_{25\text{th year}} \{ \text{patching event delays cost} \} + \text{PV}_{32\text{nd year}} \{ \text{rehabilitation event delays cost} \} \quad (7.6)$$

7.5 Results and Discussion:

7.5.1 Base case analysis

Table 7.13 illustrates the monetary present value (PV) for the initial and recurrent costs and benefits of each ice control alternative. The type of cash flow for each item should be noted. The initial cost of GHDS only occurs once (at the beginning of the life cycle), but the O & M costs recur every year. Annual safety and traffic flow enhancement occur every year, but corrosion prevention and corresponding flow enhancement benefits occur in specific years of the life cycle.

While CSRS only involves annual operation and maintenance cost of \$1000 and requires no initial investment, the GHDS has a huge initial cost of \$642,500 for construction, as well as annual recurring costs of \$18,700 for operation and maintenance. Moreover, although no benefit has been identified for CSRS, GHDS includes both one-time and recurring benefits. It is worth mentioning again that the benefit items of the GHDS are in fact the indirect costs of the CSRS.

The GHDS saves about \$405,500 over the entire life cycle of the bridge by eliminating the repair, patching, and/or rehabilitating costs incurred by corrosion in 25th and 32nd year of its life cycle. It also assists in saving the recurrent cost of \$3,500 per year by providing safe road surface conditions and preventing car crashes. Lastly, the GHDS minimizes the travel delay time of all motorists passing on a bridge. It saves the annual recurrent cost of \$14,500 that is due to motorists decelerating because of icy bridge deck surfaces and \$14,500 as the secondary effect of safety enhancement. In other words, the GHDS application prevents car accidents and deceleration due to the lack of icy roads on bridges, thereby preventing travel delays. More importantly, GHDS saves approximately \$1,963,500 over its entire life cycle by minimizing the travel delays resulting from the absence of work zones.

A comparison of the two alternatives, with a benefit-cost ratio (BCR) of 2.6 and a net present value (NPV) of \$2,442,600, shows that the GHDS is economically viable. Its large start-up costs and operating and maintenance expenses are more than compensated for by its ability to prevent corrosion, enhance safety, and facilitate good traffic flow. Its friendliness to the environment is another strong plus for the system. In this research, specific values are selected based on the available data or from valid references, but the readers are encouraged to use their own data to achieve a more appropriate economic analysis of their circumstances.

Table 7.13. Results of the base case analysis

Cost/benefit category	Conventional Snow/ice removal system	Geothermal heat-pump de-icing system	Description
Cost			
Initial construction cost	-	\$642,500	One-time expense
Operation and maintenance	\$1,000	\$18,700	Annual expense
Benefit			
Corrosion prevention	-	\$405,500	Benefits over one life cycle
Safety enhancement	-	\$3,500	Annual benefit
Traffic flow enhancement	-	\$1,963,500	Benefit over one life cycle
		\$29,000	Annual benefit

The initial construction cost of GHDS is a concern, but the main contributing parameter to the overall cost of GHDS over its entire life cycle is that of its annual operating and maintenance costs. Of the total inherent costs, 42% are directly attributable to the initial construction cost, while 58% are associated with operating and maintenance costs. It bears noting, however, that the O & M costs are expected to decline since the O & M cost of the scenario's bridge is based on the average unit cost of the first few projects of this type. These projects are conducted to investigate the feasibility of GHDS, and consequently had high O & M expenses due to more frequent inspections and maintenance. Moreover, the output of the analysis indicates that the largest portion of the benefit is due to traffic flow enhancement, which accounts for 85% of the total benefit of GHDS.

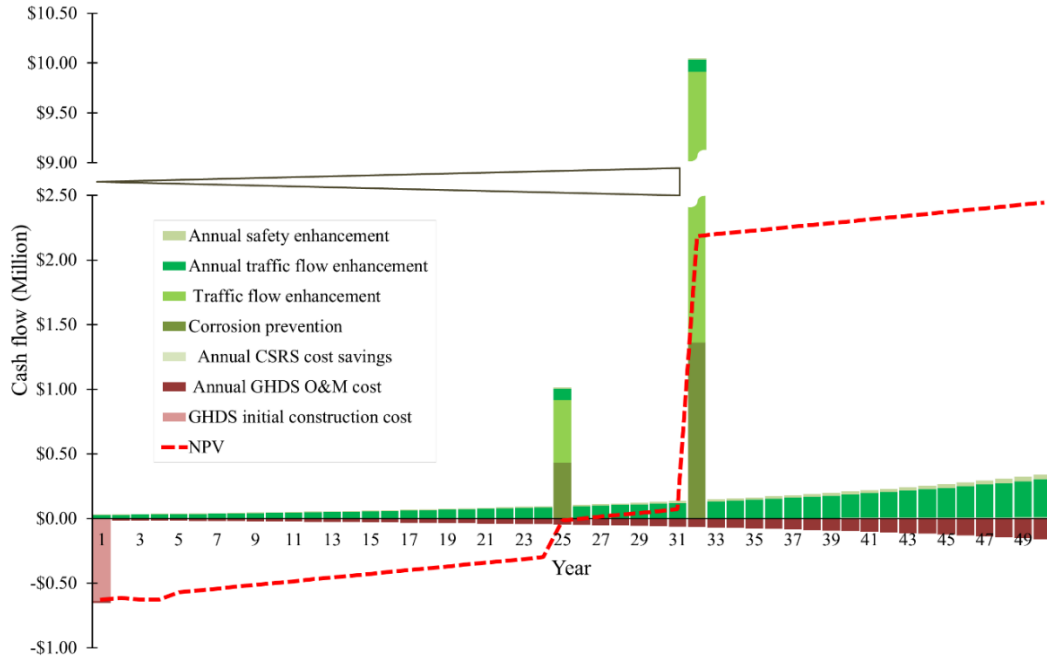


Figure 7.7. Cash flow of GHDS over one life cycle of the bridge deck

The cash flow diagram of GHDS (Figure 7.7) shows the details of cash flow for each year of the analysis. While the major cash outflow in the first year is the initial construction cost, the primary cash entries are from traffic flow enhancement benefits in the 25th and 32nd years of the analysis. The NPV line in Figure 7.7 shows that the benefits of GHDS outweigh its cost after 25 years, and after 50 years reaches \$2.4 million.

7.5.2 Sensitivity analysis

A sensitivity analysis is needed because of the lack of data and uncertainties in selecting the specific values, unit costs, and assumptions affect the result of the analysis. Monte Carlo Simulation (MCS) is employed in this research to investigate the impact of each item on the final NPV of the geothermal heat-pump de-icing system.

MCS investigates the sensitivity of each cost and benefit and reflects the maximum and minimum factors of the random variables for each item, as illustrated in Table 7.14. The factors

are extracted from available data; when data is lacking, a 25% percent variation for the variables is assumed. The results of the analysis show the total present value (PV) variation of each item over one life cycle.

Table 7.14. Input variables distributions of the Monte Carlo Simulation (MCS)

Input Items	Max	Min	St. Deviation	Distribution
CSRS				
Annual operation and maintenance	1.250	0.750	0.08	Normal
Corrosion maintenance activities	1.278	0.646	0.11	Normal
Maintenance activities travel delay	1.250	0.750	0.08	Normal
Annual car crashes and deceleration travel delay	1.250	0.750	0.08	Normal
Annual car crashes cost	1.250	0.750	0.08	Normal
GHDS				
Initial construction cost	1.408	0.592	0.14	Normal
Annual operation and maintenance cost	1.304	0.438	0.14	Normal

Figure 7.8 illustrates the results of the sensitivity analysis for the cost items of GHDS and depicts the variation range of present value (PV) for each item. The black section represents the range when a random variable factor of more than 1.0 (high input) is applied in the sensitivity analysis, and the grey shows the range when the random variable of less than 1.0 (low input) is applied. The border between the two sections indicates the value of the base case (Table 7.13), in other words, a random variable equal to one is applied in the sensitivity analysis. The output of the analysis shows that the operation and maintenance cost has a wider range and greater potential to influence the overall cost of GHDS than the initial construction cost.

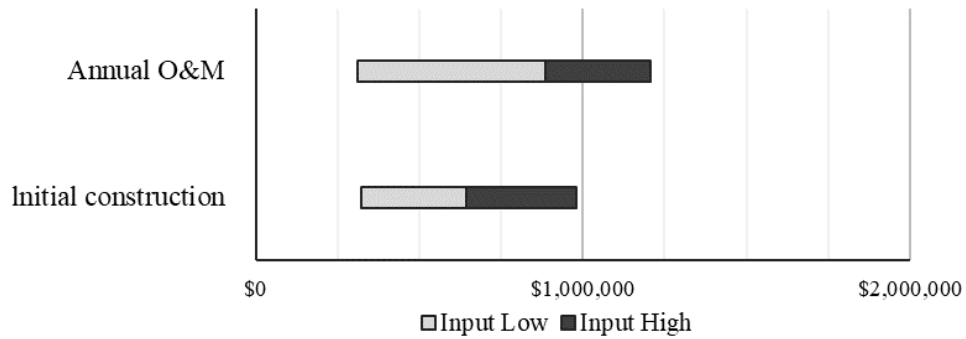


Figure 7.8. The estimated range of GHDS costs PV

Figure 7.9 shows the range of variation benefit items of the GHDS. As expected, the traffic flow enhancements are the dominant cost items and have the greatest potential to influence the overall cost.

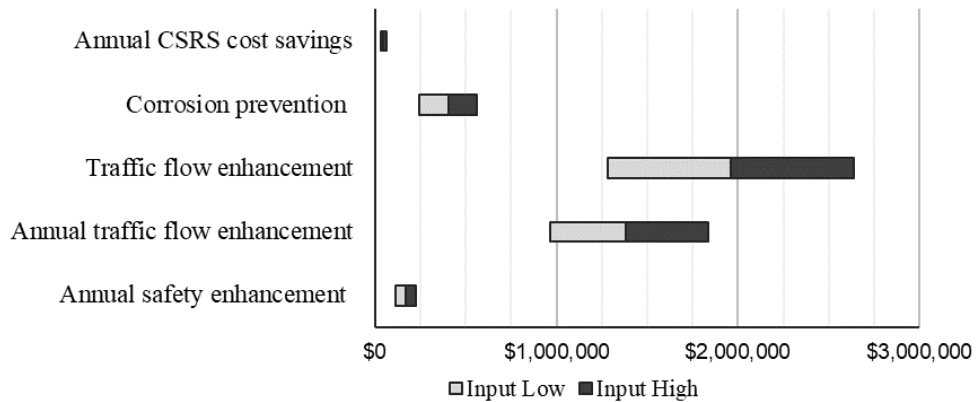


Figure 7.9. The estimated range of GHDS benefit PV

The sensitivity analysis illustrates that the NPV ranges from a maximum of \$3.5 million to a minimum of \$1.5 million (Figure 7.10). This means that the application of this system results in at least \$1.5 million, on average \$2.4 million, and maximum \$3.5 million in cost savings over one life cycle.

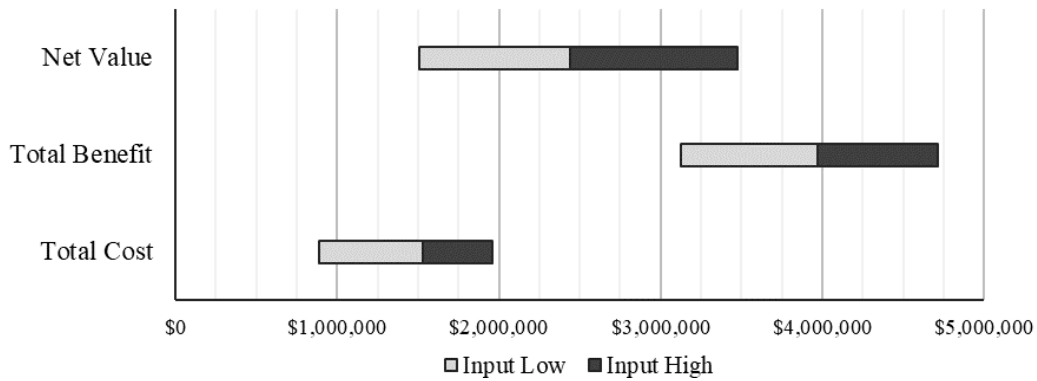


Figure 7.10. The estimated range of cost and benefit PV and NPV of GHDS

Table 7.15 shows the BCR with respect to different reliability percentages. The BCR is greater than 2.32 95% percent of the time, and more than 3.48 5% of the time, with a median value of 2.8. The results indicate that the benefits of GHDS always outweigh its cost.

Table 7.15. Benefit-cost ratios for different reliabilities

Reliability Percentage	95%	85%	75%	65%	55%	Median	45%	35%	25%	15%	5%
BCR	2.32	2.48	2.58	2.67	2.75	2.80	2.84	2.93	3.04	3.19	3.48

The sensitivity analysis shows that the application of GHDS is economically viable. The NPV and BCR of a GHDS for bridges with different average daily traffic (ADT) volumes for the base case analysis are studied to identify the circumstances under which application of GHDS is financially feasible. The results show that it is cost effective for bridges with a minimum daily traffic volume of 7000 vehicles (the BCR exceeds one). For an ADT of less than 7000 vehicles, the use of GHDS is not recommended (Figure 7.11).

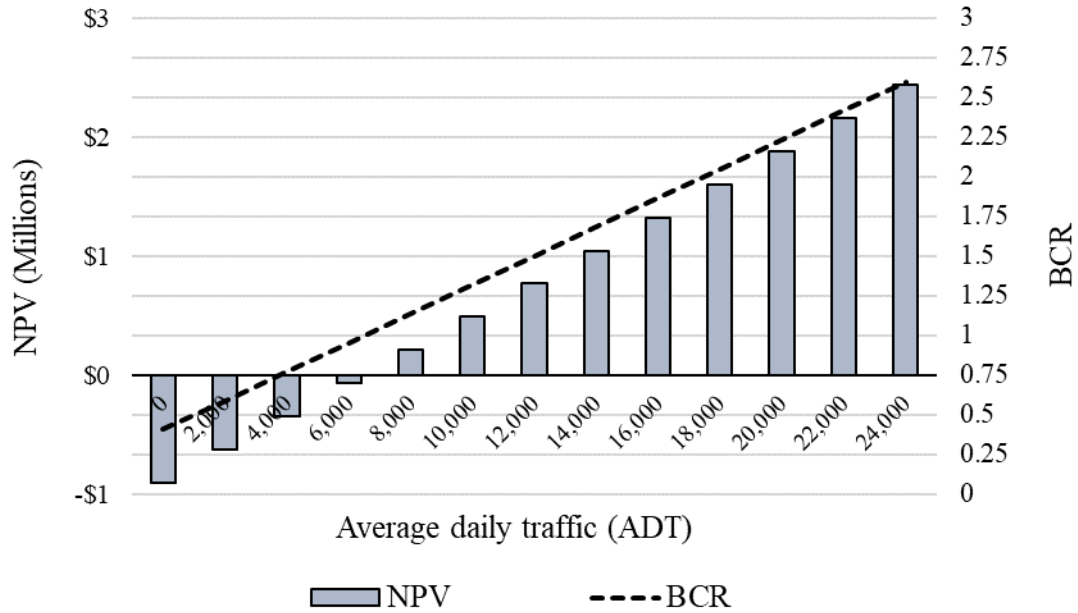


Figure 7.11. Variations of NPV and BCR of GHDS with respect to average daily traffic (ADT)

7.6 Conclusions

This paper provides a life-cycle cost-benefit analysis (LCCBA) of GHDS and assesses the economic feasibility of this system in comparison with CSRS. It specifies the costs and benefits of each alternative and estimates the monetary value of each item. In all stages of the analysis, care is taken to use assumptions and scenarios that simulate reality. The output of this study reveals the economic impacts of design and traffic parameters, as well as operation and maintenance strategies. It also provides useful information for decision makers in the transportation infrastructure sector. The main finding of this research are summarized as follows:

- A geothermal heat pump de-icing system (GHDS) is an economically viable alternative to conventional snow and ice removal for clearing bridge deck surfaces from ice and snow. It is more desirable since it prevents the negative impacts induced by CSRS.

- The benefits of GHDS are corrosion prevention, safety and traffic flow enhancement, and protection of the environment. The monetary value of the overall benefits (excluding the environmental benefits) is 2.6 times greater than the overall costs for the base case analysis. The benefits of the GHDS exceed its cost after 25 years.
- While the initial construction cost of GHDS is significant, the annual O & M cost is the main burden to the GHDS over its life cycle. However, although the value for the annual O & M is based on the actual previous project, it should be updated, using the data of more recent projects to increase the quality of the analysis.
- Traffic flow enhancement is the most sensitive variable in the analysis, and the sensitivity analysis is performed to further investigate its impact. It estimated the BCR, which ranges from 2.32 to 3.48, with 95% and 5% reliability, respectively. The GHDS is strongly recommended for bridges with high and average traffic volume but is not economically viable for bridges with an ADT below 7000 vehicles.

CHAPTER 8: SUMMARY AND CONCLUSIONS

8.1 Summary

This dissertation focused on the performance assessment of the novel external geothermal heating system for de-icing and snow-melting the bridge deck surface. Available knowledge in the field of geothermal de-icing and snow melting systems was limited to the conventional internal hydronic heating system and small laboratory scale external heating system. The research presented in this dissertation was designed to advance our current understanding of this field and assess the feasibility of the external geothermal heating system for bridge deck de-icing. The first full-scale prototype of an externally heated geothermal bridge deck was designed and constructed and the system's performance under severe cold weather conditions was monitored for two years. In addition to the primary goal of this study i.e. de-icing feasibility of the external geothermal heating system, other aspects of the system were studied. As the key component of any geothermal system, the ground heat exchanger's thermal and energy performance was studied during the heat injection and extraction tests on the bridge decks. Both heat storage and thermal balance in the soil were also investigated and showed how bridge solar collector operation can benefit the system efficiency. Moreover, this dissertation presented a computationally efficient FE model to simulate the GHE performance with a high level of accuracy and less computational time in comparison to the conventional FE model. Finally, as useful information for decision-makers in the transportation infrastructure sector, a life-cycle cost-benefit analysis was conducted to assess the economic viability of this system in comparison with conventional Ice and snow removal systems.

8.2 Conclusions

The main findings of this study are summarized in the following:

8.2.1 De-icing Operations and Bridge Deck Thermal Response

- The 17.8 m² heated area on the bridge deck was observed free of ice and maintained minimum surface temperature above freezing during all seven winter events.
- Among all the seven winter tests, the minimum surface temperature of 1.4 °C was observed during a severely cold winter with a minimum freezing temperature of -6.2 °C. The supplied fluid from the GLHE to the bridge deck was observed to have a temperature around 40°C in this coldest winter test.
- It took a minimum of 7-8 hours for the de-icing system to reach its peak performance at -3.9 °C ambient temperature. The time was less for mild winter weather.
- The monitored data illustrated an average temperature of 16.5 °C for the inlet water to the borehole, while the water returning from the 131 m deep borehole was recorded as about 16.9 °C during the system's operation in Test #5. Also, the use of a bypass operation with no geothermal heat pump in de-icing was found to be practical for mild winter weather conditions, in which the bridge deck was heated with about 16.6 °C fluid rather than 40 °C from the geothermal heat pump.

8.2.2 GHE Performance and Subsurface Thermal Response

- The analysis result revealed that the ground temperature beyond the atmospheric condition influence zone was increased as a result of the bridge solar collector test and preserved for utilization in the first de-icing test in the winter. The influence zone radius of the GHE operation was also found to be 3.45 m.

- After 74 days of heat injection during the bridge solar-collector test with an average of 5.7 W/m, the ground temperature beyond the influence zone of atmospheric condition, rose by 0.75, 0.48, and 0.35 °C at 0.45, 0.9, and 1.5 m radial distances from GHE.
- Only a small portion of the stored heat remained within the GHE surrounding soil mass, and the majority of the injected heat was lost via lateral heat transfer. It was found 31.7-39.4% of stored thermal energy was preserved for utilization in the first winter de-icing test depending on the definition of the control volume.
- The application of the heat pump in the system increased the heat extraction rate and energy efficiency to a great extent. In presence of the heat pump in the system, the heat extraction rate was 3 times and the temperature decrease in the soil was more than two times that of when the heat pump was not used. The COP was recorded 2.9 and 1.1 for the tests with and without the heat pump, respectively, based on the heat transfer in the evaporator side of the heat pump.
- The bridge solar-collector operation fully recovered the ground thermal condition by providing more than two times injected heat than the extracted from the ground. Based on analysis for over a year of operation, heat injection into the soil by bridge solar collector was 54% more than heat extraction from the ground during the six de-icing tests in the winter of 2019-2020.

8.2.3 Overall system de-icing performance

- On average, the power input to the water pumps and heat pump was about 1.4 kW. The system thermal energy output rate varied from 4.4 kW to 8.8 kW; and the system COP based on the heat transfer in the condenser side of the heat pump, varied between 3.7 and

5.4, with an average of 4.6. An increase in the heat pump operating time resulted in the higher thermal energy output of the heat pump and an increase in the COP of the system.

- The external heating system was able to transfer about 55% of the supplied heat to the bridge deck surface, implying that 45 % of the total heat was lost during the heating process. Thus, it is suggested to consider 45% heat loss of the system when calculating the design surface heat flux of the external geothermal heating system.
- For an event with a minimum ambient temperature of $-3.9\text{ }^{\circ}\text{C}$, the supplied and surface heat fluxes were found to be about 433.4 W/m^2 and 236.2 W/m^2 respectively, when the ambient temperature was below freezing. The surface heat flux on the bridge deck was sensitive to the ambient temperature and heating conditions.

8.2.4 Numerical Simulations of the U-tube heat exchanger

- A simplified computationally efficient numerical model was developed using an equivalent 1D non-isothermal pipe flow element for the GHE, which can represent the entire borehole.
- The proposed model is compared with the conventional model and together are validated against the experimental data. The result showed the proposed model output almost matches perfectly with the conventional model and provides the same level of accuracy.
- The application of the proposed model can significantly reduce the required number of mesh elements and consequently the computational time. The result showed, the required number of elements was decreased by 90% and 67% for the optimum and extra fine mesh cases and computational time was reduced by 95% and 81 % for the same mesh cases, respectively.

- As the proposed model provided the same level of accuracy as the conventional model while greatly reduced the computational time, it can be concluded that the proposed model can be recommended as a desirable alternative for the conventional model.

8.2.5 Economic Assessment

- Geothermal de-icing systems showed to be a financially feasible alternative to conventional snow and ice removal for clearing bridge deck surfaces from ice and snow. The benefits of this system outweighed the negative impacts caused by the conventional snow and ice removal system.
- The benefits of the geothermal de-icing systems were corrosion prevention, safety and traffic flow enhancement, and protection of the environment. However, traffic flow enhancement was the most significant benefit of the geothermal de-icing system. The monetary value of the overall benefits (excluding the environmental benefits) was found to be 2.6 times greater than the overall costs for the base case analysis. The benefits of the GHDS exceeded its cost after 25 years.
- Besides the initial construction cost of the geothermal de-icing system, the annual operation and maintenance cost of the system was the main burden to the geothermal de-icing system over its life cycle.
- The estimated benefit to cost ratio (BCR) of the system ranged from 2.32 to 3.48, with 95% and 5% reliability, respectively.
- The geothermal de-icing system is strongly recommended for bridges with high and average traffic volume but is not economically viable for bridges with an ADT below 7000 vehicles.

8.3 Lessons Learned

Besides detailed conclusions that are previously summarized, broader conclusions that can be drawn to form the major lessons learned from this study are present here:

- Although the system was found to be feasible for maintaining the bridge deck surface above freezing temperature, however, the operational strategy makes a great impact on the final outcome. For example, an appropriate amount of pre-heating is extremely important to ensure an adequate amount of heat is transferred to the bridge deck surface before the cold front arrives.
- Providing a good contact between pipe and concrete deck, smaller hydronic pipe spacing, and an adequate layer of insulation on the bottom surface results in greater system performance due to higher heat supply to the bridge and less heat loss.
- The system's heat loss should be accounted for designing the system for a specific required heat flux. The system's heat loss might vary for different systems according to the system and bridge deck specifications and details.
- It is feasible to store heat in the ground during the summer to utilized in the winter even for a single U-tube ground heat exchanger. However, as the heat dissipation rate to the far-field soil is two times the heat storage rate, there should not be a large gap between the bridge solar-collecting operation and de-icing operation.
- Among the two estimation errors caused by the application of the 1D pipe flow module, the error due to exact temperature coupling location is greatly less than the error of not accounting for the heat capacity in the model for the heat exchanger pipe.

- The key influencing factor in the cost-benefit analysis of the geothermal de-icing system is traffic flow enhancement. Thus, an accurate analysis cannot be done unless there is a good understanding of the traffic flow condition. The traffic data including travel time delays are extremely important.
- Although the application of the system was suggested to be cost-effective when average daily traffic is above 7000 vehicles, however, taking into account the environmental benefit, the system would be financially feasible even for smaller daily traffic volume.

8.4 Future Direction

This research has provided new insight regarding the application of the novel external geothermal heating system and geothermal de-icing systems in general. Nonetheless, these systems still demand further research and discussion on different aspects. Here are some pertinent recommendations for future research based on the work presented in this dissertation:

- As implementation of the external hydronic pipes required insulation of the entire bottom deck surface, it might raise some concerns regarding the bridge deck inspection. Therefore, a new insulation design in which only the pipe loop is insulated can be used which provides some gaps between the pipe loop section and allows inspection of the bridge deck. Also, to enhance the heat transfer from the pipe to the bridge deck, a high thermally conductive material such as aluminum can be used in the interface of the pipe and concrete.
- Application of the bridge as a solar collector and ground thermal enhancement using a single U-tube heat exchanger has proved the geothermal de-icing system can ideally incorporate with soil-borehole thermal energy storage system (SBTES)

such as the SERSO system in Switzerland (Eugster 2007). It will help to eliminate the need for the heat pump in the system and consequently an enormous reduction in electricity consumption and equipment cost. Also, another advantage of injecting heat during the summer is the reduction of extreme bridge deck temperatures in the summer and significant stabilization of the bridge deck surface temperatures. However, although a case study can be found in the literature, there is not much detailed information about this project is available in the literature. Therefore, more experimental, and numerical studies should be performed to characterize the benefits of incorporating the SBTES with geothermal de-icing systems.

REFERENCES

- Agent, K. R., and Deen, R. C. (1976). "Highway accidents at bridges." *Journal of the Transportation Research Board, Transportation Research Record*, (601).
- Ahmad, S., Abdul Mujeebu, M., and Farooqi, M. A. (2019). "Energy harvesting from pavements and roadways: A comprehensive review of technologies, materials, and challenges." *International Journal of Energy Research*, Wiley Online Library, 43(6), 1974–2015.
- Al-Habaibeh, A., Athresh, A. P., and Parker, K. (2018). "Performance analysis of using mine water from an abandoned coal mine for heating of buildings using an open loop based single shaft GSHP system." *Applied Energy*, Elsevier BV, 211, 393–402.
- Al-Khoury, R., and Bonnier, P. G. (2006). "Efficient finite element formulation for geothermal heating systems. Part II: transient." *International journal for numerical methods in engineering*, Wiley Online Library, 67(5), 725–745.
- Al-Khoury, R., Bonnier, P. G., and Brinkgreve, R. B. J. (2005). "Efficient finite element formulation for geothermal heating systems. Part I: Steady state." *International journal for numerical methods in engineering*, Wiley Online Library, 63(7), 988–1013.
- American Association of State Transportation and Highway Officials (AASHTO), Mertz, D. R., Rehm, K., and Beal, D. (2005). *Grand challenges: A strategic plan for bridge engineering*. Transportation Research Board.
- American Society of Heating, R. and A.-C. E., and American Society of Heating, R. and A.-C. E. (2015). "2015 ASHRAE handbook : heating, ventilating, and air-conditioning applications, Inch - Pound Edition."
- Anand, P., Nahvi, A., Ceylan, H., Pyrialakou, V. D., Gkritza, K., Gopalakrishnan, K., Kim, S., and Taylor, P. C. (2017). *Energy and Financial Viability of Hydronic Heated Pavement Systems*.

- Austin III, W. A. (1998). "Development of an in situ system for measuring ground thermal properties." Oklahoma State University.
- Baboian, R. (1992). "Synergistic Effects of Acid Deposition and Road Salts on Corrosion." *Corrosion Forms and Control for Infrastructure*, V. Chaker, ed., ASTM International, West Conshohocken, PA, 17–29.
- Baek, S. H., Yeo, M. S., and Kim, K. W. (2017). "Effects of the geothermal load on the ground temperature recovery in a ground heat exchanger." *Energy and buildings*, Elsevier, 136, 63–72.
- Bakirci, K. (2010). "Evaluation of the performance of a ground-source heat-pump system with series GHE (ground heat exchanger) in the cold climate region." *Energy*, Elsevier BV, 35(7), 3088–3096.
- Balbay, A., Esen, M., and A., B. (2010). "Experimental investigation of using ground source heat pump system for snow melting on pavements and bridge decks." *Scientific Research and Essays*, Academic Journals, 5(24), 3955–3966.
- Barla, M., Di Donna, A., and Perino, A. (2016). "Application of energy tunnels to an urban environment." *Geothermics*, Elsevier, 61, 104–113.
- Başer, T., Lu, N., and McCartney, J. S. (2016). "Operational response of a soil-borehole thermal energy storage system." *Journal of Geotechnical and Geoenvironmental Engineering*, American Society of Civil Engineers, 142(4), 4015097.
- Başer, T., and McCartney, J. S. (2020). "Transient evaluation of a soil-borehole thermal energy storage system." *Renewable Energy*, Elsevier BV, 147, 2582–2598.
- Beier, R. A., Smith, M. D., and Spitler, J. D. (2011). "Reference data sets for vertical borehole ground heat exchanger models and thermal response test analysis." *Geothermics*, Elsevier,

40(1), 79–85.

- Bennet, J., Claesson, J., and Hellström, G. (1987). “Multipole method to compute the conductive heat flows to and between pipes in a composite cylinder.” [Publisher information missing].
- Bernier, M. A. (2001). “Ground-coupled heat pump system simulation/Discussion.” *Ashrae Transactions*, American Society of Heating, Refrigeration and Air Conditioning Engineers, Inc., 107, 605.
- Bi, Y., Wang, X., Liu, Y., Zhang, H., and Chen, L. (2009). “Comprehensive exergy analysis of a ground-source heat pump system for both building heating and cooling modes.” *Applied Energy*, Elsevier BV, 86(12), 2560–2565.
- Bienert, W. B., Pravda, M. F., Suelau, H. H., and Wolf, D. A. (1974). “Snow and ice removal from pavements using stored earth energy.” *NASA STI/Recon Technical Report N*, 75.
- Binod, A., Kenichi, S., Peter, J., and Laloui, L. (2012). “Thermo-mechanical behaviour of energy piles.” *Geotechnique-London-*, 62(ARTICLE), 503–519.
- Bivina, G. R., Landge, V., and Kumar, V. S. S. (2016). “Socio Economic Valuation of Traffic Delays.” *Transportation Research Procedia*, Elsevier BV TS - CrossRef, 17, 513–520.
- Blackburn, R. R. (2004). *Snow and ice control. NCHRP report*, Transportation Research Board, Washington, D.C.
- Blackburn, R. R., McGrane, E. J., Chappelow, C. C., Harwood, D. W., and Fleege, E. J. (1994). *Development of anti-icing technology*. Strategic Highway Research Program, National Research Council Washington, DC.
- Bobes-Jesus, V., Pascual-Muñoz, P., Castro-Fresno, D., and Rodriguez-Hernandez, J. (2013). “Asphalt solar collectors: a literature review.” *Applied Energy*, Elsevier, 102, 962–970.
- Boockmeyer, A., and Bauer, S. (2016). “Efficient simulation of multiple borehole heat exchanger

- storage sites.” *Environmental Earth Sciences*, Springer, 75(12), 1–13.
- Bowers Jr, G. A. (2016). “Ground-Source Bridge Deck Deicing and Integrated Shallow Geothermal Energy Harvesting Systems.” Virginia Tech.
- Bowers Jr, G. A., and Olgun, C. G. (2015). “Experimental investigation of bridge deck deicing using energy piles.” *IFCEE 2015*, 1628–1637.
- Boyd, T. L. (2003). *New snow melt projects in Klamath Falls, OR*.
- Brandl, H. (2006). “Energy foundations and other thermo-active ground structures.” *Geotechnique*, Thomas Telford Ltd, 56(2), 81–122.
- Brown, H., Kraus, M., and Bowders, J. (2014). “Decision Methodology for Temperature Control of Pavements.” *Transportation Research Record*, 2403(1), 45–51.
- Chapman, W. P., and Katunich, S. (1956). “Heat requirements of snow melting systems.” *ASHAE Transactions*, 62, 359–372.
- Chi, Z., Yiqiu, T., Fengchen, C., Qing, Y., and Huining, X. (2019). “Long-term thermal analysis of an airfield-runway snow-melting system utilizing heat-pipe technology.” *Energy Conversion and Management*, Elsevier BV, 186, 473–486.
- Chiasson, A., and Spitler, J. D. (2001). “Modeling approach to design of a ground-source heat pump bridge deck heating system.” *Transportation research record*, SAGE Publications Sage CA: Los Angeles, CA, 1741(1), 207–215.
- Cho, H., and Choi, J. M. (2014). “The quantitative evaluation of design parameter’s effects on a ground source heat pump system.” *Renewable energy*, Elsevier, 65, 2–6.
- Choi, J. C., Lee, S. R., and Lee, D. S. (2011). “Numerical simulation of vertical ground heat exchangers: intermittent operation in unsaturated soil conditions.” *Computers and Geotechnics*, Elsevier, 38(8), 949–958.

- Choi, J. C., Park, J., and Lee, S. R. (2013). “Numerical evaluation of the effects of groundwater flow on borehole heat exchanger arrays.” *Renewable Energy*, Elsevier, 52, 230–240.
- Chong, C. S. A., Gan, G., Verhoef, A., Garcia, R. G., and Vidale, P. L. (2013). “Simulation of thermal performance of horizontal slinky-loop heat exchangers for ground source heat pumps.” *Applied Energy*, Elsevier, 104, 603–610.
- Churchill, S. W., and SW, C. (1977). “Friction-factor equation spans all fluid-flow regimes.”
- Claesson, J. (1981). “Model studies of duct storage systems.”
- Comsol, I. (2018). “COMSOL multiphysics reference manual, version 5.3.” *COMSOL AB*, 564, 565.
- Council, F. M., Zaloshnja, E., Miller, T., and Persaud, B. N. (2005). *Crash cost estimates by maximum police-reported injury severity within selected crash geometrics*. Turner-Fairbank Highway Research Center.
- Cuelho. (2010). “Establishing best practices for removing snow and ice from California roadways.” *Presentation to the Winter Maintenance Committee at the 89th*.
- Daghighi, A., and Nahvi, A. (2014). “Effect of different additives on fatigue behavior of asphalt mixtures.” *Construction Materials and Structures*, IOS Press, 601–607.
- Das, J. T., Banerjee, A., Chakraborty, S., and Puppala, A. J. (2018). “A Framework for Assessment of Sustainability and Resilience in Subgrade Stabilization for a High-Volume Road.” *Transportation Research Board 97th Annual Meeting* *Transportation Research Board*, (18–06711).
- Dehdezi, P. K. (2014). “Impact of concrete thermophysical properties on pavement structural design.” *Journal of materials in civil engineering*, American Society of Civil Engineers, 26(7), 4014018.

- Donnelly, D. E. (1981). *Geothermal energy for highway snow and ice control. Summary report.* Colorado Dept. of Highways, Denver (USA).
- Emmi, G., Zarrella, A., De Carli, M., and Galgaro, A. (2015). “An analysis of solar assisted ground source heat pumps in cold climates.” *Energy Conversion and Management*, Elsevier, 106, 660–675.
- Eskilson, P. (1987). “Thermal analysis of heat extraction boreholes.” Department of Mathematical Physics, University of Lund Lund,, Sweden.
- Eugster. (2007). “Road and bridge heating using geothermal energy. Overview and examples.” *Proceedings European Geothermal Congress*.
- Eugster, and Eugster, W. J. (2007). “Road and bridge heating using geothermal energy. Overview and examples.” *Proceedings European Geothermal Congress*, (June), 5.
- Fay, L., Honarvarnazari, M., Jungwirth, S., Muthumani, A., Cui, N., and Shi, X. (2015). “Manual of environmental best practices for snow and ice control.” *Clear Roads and Minnesota DOT*.
- Fay, L., Volkening, K., Gallaway, C., and Shi, X. (2008). “Performance and impacts of current deicing and anti-icing products: User perspective versus experimental data.” *87th annual meeting of the Transportation Research Board*.
- Ferrara, A. A., and Brinkman, P. (1976). *Applying Heat Pipes to Avoid the Preferential Freezing of Highway Bridge Decks*. American Society of Mechanical Engineers.
- FHWA. (2005). “Highway economic requirements system—State version.” Federal Highway Administration Washington, DC.
- FHWA. (2008). “2008 status of the nation’s highways, bridges, and transit: conditions and performance report to congress.” US DOT Federal Highway Administration.
- FHWA. (2020). *Snow and Ice*.

- Fischel, M. (2001). *Evaluation of Selected Deicers Based on a Review of the Literature. The SeaCrest Group. Louisville, CO.* Report Number CDOT-DTD.
- Fujimitsu, Y., Fukuoka, K., Ehara, S., Takeshita, H., and Abe, F. (2010). “Evaluation of subsurface thermal environmental change caused by a ground-coupled heat pump system.” *Current Applied Physics*, Elsevier, 10(2), S113–S116.
- Gao, Q., Zhou, X.-Z., Jiang, Y., Chen, X.-L., and Yan, Y.-Y. (2013). “Numerical simulation of the thermal interaction between pumping and injecting well groups.” *Applied thermal engineering*, Elsevier, 51(1–2), 10–19.
- Gardiner, E. P., Herring, D. D., and Fox, J. F. (2019). “The US climate resilience toolkit: evidence of progress.” *Climatic Change*, Springer, 153(4), 477–490.
- Gawecka, K. A., Taborda, D. M. G., Potts, D. M., Sailer, E., Cui, W., and Zdravković, L. (2020). “Finite-Element Modeling of Heat Transfer in Ground Source Energy Systems with Heat Exchanger Pipes.” *International Journal of Geomechanics*, American Society of Civil Engineers, 20(5), 4020041.
- Ghasemi-Fare, O., Bowers, G. A., Kramer, C. A., Ozudogru, T. Y., Basu, P., Olgun, C. G., Bulbul, T., and Sutman, M. (2015). *A feasibility study of bridge deck deicing using geothermal energy.* Mid-Atlantic Universities Transportation Center.
- Giordano, N., Comina, C., Mandrone, G., and Cagni, A. (2016). “Borehole thermal energy storage (BTES). First results from the injection phase of a living lab in Torino (NW Italy).” *Renewable Energy*, Elsevier, 86, 993–1008.
- Granata, R. D., and Hartt, W. H. (2009). *Integrity of infrastructure materials and structures.*
- Griffin, R. G. (1982). *Highway bridge deicing using passive heat sources.* Colorado Department of Highways.

- Habibzadeh-Bigdarvish, O., Li, T., Lei, G., Banerjee, A., Yu, X., and Puppala, A. J. (2021a). “De-icing Test of the Externally Heated Geothermal Bridge in Texas.” *4th International Conference on Transportation Geotechnics, ICTG 2021*.
- Habibzadeh-Bigdarvish, O., Li, T., Lei, G., Puppala, A. J., and Yu, X. (2021b). “Numerical Study and Experimental Validation of the Thermal Performance of a U-Tube Borehole Heat Exchanger for a Geothermal De-Icing System.” *IFCEE 2021*, American Society of Civil Engineers, Reston, VA, 109–118.
- Habibzadeh-Bigdarvish, O., Yu, X., Lei, G., Li, T., and Puppala, A. J. A. J. (2019). “Life-Cycle cost-benefit analysis of Bridge deck de-icing using geothermal heat pump system: A case study of North Texas.” *Sustainable Cities and Society*, Elsevier, 47, 101492.
- Habibzadeh-Bigdarvish, O., Yu, X., Li, T., Lei, G., Banerjee, A., and Puppala, A. J. (2021c). “A novel full-scale external geothermal heating system for bridge deck de-icing.” *Applied Thermal Engineering*, Elsevier, 185, 116365.
- Habibzadeh-Bigdarvish, O., Yu, X., and Puppala, A. J. (2020). “Externally heated geothermal bridge deck: Performance analysis of the U-tube ground heat exchanger.” *E3S Web of Conferences*, EDP Sciences, 7006.
- Hakkaki-Fard, A., Eslami-Nejad, P., Aidoun, Z., and Ouzzane, M. (2015). “A techno-economic comparison of a direct expansion ground-source and an air-source heat pump system in Canadian cold climates.” *Energy*, Elsevier, 87, 49–59.
- Han, C., and Yu, X. (2016). “Sensitivity analysis of a vertical geothermal heat pump system.” *Applied Energy*, Elsevier BV, 170, 148–160.
- Han, C., and Yu, X. (2018). “An innovative energy pile technology to expand the viability of geothermal bridge deck snow melting for different United States regions: Computational

- assisted feasibility analyses.” *Renewable Energy*, Elsevier BV, 123, 417–427.
- Han, C., and Yu, X. B. (2017). “Feasibility of geothermal heat exchanger pile-based bridge deck snow melting system: A simulation based analysis.” *Renewable energy*, Elsevier, 101, 214–224.
- Han, Z., Li, B., Ma, C., Hu, H., and Bai, C. (2018). “Study on accurate identification of soil thermal properties under different experimental parameters.” *Energy and Buildings*, Elsevier, 164, 21–32.
- He, M., Rees, S. J., and Shao, L. (2009). “Applications of a dynamic three-dimensional numerical model for borehole heat exchangers.” *Proceedings of Effstock, the 11th International Conference on Thermal Energy Storage. Stockholm International Fairs, Stockholm, Sweden.*
- Huang, Y.-H., Adams, T. M., and Pincheira, J. A. J. A. (2004). “Analysis of life-cycle maintenance strategies for concrete bridge decks.” *Journal of Bridge Engineering*, American Society of Civil Engineers, 9(3), 250–258.
- Hurley, M. (2019). “PERFORMANCE OF CONCRETE SLABS WITH EMBEDDED HYDRONIC LOOPS FOR GEOTHERMALLY BASED BRIDGE DE-ICING APPLICATIONS.”
- International Energy Agency. (2014). “Key world energy statistics.” *OECD/IEA, Paris.*
- Jalili, D., and Habibzadeh Bigdarvish, O. (2017). “On the modeling of thermo-active diaphragm walls by numerical analyses and monitoring data.” MSc thesis Politecnico di Milano, Milan, Italy.
- Javadi, H., Ajarostaghi, S. S. M., Rosen, M. A., and Pourfallah, M. (2019). “Performance of ground heat exchangers: A comprehensive review of recent advances.” *Energy*, Elsevier.
- Kavanaugh, S. P. (1997). “Design of geothermal systems for commercial and institutional

buildings.” *GROUND-SOURCE HEAT PUMPS*.

Koch, G. H., Brongers, M. P. H., Thompson, N. G., Virmani, Y. P., and Payer, J. H. (2002).

Corrosion cost and preventive strategies in the United States.

Kohl, T., and Hopkirk, R. J. (1995). “‘FRACure’—A simulation code for forced fluid flow and transport in fractured, porous rock.” *Geothermics*, Elsevier, 24(3), 333–343.

Kong, M., Alvarado, J. L., Thies, C., Morefield, S., and Marsh, C. P. (2017). “Field evaluation of microencapsulated phase change material slurry in ground source heat pump systems.” *Energy*, Elsevier BV, 122, 691–700.

Koppen, W. (1936). “Das geographische system der klimat.” *Handbuch der klimatologie*, Gebruder Borntraeger, 46.

Laloui, L., and Di Donna, A. (2013). “Energy geostructures.” *ISTE and John Wiley & Sons*, Wiley Online Library.

Laloui, L., and Loria, A. F. R. (2019). *Analysis and design of energy geostructures: theoretical essentials and practical application*. Academic Press.

Lamarche, L., Kaji, S., and Beauchamp, B. (2010). “A review of methods to evaluate borehole thermal resistances in geothermal heat-pump systems.” *Geothermics*, Elsevier, 39(2), 187–200.

Lazzari, S., Priarone, A., and Zanchini, E. (2010). “Long-term performance of BHE (borehole heat exchanger) fields with negligible groundwater movement.” *Energy*, Elsevier, 35(12), 4966–4974.

Lei, G., Yu, X., and Li, T. (2018). “Design and Numerical Analysis of an Externally Heated Geothermal Bridge Deck.” *Civil Infrastructures Confronting Severe Weathers and Climate Changes Conference*, Springer, 150–159.

- Li, B., Han, Z., Bai, C., and Hu, H. (2019). “The influence of soil thermal properties on the operation performance on ground source heat pump system.” *Renewable energy*, Elsevier, 141, 903–913.
- Li, T., Lei, G., Yu, X., Zhang, N., and Puppala, A. J. (2018). “Numerical feasibility study of an externally heated geothermal bridge deck.” *IFCEE 2018*, 758–767.
- Li, T., Yu, X., Habibzadeh-Bigdarvish, O., Lei, G., and Puppala, A. J. (2021). “Heating performance of a novel externally-heated geothermal bridge de-icing system: field tests and numerical simulations.” *Sustainable Energy Technologies and Assessments*, Elsevier, 46, 101280.
- Li, T., Yu, X., Lei, G., Habibzadeh-Bigdarvish, O., and Hurley, M. (2020). “Numerical analyses of a laboratory test of a geothermal bridge deck externally heated under controlled temperature.” *Applied Thermal Engineering*, Elsevier BV, 174(April), 115255.
- Liu, H., Maghoul, P., Bahari, A., and Kavacic, M. (2019). “Feasibility study of snow melting system for bridge decks using geothermal energy piles integrated with heat pump in Canada.” *Renewable Energy*, Elsevier BV, 136, 1266–1280.
- Liu, X., Rees, S. J., and Spitler, J. D. (2003). “Simulation of a geothermal bridge deck anti-icing system and experimental validation.” *Proceedings of the Transportation Research Board 82nd Annual Meeting. Washington, DC January*, 12–16.
- Liu, X., Rees, S. J., and Spitler, J. D. (2007). “Modeling snow melting on heated pavement surfaces. Part I: Model development.” *Applied Thermal Engineering*, Elsevier, 27(5–6), 1125–1131.
- Liu, Z., Xu, W., Zhai, X., Qian, C., and Chen, X. (2017). “Feasibility and performance study of the hybrid ground-source heat pump system for one office building in Chinese heating

- dominated areas.” *Renewable Energy*, Elsevier BV, 101, 1131–1140.
- Loomans, M., Oversloot, H., De Bondt, A., Jansen, R., and Van Rij, H. (2003). “Design tool for the thermal energy potential of asphalt pavements.” *Eighth International IBPSA Conference, Eindhoven, Netherlands*, 745–752.
- Lund, J. W. (1999). “Reconstruction of a pavement geothermal deicing system.” *Geo-Heat Center*.
- Lund, J. W. (2000). “World status of geothermal energy use overview 1995-1999.”
- Malakooti, A., Theh, W. S., Sadati, S. S., Ceylan, H., Kim, S., Mina, M., Cetin, K., and Taylor, P. C. (2020). “Design and Full-scale Implementation of the Largest Operational Electrically Conductive Concrete Heated Pavement System.” *Construction and Building Materials*, Elsevier BV, 255, 119229.
- Mallela, J., and Sadavisam, S. (2011). *Work zone road user costs: Concepts and applications*. United States. Federal Highway Administration.
- Marfin, C., Jimenez, J., Keomoungkhoun, N., Scudder, C., and Steele, T. (2021). “At least 6 dead in 133-car pileup in Fort Worth after freezing rain coats roads.” *The Dallas Morning News*.
- Marion, W., and Wilcox, S. (1995). *Solar radiation data manual for buildings*. National Renewable Energy Lab., Golden, CO (United States).
- McCartney, J. S., Sánchez, M., and Tomac, I. (2016). “Energy geotechnics: Advances in subsurface energy recovery, storage, exchange, and waste management.” *Computers and Geotechnics*, Elsevier, 75, 244–256.
- Merrill, B. D. (2002). “Texas’ use of precast concrete stay-in-place forms for bridge decks.” *Concrete Bridge Conference*.
- Mimouni, T., Dupray, F., and Laloui, L. (2014). “Estimating the geothermal potential of heat-exchanger anchors on a cut-and-cover tunnel.” *Geothermics*, Elsevier, 51, 380–387.

- Minsk, L. D. (1999). *Heated Bridge Technology-Report on ISTEA Sec. 6005 Program*. United States. Federal Highway Administration.
- Mirzananadi, R., Hagentoft, C.-E., and Johansson, P. (2018). “Numerical investigation of harvesting solar energy and anti-icing road surfaces using a hydronic heating pavement and borehole thermal energy storage.” *Energies*, Multidisciplinary Digital Publishing Institute, 11(12), 3443.
- Mirzananadi, R., Hagentoft, C.-E., and Johansson, P. (2020). “Coupling a Hydronic Heating Pavement to a Horizontal Ground Heat Exchanger for harvesting solar energy and heating road surfaces.” *Renewable Energy*, Elsevier BV, 147, 447–463.
- Mokhtarian, P. L., and Salomon, I. (2001). “How derived is the demand for travel? Some conceptual and measurement considerations.” *Transportation Research Part A: Policy and Practice*, Elsevier BV, 35(8), 695–719.
- Monsalud, A., Ho, D., and Rakas, J. (2015). “Greenhouse gas emissions mitigation strategies within the airport sustainability evaluation process.” *Sustainable Cities and Society*, Elsevier BV, 14, 414–424.
- Monzó, P., Bernier, M., Acuña, J., and Mogensen, P. (2016). “A monthly based bore field sizing methodology with applications to optimum borehole spacing.” *ASHRAE Transactions*, ASHRAE, 122(1), 111–126.
- Morita, K., and Tago, M. (2005). “Snow-melting on sidewalks with ground-coupled heat pumps in a heavy snowfall city.” *Proceedings of the World Geothermal Congress*.
- Nahvi, A., Daghighi, A., and Nazif, S. (2018). “The environmental impact assessment of drainage systems: a case study of the Karun river sugarcane development project.” *Archives of Agronomy and Soil Science*, Informa UK Limited, School of Civil Engineering, Iowa State

University, Iowa, USA School of Civil Engineering, Cleveland State University, Ohio, USA
School of Civil Engineering, College of Engineering, University of Tehran, Tehran, Iran M4
- Citavi, 64(2), 185–195.

Naito, C., Sause, R., Hodgson, I., Pessiki, S., and Macioce, T. (2010). “Forensic examination of a noncomposite adjacent precast prestressed concrete box beam bridge.” *Journal of Bridge Engineering*, American Society of Civil Engineers, 15(4), 408–418.

Nam, Y., and Chae, H.-B. (2014). “Numerical simulation for the optimum design of ground source heat pump system using building foundation as horizontal heat exchanger.” *Energy*, Elsevier, 73, 933–942.

Nixon, W. A. (2001). “Anti-icers: driving towards clearer roads.” *Snow and Ice Manager*.

NOAA’s National Weather Service. (2018). “Dallas/Fort Worth - freeze data and cold season temperatures.”

NOAA’s National Weather Service. (2021). “DFW - Temperature Extremes.”
<<https://www.weather.gov/fwd/dgr8mxmn>>.

Noorollahi, Y., Saeidi, R., Mohammadi, M., Amiri, A., and Hosseinzadeh, M. (2018). “The effects of ground heat exchanger parameters changes on geothermal heat pump performance—A review.” *Applied Thermal Engineering*, Elsevier, 129, 1645–1658.

Nwaubani, S. O., Katsanos, A., O., S., and Katsanos, A. (2014). “Effect of alternative de-icers on the corrosion resistance of reinforced concrete bridges and highway structures.” *Developments in corrosion protection*, M. Aliofkhaezai, ed., IntechOpen, Rijeka.

Nydahl, J. E., Pell, K., and Lee, R. (1987). “Bridge deck heating with ground-coupled heat pipes: analysis and design.” *ASHRAE transactions*, 93, 939–958.

Omer, A. M. (2008). “Ground-source heat pumps systems and applications.” *Renewable and*

- sustainable energy reviews*, Elsevier, 12(2), 344–371.
- Ozudogru, T. Y., Olgun, C. G., and Senol, A. (2014). “3D numerical modeling of vertical geothermal heat exchangers.” *Geothermics*, Elsevier, 51, 312–324.
- Ozyurt, O., and Ekinici, D. A. (2011). “Experimental study of vertical ground-source heat pump performance evaluation for cold climate in Turkey.” *Applied Energy*, Elsevier BV, 88(4), 1257–1265.
- Perkins, J. A., Mwakalonge, J., Jasek, D., Carson, J., Obeng-Boampong, K., and Pesti, G. (2012). *Research on best practices for winter weather operations*. Texas. Dept. of Transportation. Research and Technology Implementation Office.
- PRISM Climate Group. (2015). “Average daily minimum temperature of Jan 2015.”
- PRISM Climate Group. (2017). “Annual precipitation of 2015.” <http://www.prism.oregonstate.edu/recent/>.
- Rohde, D., Andresen, T., and Nord, N. (2018). “Analysis of an integrated heating and cooling system for a building complex with focus on long-term thermal storage.” *Applied Thermal Engineering*, Elsevier, 145, 791–803.
- Roy, D., Chakraborty, T., Basu, D., and Bhattacharjee, B. (2020). “Feasibility and performance of ground source heat pump systems for commercial applications in tropical and subtropical climates.” *Renewable Energy*, Elsevier BV, 152, 467–483.
- Salim Shirazi, A., and Bernier, M. (2014). “A small-scale experimental apparatus to study heat transfer in the vicinity of geothermal boreholes.” *HVAC&R Research*, Taylor & Francis, 20(7), 819–827.
- Sedaghat, A., Habibi, M., and Hakkaki-Fard, A. (2020). “A novel ground thermal recovery system for horizontal ground heat exchangers in a hot climate.” *Energy Conversion and*

Management, Elsevier, 224, 113350.

Shang, Y., Li, S., and Li, H. (2011). "Analysis of geo-temperature recovery under intermittent operation of ground-source heat pump." *Energy and buildings*, Elsevier, 43(4), 935–943.

Signorelli, S., Bassetti, S., Pahud, D., and Kohl, T. (2007). "Numerical evaluation of thermal response tests." *Geothermics*, Elsevier, 36(2), 141–166.

Spitler, J., and Bernier, M. (2011). "Ground-source heat pump systems: The first century and beyond." Taylor & Francis.

Spitler, J. D. (2000). "GLHEPRO-A design tool for commercial building ground loop heat exchangers." *Proceedings of the fourth international heat pumps in cold climates conference*, Citeseer.

Spitler, J. D. J. D., and Ramamoorthy, M. (2000). "Bridge deck deicing using geothermal heat pumps." *Proceedings of the Fourth International Heat Pumps in Cold Climates Conference*, Citeseer, 17–18.

Sterpi, D., Angelotti, A., Habibzadeh-Bigdarvish, O., and Jalili, D. (2017). "On the modelling of thermo-active diaphragm walls based on monitoring data." *15th International Conference of the International Association for Computer Methods and Advances in Geomechanics, IACMAG, CHN*, 1–7.

Sterpi, D., Angelotti, A., Habibzadeh-Bigdarvish, O., and Jalili, D. (2018a). "Assessment of thermal behaviour of thermo-active diaphragm walls based on monitoring data." *Journal of Rock Mechanics and Geotechnical Engineering*, 10(6).

Sterpi, D., Angelotti, A., Habibzadeh Bigdarvish, O., and Jalili, D. (2018b). "Heat transfer process in a thermo-active diaphragm wall from monitoring data and numerical modelling." *9th European Conference on Numerical Methods in Geotechnical Engineering*, Taylor and

- Francis Group, 731–736.
- Swanson, H. (1980). *Evaluation of geothermal energy for heating highway structures*.
- Texas Department of Transportation (TxDOT). (2016). *Report on Texas bridges as of September 2016*.
- Texas Department of Transportation (TxDOT). (2017). “Texas motor vehicle crash statistics.” <<https://www.txdot.gov/government/enforcement/annual-summary.html>>.
- Vitaliano, D. F. (1992a). “An Economic Assessment of the Social Costs of Highway Salting and the Efficiency of Substituting a New Deicing Material.” *Journal of Policy Analysis and Management*, JSTOR TS - CrossRef, 11(3), 397.
- Vitaliano, D. F. (1992b). “Infrastructure costs of road salting.” *Resources, Conservation and Recycling*, Elsevier BV, 7(1–3), 171–180.
- Weather Underground. (2019). *Weather history for Arlington, TX, November 2018 to March 2019*.
- White, D., Sritharan, S., Suleiman, M. T., and Chetlur, S. (2005). *Identification of the best practices for design, construction, and repair of bridge approaches*. Iowa. Dept. of Transportation.
- Wu, D., Kong, G., Liu, H., Zhu, X., and Pu, H. (2020). “Performance of a bridge deck as solar collector in a thermal energy storage system.” *E3S Web of Conferences*, EDP Sciences, 7009.
- Xi, Y., and Olsgard, P. J. (2000). *Effects of Deicing Agents (magnesium Chloride and Sodium Chloride) on Corrosion of Truck Components*. Colorado Department of Transportation, Research Branch.
- Yang, W., Sun, L., and Chen, Y. (2015). “Experimental investigations of the performance of a solar-ground source heat pump system operated in heating modes.” *Energy and Buildings*, Elsevier, 89, 97–111.

- Yoshitake, I., Yasumura, N., Syobuzako, M., and Scanlon, A. (2011). "Pipe heating system with underground water tank for snow thawing and ice prevention on roads and bridge decks." *Journal of Cold Regions Engineering*, American Society of Civil Engineers, 25(2), 71–86.
- You, T., Li, X., Cao, S., and Yang, H. (2018). "Soil thermal imbalance of ground source heat pump systems with spiral-coil energy pile groups under seepage conditions and various influential factors." *Energy Conversion and Management*, Elsevier BV, 178, 123–136.
- You, T., and Yang, H. (2020). "Feasibility of ground source heat pump using spiral coil energy piles with seepage for hotels in cold regions." *Energy Conversion and Management*, Elsevier, 205, 112466.
- Yu, X., Hurley, M. T., Li, T., Lei, G., Pedarla, A., and Puppala, A. J. (2019). "Experimental Feasibility Study of A New Attached Hydronic Loop Design for Geothermal Heating of Bridge Decks." *Applied Thermal Engineering*, Elsevier, 114507.
- Yu, X., Puppala, A. J., and Zhang, N. (2017). *Use of Geothermal Energy for Deicing Approach Pavement Slabs and Bridge Decks, Phase I*. Texas. Dept. of Transportation. Research and Technology Implementation Office.
- Yu, Y., and Olson, G. (2018). "Ground Source Heat Pump Systems." *Handbook of Energy Systems in Green Buildings*, 393–472.
- Yunovich, M., Thompson, N., and Virmani, Y. P. (2003). "Life cycle cost analysis for reinforced concrete bridge decks." *CORROSION 2003*, OnePetro.
- Zarella, A., Emmi, G., and De Carli, M. (2015). "Analysis of operating modes of a ground source heat pump with short helical heat exchangers." *Energy Conversion and Management*, Elsevier, 97, 351–361.
- Zeroual, A., Harrou, F., Sun, Y., and Messai, N. (2017). "Monitoring road traffic congestion using

- a macroscopic traffic model and a statistical monitoring scheme.” *Sustainable Cities and Society*, Elsevier, 35, 494–510.
- Zhang, C., Wang, Y., Liu, Y., Kong, X., and Wang, Q. (2018). “Computational methods for ground thermal response of multiple borehole heat exchangers: A review.” *Renewable Energy*, Elsevier, 127, 461–473.
- Zhang, D., Gao, P., Zhou, Y., Wang, Y., and Zhou, G. (2020). “An experimental and numerical investigation on temperature profile of underground soil in the process of heat storage.” *Renewable Energy*, Elsevier, 148, 1–21.
- Zhang, G., Xia, C., Sun, M., Zou, Y., and Xiao, S. (2013). “A new model and analytical solution for the heat conduction of tunnel lining ground heat exchangers.” *Cold Regions Science and Technology*, Elsevier, 88, 59–66.
- Zhao, H.-M., Wang, S.-G., Wu, Z.-M., and Che, G.-J. (2010). “Concrete Slab Installed with Carbon Fiber Heating Wire for Bridge Deck Deicing.” *Journal of Transportation Engineering*, American Society of Civil Engineers (ASCE), 136(6), 500–509.
- Zhao, W., Zhang, Y., Chen, X., Su, W., Li, B., and Fu, Z. (2020). “Experimental heating performances of a ground source heat pump (GSHP) for heating road unit.” *Energy Conversion and Management: X*, Elsevier BV, 7, 100040.
- Zhao, Z., Shen, R., Feng, W., Zhang, Y., and Zhang, Y. (2018). “Soil thermal balance analysis for a ground source heat pump system in a hot-summer and cold-winter region.” *Energies*, Multidisciplinary Digital Publishing Institute, 11(5), 1206.